

Physicochemical Properties and Synthesis of Oligothiophene Macrocycles

Dissertation

zur Erlangung des Doktorgrades Dr. rer. nat.

der Fakultät für Naturwissenschaften

der Universität Ulm

vorgelegt von

Achim Kaiser

aus Miltenberg

Ulm 2008

Physicochemical Properties and Synthesis of Oligothiophene Macrocycles

Dissertation

zur Erlangung des Doktorgrades Dr. rer. nat.

der Fakultät für Naturwissenschaften

der Universität Ulm

vorgelegt von

Achim Kaiser

aus Miltenberg

Ulm 2008

Amtierender Dekan: Prof. Dr. Klaus-Dieter Spindler

1. Gutachter: Prof. Dr. Peter Bäuerle

2. Gutachter: Prof. Dr. Nicola Hüsing

Tag der Promotionsprüfung: 27. Juni 2008

Fakultät für Naturwissenschaften

Universität Ulm

2008

The pure and simple truth

is rarely pure and never simple

Oscar Wilde

für meine “Mädels”

Danksagung (Acknowledgement)

Die vorliegende Arbeit wurde in der Zeit von November 2000 bis April 2005 in der Abteilung Organische Chemie II durchgeführt. Dabei durfte ich sowohl auf die inhaltliche als auch auf die moralische Unterstützung vieler Kollegen und Freunde zählen, bei denen ich mich nachfolgend bedanken möchte:

Bei Prof. Dr. Peter Bäuerle, der mir die spannende Arbeit ermöglicht und sie mit persönlichem Engagement begleitet hat, und der mir viele Möglichkeiten der wissenschaftlichen Weiterbildung innerhalb und außerhalb der Universität Ulm geboten hat;

bei Dr. Elena Mena-Osteritz, auf deren Erfahrung bei physikalisch-chemischen Belangen ich stets zurückgreifen konnte und deren Kondition auch bei Bergtouren bewundernswert ist;

bei Prof. Dr. Volkhard Austel und Prof. Dr. Frank Würthner für viele fruchtbare Diskussionen;

bei meinen Laborkollegen, die sowohl für experimentelle als auch für musikalische Fragestellungen stets ein offenes Ohr hatten, und die für eine gute Stimmung in und außerhalb des Labors sorgten, insbesondere Dr. Martin Ammann, Dr. Jens Cremer (den ich zu meiner Freude auch weiterhin als Kollegen bezeichnen kann), Dr. Claire Fave, Dr. Gerda Fuhrmann (der „Herrin der Ringe“, ohne deren grundlegende Arbeit diese Dissertation nicht zustande gekommen wäre), Dr. Luis Madrigal, Frank Nicklas und Markus Wilde;

bei den Laborkollegen des AK Würthner im N24-Labor, besonders Dr. Shahadat Ahmed, Dr. Zhijian Chen, Dr. Rainer Dobrawa, Dr. Christoph Thalacker und Dr. Armin Sautter;

bei allen weiteren Arbeitskreis-Mitgliedern für die gute Atmosphäre, namentlich Dr. Mohammed Abdel-Mottaleb, Felix Balser, Eduard Brier, Dr. Hang-Beom Bu, Erwaa El-Hosseiny, Dr. Michael Field, Dr. Pinar Kilickiran, Dr. Changqi Ma, Stefanie Potratz, Martin Schikora (besonders für die wertvolle Hilfe im Rahmen seines Mitarbeiter-Praktikums), Eva-Kathrin Schillinger, Dr. Sylvia Schmid, Astrid Vogt und Dr. Feng Yan;

- bitte wenden -

bei Dr. Markus Wunderlin für die massenspektrometrische Untersuchung meiner Substanzen und rege Unterhaltungen über unsere Lieblingsthemen;

bei Dr. Günther Götz und Dr. Egon Reinold für die bereitwillige technische Unterstützung, die mit außergewöhnlich viel Engagement erfolgte;

bei Dr. Werner Mästle für die fruchtbare Zusammenarbeit bei der Praktikumsbetreuung und für manche motivierenden Gespräche;

bei Dr. Dominik Auer und Dr. Daniel Schildbach für die Durchführung der Röntgenstrukturanalyse und der entsprechenden Berechnungen, sowie für die langjährige Freundschaft und die private Unterstützung bei dieser Arbeit;

bei Prof. Dr. G. Ulrich Nienhaus, der mir die Nutzung verschiedener spektroskopischer Methoden in seinem Arbeitskreis ermöglichte, sowie bei Dr. Carlheinz "Charly" Röcker für die Unterstützung bei diesen Messungen;

beim Graduiertenkolleg „Molekulare Organisation und Dynamik an Grenz- und Oberflächen" der Universität Ulm für die finanzielle Förderung durch ein Stipendium;

bei meinen Kollegen der Wacker Chemie AG, besonders Peter Hirschmann, der mir als Vorgesetzter die nötigen Freiheiten und den Ansporn gegeben hat, die Fertigstellung dieser Arbeit voranzutreiben, sowie bei Dr. Bernd Märker für die „Sklavenarbeit" beim Formelzeichnen;

bei meinen Eltern, die mich immer motiviert haben;

bei meiner Frau Andrea, die mich in jeder Entscheidung (besonders in schwierigen Phasen) unterstützt und selbst für nächtelange Messungen viel Verständnis entgegengebracht hat;

und nicht zuletzt bei meiner Tochter Elisa, deren Lächeln mich jedesmal aufs Neue inspiriert hat.

Table of Contents

Table of Contents ---------- 1

Conventions and Abbreviations ---------- 5

1 Preface ---------- 9

1.1 Introduction to Oligothiophene Macrocycles 9

1.2 Aims of this Thesis 12

1.2.1 Investigation of the Physicochemical Properties of Oligothiophene Macrocycles 12

1.2.2 Molecular Recognition of Guest Molecules 12

1.2.3 Template Synthesis of Oligothiophene Macrocycles 12

2 Introduction: The "Metal-Template" Approach to Oligothiophene Macrocycles---------- 13

2.1 Introduction to Shape-Persistent Macrocycles.....13

2.2 Preparation of Oligothiophene Macrocycles by Glaser-Type Coupling.....16

2.3 The Metal-Template Route as a Combination of Synthetic Strategies.....21

2.4 Survey of Macrocycles Comprising Pt(II) Building Blocks 24

2.4.1 Usage of Pt(II) Units as Supramolecular Building Blocks 24

2.4.2 Strategic Choice of Building Blocks for Pt(II) Macrocycles 26

2.4.3 Choice of Reaction Conditions 29

2.4.4 Characterisation of Pt(II) Macrocycles 29

2.4.5 Criteria for the Division of Different Structures 30

2.4.6 Macrocycles with Pt–N Coordination Containing Nucleobases 31

2.4.7 Macrocycles with Pt–N Coordination Containing Exocyclic Diamine Ligands 35

2.4.8 Square Pt–N Coordinated Macrocycles with Exocyclic Ligands Other than Diamines 39

2.4.9 Molecular Polygons Other than Squares (Triangles, Hexagons, Cyclodimers) and Equilibria Thereof 44

2.4.10 Macrocycles with Bridging Cyanide and Isocyanide Ligands 54

2.4.11 Macrocycles with Bridging Acetylide Ligands 57

2.4.12 Macrocycles by Pt–P Coordination 74

2.4.13 Macrocycles by Unusual Pt(II) Coordination 78

2.4.14 Concluding Remarks on Pt(II) Macrocycles 82

3 Synthesis of Aryl-Substituted Oligothienyl Macrocycles -------- 85

3.1 Synthesis of Phenyl-Substituted Precursors.....85

3.1.1 Choice of the Thiophene Substitution Pattern 85

3.1.2 Synthesis of Phenyl-Substituted Building Blocks 86

3.1.3 Synthesis of *p*-Alkylphenyl-Substituted Building Blocks 90

3.2 Solid-State and Calculated Structure of 3,4-Diphenylthiophene 93
3.3 Preparation of Phenyl-Substituted Macrocycles 97
3.4 Discussion of the Preparative Results 102
3.5 Experimental Section 104
3.5.1 Materials and Methods 104
3.5.2 Preparation of Phenyl-Substituted Building Blocks 107
3.5.3 Preparation of *p*-Alkylphenyl-Substituted Building Blocks 112
3.5.4 Preparation of Macrocyclic Compounds 117
3.5.5 Details for the Structure Discussion of 3,4-Diphenylthiophene 119

4 Photophysical Properties of Oligothienyl Macrocycles -------- 125

4.1 Theoretical Model and Selection Rules for Conjugated Macrocycles 125
4.1.1 Properties of Linear Oligothiophenes 125
4.1.2 The Frenkel Exciton Model for Linear and Cyclic Oligothiophenes 128
4.2 Absorption and Emission of Cyclic Oligo(thienylene-butadiinylene)s 131
4.2.1 Macrocycles with terthiophene (3T) units 131
4.2.2 Macrocycles with quinquethiophene (5T) units 134
4.2.3 Macrocycles with undecithiophene (11T) units 137
4.3 Pt(II) Macrocycles with Oligothienyl Monomers 139
4.3.1 C[Pt–A–3T(Bu_4)–A]$_2$ ("butyl series") 139
4.3.2 Pt(II) macrocycles with other oligothienyl monomers 141
4.4 Cyclo[*n*]thiophenes 145
4.5 Fluorescence Correlation Spectroscopy (FCS) 148
4.5.1 Theory and Experimental Setup 148
4.5.2 Results for [3T(Bu_4)–DA]$_2$–3T(Bu_4), C[3T(Bu_4)–DA]$_3$ and C[12]T 149
4.6 Low Temperature Spectroscopy of C[3T(Bu_4)–DA]$_3$ 153
4.6.1 Experimental Setup 153
4.6.2 PMMA cell restrictions 154
4.6.3 Emission at Room Temperature 155
4.6.4 Emission Spectra at Low Temperatures 156
4.7 Calculations on the Ring Strain of Cyclic Oligo(terthienyldiacetylide)s 158
4.7.1 Method of Strain Determination 158
4.7.2 Energies of the Linear Compounds 159
4.7.3 Ring Strain Energies of the Macrocycles 161
4.8 Discussion of the Photophysical Properties of Oligothiophene Macrocycles 162
4.8.1 Correlation of the UV/Vis Spectra with the Frenkel Exciton Model 162
4.8.2 Trends and Particularities of the Experimental Values 164
4.8.3 Comparison of the Diethynylene-Containing Macrocycles with Cyclo[*n*]thiophenes 168
4.8.4 Differences between Corresponding Cyclic and Linear Oligomers 170
4.8.5 Photophysical Properties of Pt(II)-Containing Macrocycles 173
4.9 Experimental Section 175

5 Electrochemical Properties of Oligothienyl Macrocycles-------177

5.1 Electrochemical Features of Shape-Persistent Macrocycles....177
- 5.1.1 Electrochemical Demands on Shape-Persistent Macrocycles 177
- 5.1.2 Influence of Pt(II) on the Electrochemical Properties 180
- 5.1.3 Electrochemical Data of Oligothiophene Macrocycles and Their Pt(II) Precursors 183

5.2 Cyclic Voltammetry of Conjugated Macrocycles with Terthienyl Units 186

5.3 Analytical Cyclic Voltammetry of Oligothienyl Diplatina-Macrocycles....189

5.4 Electrochemically Triggered Reductive Elimination of Pt(II) Centres....192

5.5 Discussion of the Electrochemical Results 197

5.6 Experimental Section 199

6 Interactions between Oligothienyl Macrocycles and Receptor Molecules----------201

6.1 The Role of Macrocycles as Host Molecules....201

6.2 Influence of Guest Molecules on the Fluorescence of Oligothienyl Macrocycles 206
- 6.2.1 Choice of the Guest Molecules 206
- 6.2.2 Addition of Fullerene C_{60} to Oligothienyl Macrocycles 206
- 6.2.3 Addition of Porphyrins to Oligothienyl Macrocycles 209
- 6.2.4 Addition of Viologene Derivatives to Oligothienyl Macrocycles 210
- 6.2.5 Formation of Gold Clusters 212
- 6.2.6 Addition of Melamine Compounds 213
- 6.2.7 Reaction of 3,4,3",4"-tetrabutylterthiophene with ferrocene 214

6.3 Discussion 216

6.4 Experimental Section 218

7 Summary ----------219

7.1 Summary of the Results 219

7.2 Zusammenfassung der Ergebnisse 224

8 Literature References ----------231

Conventions and Abbreviations

Conventions

Prefixes, symbols and units are denoted according to the conventions of the *Système International d'Unités (SI)* und the *International Union For Pure And Applied Chemistry (IUPAC)*. Exceptions come about for units which are more convenient than the SI units, such as cm, g, or °C. The unit "litre" is denoted with a capital L according to an IUPAC recommendation.

Hyphens and dashes are employed according to common British usage[1] or common English usage for chemical expressions. In the X-ray structure discussion, directional but non-covalent interactions are indicated by dots, e.g. "C–H···π".

Nomenclature

Most of the macrocyclic substances presented herein possess a lengthy and complicated IUPAC nomenclature. On the other hand, the typical counting of molecules in their order of appearance usually forces the reader to check a reference table almost every times he turns a page. To provide a better clarity, this thesis uses a more descriptive and associative approach to name molecules:

When compounds from literature are cited, they are named after the corresponding author(s) of the cited publication together with a consecutive number (i.e. **<AuthorA>1**, **<AuthorA>2**, **<AuthorsB>1** and so forth), where different structures based on the same cyclic array are grouped, e.g. **<AuthorA>1a–d**.

Names for the macrocycles and precursors with direct relevance to this thesis are built up regarding their functional moieties. Oligothiophene blocks are abbreviated as ***n*T(R$_x$)**, where *n* is the number of α-connected thiophenes and R is the type of residue in the β positions (occurring *x* times in the oligothiophene). Typical functional groups in the α positions are iodide (I), acetylide (A) and trimethylsilylacetylide (TMSA). I.e., **A–3T(Bu$_4$)–A** is a terthiophene with four butyl chains at the β and two acetylide moieties at the remaining α positions. Cyclic molecules are indicated by a leading C, followed by the cyclic repeating unit in square brackets and the number of repeating units, e.g. **C[3T(Bu$_4$)–DA]$_4$** for the cyclic tetramer of the above precursor. Please note that for such cyclic compounds the ethynylene moieties are mentioned as "DA" (for "**di**acetylide") to point out that two units — coming from two different precursor molecules — are now connected and in conjugation. All-thiophene macrocycles, which so far only exist with butyl substitution, deviate from these rules and are named **C[*n*]T** (*n* is the number of thiophenes in the cyclic array).

List of abbreviations

abbreviation	explanation
6-31+G(d)	split-valence basis set with **6** primitive **G**aussians for the core orbital
A	**a**cetylide or ethynylene
A	**a**rea
Ac	**ac**etyl
Ar	**ar**yl
AM1	**A**ustin **m**odel **1** (semi-empirical quantum-chemical Hamiltonian)
a.u.	**a**rbitrary **u**nits
B3LYP	**B**ecke **3**-parameter hybrid functional combined with **L**ee–**Y**ang–**P**arr correlation functional
BINOL	2,2'-dihydroxy-1,1'-**bin**aphthyl
bipy	2,2'-**bipy**ridine
bpz	2,2'-**bip**yra**z**in
Bn	**be**n**z**yl
Bu	**bu**tyl
c	**c**oncentration
CD	**c**ircular **d**ichroism
Chiraphos	**chira**l 2*,3*-bis(diphenyl**phos**phino)butane
CI	**c**hemical **i**onisation
COD	**c**yclo**o**cta-1,5-**d**iene
CSI	**c**old-**s**pray **i**onisation
CV	**c**yclic **v**oltammetry or **c**yclic **v**oltammogram
Cy	**cy**clohexyl
DA	**d**i**a**cetylide; diethynylene
dba	(2,6-**d**imethyl**b**enzoyl)**a**cetic acid
DDQ	2,3-**d**icyano-5,6-**d**ichloro-parabenzo**q**uinone
depe	1,2-bis(**d**i**e**thyl**p**hosphino)**e**thane
DMSO	**d**i**m**ethyl **s**ulf**o**xide
DNA	**d**eoxyribo**n**ucleic **a**cid
Dodec	**dodec**yl
dpa	9,10-**d**i**p**henyl**a**nthracene
d(pGpG)	2'-deoxy**g**uanylyl(3'→5')-2'-deoxy**g**uanosine
dppe	1,2-bis(**d**i**p**henyl**p**hosphino)**e**thane
dppee	1,2-bis(**d**i**p**henyl**p**hosphino)**e**thyl**e**ne
dppf	1,1'-bis(**d**i**p**henyl**p**hosphino)**f**errocene
dppm	1,2-bis(**d**i**p**henyl**p**hosphino)**m**ethane
dppp	1,3-bis(**d**i**p**henyl**p**hosphino)**p**ropane
ε	**e**xtinction coefficient (= molar absorptivity)
ee	**e**nantiomeric **e**xcess
en	**e**thane-1,2-diami**n**e
ESI	**e**lectron-**s**pray **i**onisation
Et	**et**hyl
FAB	**f**ast **a**tom **b**ombardment
Fc/Fc$^+$	**f**erro**c**ene/ferrocenium
FCS	**f**luorescence **c**orrelation **s**pectroscopy

abbreviation	explanation
FT-ICR	**F**ourier-**t**ransform **i**on **c**yclotron **r**esonance
fu	**fu**ryl
GC	**g**as **c**hromatography
Hex	**hex**yl
HOMO	**h**ighest **o**ccupied **m**olecular **o**rbital
HOPG	**h**ighly **o**riented **p**yrolytic **g**raphite
HPLC	**h**igh-**p**erformance **l**iquid **c**hromatography
IR	**i**nfra**r**ed
isonic	**isonic**otinate
K_a	**a**ssociation **c**onstant
L	**l**igand
LUMO	**l**owest **u**noccupied **m**olecular **o**rbital
M	**m**olar (mol L^{-1})
MALDI (TOF)	**m**atrix-**a**ssisted **l**aser **d**esorption/**i**onisation (**t**ime-**o**f-**f**light)
MCH	**m**ethyl **c**yclo**h**exane
Me	**me**thyl
MeCN	acetonitrile
MLCT	**m**etal-to-**l**igand **c**harge **t**ransfer
MO	**m**olecular **o**rbital
MP2	**2**nd order **M**øller–**P**lesset theory
MS	**m**ass **s**pectrometry
NBS	***N*-b**romo**s**uccinimide
NIS	***N*-i**odo**s**uccinimide
NMR	**n**uclear **m**agnetic **r**esonance
***o*-; *m*-; *p*-**	*ortho*-; *meta*-; *para*-
OAc	**ac**etate
Oc	**oc**tyl
OLED(s)	**o**rganic **l**ight **e**mitting **d**iode(s)
OPiv	**piv**alate
OTf	**tri**flate (trifluoro methane sulphonate)
OTP	***o*-ter**phenyl
Ph	**ph**enyl
phen	1,10-**phen**anthrolin-2,9-diyl
Piv	**piv**alyl; 2,2-dimethylpropyl
PM3	**p**arametrised **m**odel **3** (reparameterised version of AM1)
PMMA	**p**oly**m**ethyl **m**eth**a**crylate; poly(methyl 2-methylpropenoate)
Pr	**pr**opyl
Py	**py**ridinyl
R	**r**esidue/substituent
rt	**r**oom **t**emperature
SCE	**s**tandard **c**alomel **e**lectrode
STM	**s**canning **t**unnelling **m**icroscopy
T	**t**hiophene
TBDMS	***tert*-b**utyl **d**i**m**ethyl**s**ilyl
***tert*-/*t*-**	**t**e**rt**iary
T_g	**g**lass transition **t**emperature

abbreviation	explanation
THF	**t**etra**h**ydro**f**urane
TLC	**t**hin **l**ayer **c**hromatography
TMSA	**t**ri**m**ethyl**s**ilyl**a**cetylene or **t**ri**m**ethyl**s**ilyl**a**cetylide
u	**u**racilate
UV/Vis	**u**ltra**v**iolet/**vis**ible light
X	halogen atom

1 Preface

1.1 Introduction to Oligothiophene Macrocycles

One of the major requirements for functional organic compounds in electronic devices is a π-electron system with good charge transport properties. Fully conjugated oligomers are well suited for such purposes, because their defined structure with regularly repeating units guarantees homogenuous conditions and is often the basis for the formation of self-assembling monolayers.[2,3] In this rapidly growing field, α-conjugated oligothiophenes of various length and substitution patterns (figure 1) have become a common workhorse whenever conducting or semiconducting properties are required. Their unique physicochemical characteristics, especially their electronic potentials and their stability in different redox states, turn them into ideal candidates for applications such as organic light emitting diodes (OLEDs), field-effect transistors or solar cells, and led to an extensive investigation on their synthesis and behaviour.[4,5] However, the electronic characteristics of conjugated oligomers are restricted by end-effects which limit the effective extension of the π system.

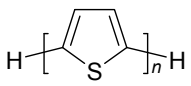

a) basic structure

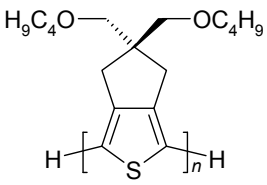

b) symmetrically β-substituted oligothiophene

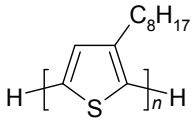

c) regioregular oligothiophene

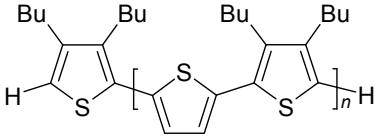

d) symmetric oligothiophene with oligomeric repeating unit

Figure 1: Examples for α-conjugated oligothiophenes

Only recently, the class of oligothiophenes was literally "rounded off" by the synthesis of cyclo[*n*]thiophenes (**C[*n*]T**) which represent the first fully α-conjugated oligothiophene macrocycles (figure 2).[6]

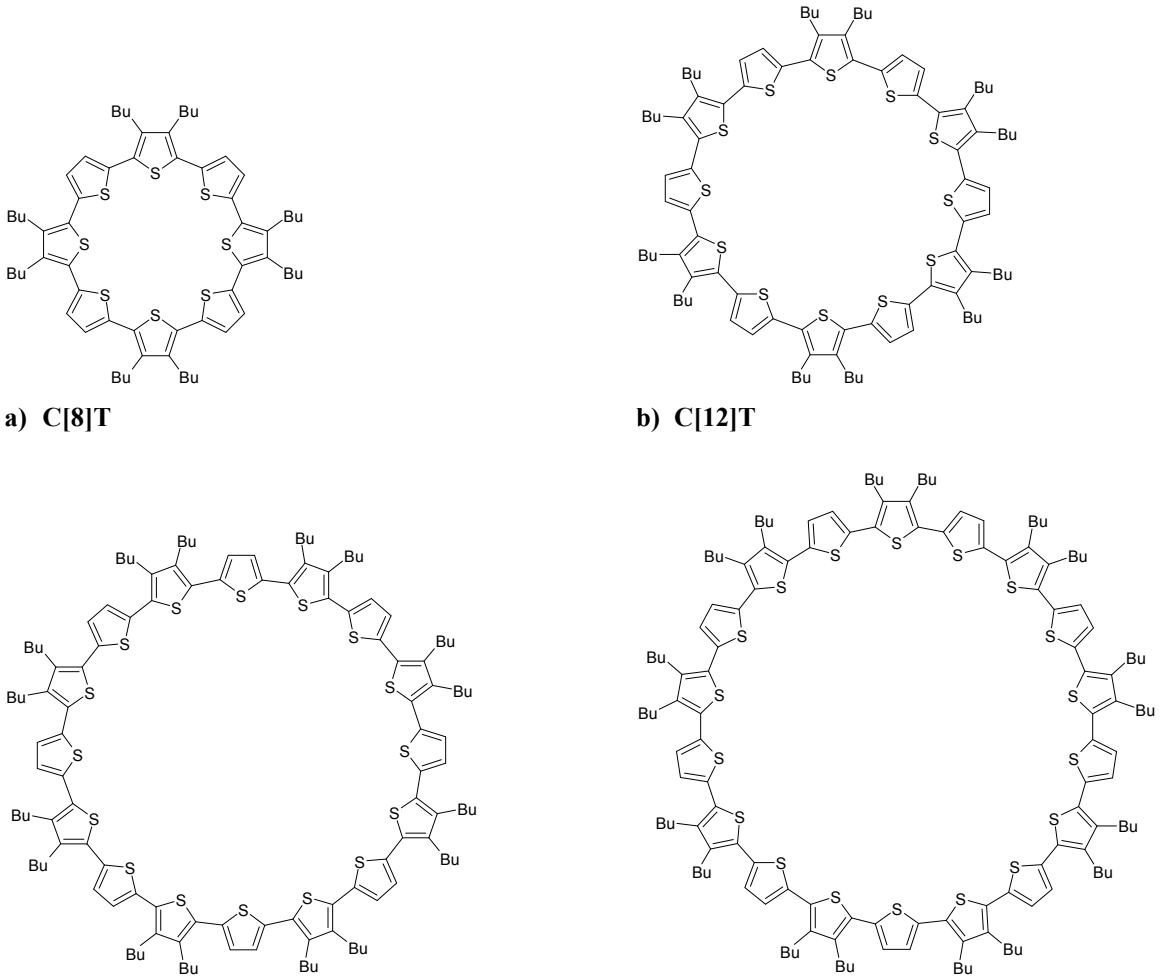

a) C[8]T **b) C[12]T**

c) C[16]T **d) C[18]T**

Figure 2: The family of cyclo[*n*]thiophenes (C[*n*]T)

This new class of materials extends the perspectives of their linear counterparts of a number of ways: First, they serve as model systems for an infinitely conjugated π-electronic chain, while at the same time they possess a much more rigid and defined structure. This corresponds to an idealised polymer without disturbing end-effects, what might lead to new electronic properties. Then, the macrocyclic cavity offers the possibility of selective inclusion of guest molecules. Such a host–guest interaction might even be triggered by the redox state of the conjugated macrocycle. Suited guest molecules, again, could possibly be used as templates to facilitate and speed up the synthesis of cyclo[*n*]thiophenes, leading to an enhanced applicability. In addition, the rather planar structure of the macrocycles allows self-organisation in two dimensions (as self-assembling monolayers) as well as in three dimensions (as "nanotubes"), with potential application in bio- and material science.

Unfortunately, the preparation of these materials still suffered from drawbacks like a rather low yield and, at the same time, statistically distributed ring sizes. Furthermore, little was known about their properties.

This thesis deals with synthetical and physicochemical aspects of oligothiophene macrocycles, and is set up on strongly interconnected cornerstones which are described in the following section.

1.2 Aims of this Thesis

1.2.1 Investigation of the Physicochemical Properties of Oligothiophene Macrocycles

The applicability of the molecules of interest mainly depends on their physicochemical properties, especially those related to the π-conjugated electron system. Therefore, the investigation of optical and electrochemical properties is a fundamental task and provides a basis for future work on these systems. Essentially, characterisation is possible by *UV/Vis spectroscopy*, *fluorescence emission spectroscopy*, and *cyclic voltammetry*.

1.2.2 Molecular Recognition of Guest Molecules

So far, quantum-chemical calculations had shown that the modelled cavity sizes are in perfect agreement with the structure parameters obtained by STM analysis of self-assembled monolayers. This provides the possibility of a theoretical evaluation of hypothetical guest molecules in terms of interaction with the macrocycles. Practical examination of these host–guest interactions can then be carried out by using the same methods of characterisation as mentioned in section 1.2.1.

Principally, the sulphur atom of thiophenes is a weak ligands for complexation, while the electron-rich nature of oligothiophenes should allow recognition of acceptor molecules like fullerenes or organic and inorganic cations. Even small metal clusters of transition metals, like Au or Ag, are conceivable as guests.

1.2.3 Template Synthesis of Oligothiophene Macrocycles

Depending on suited guest molecules with high affinities to the already existing macrocycles, a template synthesis could be designed, where precursors preorientate around the guest before being linked covalently to the macrocycle. Such a strategy would provide important advantages over the conventional “statistical” synthesis, namely higher yields and less byproducts.

2 Introduction: The "Metal-Template" Approach to Oligothiophene Macrocycles

2.1 Introduction to Shape-Persistent Macrocycles

Although cyclic oligomers like crown ethers have been known for a long time, an important impetus for large cyclic backbones was the rigidification by the use of sp- or sp^2-hybridised building blocks. So-called "shape-persistent macrocycles" mainly consist of aromatic units which are connected by one or more linear ethynylene units.[7–31] Examples for such macrocycles are shown in figure 3. Ethynylene units not only provide the desired electronic interactions, but also — in contrast to double bonds — do not alter the molecule's geometry upon rotation around an adjacent single bond. By variation of the aromatic units, functional groups with metal-binding capabilities like pyridine[16,17,18a], bipyridine[18c–d,19b,31b] or terpyridine[18b,19a] can be easily introduced. Apart from these, various other shape-persistent macrocycles with conjugated backbones are known, like zirconocene macrocycles[31], porphyrin-containing macrocycles[24], expanded porphyrins[22,23], cyclothiophenes[27] and cyclopyrroles[26]. The scientific interest in shape-persistent macrocycles is growing, because they provide a combination of unique features: They are non-collapsible, can form stable cavities with the ability to bind guest molecules[13a–c,18c–d,24a], have superior aggregation and self-assembling properties[9b,d,e,12,14b], and possess π-electronic systems that are of special interest for applications in electronic and photonic devices.

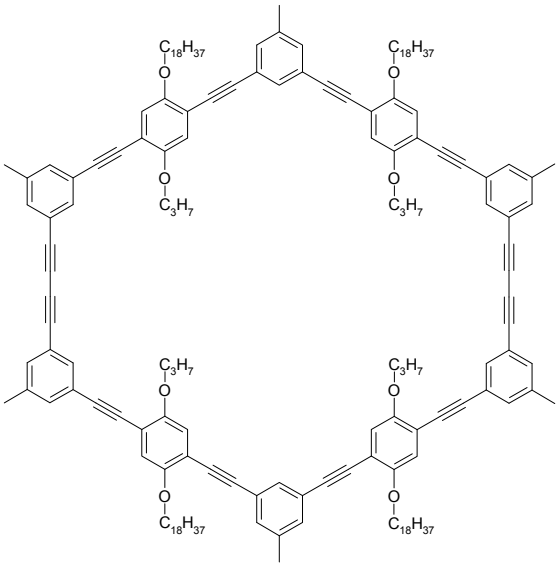

a) discotic macrocycle **Höger1** from *Höger et al.*[9f] (similar structures with diethynylene-bridged *m*-phenylene units are made, e.g., by *Tobe and coworkers*[11c,e])

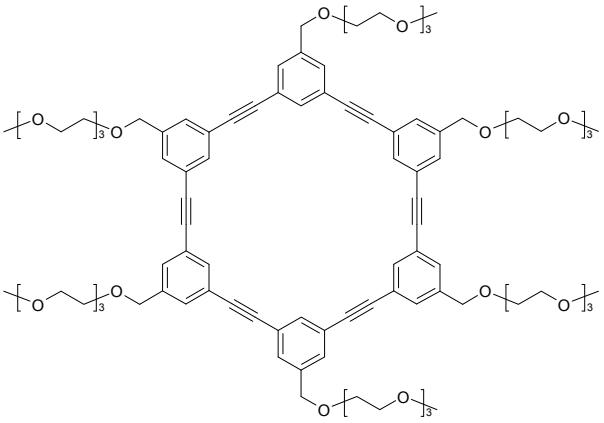

b) phenylene ethynylene macrocycle **Moore1** from *Moore and coworkers*[14b] (similar structures are made, e.g., by *Bunz and coworkers*[10])

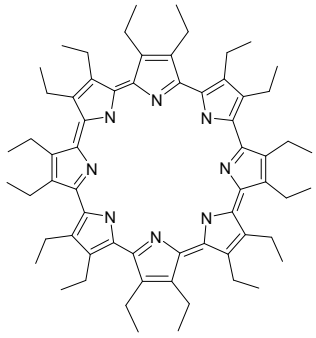

c) cyclopyrrole **Sessler1a** from *Sessler and coworkers*[26b] (cf. scheme 46 on page 179)

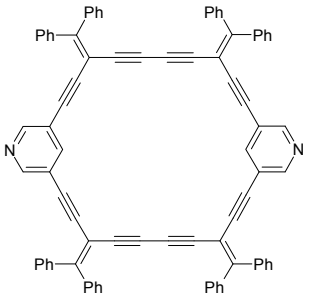

d) macrocycle **Tykwinski1** with endotopic binding sites from *Tykwinski and coworkers*[16b–d]

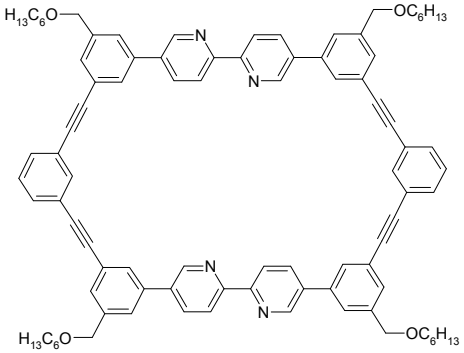

e) bipyridine macrocycle **Schlüter1** from *Schlüter and coworkers*[19b]
(similar strctures are made, e.g., by *Baxter*[18])

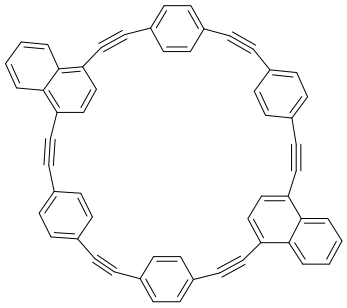

f) [6]paraphenyleneacetylene derivative **KawaseOda1** from *Kawase, Oda and coworkers*[13a,c]

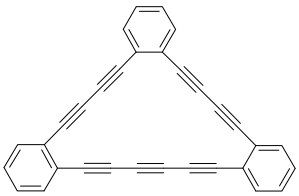

g) dehydrobenzo[20]annulene **Haley1** by *Haley et al.*[14a]

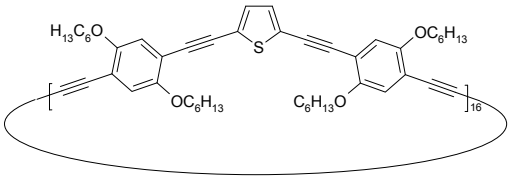

h) giant macrocycle **Mayor1** from *Mayor and coworkers*[30]

Figure 3: Examples for shape-persistent macrocycles with ethynylene units

The main disadvantages of most shape-persistent macrocycles are an interrupted conjugation by *meta*-branched aromatic corners (providing a 120° angle and leading preferredly to hexagons) and a small cavity in triangular structures with 60° *ortho*-branched benzene units. From the above-mentioned macrocycles with benzene units, only a few possess a fully conjugated cyclic structure, like the paracyclophane-type molecules of the groups of *Kawase and Oda*[13], *Ohkita and Tsuji*[15b] and *Tobe*[11d,f]. The use of five-ring heteroaromats with a native angle between the conjugated bonds at the 2- and 5-positions overcomes the geometric restrictions of conjugated benzene moieties and allows a cyclic array of a non-interrupted π system. This has been shown for *Mayor*'s giant ring[28],

Sessler's cyclopyrroles[26], and the oligothiophene macrocycles by the group of *Bäuerle*[27–29] which are described in detail in the following section.

With metal-catalysed reactions, like the commonly applied Glaser-type[32] and Sonogashira[33] coupling, or more exotic routes like alkyne metathesis[10] and aryl-aryl coupling[8,19c,d], effective methods for the ring closure are at hand. However, the assembly of macrocycles is more challenging than that of comparable linear oligomers: The latter can be built in a defined way when, i.e., at least one type of building block acts as a terminal moiety. In a cyclic array, no end groups exist, so it is necessary to provide *two* functional groups per monomeric unit, what can lead to unwanted byproducts like linear polymers or macrocycles of different sizes. In this respect, like for the platinum macrocycles presented in section 2.4, either preorientation or building blocks with a carefully adjusted geometry are major requirements for high yields of the desired macrocycle (figure 4).

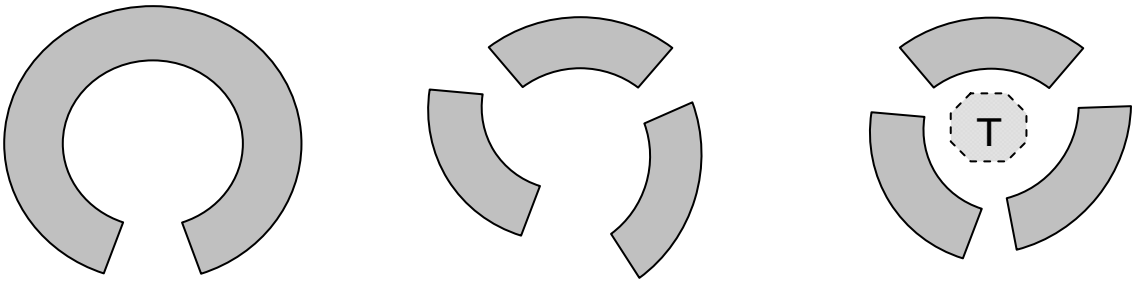

a) preorientation by "preforming" the macrocycle (intramolecular ring closure)

b) optimisation of the geometry of the building blocks

c) preorientation by the aid of a template (T = template)

Figure 4: Strategies for macrocyclisation

While preorientation (figure 4a) is the more reliable possibility, since in the final step only one int*ra*molecular bond between two close-by positions is necessary to close the ring, more steps are required to build up a longer oligomer and to attach the terminal functional groups. Meanwhile and with growing success, also optimised monomer building blocks (figure 4b) are subjected to direct macrocyclisations. Both methods have been widely used in literature for the synthesis of macrocycles.

2.2 Preparation of Oligothiophene Macrocycles by Glaser-Type Coupling

Since the direct approach to oligothiophene macrocycles by direct cross-coupling of oligothiophenes had not led to cyclic products, *Bäuerle et al.* instead successfully applied the copper-catalysed, Glaser-type alkinyl coupling to bis(ethynyl)-substituted oligothiophenes.[27e,f,28,29] Except for the very small macrocycle **C[8]T**, which was prepared by the new metal-template route (cf. section 2.3), a family of oligo(thienylene-diethynylene) macrocycles could be synthesised by this "statistical" kinetic coupling. In a final step, the diethynyl moieties were transformed into thiophene units by reaction with Na_2S, yielding the target cyclo[*n*]thiophenes.

As building blocks, butyl-substituted oligothiophenes of various lengths were employed. These compounds, in which all odd-numbered thiophene units carry butyl side-chains in the 3- and 4-position, had previously been prepared up to the 19mer.[28] Their symmetric substitution pattern with alkyl side chains had proven to be ideally suited for providing a sufficient solubility and avoiding regioisomers. The preparation of these macrocyclisation precursors is shown in scheme 1.

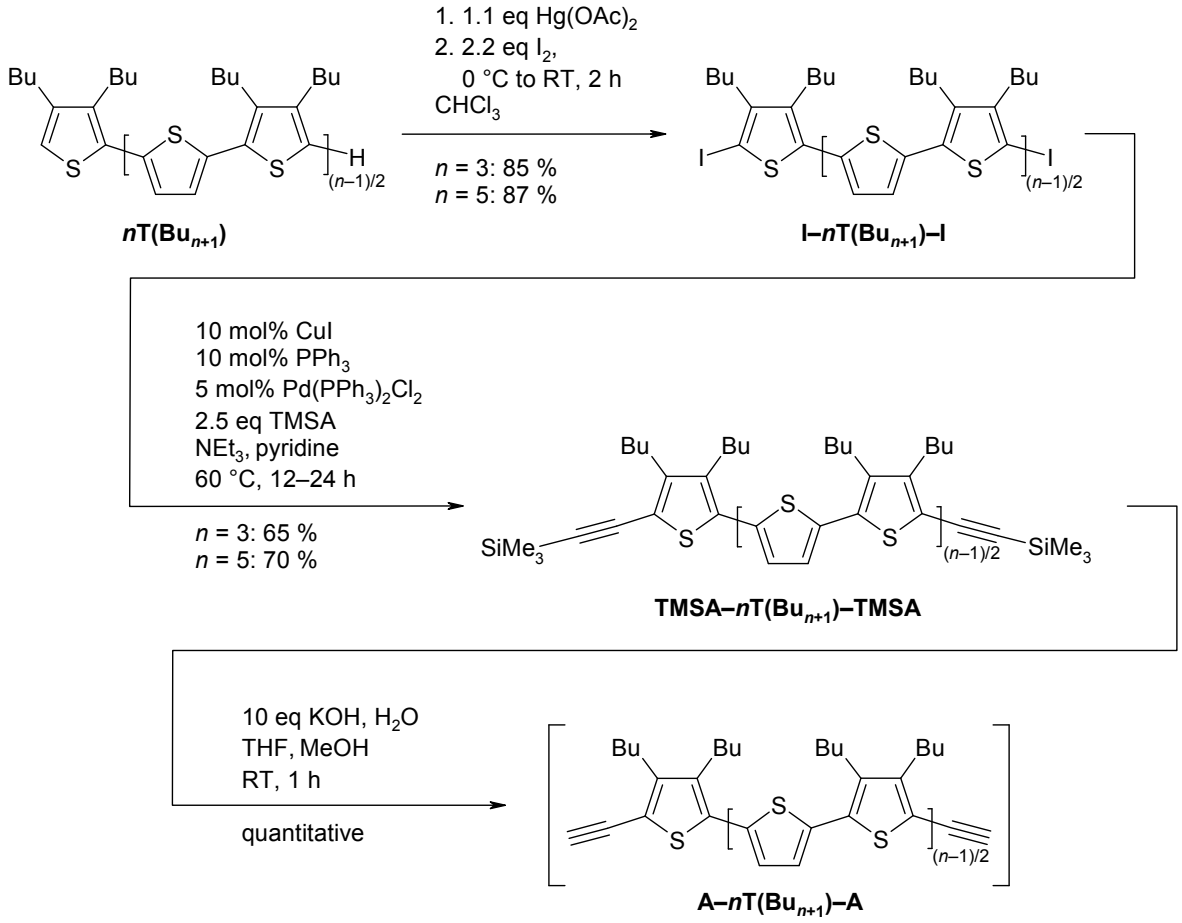

Scheme 1: Synthesis of butyl-substituted oligothienyl monomers for macrocyclisation

In a first step, the thiophenes ***n*T(Bu$_{n+1}$)** (n = 3, 5) were selectively diiodinated in the α positions by mercury(II) acetate and iodine, yielding **I–*n*T(Bu$_{n+1}$)–I** in 85–87 %. Terminal acetylenes were introduced by palladium-catalysed Sonogashira–Hagihara reaction with trimethylsilylacetylene (TMSA) in 69–76 % yield. The trimethylsilyl protection group not only facilitated the synthesis by avoiding the usage of acetylene gas, but also led to the stabilised intermediate products **TMSA–*n*T(Bu$_{n+1}$)–TMSA** in which unwanted side reactions of reactive free acetylide positions are prevented. The generally quantitative deprotection to **A–*n*T(Bu$_{n+1}$)–A** was achieved under mild basic conditions with KOH in a THF–methanol mixture, and the instable products were submitted in situ to the macrocyclisation reactions.

The optimal condition, which was evaluated by the application of Glaser[34], Eglinton[35] and Hay[36] conditions to 3,4-dibutyl-2,5-bisethynylthiophene, proved to be a modified pseudo-high-diluted Eglinton–Glaser coupling: Pyridine solutions of **A–*n*T(Bu$_{n+1}$)–A** were slowly added to a pyridine suspension of CuCl and $CuCl_2$ at room temperature by a syringe pump over a period of 3 d (scheme 2). Analysis of the crude product by ^{1}H NMR and MALDI TOF mass spectrometry clearly indicated the formation of cyclic products of different sizes, which could be separated by extensive preparative HPLC in 2–12 % yield, respectively. The detailed yields of the isolated **C[*n*T(Bu$_{n+1}$)–DA]$_m$** macrocycles are listed in table 1. Of **C[3T(Bu$_4$)–DA]$_4$**, crystals suited for X-ray crystallography could be obtained, and an analysis revealed the molecular structure as a rectangle with round edges. The maximum non-covalent S–S distance of 1.94 nm in the crystal correlates well with the calculated distance of 1.99 nm.[37]

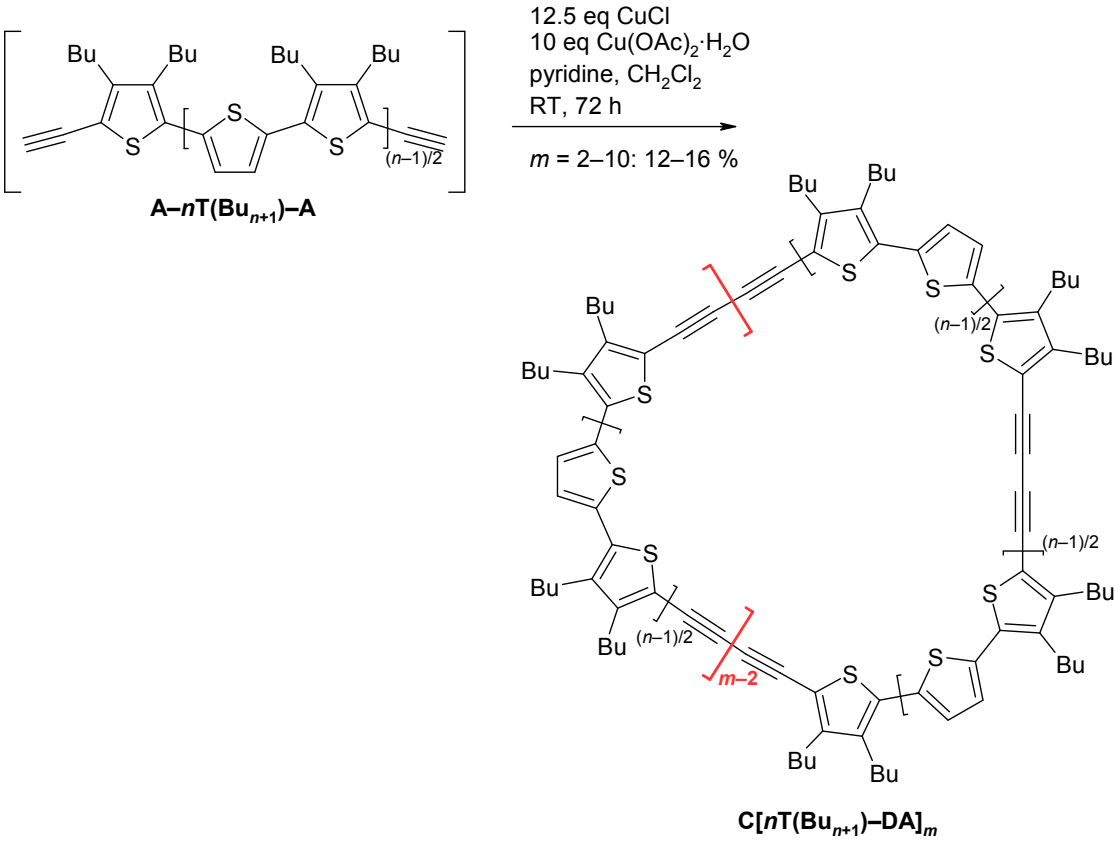

Scheme 2: **Synthesis of C[*n*T(Bu$_{n+1}$)–DA]$_m$ macrocycles by Eglinton–Glaser coupling**

number of monomer units [*m*]	yield of C[3T(Bu$_4$)–DA]$_m$ [%]	yield of C[5T(Bu$_6$)–DA]$_m$ [%]
2	0	3.0
3	2.6	8.8
4	4.0	1.5
5	1.4	0.2
6	0.5	< 0.1
7	0.2	0
8–10	< 0.1	0
all sizes	**8.7 (isolated); 12.7 (total)**	**13.5 (isolated); 16.0 (total)**

Table 1: **Yields of C[*n*T(Bu$_{n+1}$)–DA]$_m$ macrocycles prepared by Eglinton–Glaser coupling**

To improve yields and to gain control over the size of the produced macrocycle, an attempt was made for the int*ra*molecular cyclisation with an bisethynylene-undecithiophene (scheme 3). At an overall yield of ca. 50 %, the ratio of the cyclic monomer **C[11T(Bu$_{12}$)–DA]** and the dimer **C[11T(Bu$_{12}$)–DA]$_2$** could be adjusted by changing the reaction conditions: The intramolecular cyclisation is favoured by a higher dilution of ca. 10^{-4} mol L^{-1} and a high reaction temperature of 90 °C. Although in this case only the cyclic monomer and the cyclic dimer could be isolated in

improved yields, the overall yield starting from thiophene did not significantly exceed those for the shorter monomers, due to the increased number of reaction steps for obtaining the undecithiophene.

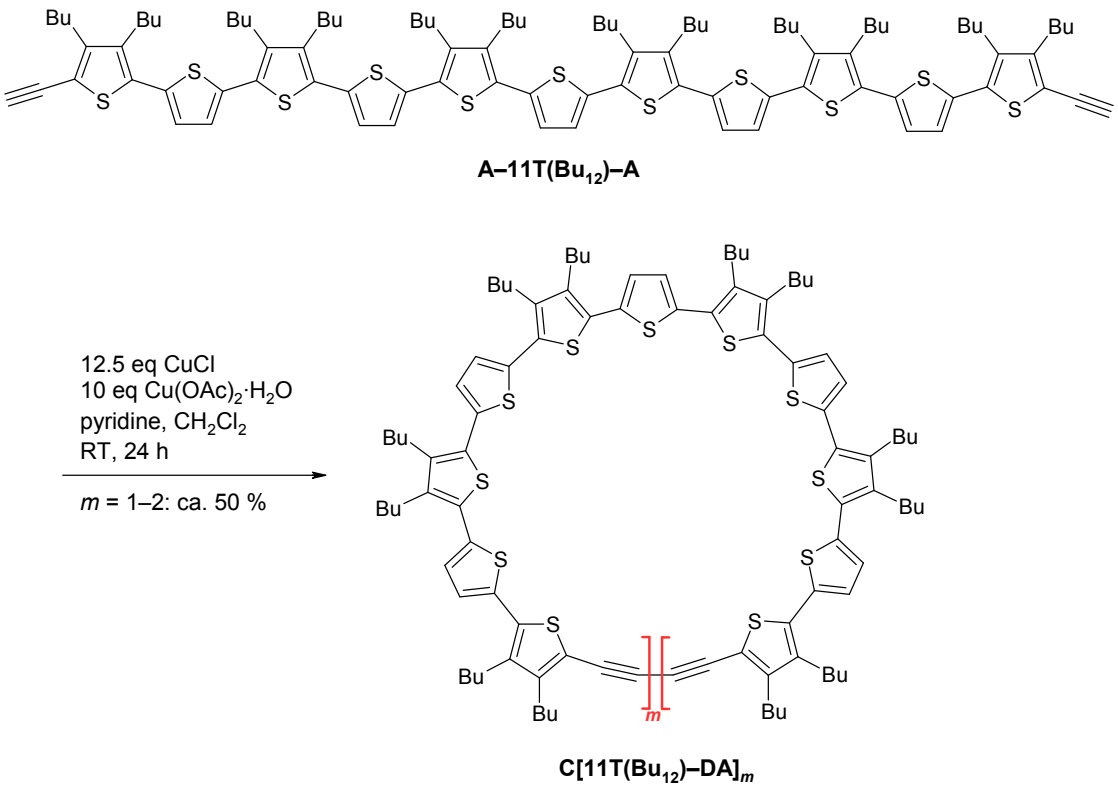

Scheme 3: Synthesis of C[11T(Bu$_{12}$)–DA]$_m$ macrocycles by Glaser-type coupling

From the initial bisethynyl-oligothienyl products, the cycles **C[3T(Bu$_4$)–DA]$_3$**, **C[3T(Bu$_4$)–DA]$_4$**, and **C[5T(Bu$_6$)–DA]$_3$** were finally available in amounts that allowed the synthesis of all-thienyl macrocycles by cyclisation of the diethynyl moieties with Na_2S (scheme 4). Due to the sterical hindrance of the butyl side chains, the reaction opted for relatively high temperatures and was carried out in a refluxing mixture of 2-methoxyethanol and *p*-xylene. The transformation yields of 52–64 % per cyclisation step, which are in agreement with comparable linear compounds,[28] resulted in 7–27 % yield of the macrocycles **C[12]T**, **C[16]T** and **C[18]T**, respectively, as stable, yellow to red microcrystalline solids that are well soluble in common organic solvents. A deeper insight into the structure was obtained by STM investigations: On highly oriented pyrolytic graphite (HOPG), the macrocycles formed self-assembled monolayers with a hexagonal environment for each molecule.[27d,f] The submolecular resolution could be perfectly correlated with a molecular model of the macrocycles, where the interdigitating alkyl side chains point downward to the HOPG substrate.

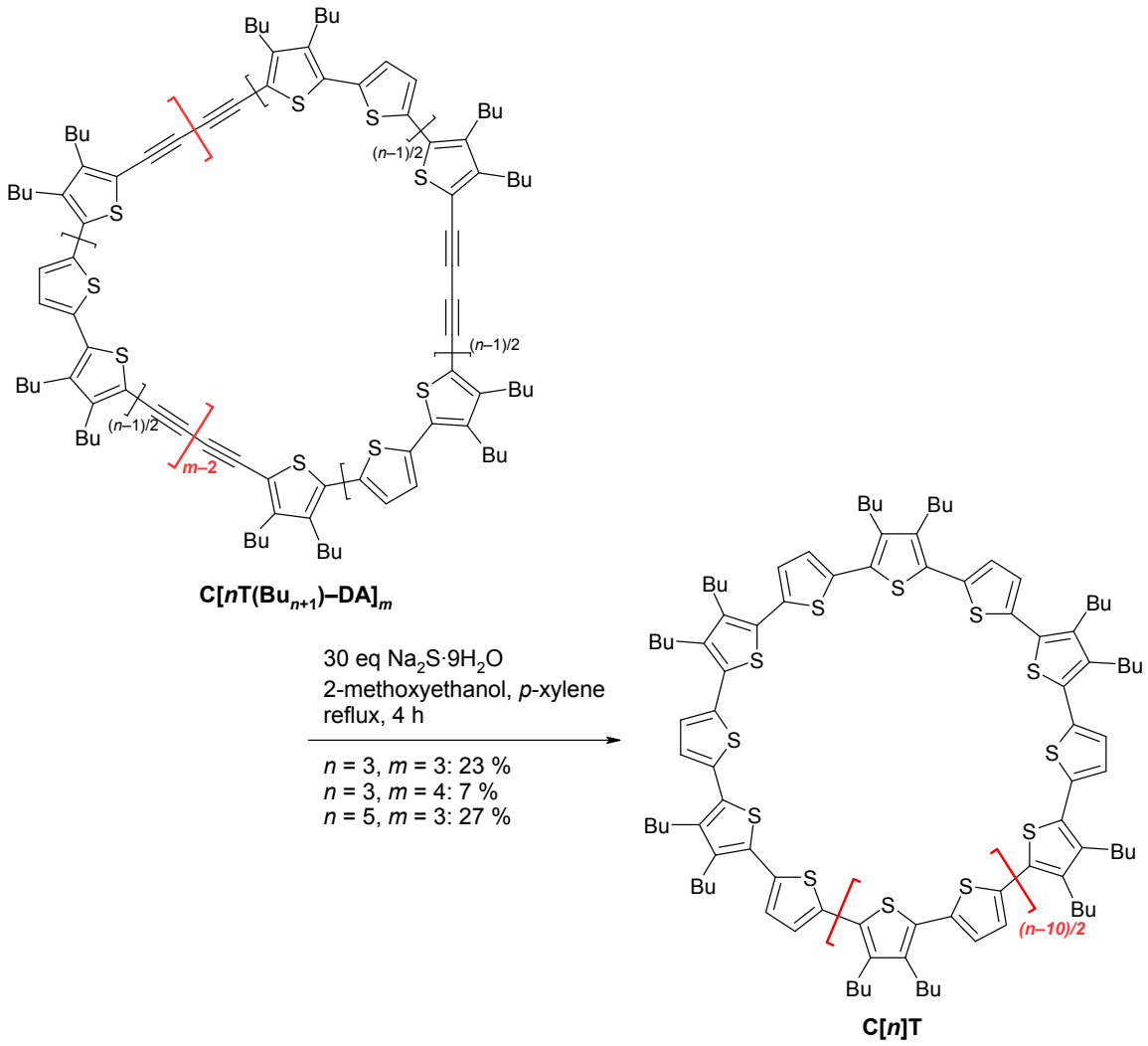

Scheme 4: Transformation of the diethynylene moieties of the macrocycles into thiophene units

2.3 The Metal-Template Route as a Combination of Synthetic Strategies

Although a whole mixture of interesting macrocyclic products are available by the Glaser-type route, this is at the same time its main disadvantage: Control over the macrocycle size is not possible; separation of the mixture is tedious and not practicable if a large-scale synthesis is required. Furthermore, the main products are cyclic trimers and tetramers, whereas the smaller dimeric macrocycles could only be seen in traces.

To overcome these problems and to reduce the product manifold to one defined (small) cycle, some kind of preorganisation is needed that relieves the strain of the diethynyl moieties. The solution was found in a combination of a template synthesis, where acyclic units are arranged around a reversibly bound template that later on is removed, and a transition-metal catalysed alkynyl homocoupling: Instead of using the typical conditions which require palladium(II) in catalytic amounts together with CuI, triethylamine and an oxidant like chloroacetone or iodine,[38] the catalytic cycle (scheme 5)[39] can be stopped at the indicated position of the proposed reaction scheme by avoiding the presence of oxidants and by usage of a *cis*-platinum complex in equimolar amounts.

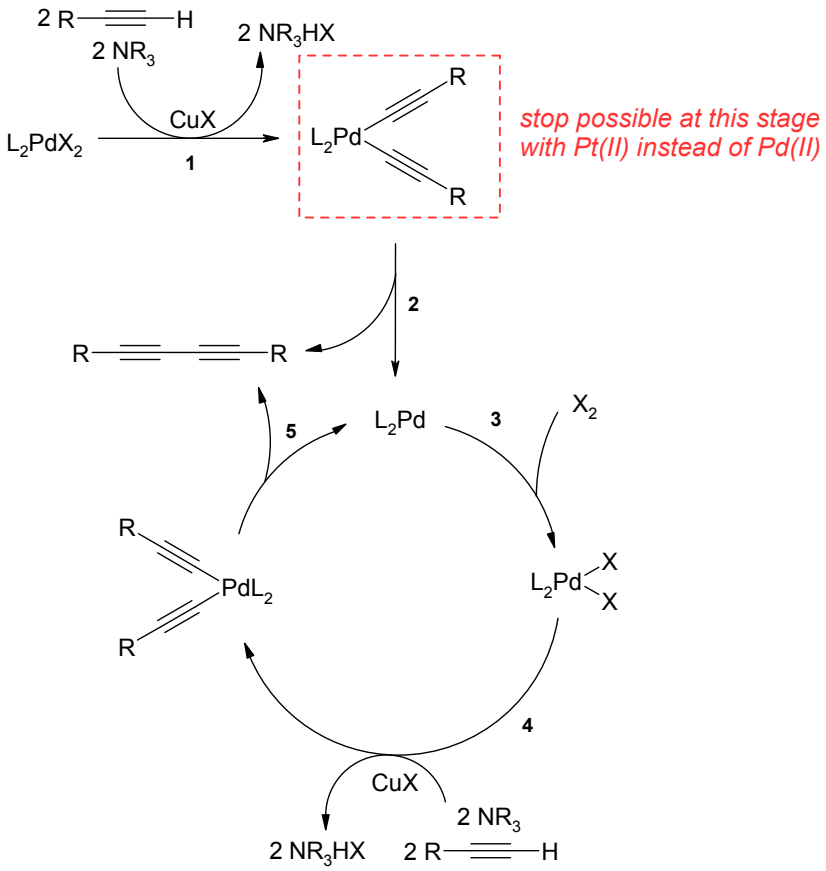

Scheme 5: Proposed reaction scheme for the palladium-catalysed oxidative homocoupling of alkynes

The advantages of the resulting platina-macrocycles are their increased stability compared with their palladium counterparts (cf. section 2.4) and the decrease of the product's ethynyl–ethynyl angle from 180° (obtained by a Glaser-type coupling) to 90°, which strongly favours the self-assembly to a dimeric metalla-macrocycle. Hence, the reaction of **A–3T(Bu$_4$)–A** with *cis*-Pt(dppp)Cl$_2$ in presence of 10 mol% CuI and two equivalents of triethylamine in toluene gave **C[Pt–A–3T(Bu$_4$)–A]$_2$** in more than 90 % yield (scheme 6).[27a,b,29]

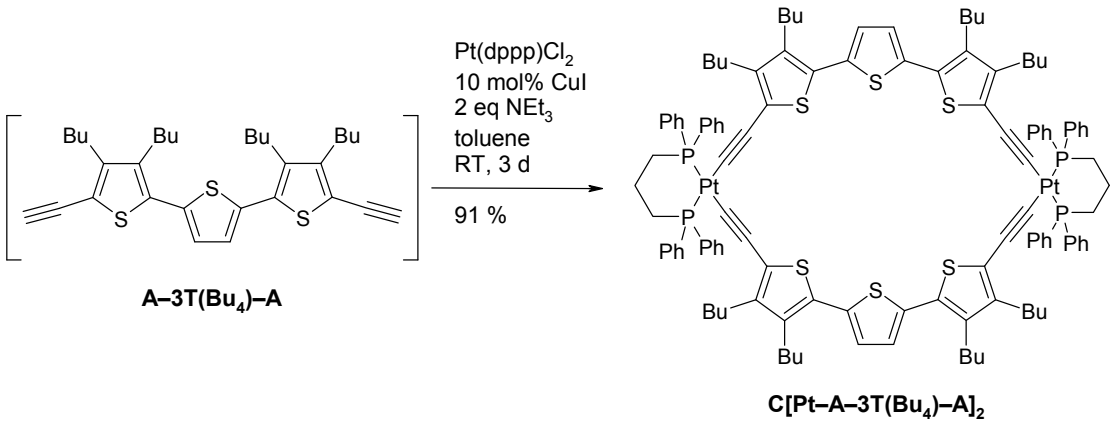

Scheme 6: Synthesis of platina-macrocycle C[Pt–A–3T(Bu$_4$)–A]$_2$

Thus preoriented, the Pt(II) template could be removed by oxidatively induced reductive 1,1-elimination to complete the catalytic cycle (step 5 of scheme 5): After addition of two equivalents of iodine (one per Pt corner) to a THF suspension of **C[Pt–A–3T(Bu$_4$)–A]$_2$** and stirring at 60 °C for 24 h, the fully conjugated macrocycle **C[3T(Bu$_4$)–DA]$_2$** was obtained selectively in 54 % yield and further transformed to **C[8]T** in 19 % yield by cyclisation with 10 eq of sodium sulfide per reaction site (scheme 7). In comparison to the larger homologues the yield of thiophene formation is only modest, which might be due to the ring strain and the steric shielding of the small cavity on one hand, and due to the high reaction temperature of 140 °C on the other hand.

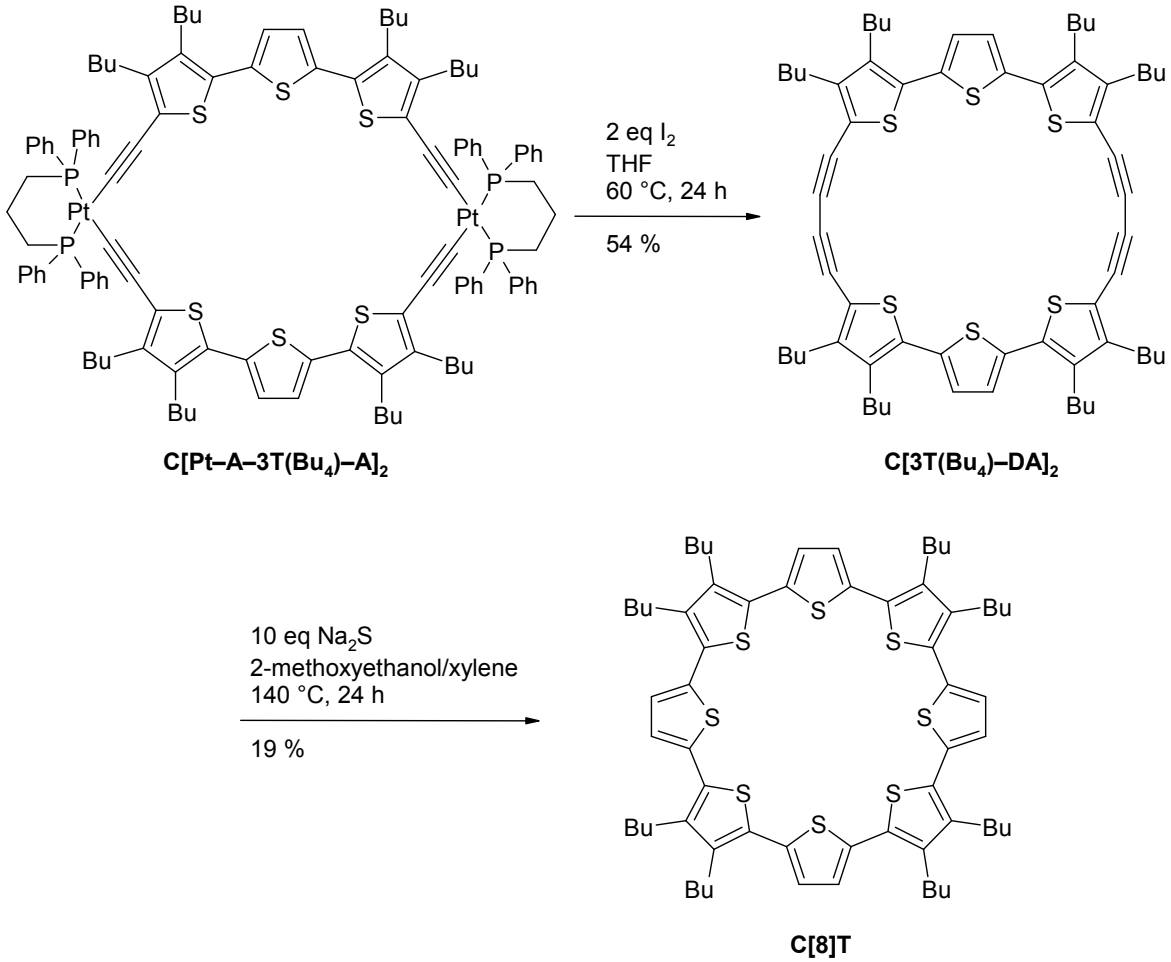

Scheme 7: Synthesis of the smallest oligothiophene macrocycle C[8]T from C[3T(Bu$_4$)–DA]$_2$

The reductive elimination, however, still remains a crucial step in the synthesis and needs to be improved so that it can be transferred to other oligothiophene macrocycles. It seems to be strongly influenced by factors like the solubility of the macrocycle, the oxidant and the substitution pattern of the thiophene rings in proximity to the Pt(II) centres. Although literature reported a promotion of reductive elimination from Pt(II) complexes by ferrocenyl groups, a study of various chelating ligands with different bite angles at the metal centre, in combination with different substitution patterns at the oligothiophenes, showed no correlation of ligand type and elimination behaviour. An improvement might be achieved by the use of electrochemical methods (cf. section 5.4):[29] After determination of the first irreversible oxidation potential by cyclic voltammetry, electrosynthesis of **C[3T(Bu$_4$)–DA]$_2$** from **C[Pt–A–3T(Bu$_4$)–A]$_2$** was carried out by application of a slightly higher voltage for several hours. The dimeric macrocycle **C[3T(Bu$_4$)–DA]$_2$** was selectively formed as the only product; nevertheless the separation of the product from the supporting electrolyte is a problematic issue.

2.4 Survey of Macrocycles Comprising Pt(II) Building Blocks

2.4.1 Usage of Pt(II) Units as Supramolecular Building Blocks

Supramolecular chemistry is of growing interest, as especially self-organisation is seen as an important way to highly functional and complex systems. In particular, chemists are increasingly fascinated by large rings, molecular polygons or more complex 3D structures, formed by supramolecular self-assembly processes. Complicated structures, which some years ago one only could dream of, can now be built from suitable precursors in one step. Recent reviews are available dealing with various aspects of this topic, such as supramolecular 2D and 3D coordination chemistry[40–46], structural and conformational control of functions[47], or the role of guest molecules interacting with supramolecular host systems[48,49], as well as for special metal-free macrocyclic systems[7].

Many examples of metalla-macrocycles rely on Pd(II) coordination chemistry as the key element. During the last decade, however, the number of interesting macrocyclic structures built with corresponding Pt(II) units has steadily increased. Since no specialised review on this most modern topic of increasing importance had been available so far, this section presents an overview and describes the up-to-date status until the first half of 2004 on self-assembled metalla-macrocycles comprising Pt(II) units as the coordinating building blocks.[50]

At first glance, the trend to use Pt(II) as crucial building block seems not quite reasonable, since platinum chemicals are rather expensive and the low solubility or product mixtures often cause experimental problems. The reason for this contradiction is given by the unique properties of Pt(II) complexes.

As a late d^{10} transition metal, the element platinum comprising *5d*, *6s* and *6p* orbitals prefers a 16-electron valence shell rather than an 18-electron configuration. Consequently, the most important oxidation state of Pt is Pt(II), having a d^8 valence electron configuration that fully contributes to Pt(II) complexes. The remaining eight electrons come from four ligands around the central metal to form Pt(II)L_4 complexes.

A square planar coordination is energetically more favourable than a tetrahedral coordination due to the splitting of the originally degenerated metal *d* orbitals, as shown in scheme 8a. Scheme 8b depicts a more detailed MO scheme for such a square planar d^8 complex, reflecting the symmetrically allowed valence orbital interactions. In this case, the 16 electrons occupy the

energetically lowest lying bonding and non-bonding orbitals, while the anti-bonding orbitals remain unoccupied.

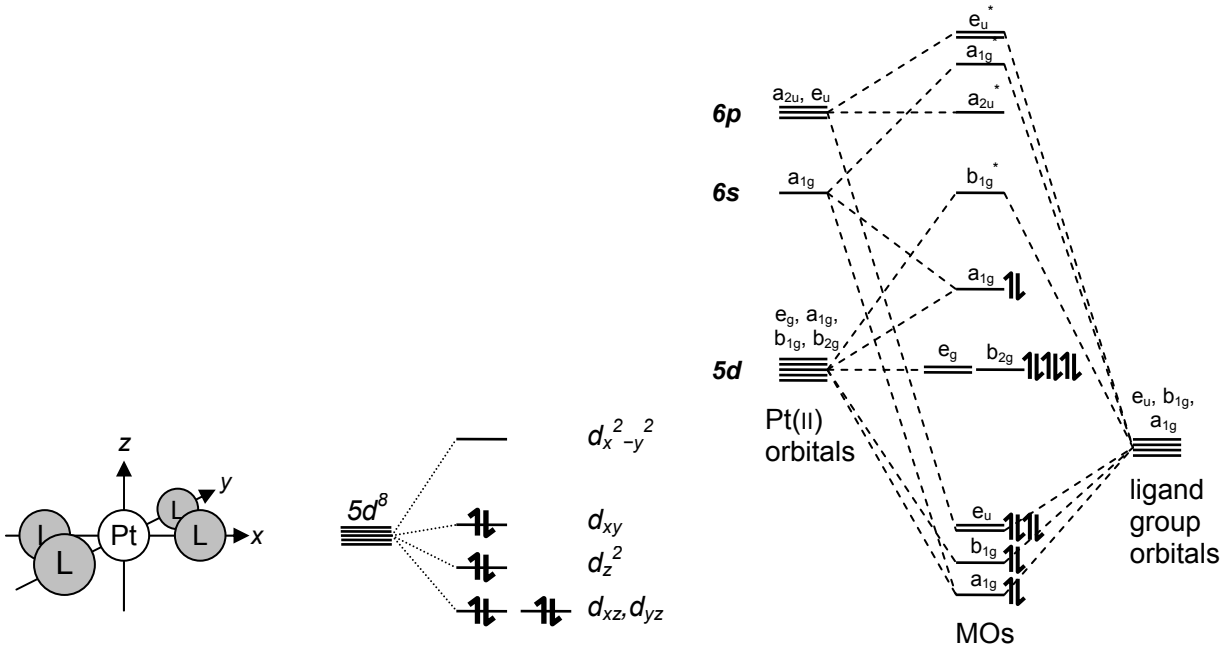

a) splitting of the *d* orbital levels due to the influence of the ligand electrons

b) MO scheme of the metal and ligand valence orbitals, considering symmetry-allowed interactions

Scheme 8: Qualitative picture of the orbital levels in square planar Pt(II) complexes

The main attractivity and value for the use of Pt(II) units in supramolecular chemistry comes from their inherent stability and rather low reactivity in the final complex. The geometry aspect adds to these advantages and opens up structural variations: Square planar Pt(II) complexes can either act as important 90° building blocks, i.e. as corner elements for the construction of molecular squares when the bridging ligands are *cis*-connected to the Pt(II) atoms, or as 180° linear spacers having a *trans*-Pt(II) arrangement. When macrocycles comprise a *cis*-arranged Pt(II) unit, the so-called bite angle can be fine-tuned to a certain extent by the use of different chelating ligands. Ligand variation at the metal is a valuable factor in general, since additional modification of the resulting macrocyclic structure becomes possible.

Recently, host–guest chemistry has become an important topic in the field of macrocycles. In particular, multiply charged platina-macrocycles are the result of incorporation of Pt–N coordinated moieties. This leads to enhanced solubility in polar or protic organic solvents, and furthermore provides ionic interactions for the inclusion of anionic guest molecules.

Another major interest in the implementation of Pt(II) into large cyclic structures is the expectation of special physical and materials properties, such as non-linear optical effects. The *d* orbitals of the

metal often give important contributions to the MOs of the whole macrocyclic system. This may lead to a polarisation of the excited state, which in particular provides hyperpolarisability as a basic requirement for non-linear optics.

2.4.2 Strategic Choice of Building Blocks for Pt(II) Macrocycles

For the preparation of Pt(II) macrocycles several considerations have to be made concerning the building blocks and the reaction conditions. This section will give a brief introduction to the choice of appropriate building blocks, while the following sections 2.4.3 and 2.4.4 treat the reaction conditions in order to successfully prepare these compounds and the characterisation of the products.

Of course, the synthesis of Pt(II) macrocycles always involves a suitable Pt(II) precursor complex. Already at this point, questions concerning the type of ligands and the configuration of the resulting complex have to be addressed. Typically, the configuration (*cis*/*trans*) at the metal centre is retained during reactions, and from these the *trans* configuration is the more stable one. In several cases *cis*-to-*trans* isomerisations have been reported (e.g. structure **Bosch1**[51] on page 63), while the reverse way is more difficult to achieve[52]. To ensure the retention of a desired *cis* configuration in the resulting macrocycle, chelating ligands such as 1,2-bis(diphenylphosphino)ethane (dppe), 1,1'-bis(diphenylphosphino)ferrocene (dppf), 1,3-bis(diphenylphosphino)propane (dppp), or ethane-1,2-diamine (en) may be used. With such bidentate ligands, the bite angle at the Pt centre may be fine tuned: a larger bridge in the chelating ligand ensures an increased bite angle, but at the same time the disadvantage of steric hindrance might arise.

As leaving groups in the Pt(II) precursor complexes, weakly bound ligands such as cycloocta-1,5-diene (COD), halogenides (X^-), triflate (OTf^-), or nitrate (NO_3^-) are quite useful. When these leaving groups act as counter anions for the resulting charged Pt(II) macrocycles, and this is in particular true for NO_3^-, they might have an important impact on the stability of the macrocyclic complex. Furthermore, they may influence the dynamic equilibria that sometimes come into play.

In most cases, the macrocycles are intentionally prepared by a directional bonding method: the "binding vectors" (representing the directions of the coordination bonds to which the difunctional ligand and metal precursors are capable) form angles that can be assigned to geometric structures and polygons. As already pointed out in the previous section, Pt(II) can thereby act as a 90° (*cis*) or 180° (*trans*) building block, which directly results in basic frameworks of cyclic tri- and tetranuclear Pt(II) complexes (scheme 9). The combination of Pt(II) with ligands of different bite

angles may result in a variety of geometric structures and molecular polygons, some of which are depicted in scheme 10.[45b,c]

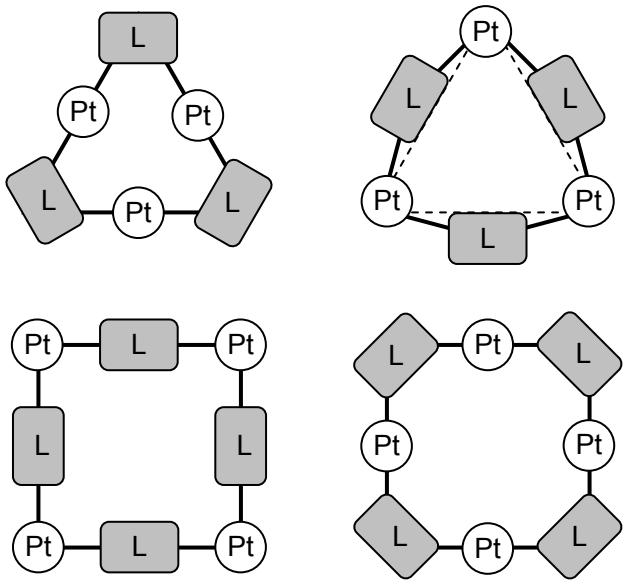

Scheme 9: **Possible approaches to molecular coordination triangles and squares** (L = bridging ligand)

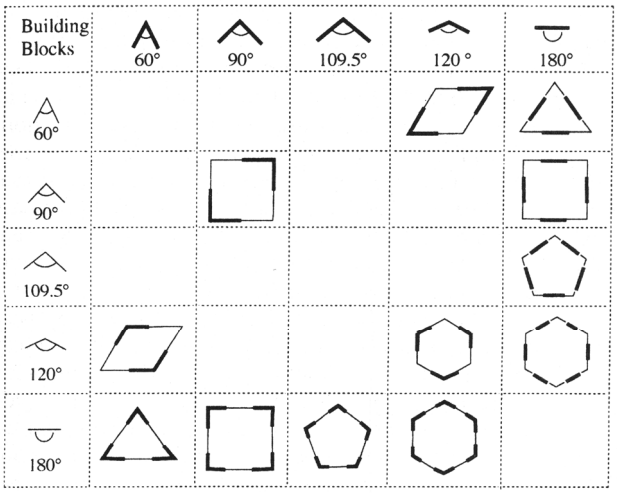

Scheme 10: **Selective formation of different geometric structures by appropriate choice of corner and bridging units**[45b,c]

Typically, these frameworks are formed by self-assembly processes. If this strategy is not applicable, which is mostly the case for the preparation of mixed metal macrocycles, the following general strategies depicted in scheme 11 might be used for the construction of corresponding coordination macrocycles.

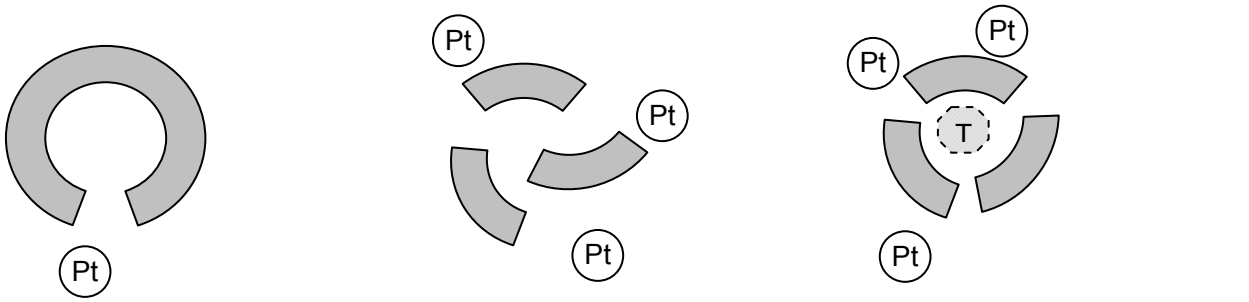

a) "preformed" macrocycle **b)** self-assembly **c)** template synthesis (T = template)

Scheme 11: Strategies for the synthesis of coordination macrocycles

Preformed cycles: The macrocycle is already preformed to a certain extent and intramolecular ring closure is the crucial step. In order to allow efficient ring-closure reactions, a configuration or conformation of the precursor is needed in which the end-groups (that are to be connected) come into close proximity to each other. This method probably gives the best control over product formation.

Self-assembly: Rather rigid bifunctional building blocks and Pt(II) precursors with predefined geometry (size and angles) are reacted in a specific stoichiometry to form the macrocycle. Typically, a mixture of various ring sizes and number of metal centres should be expected as well as linear oligomers or polymers. Therefore, well-defined and optimised geometries of the building blocks are necessary so that finally the multi-component system can self-organise into distinct structures. Thermodynamically, the cyclic structures are in almost all cases the most stable compounds. If the Pt–ligand bond formation is reversible, which is usually true for Pt–N bonds, long reaction times and heating are favourable for macrocycle formation. Entropy usually yields smaller ring sizes, hence, strained macrocycles become available with this method.

Template synthesis: The addition of a template leads to a preorganisation of one component around the template due to hydrophobic or ionic interactions. Efficient formation of the macrocyclic product is then obtained by connecting these prearranged moieties with the second component. Finally, the template is removed to yield the desired macrocycles. The template approach is especially important and useful for the formation of complex 3D structures.

2.4.3 Choice of Reaction Conditions

Although the reactions work at room temperature for most Pt–N and Pt–P complexes, heating might be necessary to drive the equilibrium from kinetically formed linear oligomers to thermodynamically favoured macrocyclic products. This reaction control can be applied in particular to Pt–N coordinated compounds, where the Pt–N bond is stable at room temperature but becomes labile when heated up to about 100 °C. Typically, the metalla-macrocycle is formed as a multiply charged salt that precipitates from aqueous or non-polar organic solvents, shifting the equilibrium towards the macrocyclic products.

In contrast to Pt–N and Pt–P coordination chemistry, Pt–C bond formation is not reversible. Here, the macrocyclisation is kinetically controlled and does not need a long reaction time. In the case of acetylide ligands, the precursors are rather instable and are therefore generated in situ from trialkylsilyl-protected reactands. Pt(II)–acetylide complex formation can then be achieved by using copper(I) iodide as a catalyst.[53]

2.4.4 Characterisation of Pt(II) Macrocycles

Characterisation and structure elucidation of Pt(II) systems can be best done by NMR, IR and mass spectrometry methods. In most Pt(II)-based systems phosphorus-containing ligands are involved. Therefore, ^{31}P NMR is (besides other NMR methods) an excellent tool. The position of the phosphorus signal represents a good indication for the environment, i.e. the geometry at the Pt centre.

Further characterisation of Pt(II)-macrocyclic systems is often provided by IR spectroscopy. Especially in the case of Pt(II)–acetylide complexes, characteristic bands for the C≡C triple bond are found .

The complicated structures are typically well supported by mass spectrometry using fast atom bombardment (FAB) as ionisation method.[54] For more labile compounds, which may decompose even under mild ionisation conditions such as FAB, matrix-assisted laser desorption/ionisation (MALDI) or electron-spray ionisation (ESI) can be used. *Yamaguchi, Fujita et al.* developed cold-spray ionisation (CSI) mass spectrometry as a modification of ESI at low temperatures[55], whereas *Schalley, Lützen et al.* successfully utilised advanced Fourier-transform ion cyclotron resonance mass spectrometry (FT-ICR MS) for high-resolution measurements[56].

2.4.5 Criteria for the Division of Different Structures

The following sorting criteria for the numerous Pt(II) macrocycles can be used:

Geometry of the macrocycle: The large group of molecular squares and triangles is frequently the topic of reviews on coordination-driven self-assembly. However, some macrocycles that are not shape-persistent cannot be accounted to a specific geometry. Furthermore, in several cases equilibria between two different geometries are observed.

Configuration of the Pt moiety: Either *cis* or *trans* configurations of the bridging ligands are possible at the Pt(II) centres. Since some macrocycles include both *cis*- and *trans*-arranged Pt units within the same molecule, this criterion is not well suited.

Synthetic strategy: As presented in section 2.4.2, there are different approaches for the construction of Pt(II) macrocycles. Because they all may lead to very similar structures, a good comparison is not possible.

Properties of the macrocycles: Some of the macrocycles presented in this review have been investigated in terms of their chemical and physical behaviour, such as host–guest chemistry, subsequent modification, chirality or non-linear optical properties. A satisfying comparison might be difficult because large differences in these properties might arise from only small structural modifications.

Coordination type of the bridging ligand: Typically, the bridging ligands such as N-hetarenes, phosphines or acetylides are bound to the metal centre by Pt–N, Pt–P or Pt–C coordination, respectively. This aspect is often congruent with the synthetic strategy for the preparation of Pt(II) macrocycles. Since only few exceptions exist in which several binding modes are operative in one molecule, the coordination type of the bridging ligands to the Pt(II) centre was chosen as the main criterion to divide the cited examples into the corresponding sections 2.4.6 to 2.4.13. Within these sections the members were grouped according to their geometry.

2.4.6 Macrocycles with Pt–N Coordination Containing Nucleobases

Coordination of heteroaromatic nitrogen ligands to Pt(II) is the key to many synthetic Pt(II) macrocycles, including the first examples inspired by biochemical research in the 1980s. The biological importance of the anticancer drug "Cis-platin" led to detailed studies on the binding modes of Pt compounds to nucleobases, resulting in various macrocyclic structures.

As an example, in the 1970s *Lock et al.* reported a cyclic dimer formed from *cis*-$Pt(NH_3)_2Cl_2$ and 1-methylthymine, in which the nucleobase binds to the Pt(II) moieties by nitrogen and oxygen atoms.[57] Further reports on similar structures followed, e.g. by *Lippert et al.*[58] or *Fanchiang*[59]. As these complexes might rather be considered "macrochelates" than "macrocycles", their structures are not shown here. Meanwhile, the investigation of Pt insertion into DNA fragments has developed into an important field of research on its own. On the following pages, some representative examples will be described; a complete survey would go far beyond the scope of this section.

In 1985, *Lippard and coworkers* presented the first X-ray structure analysis of platina-macrocycle **Lippard1**, which is assembled from $\{Pt(NH_3)_2\}^{2+}$ and the DNA intrastrand $d(pGpG)^{2-}$. The Pt(II) centre here is surrounded by four nitrogen ligands: two ammonia and two guanosine moieties, the latter being linked by a phosphate unit (figure 5).[60]

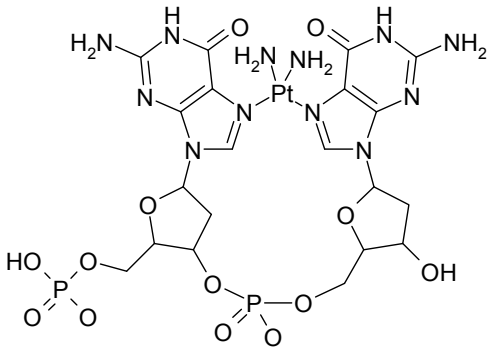

Figure 5: Macrocycle Lippard1

Longato and coworkers reported in 1995 the impressive hexaplatina-macrocycle **Longato1**, which readily self-assembles in D_2O from six 9-methylguanine and six $Pt(PMe_3)_2(NO_3)_2$ precursor molecules (figure 6).[61a] The structure was confirmed by X-ray structure analysis and shows an S_3-symmetric compound, in which the bridging guanine units are alternately located below and above the ring plane of the six Pt(II) centres.

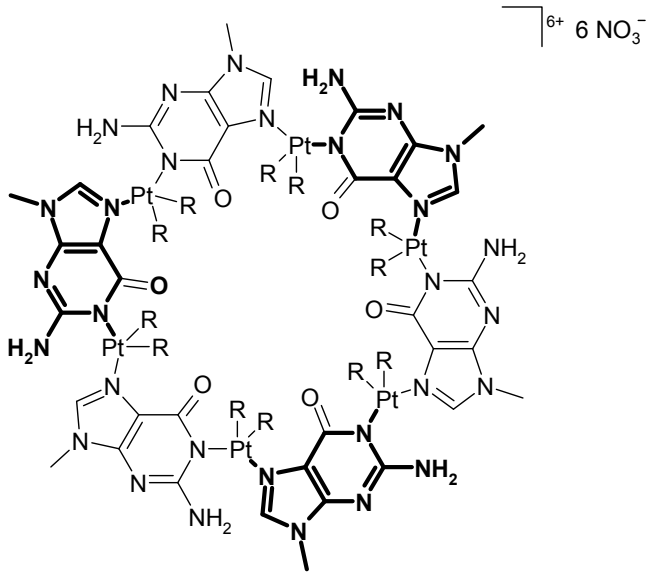

Figure 6: **Macrocycle Longato1**
in the 3D structure, the ligands R = PMe_3 point outwards of the cycle;
parts of the structure pointing upwards are marked in bold

Besides these examples, the cyclic trimer **Longato2** is formed from $Pt(PMe_3)_2(OH)_2$ and 1-methylcytosine as the nitrate or the perchlorate salt (the latter being described as "unpredictably explosive") after heating in water for 6 days at 80 °C (figure 7).[61b] In this trisplatina-macrocycle, the cytosine units are arranged on one side of the plane which is formed by the three Pt(II) corners, whereas the six phosphine ligands face the opposite side.

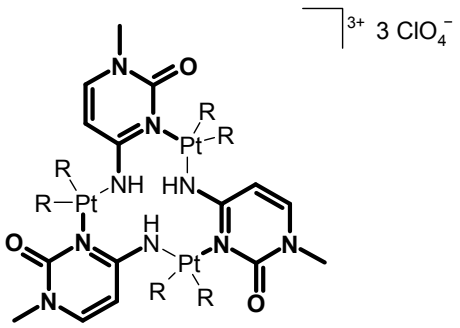

Figure 7: **Macrocycle Longato2**
R = PMe_3; parts of the structure pointing upwards are marked in bold

Lippert and coworkers broadly investigated macrocycles consisting of Pt(II) and nucleobases, and later on extended their research to related Pt(II) macrocycles in which other N-heterocyclic systems act as bridges between the Pt centres.[62,63] By 1981 *Lippert* had already postulated the cyclic tetranuclear Pt(uracilate) complex $\{Pt(en)(u\text{-}N^1,N^3)\}_4$ **Lippert1** (scheme 12).[63o] However, a thorough characterisation of this "molecular box" by crystal structure analysis only appeared in

1992.[63n] **Lippert1** results from an initially formed mixture of linear complexes after stirring for several days at room temperature. In contrast to most of the existing Pt–N coordinated complexes (vide ultra), one nitrogen atom in a uracil ligand is bound as an anion. The OH groups of the resulting positively charged complex can be deprotonated around pH 8 to a neutral, highly soluble product. From its structure, **Lippert1** can be considered as a metal analogue of calix[4]arenes. An equilibrium between various conformations was observed due to the rotational freedom around the Pt–N bonds, whereby the "1,3-alternate" form is the predominant one (scheme 12). By deprotonation, or addition of metal ions such as Ag(I), the equilibrium can be shifted to a "(pinched) cone" conformation. Each of the possible conformations can be stabilised by additional metal cations.[63d,e,k,l] In recognition experiments it was found that only the "cone" conformation is able to complex sulfonate anions.[63e] *Navarro, Lippert et al.* and *Mutikainen, Randaccio, Lippert et al.* also reported an analogous tetrameric macrocycle with 2-hydroxyprimidine ligands, as well as several mixed hexa- or octanuclear cycles comprising uracilate and *trans*-Pt(II), which represent further interesting examples.[63c,k]

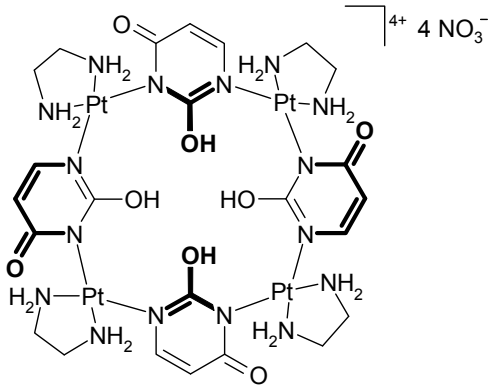

a) molecular structure (parts of the structure pointing upwards are marked in bold)

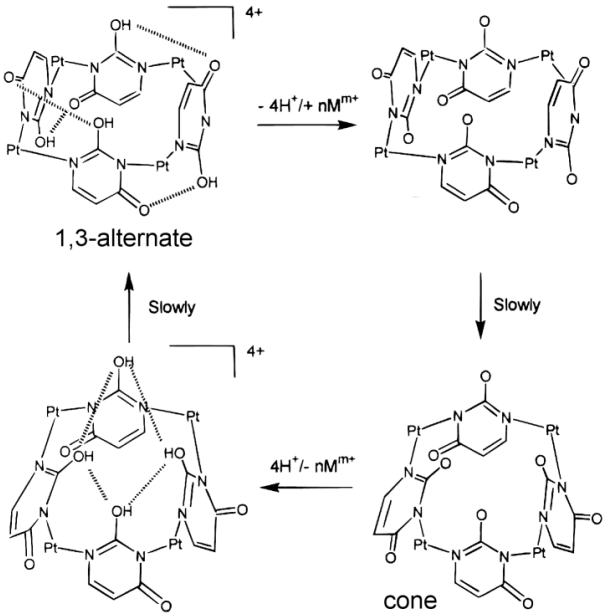

b) conformational equilibria (Pt = Pt(en); M is omitted in the structures for sake of clarity)[63e]

Scheme 12: Macrocycle Lippert1

The molecular rectangle **Lippert2**, consisting of *trans*-Pt(II), linear Hg(II) and guanine units, is quantitatively formed due to the ideal binding vectors of guanine which virtually adopt a 90° angle (figure 8).[63i,j,m]

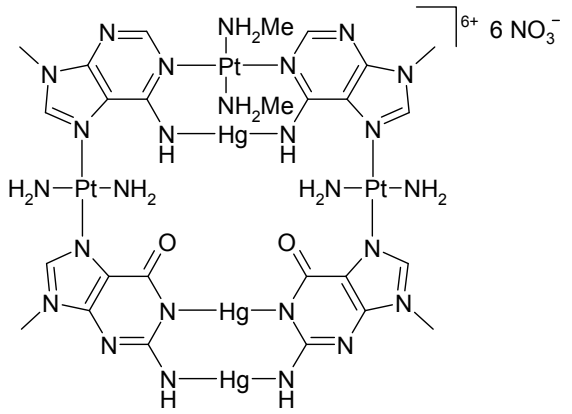

Figure 8: Macrocycle Lippert2

The similar "molecular rectangle" **Lippert3** with two Ag(I) and two Pt(II) moieties could be obtained by reaction of $AgNO_3$ and a *trans*-Pt(II) precursor comprising 9-methyladenine and 9-methylhypoxanthinate as ligands (figure 9).[63a]

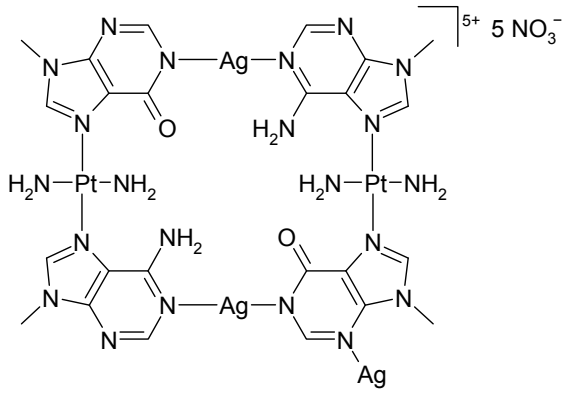

Figure 9: Macrocycle Lippert3

As successfully applied for **Lippert1**, the concept of switching the ligand conformation by postmodification of the metalla-macrocycle was extended to cyclic trimers containing 2,2'-bipyrazine (bpz) units.[63b,f–h] The bpz ligand connects to the Pt(II) corners by a *trans*-4,4' coordination to form the molecular triangle **Lippert4a** in 35 % yield (scheme 13). In this macrocycle the pyrazine rings are distorted by 21–27° and remain more or less perpendicular to the molecular plane.[63h] This coordination mode allows the formation of a triangle because the favourable 90° angles at the Pt corners remain intact. The addition of an second metal precursor complex such as Pd(II)(en) results in the formation of hexametalla-macrocycle **Lippert4b** in which the bipyrazines are twisted and chelate three Pd(II) units by 2,2'-coordination at the remaining nitrogen atoms.[63b,f] The three Pt and Pd centres are arranged in an alternating up-and-down fashion which, similar to macrocycle **Lippert1,** resembles a calix[3]arene and is capable of complexing

anions such as PF_6^- and NO_3^-. In the solid state, the macrocycles are stacked, forming anion channels with a diameter of 6.24–6.42 Å.[63g]

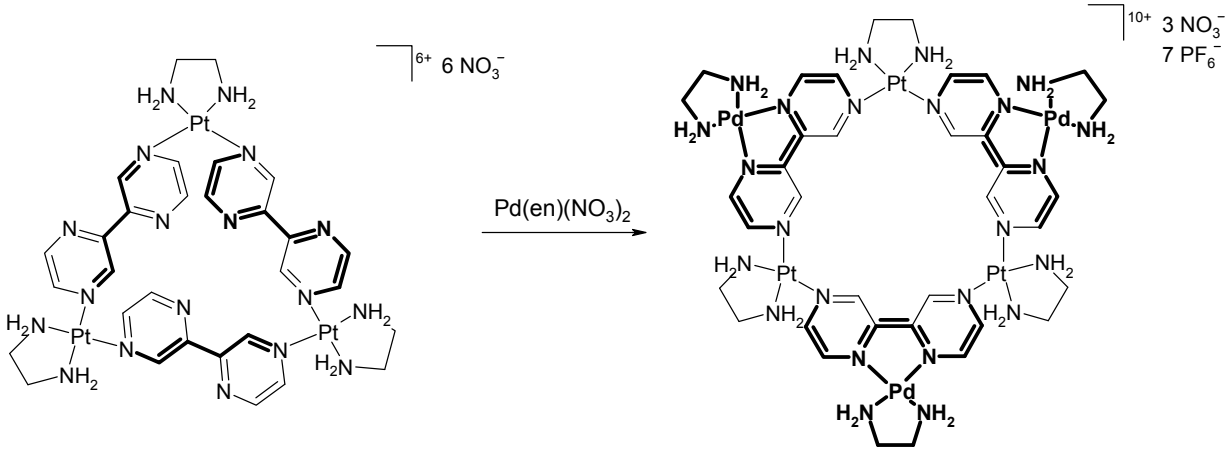

Lippert4a **Lippert4b**

Scheme 13: Macrocycle Lippert4a and conversion to Lippert4b
parts of the structures pointing upwards are marked in bold

2.4.7 Macrocycles with Pt–N Coordination Containing Exocyclic Diamine Ligands

While the examples described so far have concentrated on bridging ligands with biologic relevance, it was the ground-breaking work of *Fujita et al.* and *Stang et al.* that established a huge variety of novel metalla-macrocyclic structures formed by self-assembly processes. Molecular polygons or more sophisticated molecular topologies, such as catenanes or Platonic and Archimedean structures, boosted a field on its own which receives much attention (cf. reviews of *Fujita et al.*[44] and *Stang et al.*[45]). In 1991, *Fujita, Ogura and coworkers* were in fact the first to report a molecular square comprising *cis*-Pt(II)(en) corners and 4,4'-bipyridine bridging ligands.[64b–d] The reaction of Pt(II)(en)$(NO_3)_2$ and the bipyridine in D_2O first resulted in a mixture of linear oligomers. Nevertheless, after heating up the reaction mixture to 100 °C for 4 weeks (!), the macrocycle **Fujita1** (figure 10) could be identified and its formation could be monitored by ^{1}H NMR.[64d] NMR studies in aqueous solutions showed that the macrocycle is capable of complexing small aromatic ether molecules, however, with relatively small association constants around 10^2 L mol^{-1}.[64c] The intermolecular interactions are most probably of hydrophobic nature and are due to the quasi-perpendicular conformation of the 4,4'-bipyridine units.

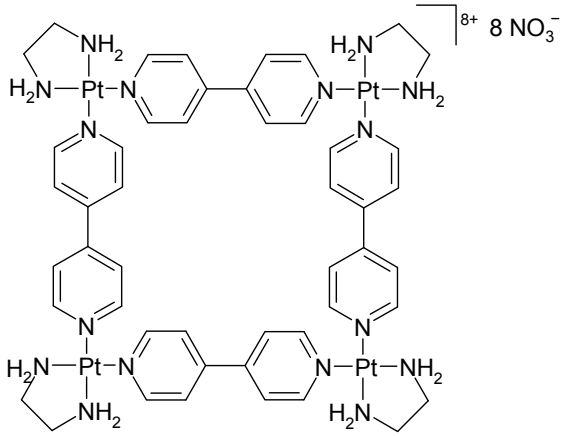

Figure 10: Macrocycle Fujita1

When [4,7]phenanthroline is used as a bridging ligand instead of 4,4'-bipyridine, a completely different macrocyclic structure results, which is quantitatively formed in D_2O within minutes, as reported by *Yu et al.*[64a] Due to the 60° angle of the binding vectors of the nitrogen lone pairs in [4,7]phenanthroline, three *cis*-arranged Pt(II)(en) corners form a triangle with a crown-like structure. Replacement of the bidentate en ligands at the Pt(II) centres by 2,2'-bipyridine or [1,10]phenanthroline, which occurs at 100 °C in the presence of excess $NaNO_3$, gives the crown-like structure **Yu1** comprising strong aromatic receptor moieties (figure 11).

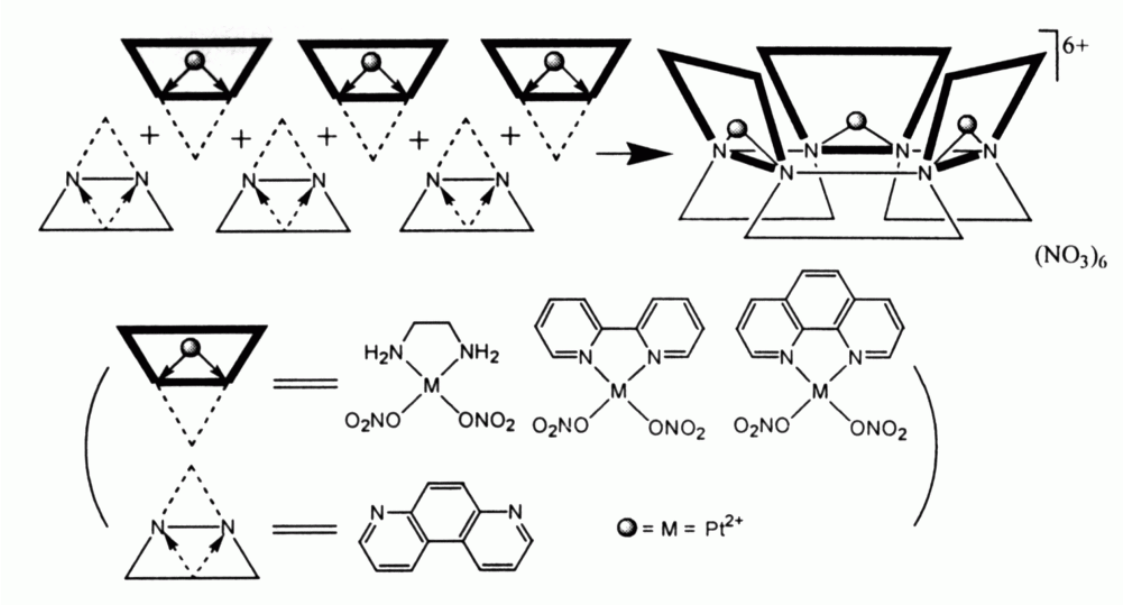

Figure 11: Structure of macrocycle Yu1[64a]

An interesting mixed-metal motif was presented by *Dunbar et al.*, who obtained the square **Dunbar1** (figure 12) comprising isonicotinate (isonic) bridging ligands and mixed Pt and Re corners in 42 % yield.[65] Here, each Re corner consists of two linked Re atoms, each of them coordinating to one of the oxygen atoms of the carboxylate moieties. A further cyclic assembly with isonic ligands, in which Pt is not only bound by nitrogen, but also via oxygen, is presented in section 2.4.13.

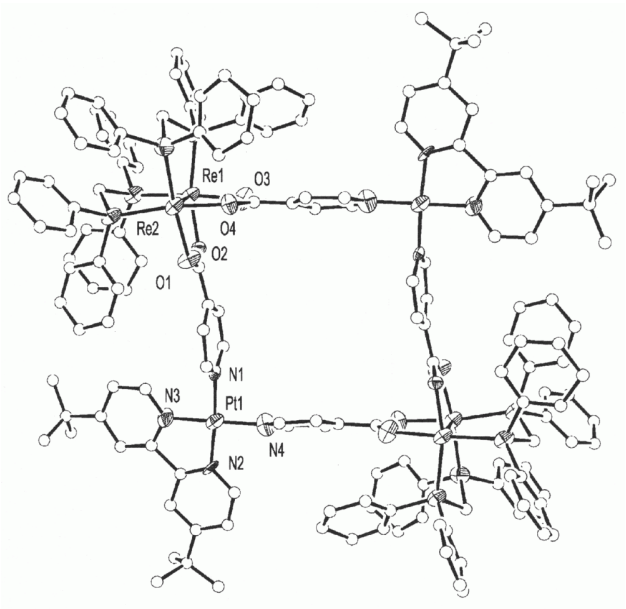

Figure 12: X-ray structure of macrocycle Dunbar1[65b]

A kind of strain-free truncated triangle, in which the Pt corners comprise a bite angle of 90°, was reported by *Kim et al.* who used flexible linkers to build the macrocyclic oligorotaxane (or "necklace") **Kim1** (figure 13).[66] The interlocked ring system was obtained in 90 % yield in a one-pot reaction by stirring a mixture of the Pt(II) precursor, the exocyclic en ligand and cucurbituril in refluxing water. The reaction could be monitored by NMR and the structure was confirmed by X-ray structure analysis. With longer reaction times, an equilibrium between the molecular triangle and a corresponding square evolved, yielding an almost 1:1 mixture of the trimeric and tetrameric necklace. On the other hand, the cyclotetramers could be selectively obtained by tuning the threading ligands in terms of length and connectivity to the coordinating groups (3-pyridyl vs. 4-pyridyl).[66a]

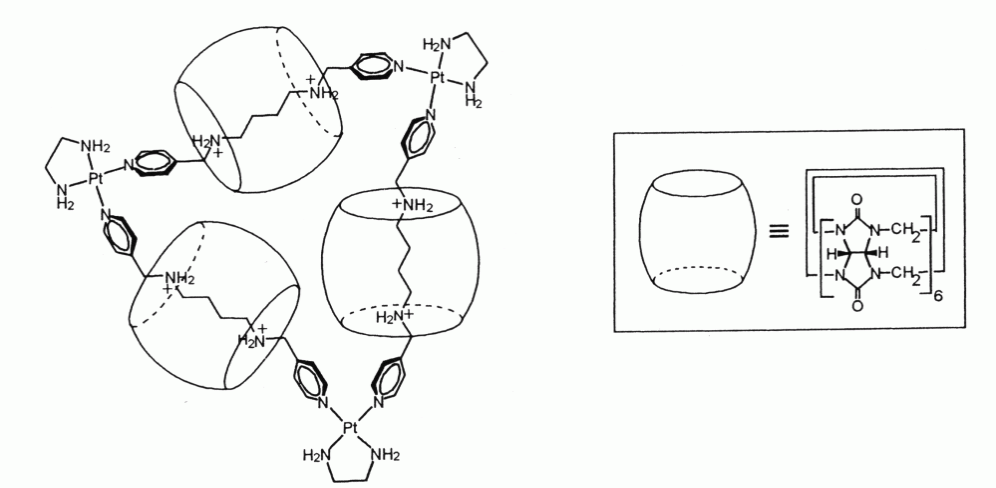

Figure 13: Macrocycle Kim1[66b]

A similar and also flexible molecular triangle with the non-symmetric bridging ligand *N*-(4-pyridinyl)isonicotinamide was reported by *Puddephatt and coworkers*.[67] From the two different possible combinations, the less symmetric trimer **Puddephatt1** (figure 14) is formed in favour of a potential triangle with C_3 symmetry, as was confirmed by X-ray structure analysis. The packing pattern in the crystal reveals association of the molecules by stacking, which is caused by hydrogen bonding between the amide groups. However, the authors do not exclude the possibility that in solution other structures such as molecular squares may exist.

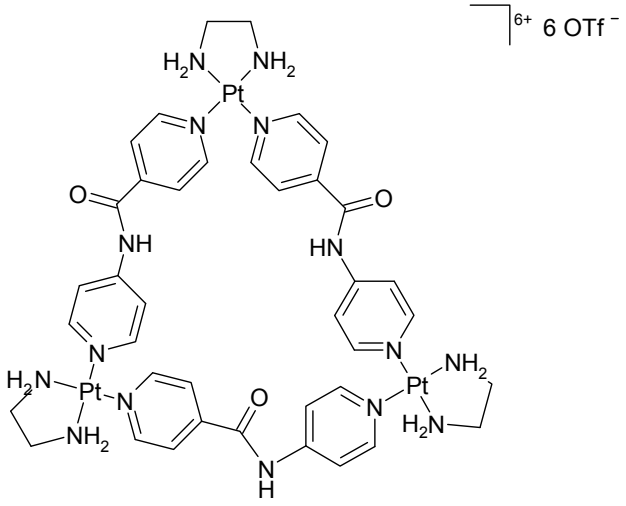

Figure 14: Macrocycle Puddephatt1

2.4.8 Square Pt–N Coordinated Macrocycles with Exocyclic Ligands Other than Diamines

The same type of self-assembled molecular square such as **Fujita1** was reported in 1994 by *Stang et al.*[54,68f,g] In contrast to **Fujita1**, the square **Stang1** forms at room temperature with 4,4'-bipyridine when, instead of the en ligand, the bidentate phosphine ligand dppp is used in the Pt(II) precursor complex (figure 15). Interestingly, the successful implementation of PEt_3 instead of dppp proved that a chelating ligand is not absolutely necessary to retain the *cis* geometry at the metal centre.

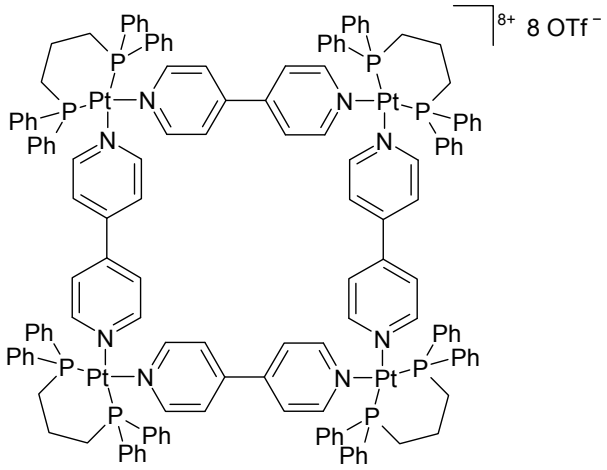

Figure 15: Macrocycle Stang1

In the following years, *Stang et al.* reported a variety of metalla-macrocycles based on the previous type including Pt(II)–diphosphine corner units. Various bridging ligands, e.g. diazapyrene and diazabenzoperylene, have been used yielding macrocycles with extended cavities. Furthermore, variations of the structures were achieved at the exocyclic bidentate ligands of the Pt(II) centres or by replacement of two opposite Pt(II) corners with other 90° elements such as Pd(II), T-shaped iodonium moieties or oxygen-bonded $TiCp_2$ units. Since much of this work has already been covered by reviews published in 1997[45d] and 1998[45c], only some prominent examples will be discussed here.

Very aesthetic and complex multimetallic structures result when *meso*-(4'-pyridyl)-substituted metalloporphyrins are reacted with Pt(II) precursors to form the comparable molecular squares **Stang2** (by *Stang and coworkers*; figure 16)[68e] and **Lehn1** (by *Lehn and coworkers*; figure 17)[69]. Such a cyclic arrangement of porphyrin moieties is particularly striking because one can regard them as a mimic for the natural light harvesting systems in the photosynthesis reaction centre. Detailed structural analyses of the porphyrin squares by NMR indicate that, in contrast to macrocycles such as **Fujita1** (vide infra), only the pyridine rings are twisted perpendicular to the

molecular plane, while the porphyrins, representing the larger part of the bridging ligand, remain in the plane of the square. As had been seen before with self-coordinated Zn–porphyrin arrays, the coordinated metal has a strong influence on their spectroscopic behaviour: for example, the Soret- and Q-band absorptions are strongly enhanced.[68e] *Stang et al.* further demonstrated the possibility of using substituted porphyrins not only as a linear building block, but also as 90° corner elements for molecular Pt(II) squares.[68a]

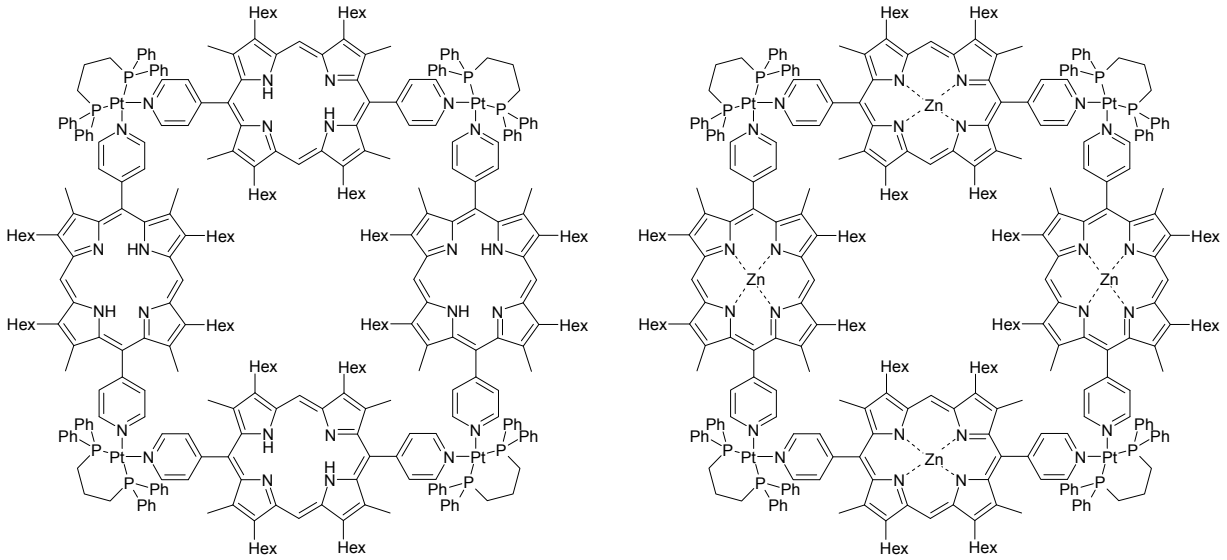

a) Stang2a **b) Stang2b**

Figure 16: Macrocycles Stang2

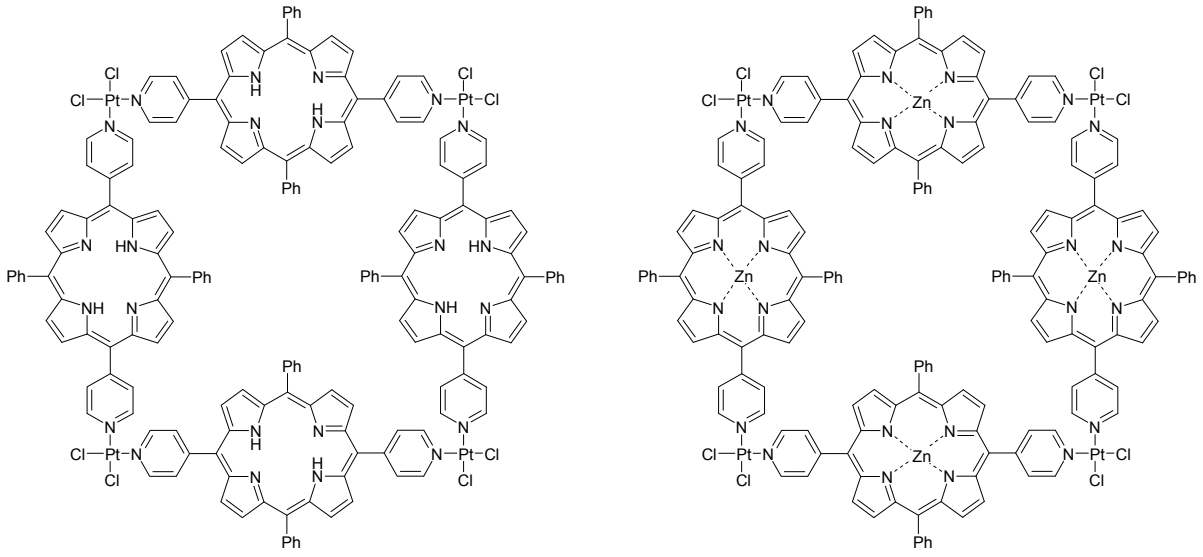

a) Lehn1a **b) Lehn1b**

Figure 17: Macrocycles Lehn1

The replacement of the porphyrin unit by other dye molecules leads, e.g., to the molecular squares **Würthner1**, which are formed by self-assembly in excellent yields and comprise *N,N*-dipyridyl-substituted perylene tetracarboxylic acid diamides as the bridging ligands (figure 18).[70] This type of novel supramolecularly arranged dye aggregate shows intriguing photophysical data. Among them, the high fluorescence quantum yield of the ligand remains almost unchanged in the Pt(II) molecular square. The authors ascribe this effect to a decoupling of the perylene chromophore and the metal binding sites, caused by the perpendicular arrangement of the ligands with respect to the molecule plane. A similar macrocycle, which exhibits a triangle–square equilibrium, is presented in section 2.4.9.

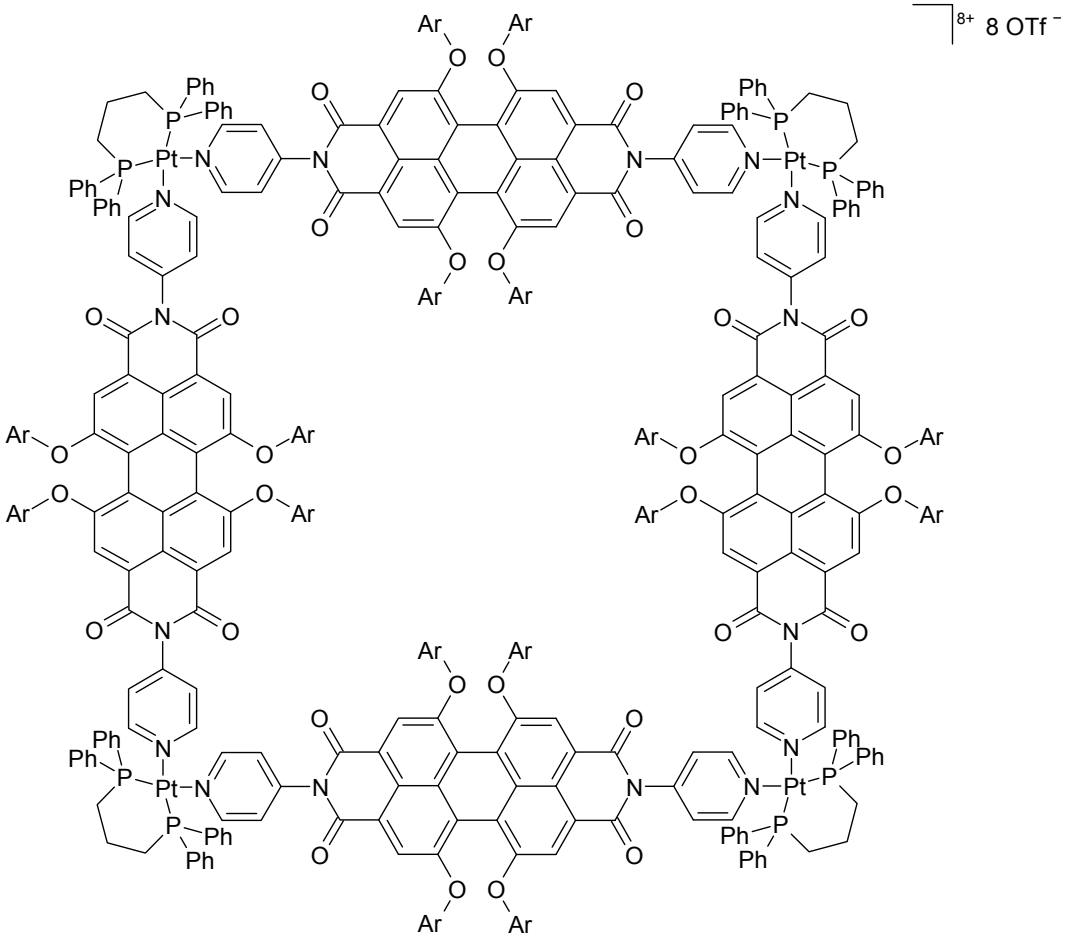

Figure 18: **Macrocycles Würthner1**

Würthner1a: Ar = 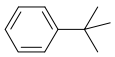

Würthner1b: Ar = 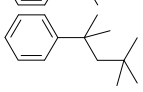

The resulting cavity of the molecular squares may be suited for the inclusion of guest molecules, which was shown by *Stang and coworkers* for mixed metallic macrocycles such as **Stang3** (figure 19).[68b–d] Although only little interaction was found with electron-rich compounds such as 1,4-dihydroxybenzene, it was possible to bind Ag(I) cations from silver triflate in a "tweezer" fashion, in which Ag(I) is bridging two ethynyl units adjacent to the Pt(II) corners. This coordination mode could be proven by NMR, IR and mass spectrometry. Remarkably, the resulting Ag(I) complexes of **Stang3** can themselves capture guest molecules, such as pyrazines or phenazines, which form a "diagonal" in the molecular square (figure 19).[68b]

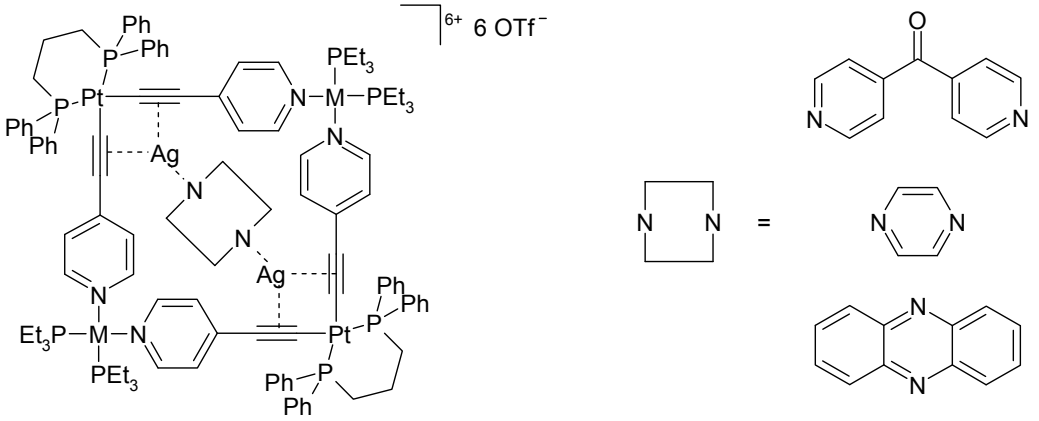

Figure 19: Silver complexes of macrocycles Stang3 with different guest molecules
Stang3a: M = Pt
Stang3b: M = Pd

Post-modification of molecular squares by photoisomerisation of reactive bridging ligands was attempted by *Lees et al.*[71a] Among other mixed metal molecular squares that have been reported by this group (cf. p. 57),[71b] the structures **Lees1–2** (figure 20) are particularly interesting due to their *trans*-stilbene or *trans*-diazo units, which constitute the bridging ligands between the two Pt(II) and Re(III) corners. The ligand configuration at the double bond can be isomerised by light and thermally reverted. In contrast to the corresponding Pd(II) macrocycles, which due to the *cis* configuration of the bridging ligand convert to a cyclic dimer by irradiation, the Pt(II) analogues dissociate and do not form dimers upon irradiation. This was accounted for by the more stable nature of the Pt–N bond compared to the Pd–N bond, which prevents reorganisation. However, after heating up the solution of the follow-up products for 2 days, the original mixed metalla-macrocycles **Lees1–2** could be fully recovered.

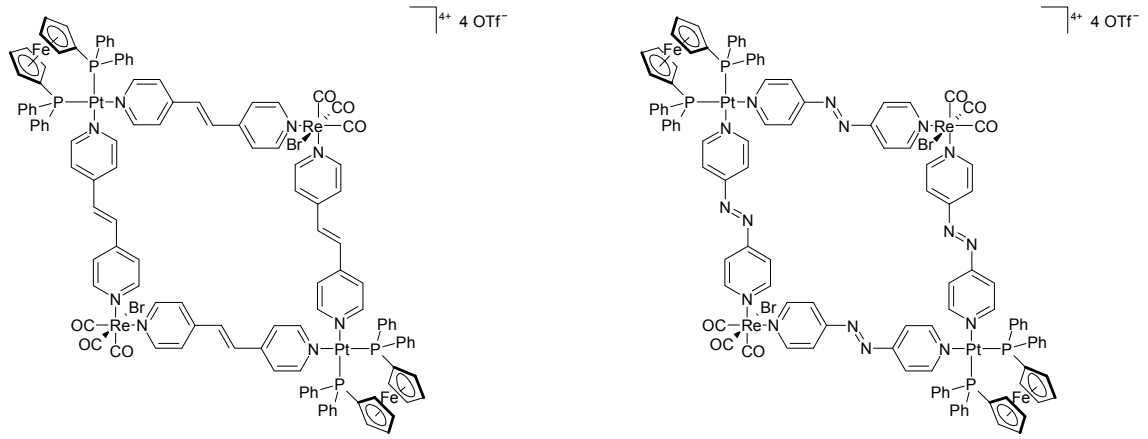

a) Lees1 **b) Lees2**

Figure 20: Macrocycles Lees1–2

The group of *Hong* used a BINOL (2,2'-dihydroxy-1,1'-binaphthyl) ester of isonicotinic acid as a bridging ligand. In the reaction of the racemic mixture of the BINOL ester with Pt(II)(dppf), the rectangular bisplatina-macrocycle **Hong1** (figure 21) was selectively formed.[72] NMR and X-ray structure analysis showed that one *S* and one *R* ligand are incorporated in the macrocycle, revealing a self-discrimination process.

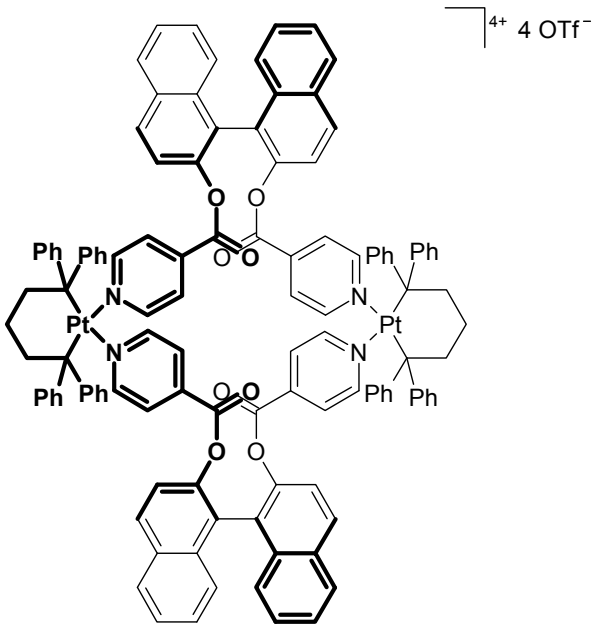

Figure 21: Macrocycle Hong1
parts of the molecule are marked in bold for a better differentiation of superimposed structures

2.4.9 Molecular Polygons Other than Squares (Triangles, Hexagons, Cyclodimers) and Equilibria Thereof

Due to the ideal 90° angle of the frequently used Pt(II)–diphosphine precursors, most examples of Pt(II) macrocycles take the shape of a square or a rectangle. However, other molecular geometries, which may be strained, recently came up when the resulting binding angles either at the bridging ligands or at the Pt centre differ from 90° or 180°. Since metal–ligand interactions are typically reversible, equilibria between various molecular geometries may arise.

In this respect, the reversible transformation of a molecular square to a corresponding triangle was found by *Stang et al.* for the macrocycle **Stang4**, in which the more or less flexible linkers *trans*-bis(4-pyridyl)ethylene are used as bridging ligands (scheme 14).[73d] The equilibration is accelerated by addition of water and was monitored by NMR spectroscopy. Although the squared configuration tends more to crystallisation, in solution the formation of a triangular structure is strongly favoured. Exchange of the triflate counter ions by the larger cobalticarborane anion $CoB_{18}C_4H_{22}^-$ led to a further stabilisation, so that for the triangular form crystals suitable for X-ray analysis could be grown.

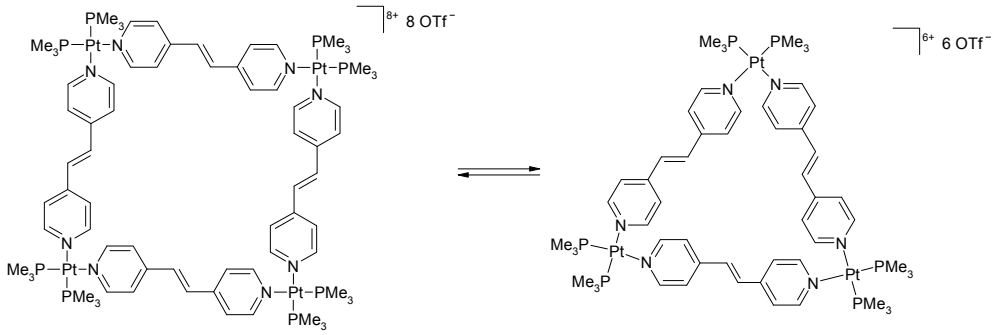

Scheme 14: Equilibrium between square Stang4a and triangle Stang4b

In the case of the similar macrocycles **Ferrer1** (scheme 15) comprising 1,4-bis(4-pyridyl)butadiyne linkers, by increasing the concentration a shift of the square–trimer equilibrium towards the squared forms resulted while the triangles are still the predominant species.[74] For the assembly process and equilibrium formation, length, basicity and flexibility of the spacer seem to play a major role, whereas the bite angle of the diphosphine ligand has rather less influence. Host–guest experiments with the macrocycles **Ferrer1** gave different results for PF_6^- and OTf^- anions: in the former case enhancement of the luminescence of the macrocycles was found by the addition of the anion; in the latter case the fluorescence was quenched.

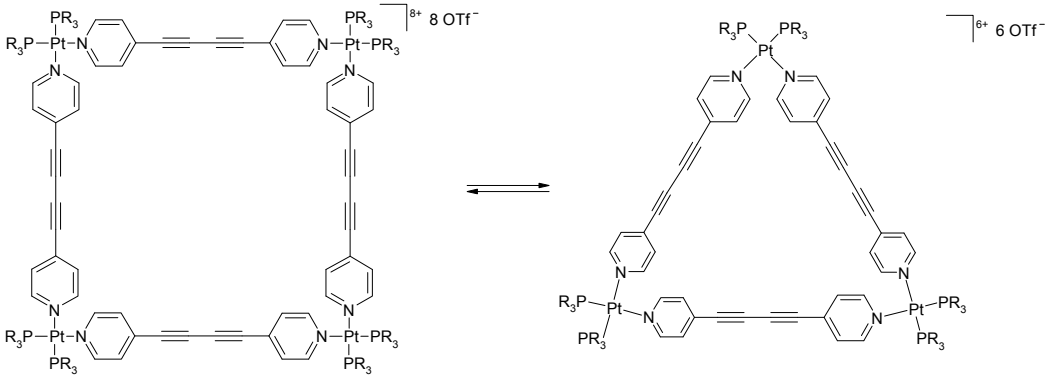

Ferrer1a–c **Ferrer1d–f**

Scheme 15: Equilibrium between squares Ferrer1a–c and triangles Ferrer1d–f
Ferrer1a/1d: PR_3 = dppp (chelating)
Ferrer1b/1e: PR_3 = dppf (chelating)
Ferrer11c/1f: PR_3 = depe (chelating)

Equilibria between molecular squares and triangles seem to be a quite general phenomenon. *Würthner and coworkers* synthesised the enlarged Pt(II) macrocycles **Würthner2** (scheme 16) comprising diazadibenzoperylenes as bridging ligands.[75] NMR studies in deuterated nitromethane clearly showed almost 1:1 ratios of the squares and the corresponding triangles. The structures were assigned based on NMR and ESI-FT-ICR-MS results as well as on molecular modelling, which gave insight into the steric situations of the two related geometries. Repulsion between the phenyl groups of the exocyclic dppp ligand and the phenoxy substituents at the bay region of the diazadibenzoperylene is more pronounced for the molecular squares. Therefore, most likely this steric interaction seems to be the driving force for the formation of the less hindered triangles. In contrast to the Pt(II) macrocycles **Würthner1** (vide infra), spectroscopic investigations on these macrocycles showed effective quenching of the pyrene fluorescence.

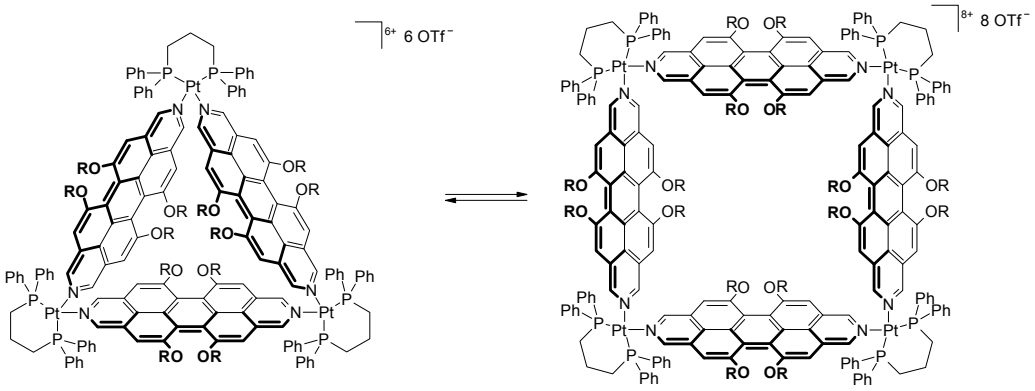

Würthner2a–b **Würthner2c–d**

Scheme 16: Equilibrium between triangles Würthner2a–b and squares Würthner2c–d
Würthner2a/2c: R = Ph
Würthner2b/2d: R = *t*-BuPh

A very thorough investigation of square–triangle equilibria for the related Pt(II) macrocycles **SchalleyLützen1** to **SchalleyLützen3** (figure 22)**,** containing 4,4'-bipyridine, *trans*-di(4-pyridyl)-ethylene and *trans*-4,4'-azopyridine as bridging ligands, was recently described by *Schalley, Lützen and coworkers*.[56] The equilibrium and the ligand-exchange behaviour of these dynamic systems were examined by different techniques such as FT-ICR and tandem mass spectrometry as well as by gas-phase experiments. Thus, very important insight in the defragmentation pathways of the investigated Pt(II) macrocycles was obtained.

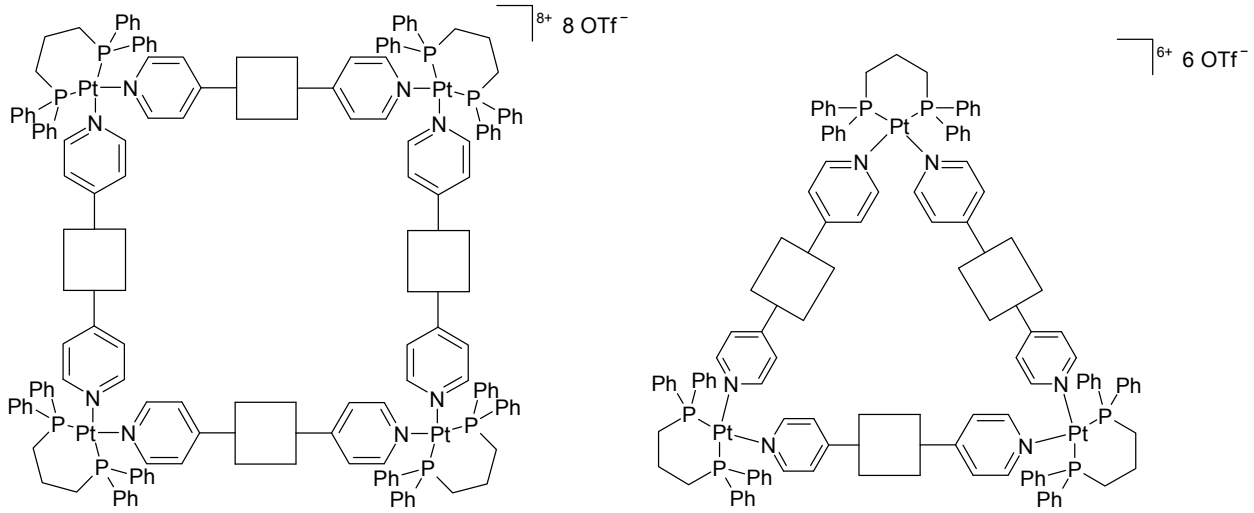

a) SchalleyLützen1a–3a **b) SchalleyLützen1b–3b**

Figure 22: Square molecules SchalleyLützen1a–3a and corresponding triangles SchalleyLützen1b–3b

SchalleyLützen1a/b: ☐ = ·⁄⁄·

SchalleyLützen2a/b: ☐ = ·N=N·

SchalleyLützen3a/b: ☐ = direct bond (i.e., bridging ligand is ·N⟨⟩N·)

In the preceding examples, the molecular triangles were difficult to isolate from the square–triangle equilibria because, due to the 90° *cis*-Pt(II) corners, they only exist in a truncated or strained form. However, *Stang et al.* showed that a true 60° tecton results from a phenanthrene that is disubstituted in the 2- and 9-positions with reactive Pt(II) units.[73c] Reaction of this corner element with the linear bridging ligand *trans*-[bis(4-pyridylethynyl)-bis(triethylphosphine)]platinum(II) in acetone gives the unique and stable molecular triangle **Stang5** (figure 23) in excellent yield within a few hours. Interestingly, in the solid state the nonaplatina triangles stack and form large channels.

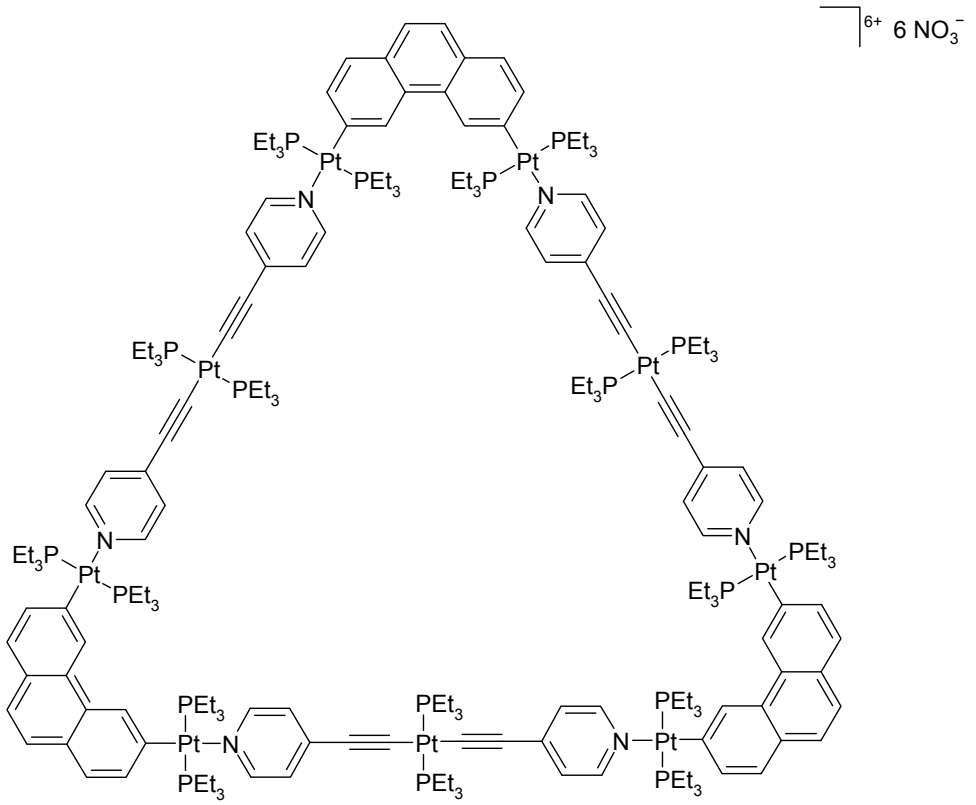

Figure 23: Macrocycle Stang5

Surprisingly, reaction of *cis*-Pt(PMe$_3$)$_2$(OTf)$_2$ with the rather small pyrazine in nitromethane resulted in the formation of the molecular triangle **Stang6** (figure 24) instead of the expected molecular square.[73f] Entropic reasons are considered to be the driving force for the formation of this strained structure. The strain is not only accommodated by the reduced N–Pt–N angle of 82–83°, but also by the reduced centroid(pyrazine)–N–Pt angles of 167–171°. These values are remarkable, as Pt(II) typically tries to keep a perfect square coordination even in strained macrocycles (compare, e.g., **Bosch1** in section 2.4.11).

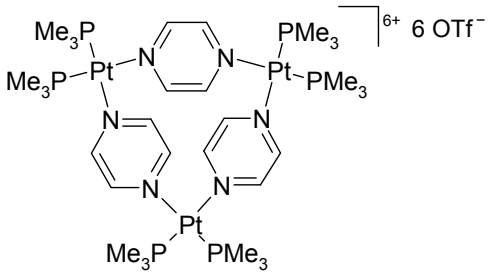

Figure 24: Macrocycle Stang6

Precursor complexes that can function as 60° tectons and exclusively form triangles are quite rare. In this respect, *Chan, Che and coworkers* took benzimidazole as a bridging ligand in which the nitrogen atoms span binding vectors of approximately 150°.[76] Reaction of benzimidazole with *cis*-Pt(II) as the corner element resulted in truncated triangle **ChanChe1** (figure 25). The crystal structure analysis of **ChanChe1** revealed a slight distortion of the Pt coordination sphere from the plane, which probably causes the *syn–anti–anti* orientation of the benzimidazole units with respect to the plane of the triangle.

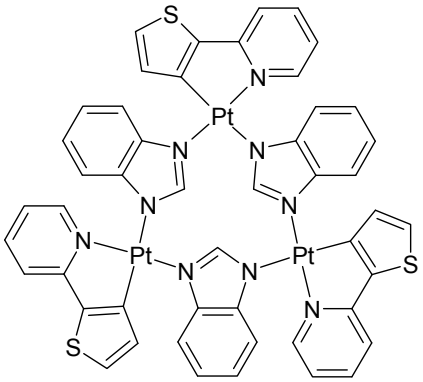

Figure 25: Macrocycle ChanChe1

That geometric structures other than squares, rectangles or triangles can be selectively formed was shown by *Chi, Addicott, Stang and coworkers* when various Pt(II) precursor complexes were used that allow 90°, 120° or 180° angles in combination with di(3-pyridyl)ethyne or 1,4-di(3-pyridyl)-1,3-butadiyne, respectively.[73b] The strain-free hexagons **ChiAddicottStang1–4** or the truncated hexagons **ChiAddicottStang5–6** (scheme 17) were formed, although entropy should favour smaller macrocycles.

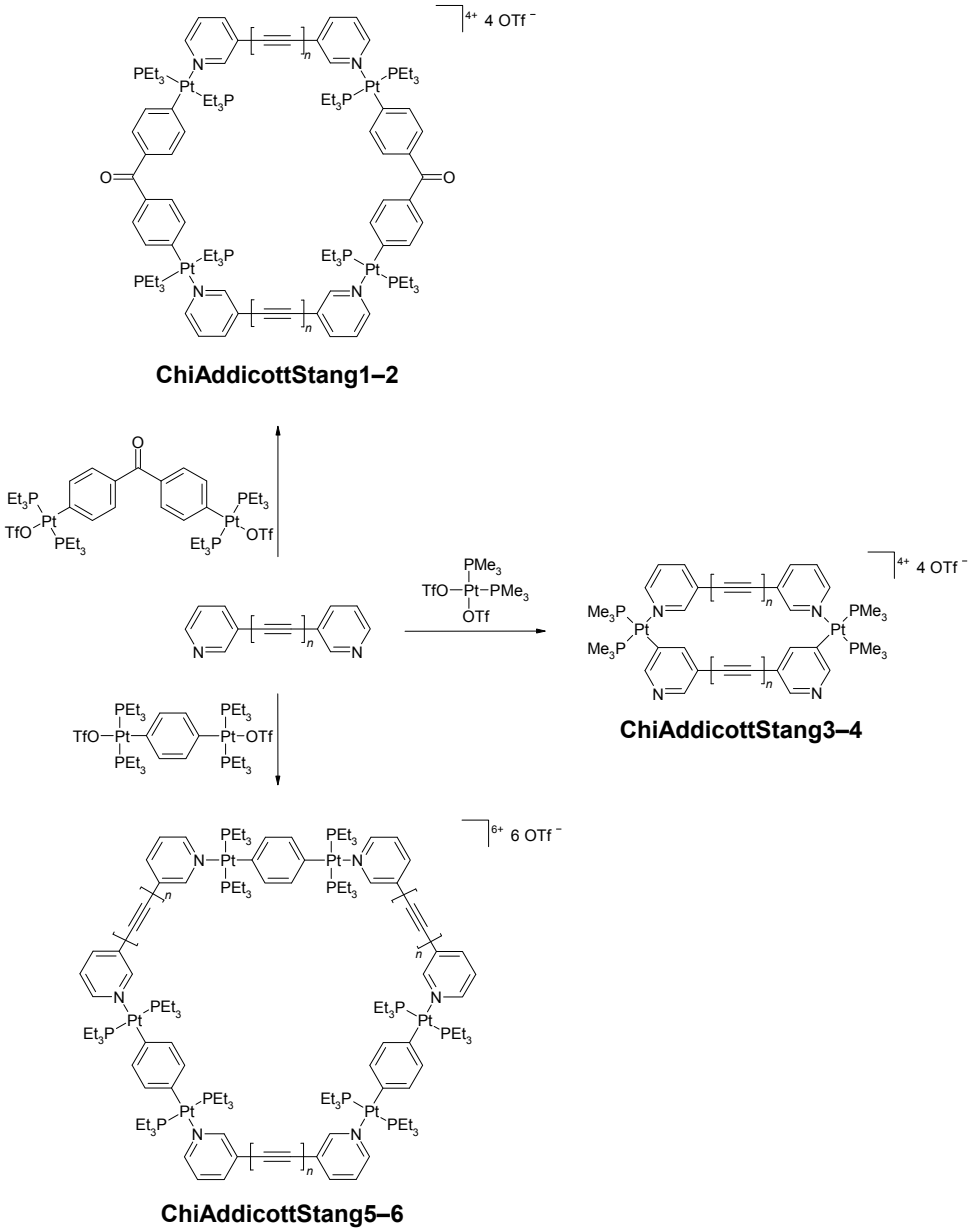

Scheme 17: Preparation of macrocycles ChiAddicottStang1–6 from the same bridging ligand with three different Pt(II) precursors
ChiAddicottStang1/3/5: $n = 1$
ChiAddicottStang2/4/6: $n = 2$

Utilising the same type of building blocks, the formation of the molecular hexagons **Rendina1** and **Rendina2** (figure 26) from isonic and *trans*-configured Pt(II) precursors by self-assembly was reported by *Rendina et al.*[77] The rather rare non-covalent Pt(II) hexagons are kept together by hydrogen bonding due to the typical dimerisation of carbonic acid groups. Appreciable association constants of up to 10^4 L^2 mol^{-2} were determined.

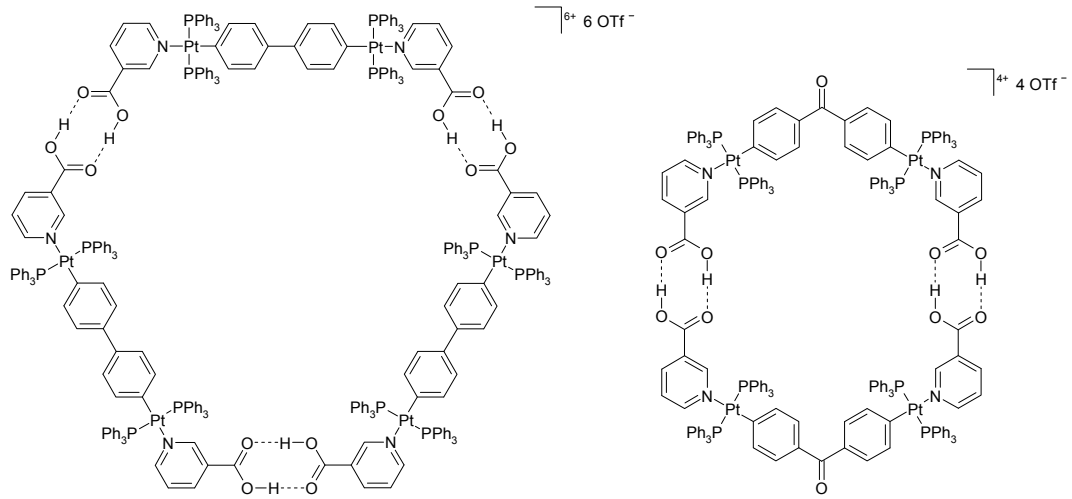

a) Rendina1 **b) Rendina2**

Figure 26: Macrocycles Rendina1 and Rendina2

The hexagonal Pt(II) macrocycle **Stang7** (scheme 18) was obtained by reaction of bis(4-pyridyl)ketone, which opens a perfect 120° angle, and *cis*-$Pt(PEt_3)_2(OTf)_2$.[73g] If the trisplatina-macrocycle is crystallised from an acetone/water mixture, the original structure is not retained and the corresponding cyclodimer **Stang8** is obtained instead. Hydration of the keto groups leads to a reduction of the binding vectors from 120° to 109° and equilibration to a more favourable cyclodimer, which then precipitates and shifts the equilibrium. A similar cyclodimer was directly obtained by reaction of *cis*-Pt(II) diphosphine and bis(4-pyridyl)silanes.[73g] X-ray structure analysis showed that the pyridyl rings are twisted out of the rhomboidal plane and that the N–Pt–N angle is decreased to 81–82°, similar to the molecular triangle **Stang6**.

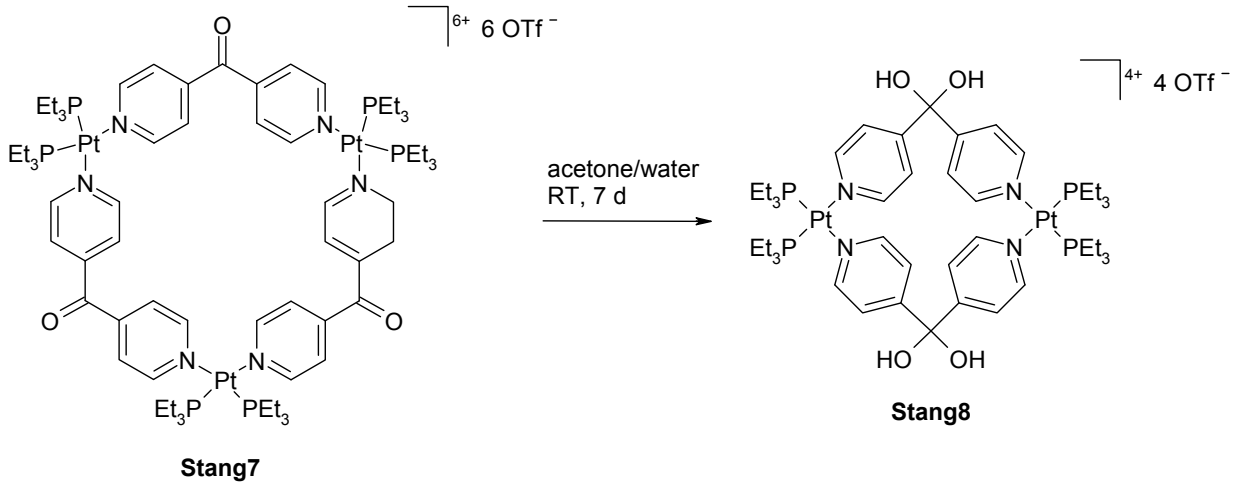

Stang7 **Stang8**

Scheme 18: Macrocycle Stang7 and conversion to Stang8

On the other hand, a dynamic equilibrium between a rhomboidal bisplatina-structure **Stang9a** and the corresponding hexagonal trisplatina-macrocycle **Stang9b** (scheme 19) was observed for the self-assembly of *cis*-Pt(II) diphosphine and (4-pyridylethynyl)pyridine.[73a] The crystal structure analysis of the cyclodimer shows that ring strain is accommodated at the Pt corners at which, similar to the structures **Stang8** and **Stang6**, the N–Pt–N angle is reduced from 90° to 81.3°. Most of the remaining strain is presumably accommodated in the acetylene connected bridging ligands and in the distortion of the rhomboidal structure from planarity.

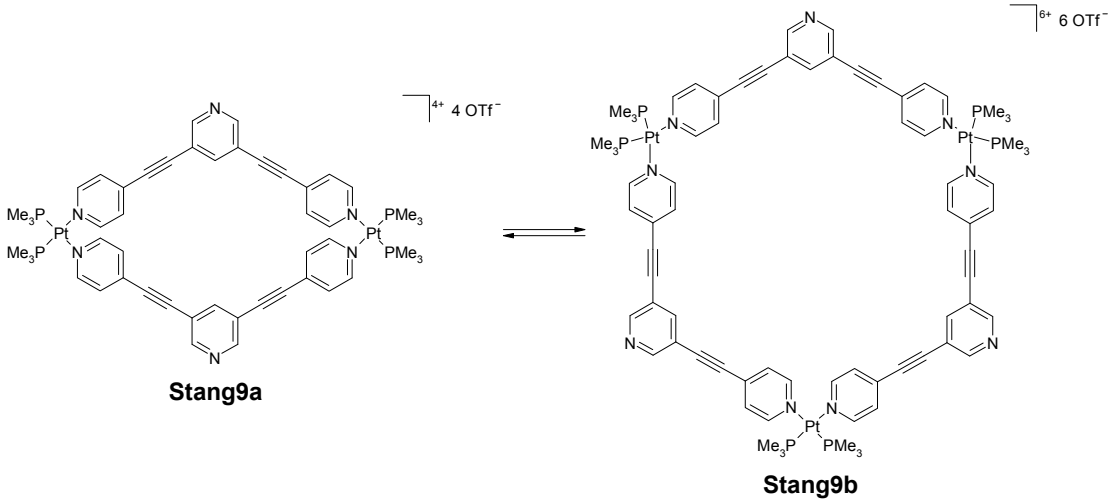

Scheme 19: Equilibrium between rhomboid Stang9a and hexagon Stang9b

Very similar to the cyclodimeric Pt(II) macrocycle **Stang8**, *Diederich et al.* reported the synthesis of the C_{60}-functionalised bisplatina-cyclodimer **Diederich1** (figure 27).[78] The macrocycle was rapidly obtained in quantitative yield only after the fullerene moieties had been exhaustively substituted with malonic ester groups in order to enhance the solubility of the precursor. As was the case for the previously described structures, the coordination of the ligands at the Pt(II) centre proves to be quite flexible, showing a reduced N–Pt–N angle of 82–83°.

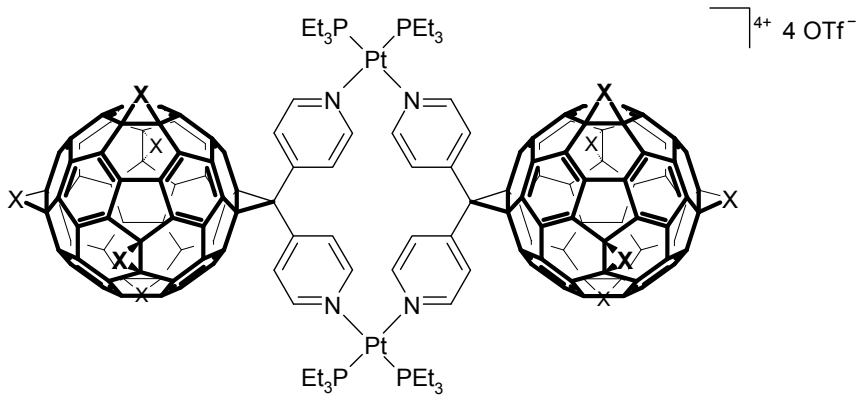

Figure 27: Macrocycle Diederich1
X = :C(CO_2Et)$_2$
parts of the molecule are marked in bold for a better differentiation of superimposed structures; for the same reason the background double bonds of the C_{60} moieties are shown as single bonds

The truncated tetrakisplatina-hexagon **KuehlStang1** was obtained when a bent bridging ligand such as 2,5-bis[(4-pyridyl)ethynyl]furane is combined with Pt "clips" comprising an 1,8-anthracenyl ligand and *trans*-Pt(II) diphosphines (figure 28).[73e] Here, the counterions obviously play an important role: mechanistic investigations showed that anion exchange of the initially released nitrate anions with hexafluorophosphate stabilised the product. On the other hand, an immediate addition of a PF_6^- salt to the reaction mixture prevented kinetic formation of the macrocycle and resulted in an excess of linear oligomers. This result clearly underlines the importance of nitrate as a counterion in substitution reactions at Pt(II) centres.

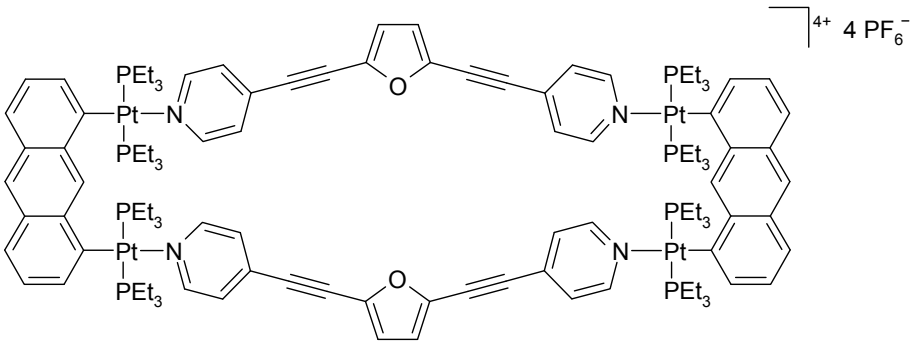

Figure 28: Macrocycle KuehlStang1

Flexibility in terms of structural isomerism was found by *Hanan et al.* for the cyclodimeric macrocycles **Hanan1** (figure 29) built from *cis*-Pt(II) diphosphines and *N*,*N*'-bis(3-pyridyl)-2,6-pyridinedicarboxamide.[79] A rotation of the 3-pyridyl units in the bridging ligand leads to either a *syn* or an *anti* conformation with respect to the plane of the Pt(II)–diphosphine corners. Temperature-dependent NMR spectroscopy revealed a rotational energy barrier of 30 kJ mol^{-1},

which allows "flipping" of the macrocycles without the need for breaking bonds. This flexibility permits an induced fit to bind BF_4^- anions in a 1:1 stoichiometry, which consequently raised the rotational energy barrier to about 45–50 kJ mol^{-1}.

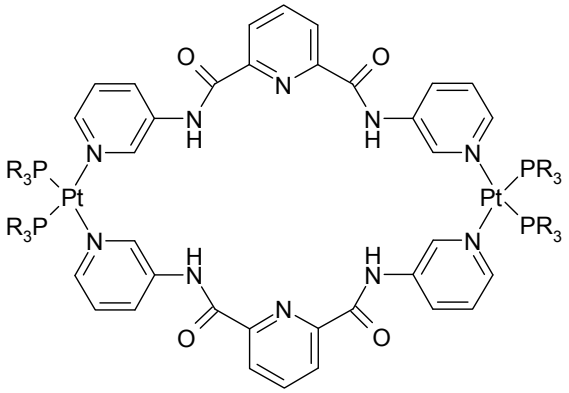

Figure 29: **Macrocycles Hanan1**
Hanan1a: R = Et
Hanan1b: R = Bu

A rather exceptional monoplatina-macrocycle involving one Pt(II)(dppp) corner and a bispyridyl bridging ligand was synthesised by a ring-closure reaction and has been used as the encircling ring in rotaxane **Jeong1** (figure 30).[80] In contrast to the previously described rotaxane **Kim1** (vide infra), here, the threading of a linear chain through the macrocycle is subsequently obtained due to directed hydrogen bondings. As the rotaxane formation was slow on the NMR time scale, the rate constant was determined to be 6.2 ± 0.1 s^{-1}.

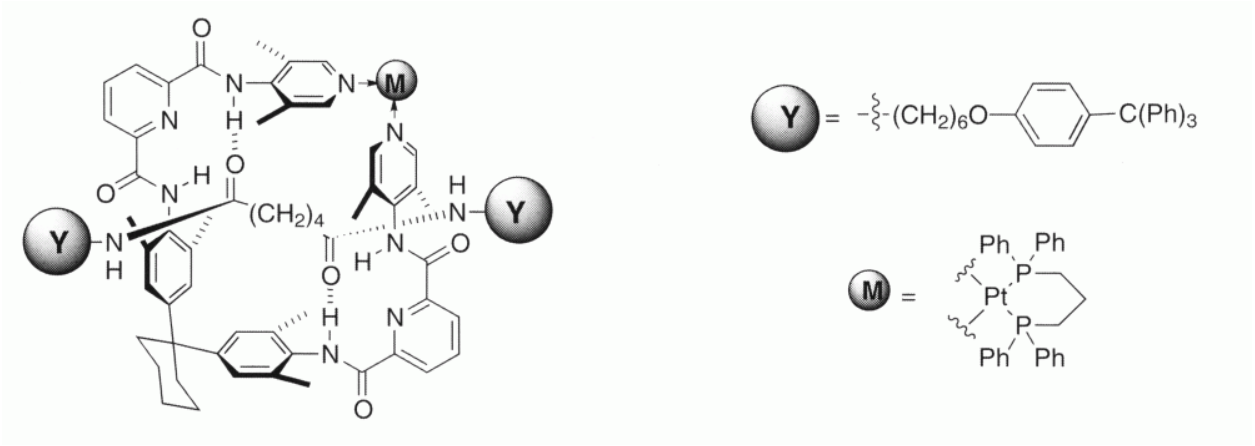

Figure 30: **Macrocycle Jeong1[80]**

2.4.10 Macrocycles with Bridging Cyanide and Isocyanide Ligands

Another larger group of Pt(II) macrocycles comprises Pt–C coordination modes when typically cyanides, isocyanates or acetylides are used as bridging ligands.

For example, a mixed Pt–C and Pt–N bonded macrocycle was obtained by *Che et al.*[81] Reaction of $K_2[PtCl_4]$ with hydrazine hydrate and *tert*-butyl isocyanide in refluxing water surprisingly yielded hexagon **Che1** (figure 31) in which the six Pt corners are bridged with cyanide spacers and are further coordinated to exocyclic carbene ligands formed from hydrazine and the isocyanide. Due to the almost 90° angles at the Pt(II) and the linear coordination mode of the cyanide ligands, the structure of the macrocycle is not planar and instead resembles a cube with two missing opposite corners. Unlike the majority of the Pt(II) macrocycles, **Che1** shows luminescence because of metal-to-ligand charge transfer (MLCT) to the exocyclic carbene ligands.

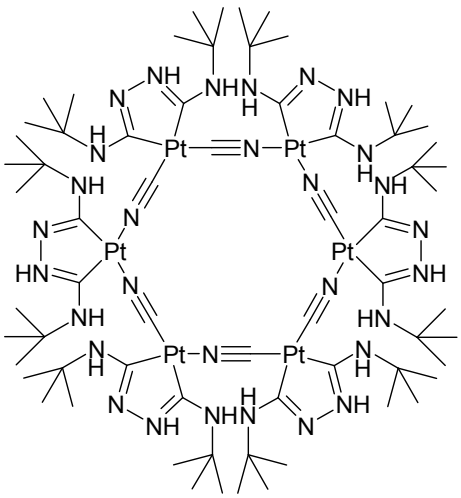

Figure 31: **Macrocycle Che1**
the true constitution with respect to direction of the bridging cyanide ligands is unknown and might be statistically distributed

By mixing a tetracyanoplatinum(II) precursor with Cu(II) and 2,2'-bipyridin, *Falvello and Tomás* prepared the cyanide-bridged molecular square **FalvelloTomás1** (figure 32) in which the Pt(II) corners are coordinated to four carbons and the Cu(II) corners to four nitrogens and one aqua ligand, providing a square planar configuration for each Pt centre and a distorted square pyramidal coordination environment for each Cu unit.[82] Additionally, by analogous reactions the corresponding Rh- and Ir-containing Pt(II) macrocycles could be synthesised. The mixed macrocycles showed very low solubility. Single crystals could only be obtained by dissolution of the macrocycles in ammonium hydroxide, which probably caused a break-up of the solid-state

structure due to coordination, while slow evaporation of NH_3 from this solution resulted in the precipitation of single crystals.

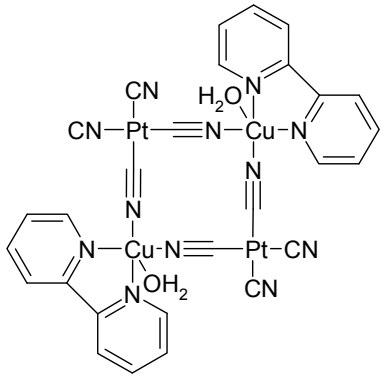

Figure 32: Macrocycle FalvelloTomás1

Using a similar *cis*-dicyanoplatinum(II) precursor, *Forniés, Lalinde et al.* synthesised the molecular trisplatina-triangles **ForniésLalinde1** and the mixed metal molecular squares **ForniésLalinde2** (figure 33), comprising two Rh or Ir corners, in moderate yields.[83] Both macrocycles comprise Pt centres that are coordinated to four carbons as typical structural elements. The macrocycles **ForniésLalinde2** can be further modified by two additional Pt(II) ligands that bind to two exocyclic acetylide ligands by σ and π coordination and thus form hexanuclear metalla-macrocycles.

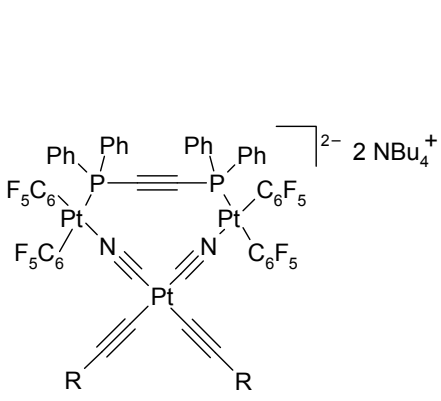

a) ForniésLalinde1
ForniésLalinde1a: R = *t*-Bu
ForniésLalinde1b: R = Ph

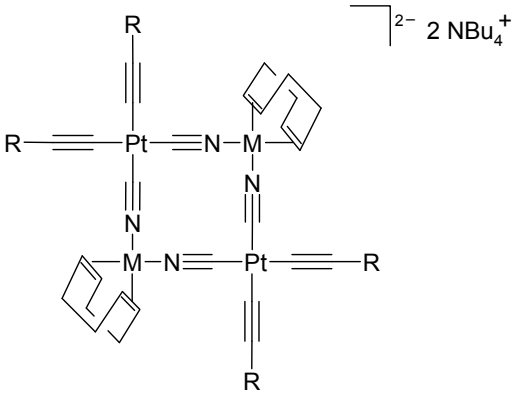

b) ForniésLalinde2
ForniésLalinde2a: M = Rh; R = *t*-Bu
ForniésLalinde2b: M = Rh; R = Ph
ForniésLalinde2c: M = Ir; R = *t*-Bu
ForniésLalinde2d: M = Ir; R = Ph

Figure 33: Macrocycles ForniésLalinde1 and ForniésLalinde2

The same authors further extended the size of molecular Pt(II) squares incorporating cyanide ligands by reacting *cis*-Pt(II) diacetylide with one equivalent of a triphenyltin cation in acetone.[83] The macrocycles **ForniésLalinde3**, which are hardly soluble, precipitated from the solution and

were characterised by IR as well as ^{1}H NMR spectroscopy. The structures comprise linear (CN)$SnPh_3$(NC) edges connecting four Pt(II) corners (figure 34).

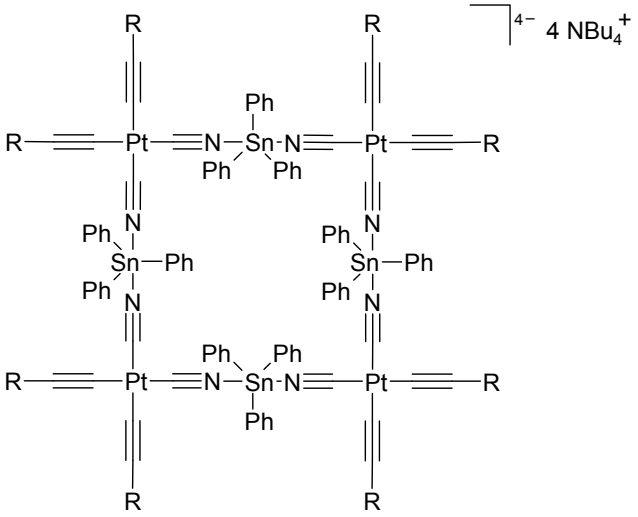

Figure 34: Macrocycles ForniésLalinde3
ForniésLalinde3a: R = *t*-Bu
ForniésLalinde3b: R = Ph

A rare example of an equilateral molecular triangle was reported by *Espinet et al.*[84] The trisplatina-macrocycle **Espinet1** (figure 35) was obtained in good yield by stirring 1,2-phenylene diisocyanide and *trans*-$Pt(C_6F_5)_2(AsPh_3)_2$ for 2 h in dichloromethane. The small distance (ca. 5.65 Å) of the three Pt(II) moieties causes an unusual arrangement of the pentafluorophenyl ligands: while the phenyl plane normally is perpendicular to the Pt(II) coordination plane, X-ray structure analysis of **Espinet1** revealed an average torsion of 54° instead of 90°. The six phenyl units are twisted in the same sense, leading to a C_{3h} symmetry.

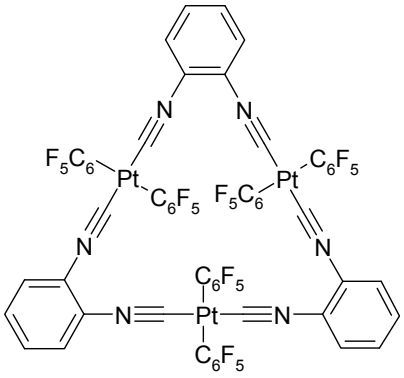

Figure 35: Macrocycle Espinet1

2.4.11 Macrocycles with Bridging Acetylide Ligands

Although the diversity of macrocycles with Pt(II)–acetylide bonds is as vast as for those with Pt–N bonds, there are structural motifs that exist for both types of macrocycles. An important "trick" for the construction of Pt–C macrocycles is the preassembly of Pt(II) corners already bearing the bridging ligands. For example, *Lees et al.* reported the Pt(II)–acetylide square **Lees3** (figure 36), comprising two Pt(II) and two Re(I) corners, in analogy to the Pt–N coordinated hybrid macrocycles **Lees1–2** (p. 43) and **Lees4–5**.[71b] In contrast to the latter, in **Lees3** the Pt(II) moiety bearing the *cis*-connected bridging ligands was assembled first and then reacted with $Re(CO)_5Br$.

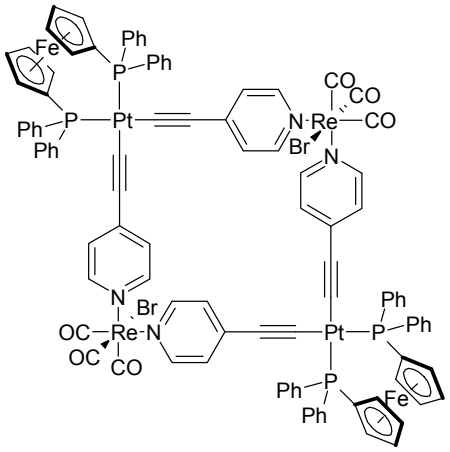

a) Lees3

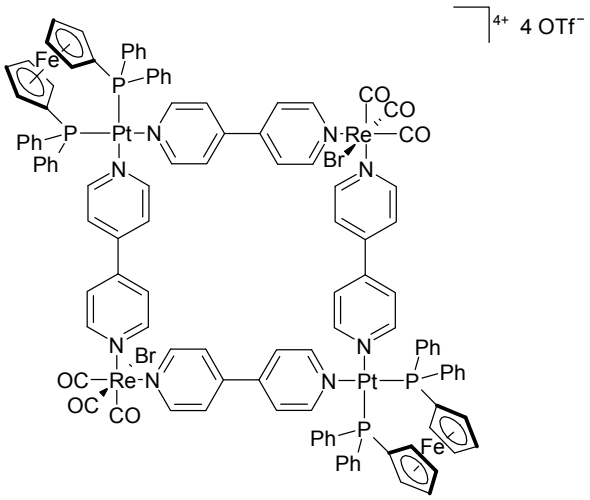

b) Lees4

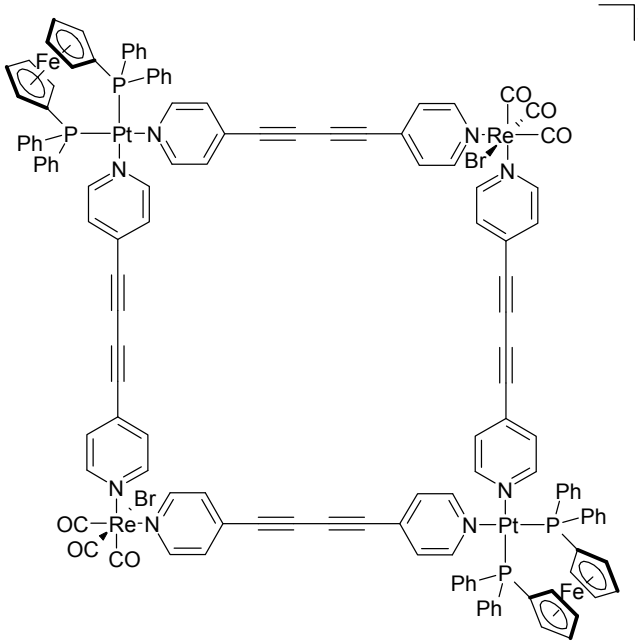

c) Lees5

Figure 36: Macrocycles Lees3–5

The photophysical properties of **Lees3** are different in comparison to the Pt–N bonded counterparts, i.e. the luminescence is quenched. In NMR experiments no evidence for host–guest assemblies of **Lees3–5** with 1,3,5-trimethoxybenzene or aromatic sulfonates could be detected, indicating that no π–π or hydrophobic interactions are operative.

For *Bruce et al.'s* butadiyne-bridged molecular squares **Bruce1** (figure 37), two assemblies of *cis*-Pt(II) with bridging ligands were coupled with the two remaining Pt(II) corners under high dilution conditions in the presence of sodium acetate.[85] Alternative usage of diethylamine resulted in the formation of dialkylammonium–macrocycle adducts, which in mass spectrometric characterisations gave additional peaks. Apparently, a triangular structure with a missing Pt(II)–diphosphine group was formed by reductive elimination. *Bruce et al.* furthermore investigated whether Cu(I) or Ag(I) cations would interact with the acetylide triple bonds in a "tweezer"-like coordination, but a clear proof for such a structure could not be presented.

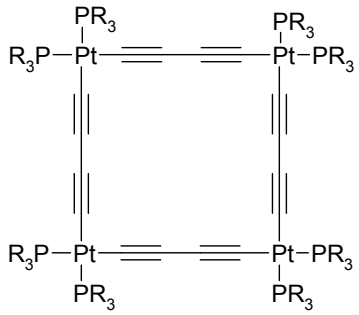

Figure 37: **Macrocycles Bruce1**
Bruce1a: $PR_3 = PEt_3$
Bruce1b: PR_3 = dppe (chelating)
Bruce1c: PR_3 = dppp (chelating)

By copper-catalysed oxidative dimerisation of a *trans*-Pt(II) component with a U-shaped structure bearing terminal acetylene units, *Diederich and coworkers* were able to synthesise molecular square **Diederich2** (figure 38) in 92 % yield.[86] Here, perfect 90° angles are provided by the cross-conjugated (1,1-diethynylene)ethene units. The macrocycle could be characterised by NMR and MALDI TOF mass spectrometry, while FAB-MS led to a complete fragmentation of the molecule.

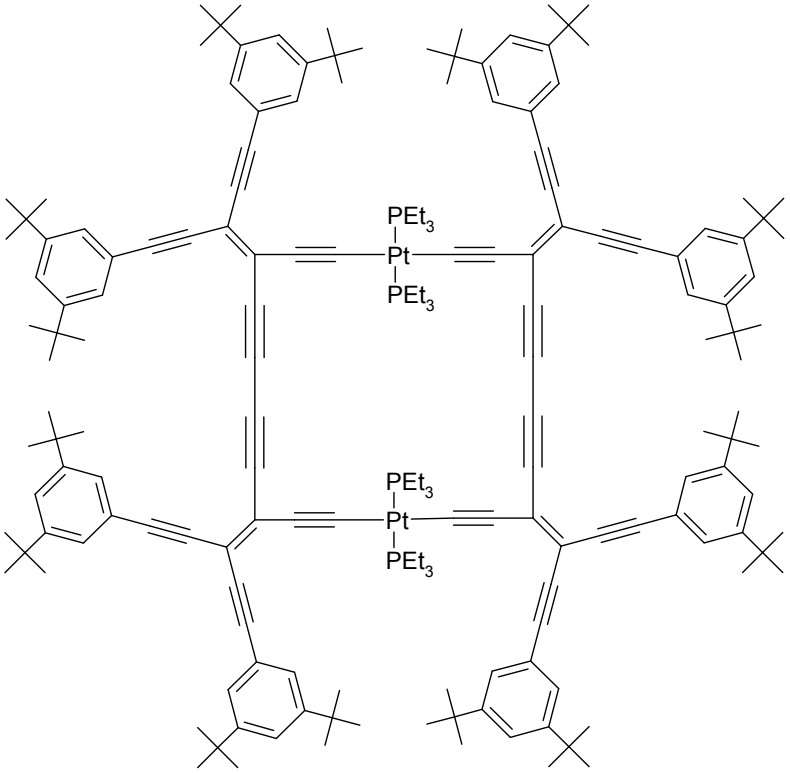

Figure 38: Macrocycle Diederich2

Tessier, Youngs and coworkers used the preassembly approach to build the molecular square **TessierYoungs1** (figure 39).[87a] Therefore, a *cis*-Pt(II)–diphosphine–diacetylide precursor was reacted with *cis*-$Pt(PR_3)_2Cl_2$ in almost quantitative yield. The product was found to be air-stable, but decomposed slowly in halogenated solvents. In contrast, the larger octaplatina-square **TessierYoungs2** (figure 39) was prepared by self-assembly of the Pt(II) corners and spacers consisting of *trans*-Pt(II)–diphosphine–diacetylide.[87a] **TessierYoungs2** represents a most interesting structure comprising four *cis*-arranged and four *trans*-arranged Pt(II)–bisacetylide moieties. Reaction of the macrocycle with an excess of Ag(I) salts gave "tweezer" complexes which contain Ag(I) in ratios of 1:1 to 1:4.

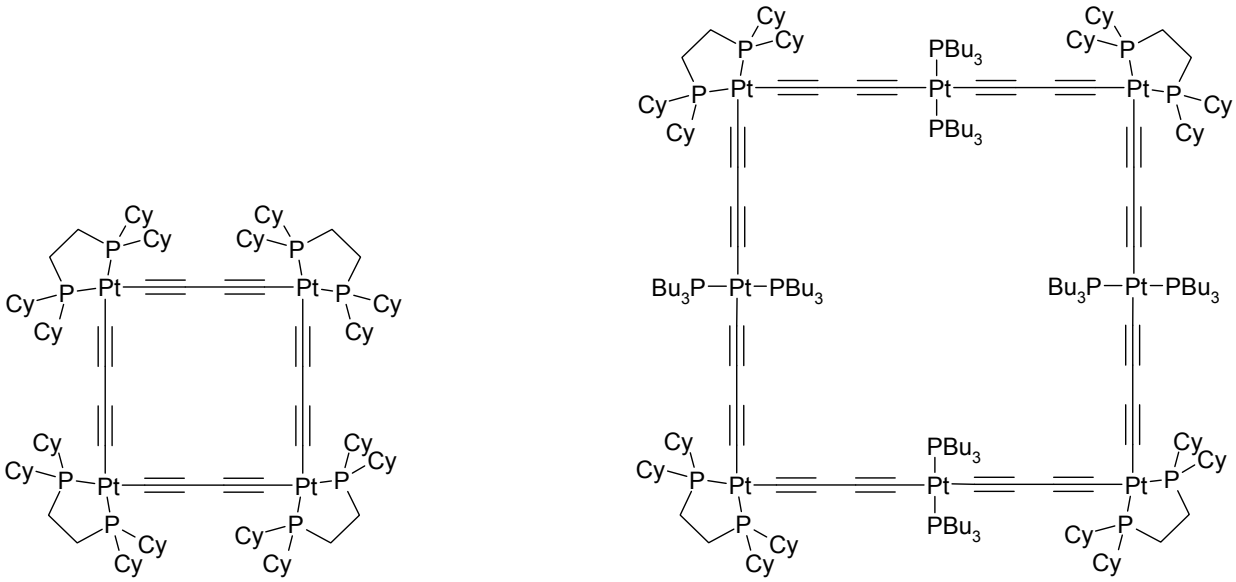

a) TessierYoungs1 **b) TessierYoungs2**

Figure 39: Macrocycles TessierYoungs1 and TessierYoungs2

Further macrocycles prepared by the group of *Tessier and Youngs* take advantage of preformed, almost cyclic fragments with terminal acetylide functions. In the final step, under high dilution conditions and Cu(I) catalysis, these fragments are reacted in good yields with Pt(II) corners to the triangular shaped structures **TessierYoungs3** and **TessierYoungs4** (figure 40).[87c] Due to the high strain of the molecular triangle, the C–Pt–C angles are reduced to 81–83° and the Pt–C–C angles to 170–175°. To further accommodate the strain, the planes spanned by the P–Pt–P (exocyclic ligands) and the C–Pt–C atoms (macrocyclic plane) are distorted against each other by 18°.



a) TessierYoungs3 **b) TessierYoungs4**

Figure 40: Macrocycles TessierYoungs3 and TessierYoungs4

Similarly, the butterfly-like, bicyclic structure **TessierYoungs5a** (scheme 20) was synthesised, in which the Pt(II)–tetraacectylide centre connects two triangular moieties.[87b] Addition of $HgCl_2$ results in the "double-tweezer" complex **TessierYoungs5b** by coordination of two Hg(II) atoms to acetylene units at the outer "pockets", what was deduced from X-ray structure analysis.

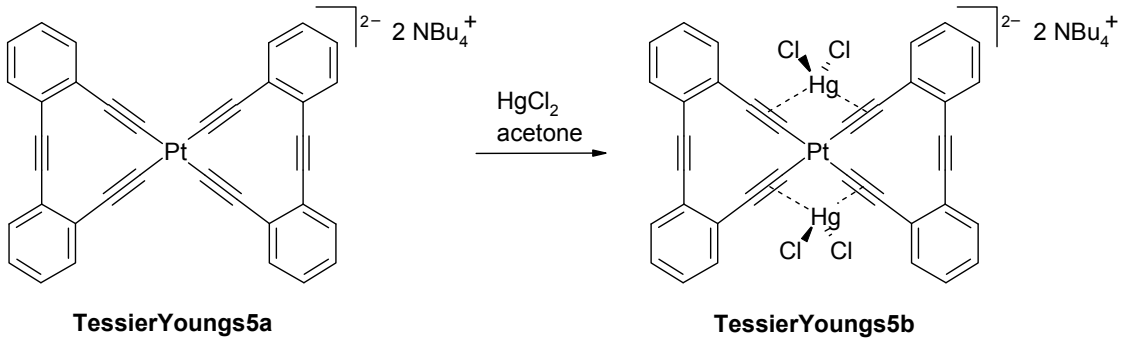

TessierYoungs5a **TessierYoungs5b**

Scheme 20: Macrocycle TessierYoungs5a and conversion to TessierYoungs5b

Haley and coworkers described the synthesis of the triangular monoplatina-macrocycle **Haley2** (figure 41) which, in contrast to **TessierYoungs3**, contains a *trans*-configured Pt(II)–diacetylide fragment in one edge of the triangle.[88a] The synthesis started from a "preoriented" acyclic precursor having triisopropyl–silanyl-protected terminal acetylene groups. After deprotection with base, stannylation and Cu(I)-catalysed transmetallation with a *trans*-Pt(II) diphosphine, the macrocycle was isolated in 65 % yield. Since the insertion of the Pt(II) moiety exerts some strain in the macrocycle, a slight deviation of the square planar Pt(II) geometry from the ideal 180° *trans* coordination and from the plane of the macrocycle was detected by X-ray structure analysis. Compared to the corresponding Pt-free dehydrobenzo[18]annulene, in UV spectra the absorption maximum of **Haley2** exhibits a bathochromic shift. This finding is in contrast to linear systems, where insertion of a *trans*-Pt(II) unit leads to a small hypsochromic shift.[86]

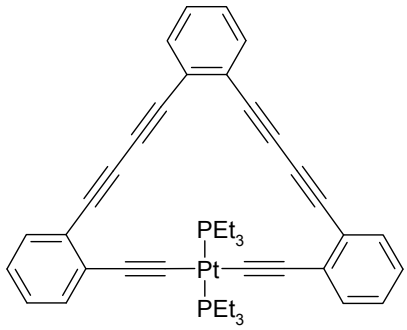

Figure 41: Macrocycle Haley2

In an analogous way *Haley and coworkers* synthesised the corresponding dehydrobenzo-[15]annulene and dehydrobenzo[14]annulene platina-macrocycles **Haley3** (figure 42) and **Haley4** (figure 43).[88b] In **Haley3**, a *trans*-Pt(II)–diphosphine unit was used to close the ring, whereas for **Haley4** ring formation could only be achieved by the use of a *cis*-Pt(II)(dppe) precursor.

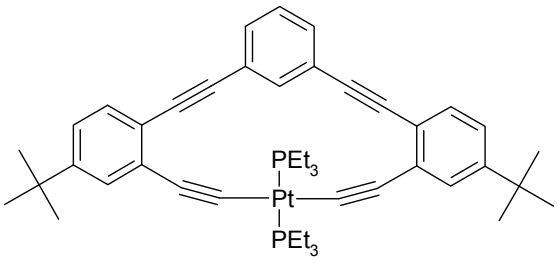

Figure 42: Macrocycle Haley3

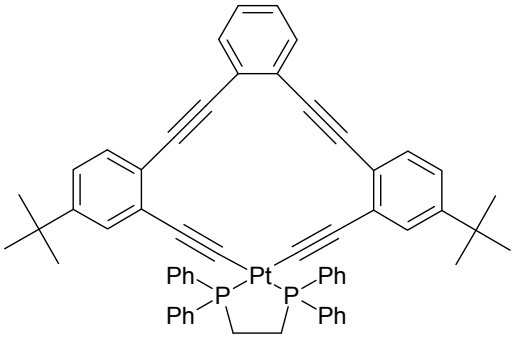

Figure 43: Macrocycle Haley4

Using the same synthetic route, the more complicated "bowtie"-shaped bimacrocycle **Haley5** (figure 44), which contains two *trans*-arranged Pt(II) units, was synthesised in 21 % yield.[88b].

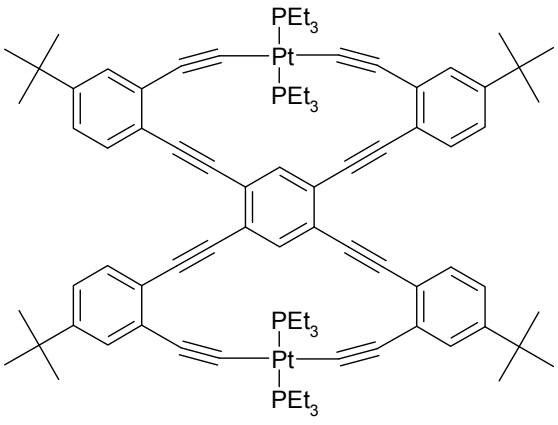

Figure 44: Macrocycle Haley5

Similar to the strained macrocycle **Haley3**, *Bosch et al.* reported the synthesis of the monoplatina-macrocycle **Bosch1** (figure 45), which contains a *meta*-branched pyridyl unit instead of a *meta*-phenylene unit as for **Haley3**.[51] Although a *cis*-Pt(II)–diphosphine precursor was used as starting material, a *trans* configuration at the Pt(II) centre is found in the macrocycle and unequivocally proven by X-ray structure analysis. *Cis*-to-*trans* isomerisations at Pt(II) centres are known and might be induced by the usage of CuI and diethylamine for the cyclisation reaction. In the case of macrocycle **Bosch1**, the isomerisation is dictated by the steric environment of the small dialkyne ligand.

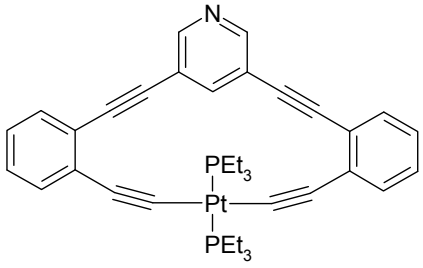

Figure 45: Macrocycle Bosch1

Tykwinski and coworkers used similar structural elements to build up the platina-macrocycles **Tykwinski2a** and **Tykwinski3a** (scheme 21 and scheme 22).[16a,52] 3,5-Diethynylated pyridine and exocyclic (1,1-diethynyl)ethene units as tectons provide curvature, so that ring closure reaction with *trans*-Pt(II) diphosphine effectively gave the monoplatina-cyclyne **Tykwinski2a** in 70 % yield and the bisplatina-hexagon **Tykwinski3a** in 45 % yield. In comparison to the previously described system **Bosch1** (vide infra), metalla-cyclyne **Tykwinski2a** is substantially larger and less strained showing a non-distorted C–Pt–C angle of 178° to 180°. Furthermore, the pyridine unit provides an exocyclic binding site that can react with another Pt(II) complex. While the preparation of macrocycle **Bosch1** included a *cis*-to-*trans* isomerisation at the Pt(II) centre, *Tykwinski and coworkers* showed the very interesting switching of the *trans*-configured Pt(II) macrocycles **Tykwinski2a** and **Tykwinski3a** to the corresponding *cis* systems **Tykwinski2b** and **Tykwinski3b** which were obtained in 87 % and 71 % yield, respectively.[52b] This highly effective ligand exchange reaction is triggered when the *trans* complexes are treated with the chelating ligand 1,2-bis(diphenylphosphino)ethylene (dppee) in dichloromethane. The *cis* complex **Tykwinski2b** shows increased strain, since the Pt(II) moiety bends out of the plane of the macrocycle to retain an 89° C–Pt–C angle, while the Pt–C–C and C–C–C angles are reduced to about 170°. Very recently, this exchange reaction was extended to chiral chelating phosphine ligands, when *trans* macrocycle **Tykwinski2a** was treated with *S*,*S*-Chiraphos to form enantiopure **Tykwinski2c** in 73 %.[52a] In the

same way, **Tykwinsky3a** was reacted with either *R*,*R*- or *S*,*S*-Chiraphos to give the corresponding chiral macrocycles **Tykwinsky3c** in 92 % and 96 % yield, respectively.

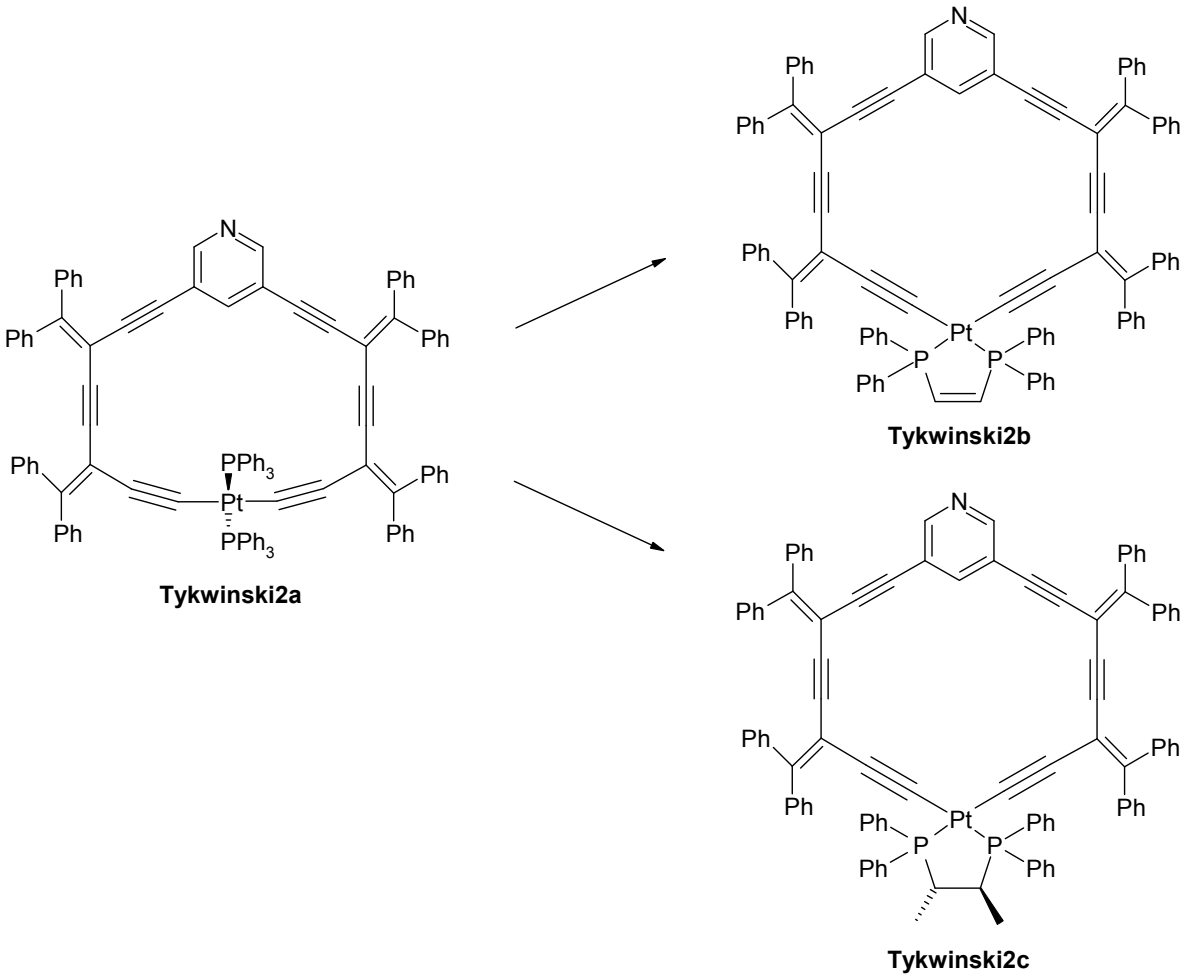

Scheme 21: Macrocycle Tykwinski2a and conversion to Tykwinski2b and Tykwinski2c, respectively

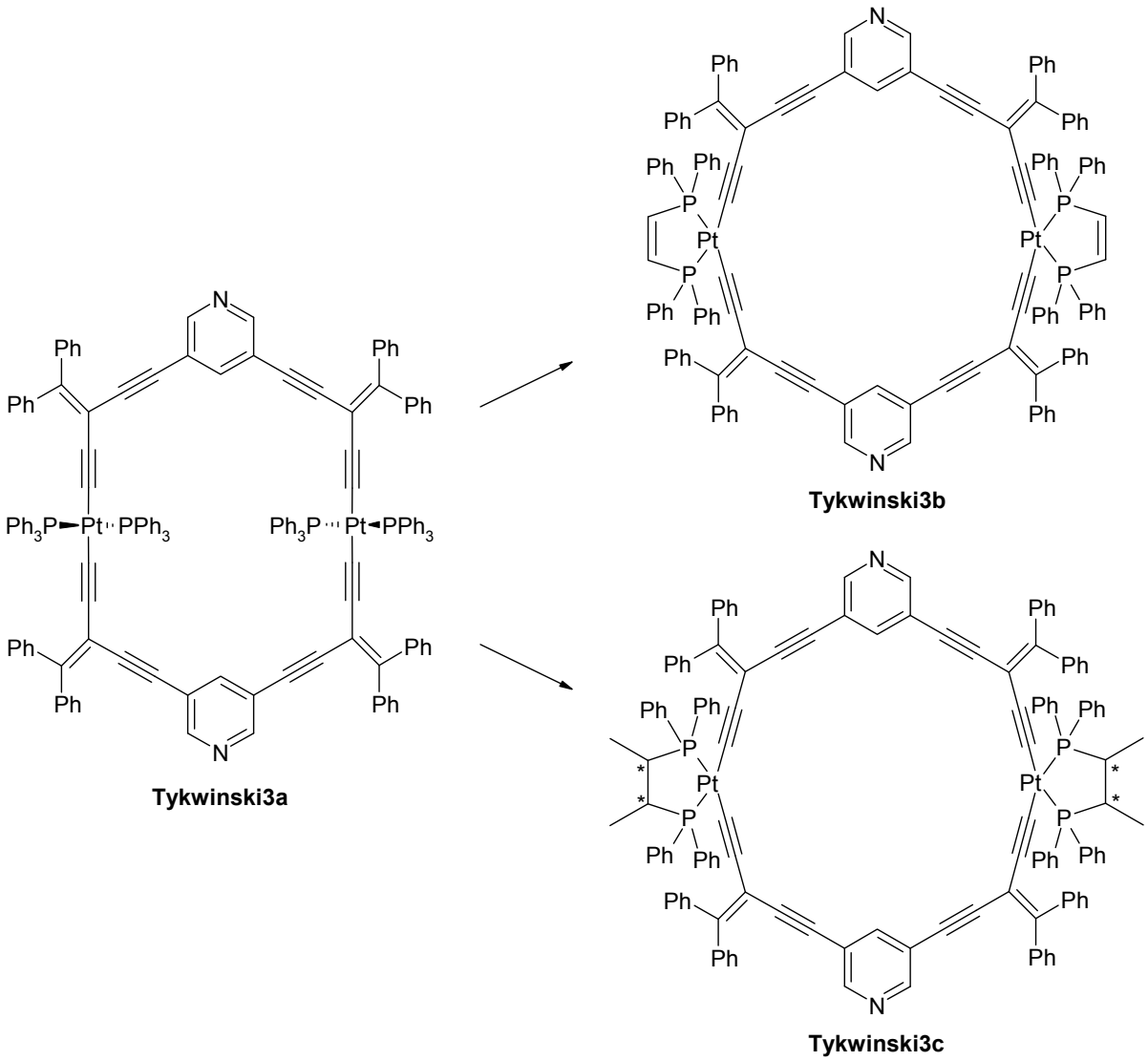

Scheme 22: Macrocycle Tykwinski3a and conversion to Tykwinski3b and Tykwinski3c, respectively

Ligand exchange as the penultimate step bears a major advantage over the use of chiral precursors for macrocycle formation, as both enantiomers are easily accessible from the same macrocyclic precursor compound. CD spectra of the chiral molecules **Tykwinski3c–5c** (scheme 22 to scheme 24) showed that the chirality of the ligand is transducted to the whole macrocycle, caused by an energetically favoured ligand conformation and the resulting steric interaction of the phosphine phenyl groups with the acetylide ligands.[52a] This chiral influence is somewhat reduced for the rather strained macrocycle **Tykwinski3c**, while the fully conjugated chromophore system of **Tykwinski5c** shows the strongest response.

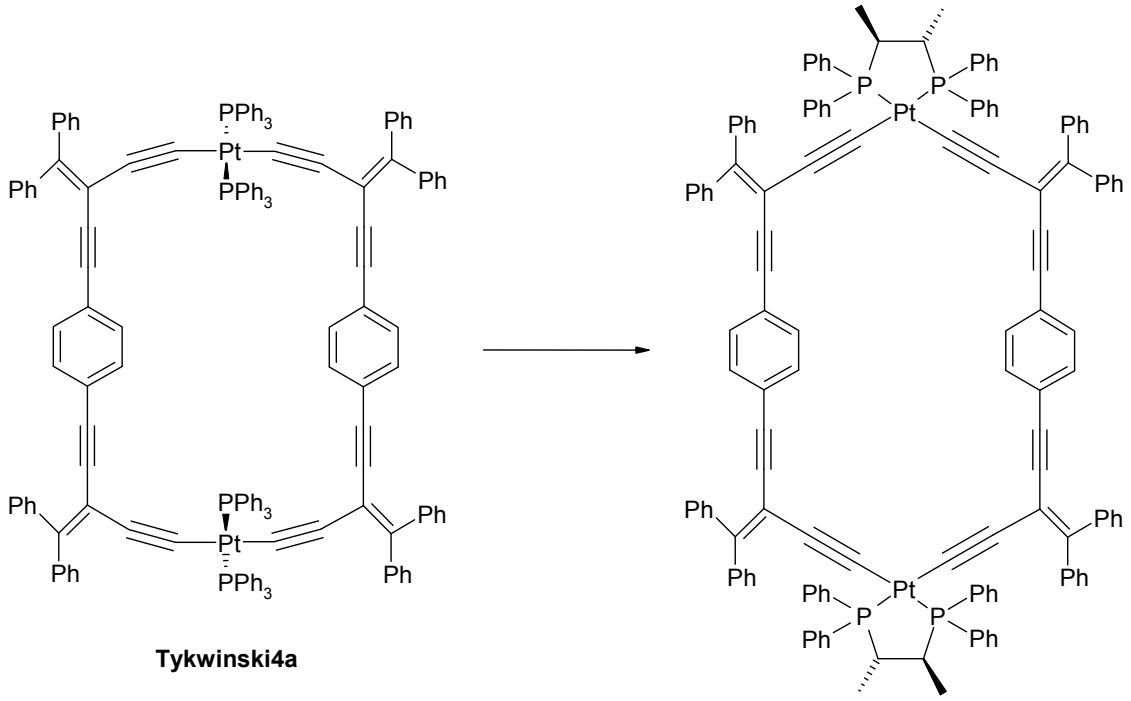
Ph
PPh3
Pt
PPh3
Ph
Ph
Ph

aldehydes with $Ti(O^iPr)_4$ and $ZnEt_2$. The resulting chiral alcohols were obtained with *ee* values higher than 90 %, while catalysis with the free ligand only led to excesses less than 80 %.

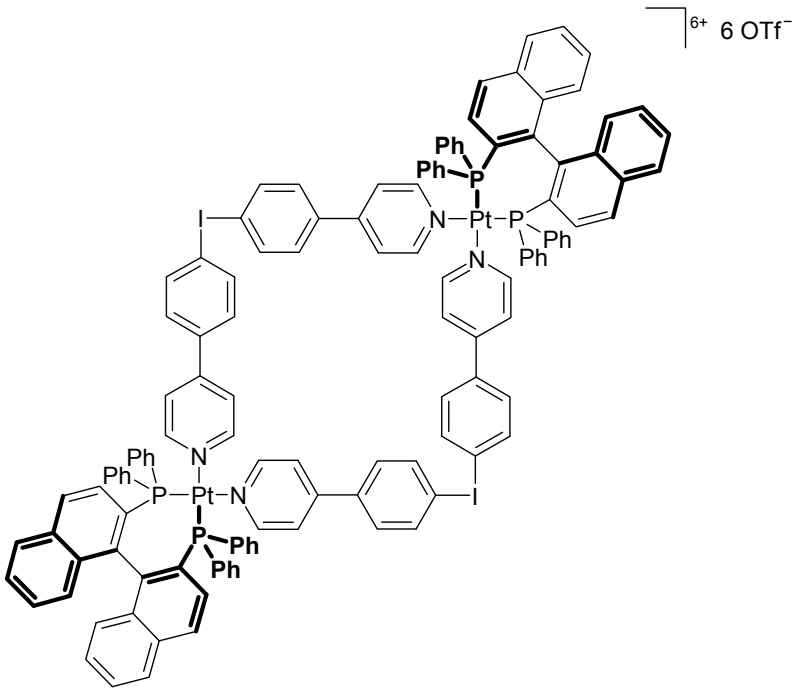

Figure 46: **Macrocycle Stang10**
parts of the structure are marked in bold to depict the chirality of the molecule

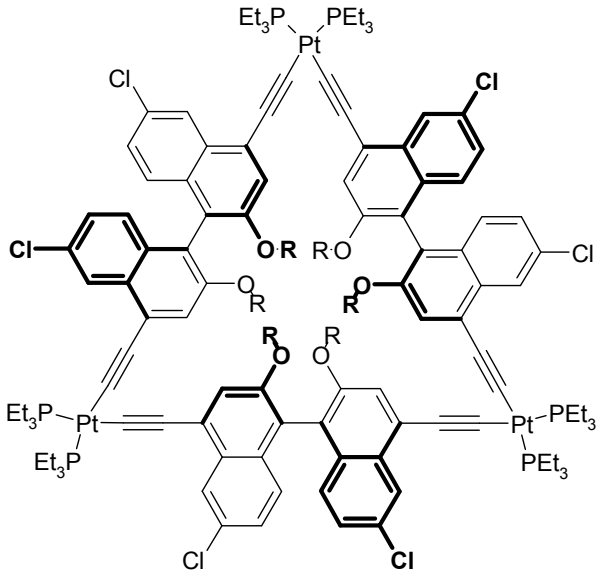

Figure 47: **Macrocycles Lin1**
Lin1a: R = Et;
Lin1b: R = Me;
Lin1c: R = TBDMS;
Lin1d: R = H;
parts of the structure are marked in bold to depict the chirality of the molecule

Alkynyl substitution at the 6,6'-positions of BINOL turned the bridging ligand to a corner building block, which by reaction with a *cis*-Pt(II) diphosphine gave rhomboids **Lin2** (figure 48) in 49–59 % yield.[90c] X-ray structure analysis showed a slightly distorted geometry at the Pt(II) centre comprising C–Pt–C angles from 82.4–101.3°. Similar to **Lin1**, this type of structure was used in a deprotonated form for asymmetric reduction of aldehydes, yielding chiral alcohols with very good *ee* values.

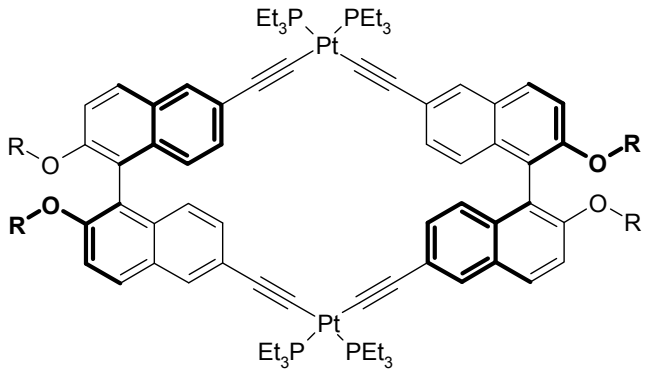

Figure 48: **Macrocycles Lin2**
Lin2a: R = Et;
Lin2b: R = Ac;
Lin2c: R = H;
parts of the structure are marked in bold to depict the chirality of the molecule

3,3'-Bis(alkynyl)-substituted BINOL and *cis*-Pt(II) diphosphine provided the analogous rhomboids **Lin3** (figure 49) in 79–81 % yield.[90a] In this case, deprotonated **Lin3c** was not catalytically active in stereoselective aldehyde reductions due to the steric hindrance around the inwards-pointing hydroxy groups. Therefore, the active Ti–BINOLate complex could not be formed. The reaction of the 3,3'-disubstituted BINOL derivative with *trans*-Pt(II) units resulted in polymers instead of cyclic oligomers.[91]

While the aforementioned substitution patterns at the BINOL moieties in combination with *cis*-Pt(II) precursors resulted in discrete macrocycles, reaction of a 6,6'-disubstituted BINOL with *trans*-Pt(II) yielded a mixture of macrocycles **Lin4** (figure 50), ranging from the cyclotrimer to the cyclooctamer.[90b] The individual macrocycles could be obtained after chromatography in 5–18 % yield. A reason for the statistical formation of various ring sizes might be the flexibility of the dihedral angle at the BINOL building block, which is able to adopt different bite angles and binding vectors without generating much strain.

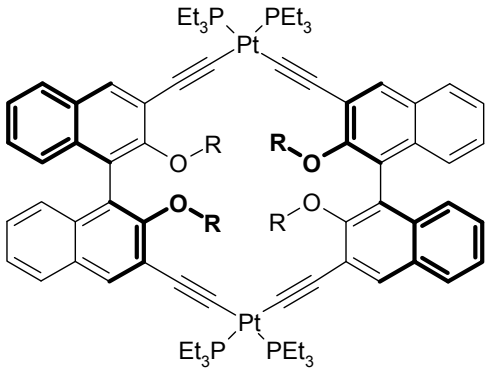

Figure 49: **Macrocycles Lin3**
Lin3a: R = Me;
Lin3b: R = Ac;
Lin3c: R = H;
parts of the structure are marked in bold to depict the chirality of the molecule

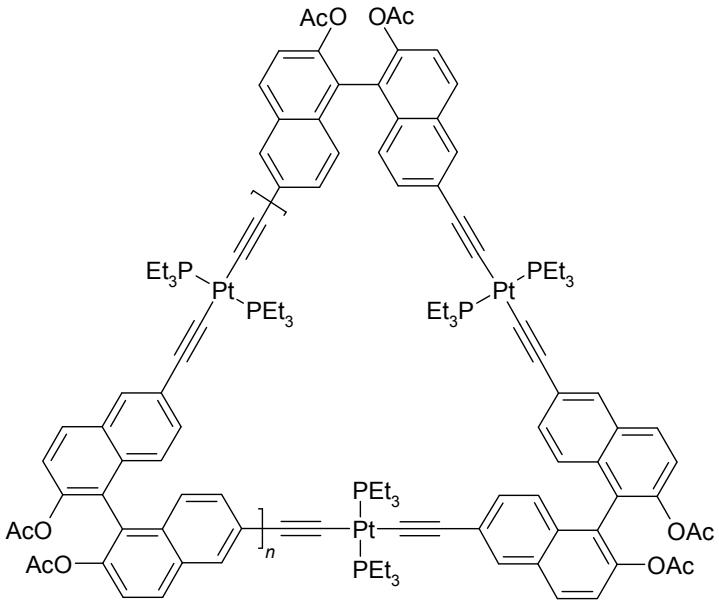

Figure 50: **Macrocycles Lin4**
isolated compounds and yields:
Lin4a (*n* = 1): 5 %
Lin4b (*n* = 2): 18 %
Lin4c (*n* = 3): 16 %
Lin4d (*n* = 4): 10 %
Lin4e (*n* = 5): 5 %
Lin4f (*n* = 6): 4 %

A diethynylated biferrocene was used by *Yamazaki, Haga and coworkers* as a similar non-rigid building block in a Cu(I)-catalysed macrocyclisation with *cis*-Pt(II) diphosphine.[92] Compounds **YamazakiHaga1** (figure 51) form as a mixture of cyclic oligomers ranging from the cyclodimer to the cyclotetramer, which were isolated in rather low yields. Employment of PMe_3 instead of PBu_3 as exocyclic Pt(II) ligands yielded rather selectively the cyclic tetramer in 22 % yield. The X-ray structure analysis of this molecule revealed a rhomboidal geometry comprising two *trans*-Pt(II) moieties and two biferrocenyl units as opposite edges. Electrochemical investigations by cyclic and differential pulse voltammetry revealed only weak interaction and conjugation of the biferrocene units due to the rather insulating character of the Pt(II) spacers.

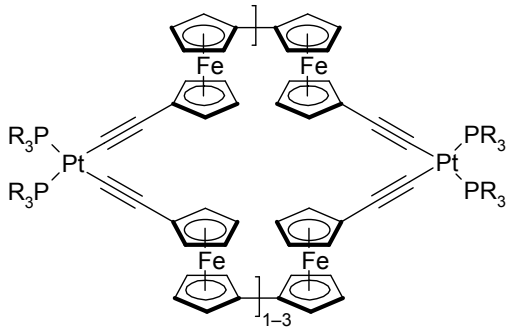

Figure 51: Macrocycles YamazakiHaga1

A series of oligothiophene-containing platina-macrocycles were synthesised by *Bäuerle and coworkers* in excellent yields. Reaction of an α,α'-diethynylated terthiophene with Pt(II)(dppp) units did not give the expected square, but the strained cyclodimer **C[Pt–A–3T(Bu_4)–A]$_2$** (scheme 25) by a four-component self-assembly process in 91 % yield.[27a,29] As has been described more in detail in section 2.3, this cyclodimer subsequently served as a template for an oxidatively induced reductive elimination of the Pt(II) corners with iodine and led to the highly strained and fully conjugated metal-free macrocycle **C[3T(Bu_4)–DA]$_2$** in 54 % yield. Therefore, this novel Pt(II) metal template approach was a major improvement to the former "statistical" route[27e,f,29] and one of the first applications of effectively formed Pt(II) macrocycles as intermediates for the synthesis of conjugated macrocycles.

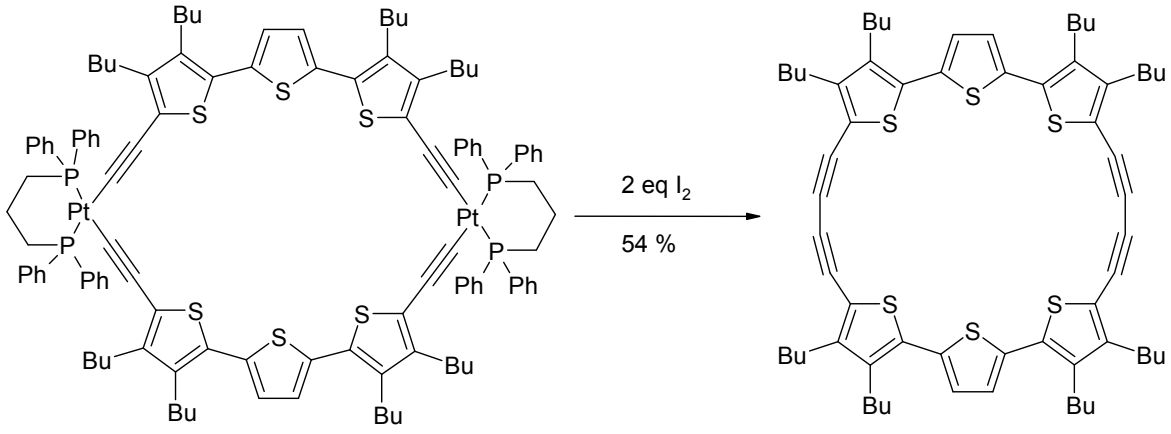

C[Pt–A–3T(Bu$_4$)–A]$_2$ **C[3T(Bu$_4$)–DA]$_2$**

Scheme 25: Macrocycle C[Pt–A–3T(Bu$_4$)–A]$_2$ and reductive elimination to C[3T(Bu$_4$)–DA]$_2$

Meanwhile, in the course of the efforts of the group to work out a generally applicable synthetic protocol for the transition-metal-directed synthesis of diacetylene-bridged macrocycles, differently substituted α,α'-diethynylated terthiophenes were reacted with the Pt(II)(dppp) precursor to give the corresponding Pt(II) cyclodimers **C[Pt–A–3T(Bu$_2$)–A]$_2$** and **C[Pt–A–3T(Dodec$_2$)–A]$_2$** in 86 % and 80 % yield, respectively (figure 52).[27b,93]

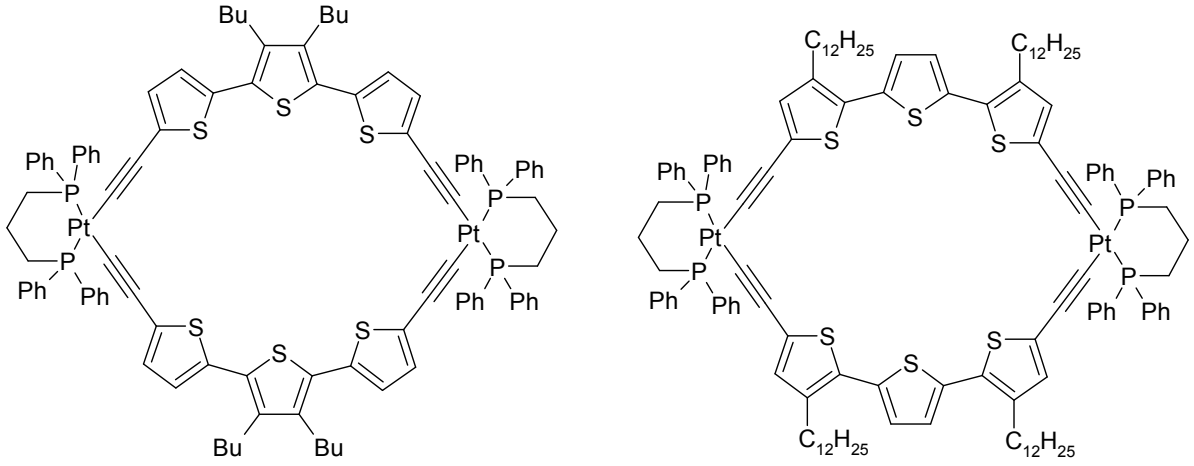

a) C[Pt–A–3T(Bu$_2$)–A]$_2$ **b) C[Pt–A–3T(Dodec$_2$)–A]$_2$**

Figure 52: Terthienylene macrocycles with substitution patterns other than (Bu$_4$)

Furthermore, the length of the bridging oligothiophene unit could be extended to a quater-, quinque- and septithiophene, yielding platina-macrocycles **C[Pt–A–4T(Dodec$_2$)–A]$_2$**, **C[Pt–A–5T(Bu$_6$)–A]$_2$** and **C[Pt–A–7T(Bu$_8$)–A]$_2$** in 80–86 % yield (figure 53).[27b,93]

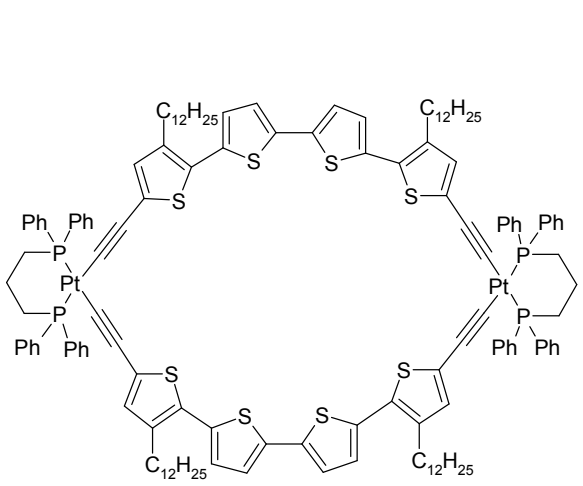

a) C[Pt–A–4T(Dodec$_2$)–A]$_2$

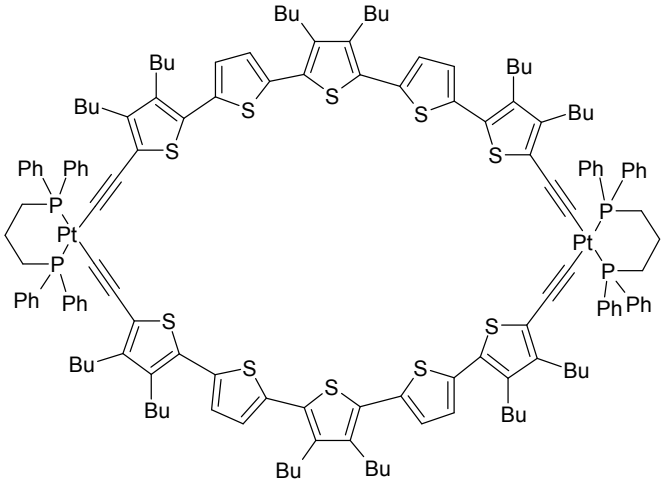

b) C[Pt–A–5T(Bu$_6$)–A]$_2$

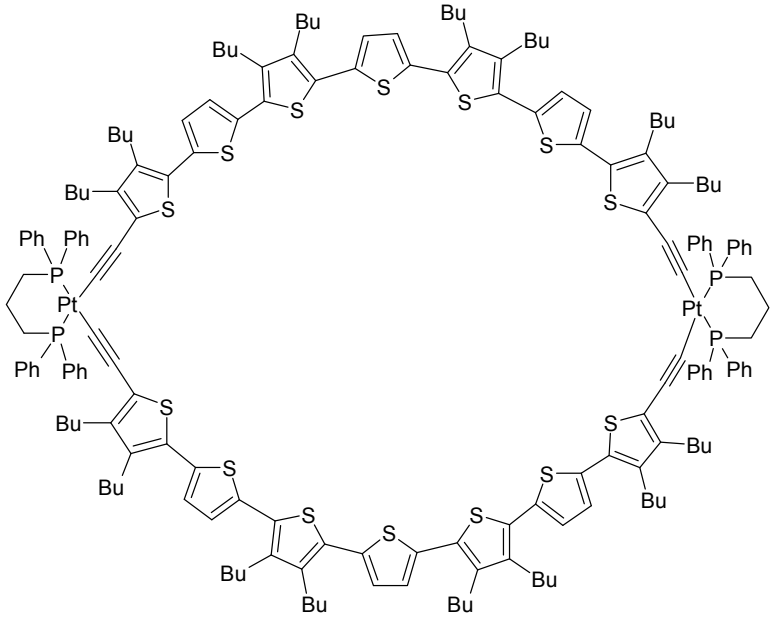

c) C[Pt–A–7T(Bu$_8$)–A]$_2$

Figure 53: Pt(II) macrocycles with longer oligothienylene moieties

The broad applicability of the metal-template approach was further shown by the synthesis of the monoplatina-macrocycles **C[Pt–A–*n*T(Bu$_{n+1}$)–phen–*n*T(Bu$_{n+1}$)–A]** (with $n = 1, 2$) and **C[Pt–A–4T(Bu$_4$)–phen–4T(Bu$_4$)–A]**, in which a Pt(II)(dppp)–diacetylide corner is connected to a bent bis(oligothienyl)phenanthroline unit (figure 54).[27b,94] Good yields of 70 % are obtained only in the case of the terthienyl derivative, whereas the corresponding longer quater- and quinquethiophenes — probably due to unfavourable conformations of the precursor molecules for the macrocyclisation process — only lead to low yields of 23 % and 9 %.

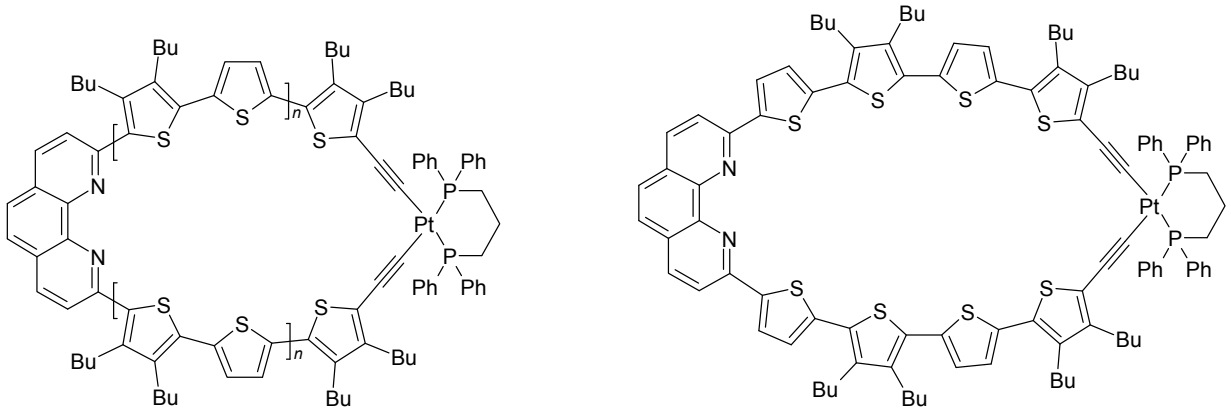

a) C[Pt–A–3T(Bu$_4$)–phen–3T(Bu$_4$)–A] (n = 1) and **C[Pt–A–5T(Bu$_6$)–phen–5T(Bu$_6$)–A]** (n = 2)

b) C[Pt–A–4T(Bu$_4$)–phen–4T(Bu$_4$)–A]

Figure 54: Pt(II) macrocycles comprising phenanthroline moieties

With respect to the subsequent elimination reaction that is applied to this type of platina-macrocycles to form the conjugated macrocycles, *Bäuerle and coworkers* also varied the bite angle at the Pt(II) corner by using bidentate phosphine ligands other than dppp which opens an angle of 91°. Dppm and dppf span extreme angles of 72° and 108°, respectively, are well tolerated and gave platina-macrocycles **C[Pt(dppm)–A–3T(Dodec$_2$)–A]$_2$** and **C[Pt(dppf)–A–3T(Dodec$_2$)–A]$_2$** in 80–85 % yield (figure 55).[95]

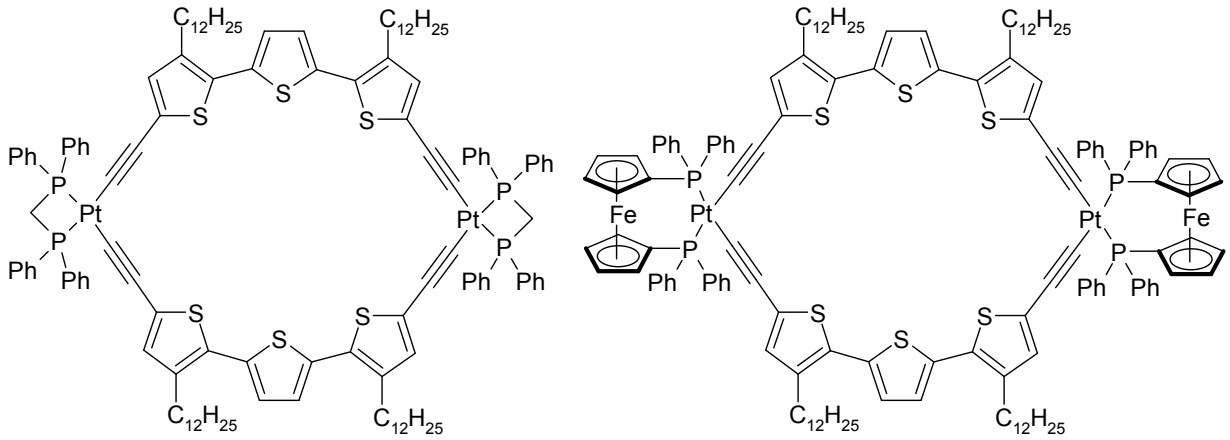

a) C[Pt(dppm)–A–3T(Dodec$_2$)–A]$_2$

b) C[Pt(dppf)–A–3T(Dodec$_2$)–A]$_2$

Figure 55: Terthienylene macrocycles with ligands other than dppp at the metal centre

Haley and coworkers synthesised the monoplatina-macrocycle **Haley6**; however in this case, reductive elimination to conjugated macrocycle **Haley7** was not successful, as the still-unknown **Haley7** would probably bear too much strain (scheme 26).[7f]

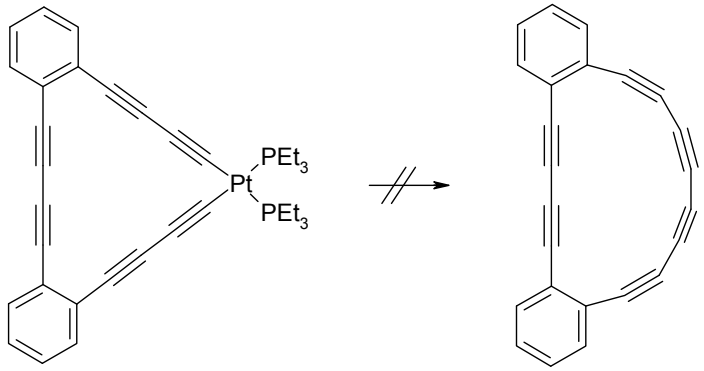

Haley6 **Haley7**

Scheme 26: Attempted route to obtain macrocycle Haley6 from Haley7

2.4.12 Macrocycles by Pt–P Coordination

Although they are commonly used as exocyclic ligands for Pt(II), phosphines are not that often used as bridging ligands for platina-macrocycles. One reason for this might be the lack of rigidity of the phosphine-containing macrocycles, as rotation around the Pt(II)–P bond is easily possible. More flexible spacers, though, make a directional-bond approach to macrocycles tedious or even impossible, and result in structures that are not shape-persistent. Nevertheless, the geometric behaviour of Pt(II) compounds is often controlled by diphosphine ligands, and a lot of work has been devoted to the field of Pt(II)–diphosphine complexes. For example, *Bessel, Takeuchi et al.* reviewed *trans*-spanning diphosphine ligands, giving a very detailed picture of research in this area.[96] Here, only a few examples will be discussed.

Gladysz et al. achieved the cyclisation to a *trans*-Pt(II)–diphosphane macrocycle by first preparing an acyclic Pt(II) precursor with two phosphine moieties in *trans* position. The alkene end-groups of the phosphine ligands were then linked by an intramolecular metathesis cyclisation to form macrocycles **Gladysz1–4** (figure 56) as mixture of *E* and *Z* isomers in typically 78 % yield.[97b,e] The macrocycles were subsequently hydrogenated over Pd/C to remove the double bond in ca. 54 % yield.

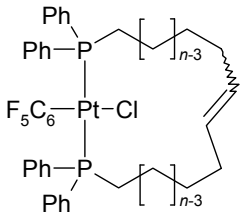

Figure 56: Macrocycles Gladysz1–4
Gladysz1: $n = 4$
Gladysz2: $n = 6$
Gladysz3: $n = 8$
Gladysz4: $n = 9$
the zigzag bond indicates the possibility of both *cis* or *trans* configuration at the double bond

Using the same method with a precursor carrying four alkene groups, the bimacrocyclic system **Gladysz5** (figure 57) could be obtained after hydrogenation in moderate yield as a mixture of *syn* (31 %) and *anti* (7 %) isomers (regarding the two phosphine phenyl groups).[97a,e] Shorter alkyl chains at such a precursor complex, however, mainly resulted in products with separate rings on each side of the Pt atom.

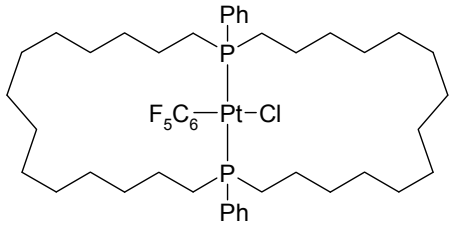

Figure 57: Macrocycle Gladysz5

More recently, this strategy was extended to prepare *trans*-Pt(II)–diphosphane macrocycle **Gladysz6** (figure 58) by alkyne metathesis.[97c] Hydrogenation of the alkyne moiety with Pd/C and hydrogen led, in 87 % yield, to the same saturated product as hydrogenation of **Gladysz2**.

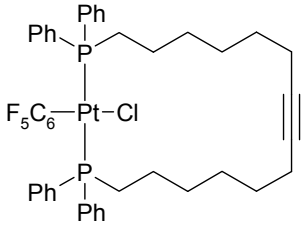

Figure 58: Macrocycle Gladysz6

When *cis*-configured Pt(II) precursors are used instead of *trans*-Pt(II) complexes, monoplatina- and bisplatina-macrocycles **Gladysz7a/7b** (scheme 27) are formed in equilibrium and seem to interconvert having the equilibrium on the side of the cyclic monomer **Gladysz7a**.[97b]

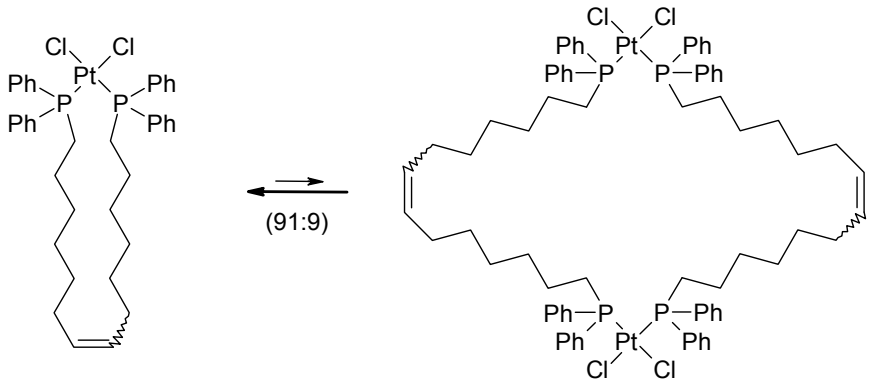

Gladysz7a **Gladysz7b**

Scheme 27: Equilibrium between cyclic monomer Gladysz7a and cyclic dimer Gladysz7b

A directional bond formation strategy was elaborated by *Faraone et al.* Upon mixing diphosphinito ligands in a 1:1 ratio with Pt(COD)I_2, the cyclic dimers **Faraone1a/b** (figure 59) precipitate from the solution.[98] From X-ray structure analysis the authors concluded that the cavity of the macrocycles, with critical interatomic distances of ca. 4 Å, is too small to allow binding of even small guest molecules. While cyclic trimers or tetramers would certainly increase the chances of establishing host–guest chemistry, formation of such species was not observed. The preference of the cyclodimer over larger cyclooligomers is assumed to be due to both the geometry of the ligands and the strong Pt–P bonds.

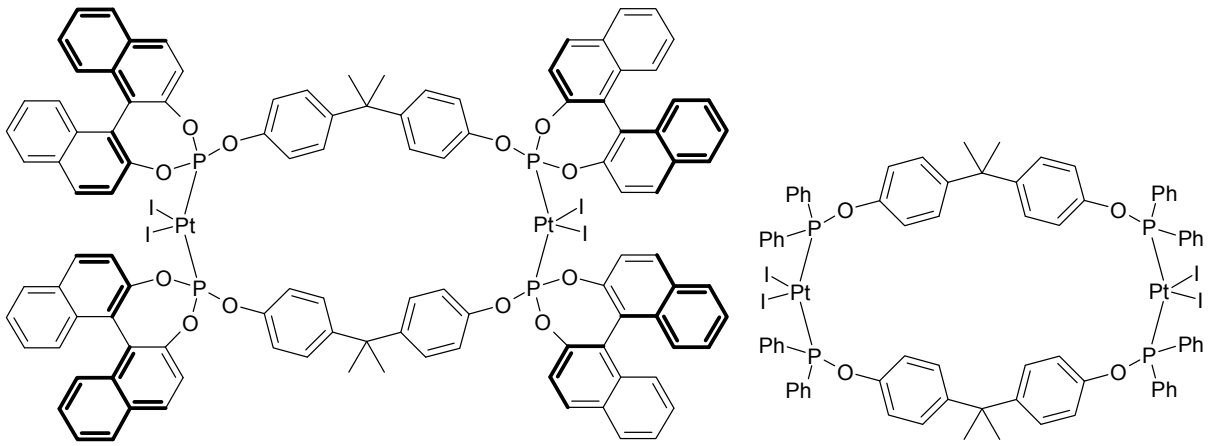

a) Faraone1a **b) Faraone1b**

Figure 59: Macrocycles Faraone1a and Faraone1b
parts of structure a) are marked in bold to depict chiral moieties

By starting with a 2,2'-bipyridyl-containing diphosphine ligand, *Lindner and coworkers* introduced functionality in terms of endotopic binding sites to their macrocycles. Although the diplatina-macrocycles **Lindner1a/1b** (figure 60) are formed in only 20–23 % yield, their solubility was much higher than that of a corresponding cyclodimer comprising longer alkyl spacers and chlorine substituents at the Pt(II) corners, which forms in excellent yields under high-dilution conditions (not shown here).[99] After addition of $[Cu(CH_3CN)_4][BF_4]$ to **Lindner1a**, the trismetallated Pt(II)–Cu(I)–Pt(II) complex **Lindner1c** (figure 60) could be obtained in good yields. This macrocyclic system should exhibit a "figure-eight"-conformation due to the tetrahedral coordination of Cu(I) and the bipyridine bridging ligands.

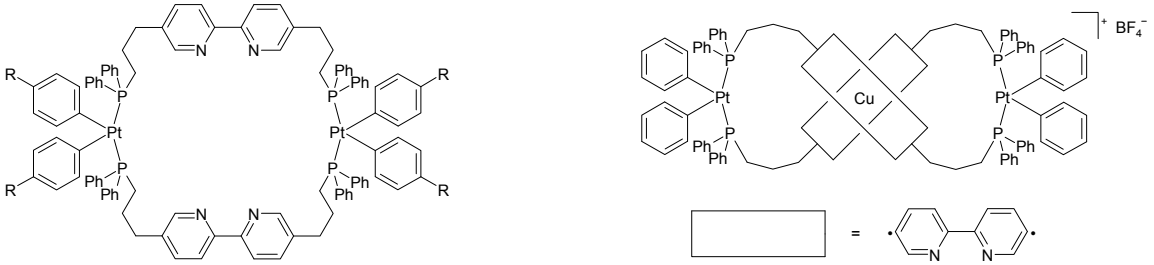

a) Lindner1a/1b
Lindner1a: R = H
Lindner1b: R = *t*-Bu

b) Lindner1c

Figure 60: Macrocycles Lindner1a/1b and the resulting mixed metalla-macrocycle Lindner1c

A more rigid system has been prepared by *Manners and coworkers* by using a linear phosphinoacetylene ligand. Thus, the reaction of a 1,4-diethynylbenzene-based diphosphine and K_2PtCl_4 selectively gave the trisplatina-triangle **Manners1** (scheme 28) in quantitative yield.[100] The macrocycle is strained, what is indicated by the X-ray structure that showed dihedral angles of 59–69° between the P–C–C moieties. Addition of KI to **Manners1** in a 1:1:1 mixture of chloroform, dichloromethane and acetonitrile resulted in a cyclisation reaction and a rearrangement, providing the triangle **Manners2** which comprises helical chirality.

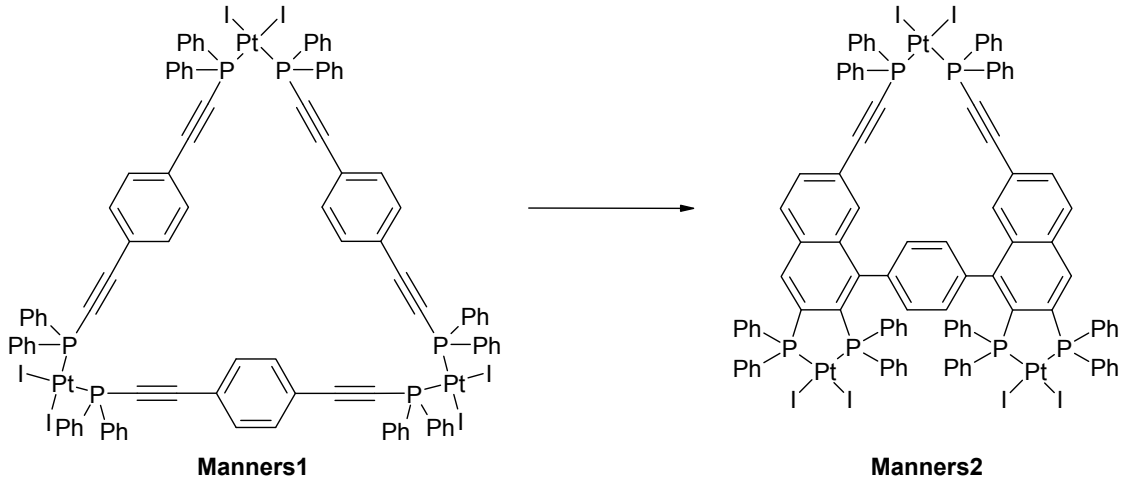

Scheme 28: Macrocycle Manners1 and conversion to Manners2

Interestingly, by the use of shorter diphosphinoalkynyl ligands, cyclodimers are formed in high yields, as presented in the hexagons **ForniésLalinde4** (figure 61) reported by *Forniés, Lalinde et al.*[101]

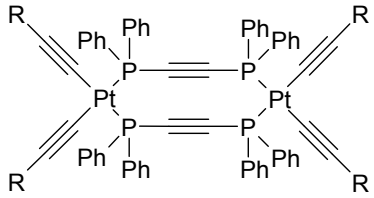

Figure 61: Macrocycles ForniésLalinde4
R = *t*-Bu or Ph

This type of structure has been known for a longer time; and a variety of corresponding dinuclear Pt(II) cycles with other diphosphine ligands is known.[102] Early work on 1,2-bis(diphenylphosphino)methane (dppm) bridged compounds is, e.g., summarised in a review by *Puddephatt*.[103] Although these complexes sometimes are named "macrocyclic", the expression "macrochelate" would be more appropriate (cf. section 2.4.6).

2.4.13 Macrocycles by Unusual Pt(II) Coordination

Bonds between the soft metal Pt(II) and hard oxygen atoms are considered to be rather instable.[104,105] Only very recently, *Mukherjee, Stang et al.* reported for the first time Pt(II) macrocycles with Pt–O coordinated bridging ligands. E.g., reaction of a bis-Pt(II)–phenanthrenyl precursor with various dicarboxylates in aqueous acetone resulted almost quantitatively in macrocycles **MukherjeeStang1–4** (figure 62).[104a]

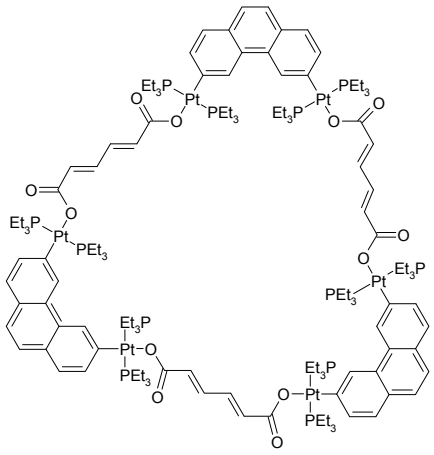

a) MukherjeeStang1

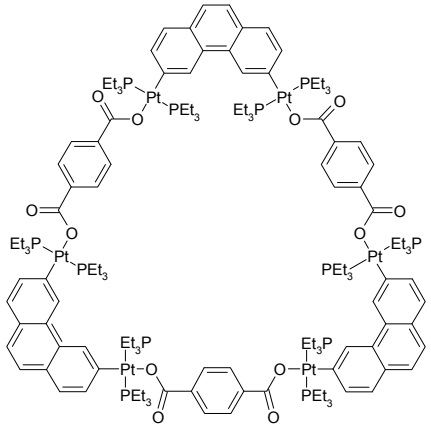

b) MukherjeeStang2

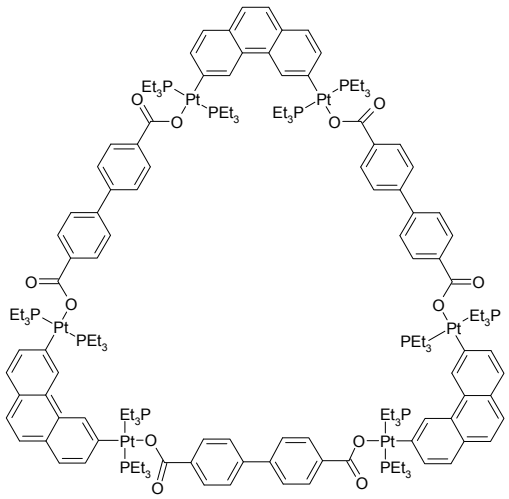

c) MukherjeeStang3

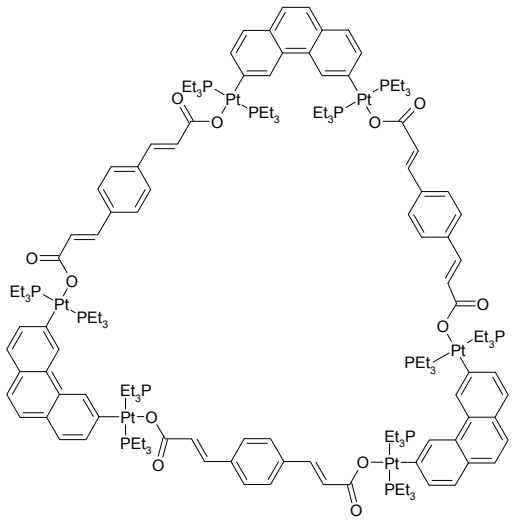

d) MukherjeeStang4

Figure 62: Macrocycles MukherjeeStang1–4

More generally speaking, the concept of directional bonding was shown to work very effectively for Pt–O bound macrocycles: reaction of the 60° bis-Pt(II)–phenanthrenyl precursor with linear or quasi-linear bridging ligands resulted in the triangularly shaped systems **MukherjeeStang1–4**. The same bis-Pt(II) tecton reacted with a dicarboxylate, which spanned a 120° angle, to yield the rhomboids **MukherjeeStang5–6** (figure 63).[104a] In contrast, the U-shaped bis-Pt(II)–anthracenyl "clamps" formed rectangles **MukherjeeStang7–11** (figure 64)[104] by reaction with linear or quasi-linear ligands. The structures of these macrocycles have been confirmed by X-ray structure analysis. Interestingly, only few of these molecules form stacks with cavities or channels in the solid state, while this is quite common for nitrogen bonded macrocycles.

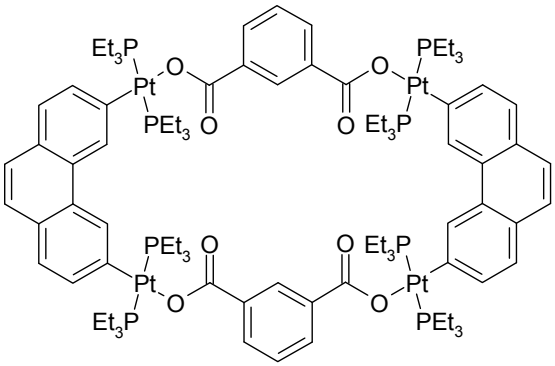

a) MukherjeeStang5

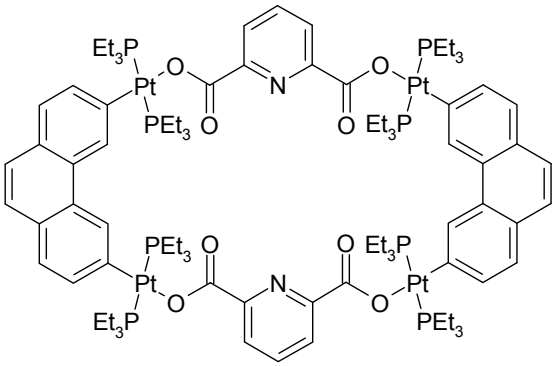

b) MukherjeeStang6

Figure 63: Macrocycles MukherjeeStang5–6

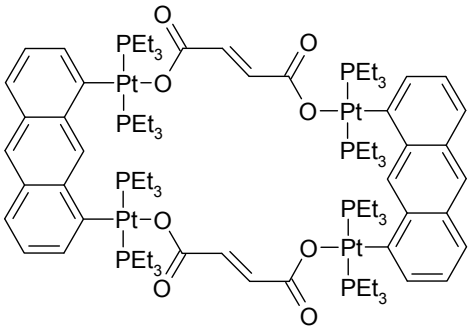

a) MukherjeeStang7

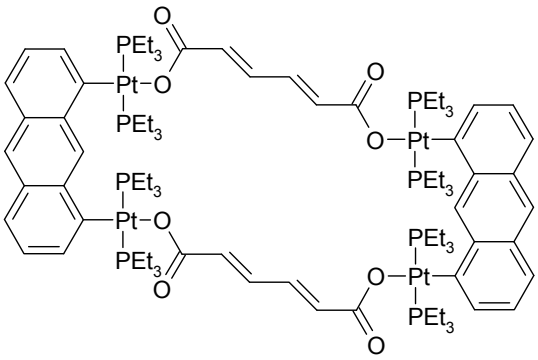

b) MukherjeeStang8

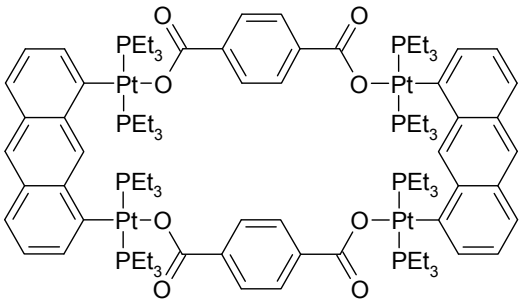

c) MukherjeeStang9

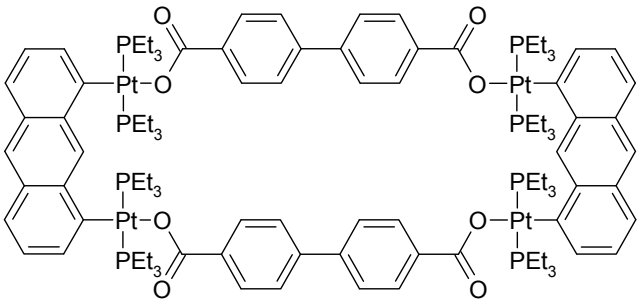

d) MukherjeeStang10

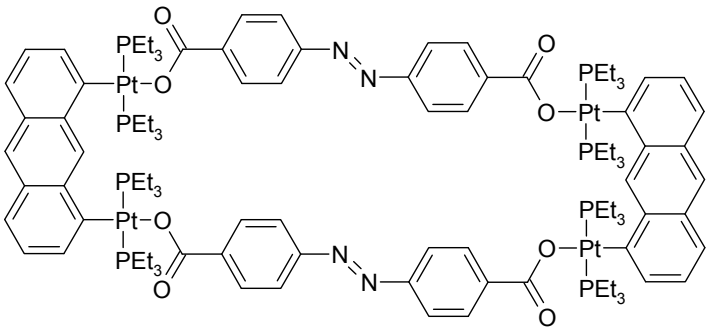

e) MukherjeeStang11

Figure 64: Macrocycles MukherjeeStang7–11

Hor and coworkers presented the Pt(II) square **Hor1** (figure 65) in which the Pt(II) corners are bound to the N and O atoms of isonicotinic acid.[106] For the reaction, a bis-Pt(II)–bithienyl precursor was used, which reacted upon mixture with isonicotinic acid to the C_4-symmetric macrocycle **Hor1**, releasing 2,2'-bithiophene. In contrast to the macrocycle **Dunbar1** (cf. section 2.4.7), the oxygen atom of the C=O moiety is not involved in a coordinative bond.

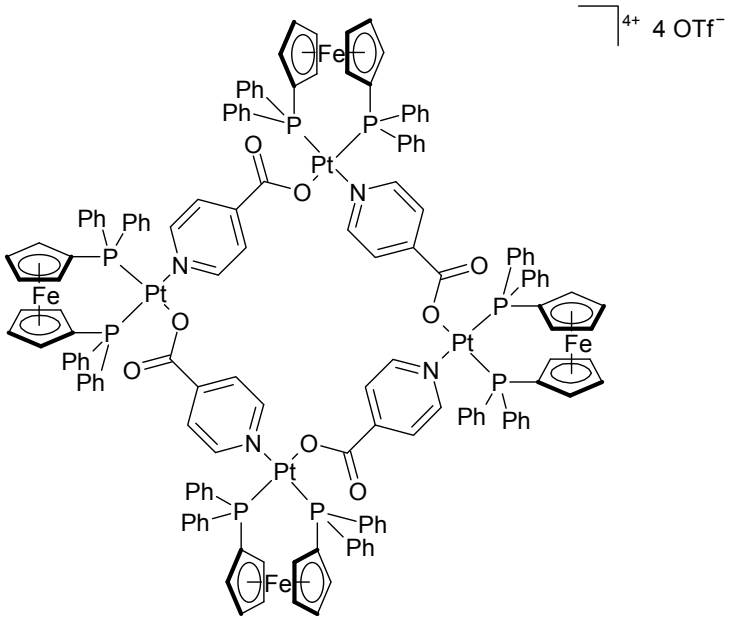

Figure 65: Macrocycle Hor1

Using the same metathesis strategy as for the phosphine macrocycles, *Gladysz and coworkers* synthesised the sulphur-coordinated cycles **Gladysz8a** and **Gladysz8b** (figure 66) which could be obtained in 55 % and 24 % yield, respectively.[97d] Unlike the macrocycles **Gladysz7a/7b**, these two forms did not interconvert. *tert*-Butyl substitution at the sulphur suppressed the formation of dinuclear cycles.

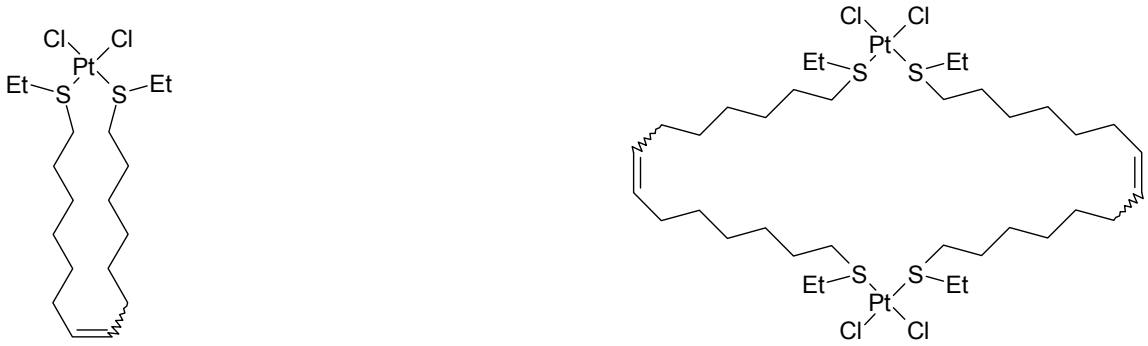

a) Gladysz8a **b) Gladysz8b**

Figure 66: Cyclic monomer Gladysz8a and dimeric byproduct Gladysz8b
the zigzag bonds indicates the possibility of both *cis* or *trans* configuration at the double bond

2.4.14 Concluding Remarks on Pt(II) Macrocycles

In the previous sections, an overview of the state-of-the-art in the use of Pt(II) moieties in macrocyclic and topological chemistry was given. The many examples show that a lot of very creative work has already been done in this strongly growing field.

However, some closely related aspects should be stressed at this point. Many reports on the formation of Pt(II) macrocycles are in conjunction with corresponding Pd(II) compounds; therefore by comparison one general conclusion can be drawn: the Pd(II) analogues possess weaker bonds and are therefore prone to undergo equilibration. Because of this feature, it is easier to build up 3D structures or to achieve the thermodynamically most stable product with Pd(II) precursors instead of Pt(II) building blocks, where bond formation is less reversible and, hence, unwanted side products are much more probable. *Fujita et al.* reported the equilibrium between the strain-free square assemblies **Fujita2a–5a** — the Pd analogues of **Fujita1** (cf. section 2.4.7) — and the entropically favoured triangles **Fujita2b–5b** (scheme 29).[107] The ratio between these two forms can be adjusted even at room temperature by simply varying the concentration, whereas the Pt(II) square **Fujita1** is completely stable. If acetylides are reacted with Pd(II), very often only the C–C coupling product is observed, because elimination from the Pd–bisacetylide complex is very fast, which is in contrast to the corresponding isolable Pt complexes.[108]

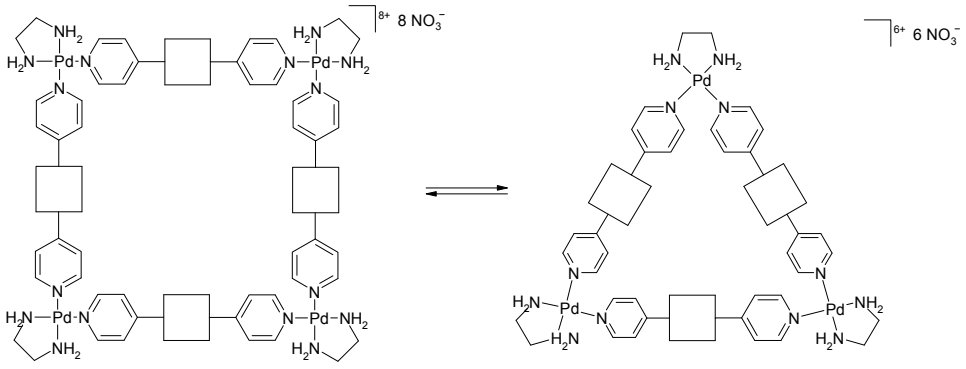

Fujita2a–5a **Fujita2b–5b**

Scheme 29: Equilibrium between squared Pd(II) macrocycles Fujita6a–9a and their triangular forms Fujita2b–5b

Fujita2a/b: □ = ·≡·

Fujita3a/b: □ = ·⁄⁄·

Fujita4a/b: □ = ·≡—≡·

Fujita5a/b: □ = ·⬡·

The coordination patterns for Pt(II), especially coordination to acetylides, are also seen in a number of linear structures. Pt(II) has been incorporated into a number of molecular wires, polymers and networks. The interest thereby is mainly in the electronic nature and conductivity of these compounds and the change upon the addition of Pt. Although they are not part of this chapter, their structures are often closely related to the discussed macrocycles.

In summary, the increasing number of Pt(II) macrocycles shows that Pt(II) is a very valuable building block for macrocyclic and topological chemistry. Its major advantages are good stability towards air and moisture, especially compared to the Pd(II) analogues, the usually good to excellent yields in formation, and the applicability both as a 90° and 180° construction element with which the directional synthesis of a specific structure (e.g. a molecular square) can be achieved. Beyond this, Pt(II) can act as a building block for more sophisticated 3D structures, and function as a template for the synthesis of strained conjugated macrocycles and even catenanes.[see, e.g., 45,94,109,110]

3 Synthesis of Aryl-Substituted Oligothienyl Macrocycles

3.1 Synthesis of Phenyl-Substituted Precursors

3.1.1 Choice of the Thiophene Substitution Pattern

While previous attempts to synthesise oligothienyl macrocycles employed alkyl-substituted oligothiophenes (as described in sections 2.2 and 2.3), here, a terthiophene with phenyl rings at the 3- and 4-positions of the terminal thiophenes was chosen as the acyclic building block (scheme 30).

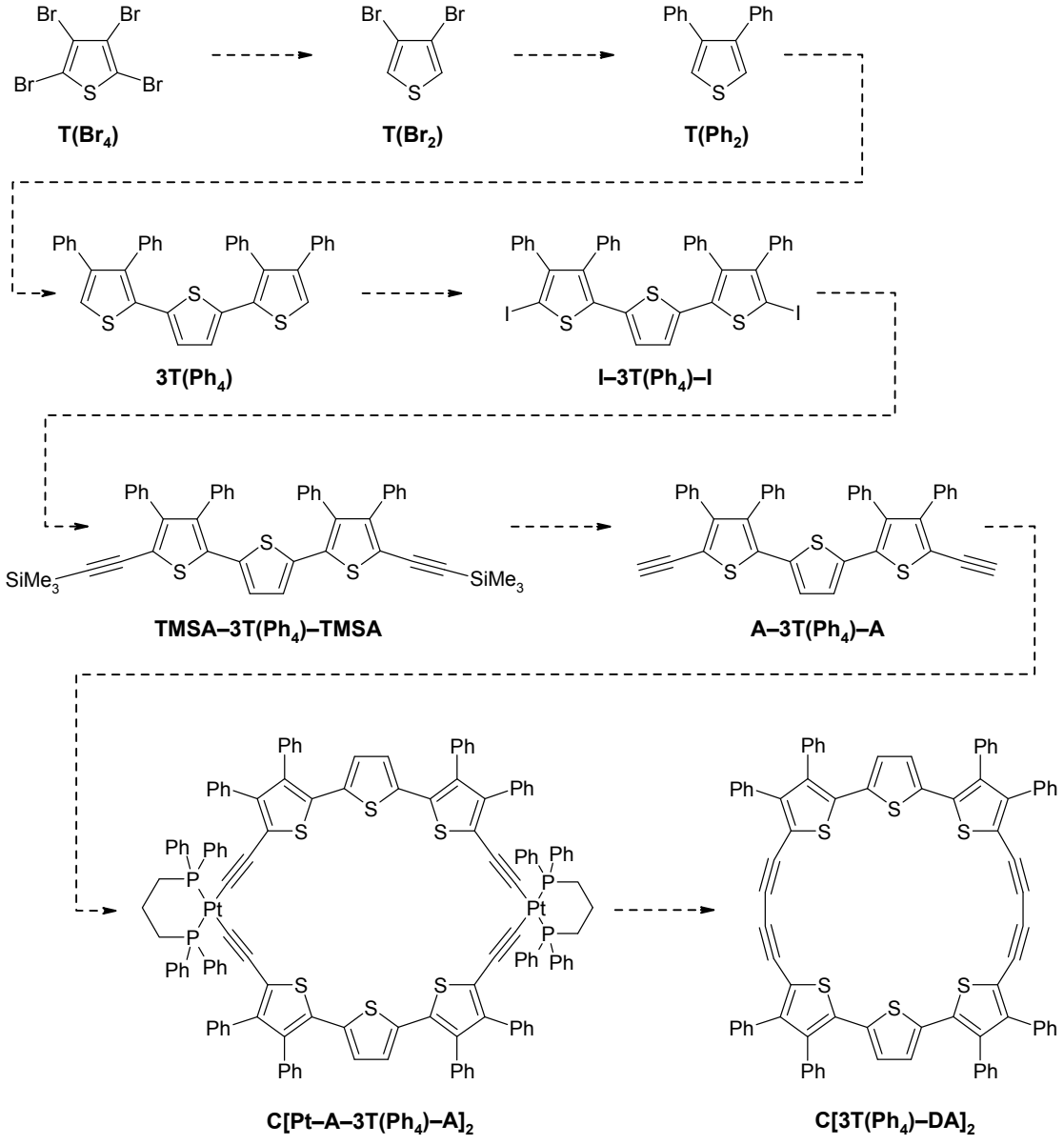

Scheme 30: Strategy for the synthesis of a phenyl-substituted macrocycle

Main reasons for the choice of this pattern were the interest to evaluate the influence of aromatic substituents on the physical properties of the macrocycles — as the phenyl π systems can contribute to the π system of the oligothiophene by conjugation — and the steric "pressure" of the outer phenyl units which should have a positive effect on the reductive elimination of the Pt(II) centres. Furthermore, a symmetric structure like the butyl substitution of the successfully macrocyclised oligothiophenes avoids the formation of hardly separable regioisomers and would allow a direct comparison with the alkyl-substituted macrocycles.

3.1.2 Synthesis of Phenyl-Substituted Building Blocks

For a symmetrical substitution of the thiophene β positions, 3,4-dihalogenated thiophenes as starting materials are commonly subdued to Kumada or Negishi coupling reactions. 3,4-dibromothiophene **T(Br$_2$)** was prepared from tetrabromothiophene **T(Br)$_4$** by bromine elimination from the α positions with zinc in diluted acetic acid (scheme 31).[111] The product was removed from the mixture by azeotropic distillation and purified by vacuum distillation to yield 70 % of **T(Br$_2$)**.

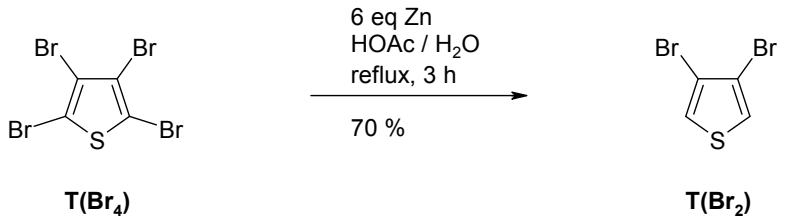

Scheme 31: Synthesis of T(Br$_2$)

To obtain the diaryl-substituted thiophene **T(Ph$_2$)**, a Kumada coupling of **T(Br$_2$)** and a solution of the Grignard reagent of bromobenzene was carried out in diethyl ether (scheme 32).[112] After several days under reflux the reaction was stopped since TLC control showed no more change, although the intermediate 3-bromo-4-phenylthiophene still was present. After workup, a white crystalline substance, whose NMR spectra did not match the structure of 3,4-diphenylthiophene, was obtained from the solution by recrystallisation from petrol ether. From further recrystallisation fractions in petrol ether and ethanol, the desired pure 3,4-diphenylthiophene was isolated in 32 % yield. The main byproduct in form of the above-mentioned white crystals was identified as biphenyl, resulting from a homo-coupling of the aryl compound.

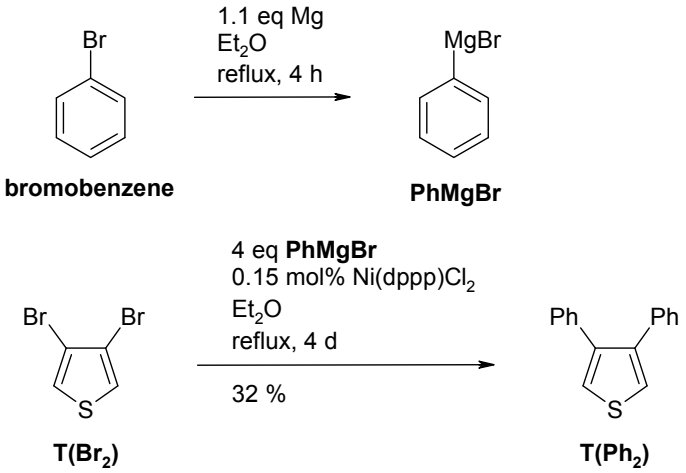

Scheme 32: Synthesis of T(Ph_2)

For the terthiophene synthesis, a different route compared to the alkyl-substituted building blocks was chosen. The tetrabutyl-substituted terthiophene, which was the starting material for the macrocycle synthesis presented in section 2.2, had been prepared by the nickel-catalysed Kumada coupling of 2-bromo-3,4-dibutylthiophene with 2,5-diiodothiophene.[113] Bromination of the 3,4-dibutylthiophene with *N*-bromosuccinimide (NBS) to yield 2-bromo-3,4-dibutylthiophene had required an extensive chromatographic separation of the mono- and dibrominated thiophene, resulting in a decreased yield.[114] To avoid this problem, the palladium-catalysed Negishi coupling[115] was envisaged for the synthesis of the tetraphenyl-substituted terthiophene **3T(Ph_4)** from 3,4-diphenylthiophene **T(Ph_2)**. This route benefits from directly leading to the desired product without the need of isolating an intermediate compound like an α-halogenated thiophene: Instead, a lithiated thiophene could in one step be quenched with $ZnCl_2$ and reacted with 2,5-diiodothiophene. While the quenching with $ZnCl_2$ usually happens quantitatively, lithiation as the crucial step for this sequence had to be investigated for its efficiency. Hence, **T(Ph_2)** was reacted with 1 eq of *n*-butyllithium (*n*-BuLi) in THF at −78 °C. After warming up to room temperature, the solution was quenched with an excess of I_2 (scheme 33). ^{1}H NMR and GC proved that mono-lithiation (and hence mono-deprotonation) was selective by greater 99 %, with an isolated yield of 95 %.

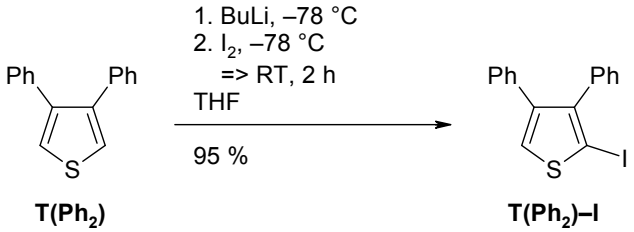

Scheme 33: Synthesis of T(Ph_2)–I

This result indicated that the Negishi coupling should be well suited for the synthesis of terthiophenes. Therefore, **T(Ph$_2$)** was again lithiated at −78 °C, a $ZnCl_2$ solution was added, and the resulting mixture was transferred at room temperature to a suspension of 2,5-diiodothiophene and the Pd catalyst (scheme 34). After stirring for 16 h and aqueous workup, the crude product could be purified by recrystallisation from toluene to yield 62 % of pure **3T(Ph$_4$)**.

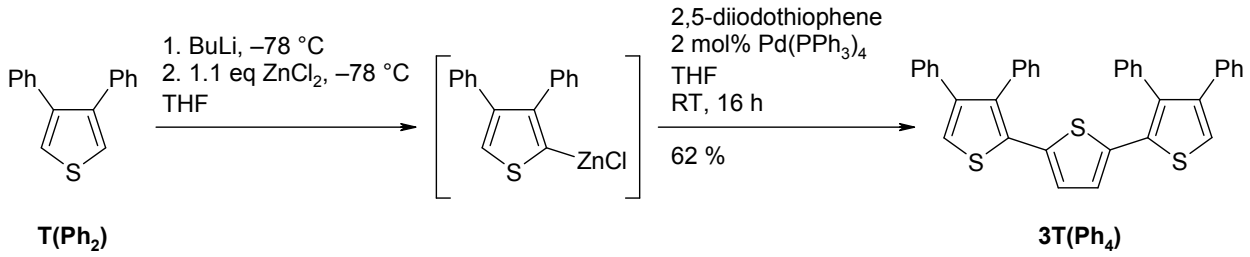

Scheme 34: Synthesis of 3T(Ph$_4$)

Iodination of the terthiophene in the free α positions was first tried by stirring **3T(Ph$_4$)** with 2.2 eq of mercury(II)acetate and acetic acid in dichloromethane over night and subsequent quenching with 4.4 eq of I_2 at 0 °C (scheme 35).[113]

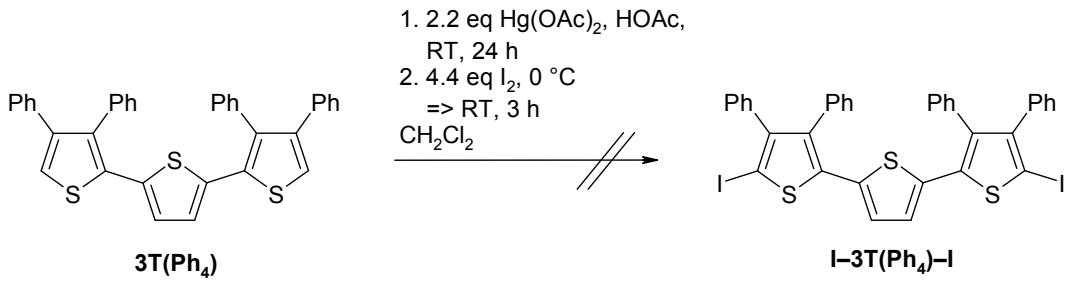

Scheme 35: Attempted synthesis of I–3T(Ph$_4$)–I using Hg(OAc)$_2$

^{1}H and ^{13}C NMR data indicated that, after workup with sodium thiosulfate and chromatography, only monoiodinated product was obtained: A singlet, expected at ca. 6.7 ppm for the β hydrogen atoms of the centre thiophene, appeared at 6.87 ppm; the integrated peak area was lacking one hydrogen atom and the ^{13}C spectrum had substantially more peaks than were expected for a symmetric compound. Obviously, the solubility of the Hg(II) salt in dichloromethane was not sufficient to exchange both terminal protons. To enhance the reactivity of the mercuration and such the yield of the diiodo product, the better soluble pivalylic acid salt of Hg(II) was used in a second approach in chloroform (scheme 36). After stirring for 36 h, the product was worked up with sodium bisulfate, potassium iodide and sodium hydroxide (to remove free pivalylic acid), and

finally filtered over basic alumina. The desired product **I–3T(Ph$_4$)–I** was obtained in 98 % yield with an HPLC purity of 98 %.

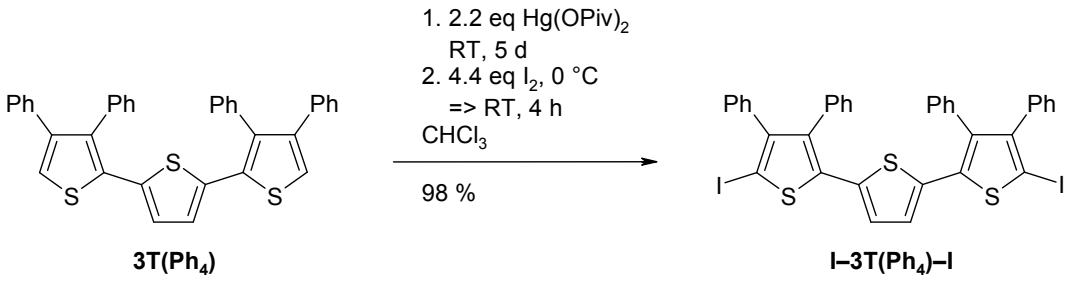

Scheme 36: Synthesis of I–3T(Ph$_4$)–I using Hg(OPiv)$_2$

For reasons of comparison, the before obtained monoiodinated terthiophene was reacted with 1 eq of the Hg(II) salt of pivalylic acid. Unfortunately, the monoiodo compound was recovered as the main product. Hg(II) obviously prefers to insert into the C–I bond instead of replacing the remaining α hydrogen atom. Hence, for a successful conversion to the diiodo product, 2 eq of mercury salt should be used.

As a larger batch of the mercuration–iodination reaction only yielded 70 % instead of > 95 %, iodination of **3T(Ph$_4$)** was additionally tried with *N*-iodosuccinimide (NIS; scheme 37). After workup and purification by column chromatography, the yield of pure product was only slightly higher than 70 %, so the mercuration–iodination route still seems to be the best way to obtain **I–3T(Ph$_4$)–I**.



Scheme 37: Synthesis of I–3T(Ph$_4$)–I using NIS

Finally, the acetylene moieties were introduced by a palladium-catalysed Sonogashira–Hagihara coupling.[116] Trimethylsilylacetylene (TMSA) was added to **I–3T(Ph$_4$)–I** and the catalyst CuI/Pd(PPh$_3$)$_2$Cl$_2$/PPh$_3$ in a mixture of triethylamine and pyridine (scheme 38). Depending on the results of an HPLC reaction control, additional TMSA was added several times in the course of the reaction. With this method, yields of up to 91 % of pure **TMSA–3T(Ph$_4$)–TMSA** were obtained.

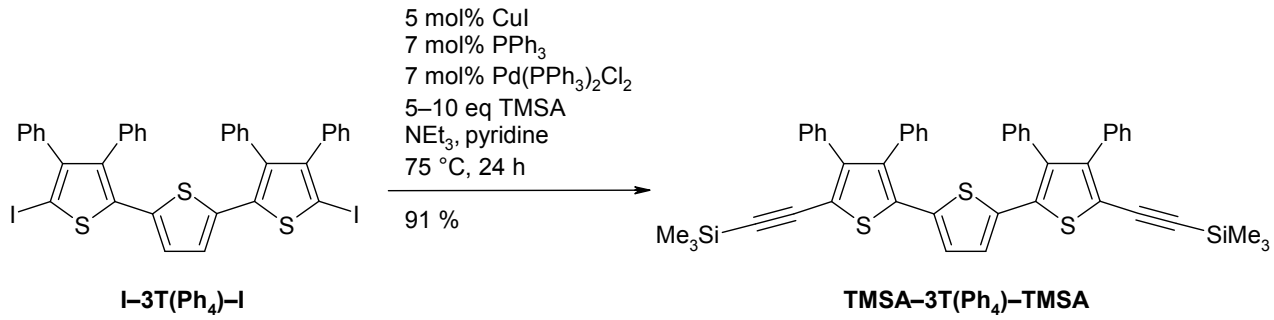

Scheme 38: Synthesis of TMSA–3T(Ph$_2$)–TMSA

In contrast, reactions of **I–3T(Ph$_4$)–I** with TMSA with Pd_2dba_3/PCy_3 instead of $Pd(PPh_3)_2Cl_2/PPh_3$ yielded only HPLC purities of 60 to 75 %, even after further amounts of the catalyst were added.

3.1.3 Synthesis of *p*-Alkylphenyl-Substituted Building Blocks

The main problem for the characterisation of platinamacrocycles, which constitute the crucial intermediates on the way to the conjugated macrocycles, is their general bad solubility. This might be overcome by attaching aryl side chains to the phenyl-substituents in order to increase the solubility. Therefore, an approach was made to build up a terthiophene unit with *p*-dodecylphenylene substituents.

Starting from bromobenzene, 4-bromododecylbenzene **BrPh'** was prepared by Friedel–Crafts acylation with lauroyl chloride, followed by a Wolff–Kishner reduction (scheme 39).[117] While the acylation to ketone **BrPh'(O)** worked well with 70 % yield after recrystallisation, the reaction was stopped after 7 h due to a darkening of the solution, although still gas evolved from the mixture. After destillation of the crude product, a byproduct was still present, which was finally identified as 4-dodecylaniline and removed by an acidic washing step. **BrPh'** was then isolated as a yellow oil in 54 % yield.

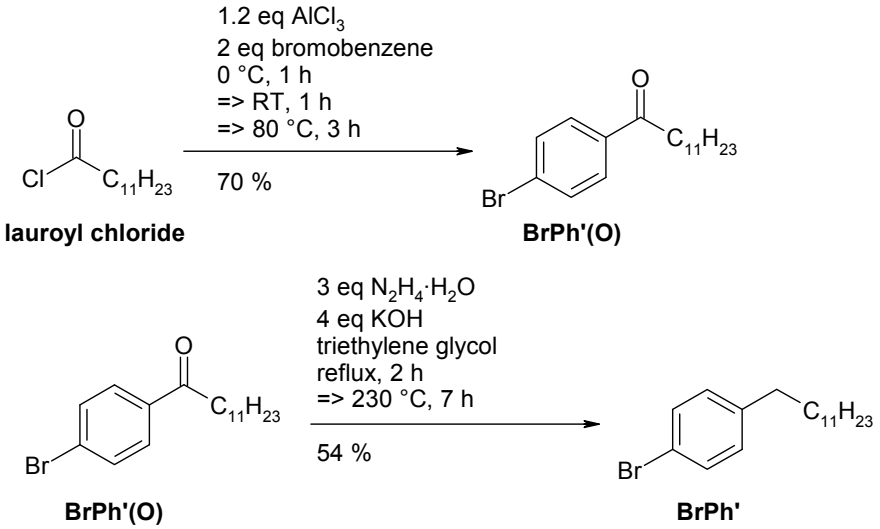

Scheme 39: Synthesis of BrPh'

As was expected for a compound with such a long alkyl chain, the Grignard reaction of **BrPh'** did not show the typical exothermic behaviour and had to be heated to reflux for 2 d. This mixture was then transferred to a flask with 3,4-dibromothiophene and the Kumada catalyst, refluxed for 4 d and worked up. After purification by column chromatography, **T(Ph'$_2$)** was isolated in 41 % yield (scheme 40). The major byproducts were identified as the mono-coupling product 3-bromo-4-(4-dodecylphenyl)thiophene (17 % yield), the hydrolysed Grignard reagent 4-dodecylbenzene and the debrominated intermediate 3-(4-dodecylphenyl)thiophene.

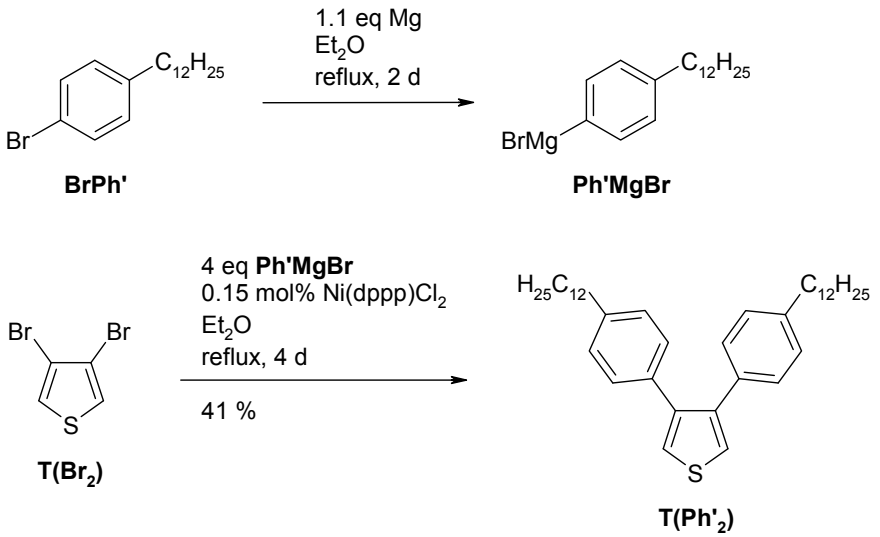

Scheme 40: Synthesis of T(Ph'$_2$)

As **BrPh'** had to be used in a 4-fold excess for the coupling, it was desired to increase the yield of this reaction. Therefore, the reaction was repeated in THF which allowed higher reaction temperatures. The higher temperatures, however, also increased side reactions, leading to 4,4'-bisdodecylbiphenyl as a major byproduct, while the desired **T(Ph'$_2$)** could only be isolated in 19 % yield. Negishi coupling, as an alternative way, failed already at the lithiation step: Upon cooling to −78 °C, the starting material **BrPh'** precipitated, and — even after several heating/cooling steps during which the suspension turned clear for short periods —, a GC spectrum of an iodine-quenched sample showed only a small amount of lithiation.

Reactivity problems also limited the application of the Negishi coupling to the desired terthiophene **3T(Ph'$_4$)**: After 4 d of stirring at room temperature, the yield of pure terthiophene was only 18 % (scheme 41). ESI mass spectra of column chromatography fractions showed that the main product was the mono-coupled intermediate, so — probably due to steric reasons — the second coupling is the limiting step for this reaction.

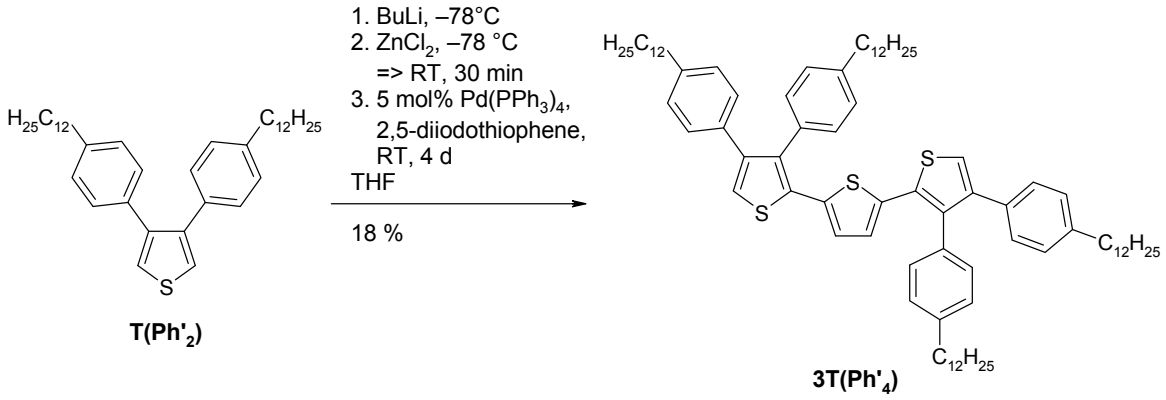

Scheme 41: Synthesis of 3T(Ph'$_4$)

Suzuki coupling was considered an alternative pathway to the preparation of **3T(Ph'$_4$)**. Hence, **T(Ph'$_2$)** was lithiated, reacted with triisopropyl borate, and the ligand was then exchanged with pinacol. Unfortunately, ^{1}H NMR spectra of a reaction mixture showed that there was still a substantial amount of starting material left. Purification was not possible, as the pinacol boronic ester decomposes on the silica column and the amount of substance was too large for Kugelrohr distillation.

Due to these severe experimental problems, the pathway using *p*-alkylated aryl substituents was not persued further.

3.2 Solid-State and Calculated Structure of 3,4-Diphenylthiophene

In contrast to alkyl side chains, phenyl substituents can interact with the aromatic system of thiophene. This conjugation could be used to tune properties of the whole π-electronic system in oligomers, e.g. redox potentials or the absorption, by introduction of donor- or acceptor-modified phenyl groups. The extent of the conjugation is determined by the overlap of the π systems and therefore related to the torsion angle between the substituents and the thiophene. As the two phenyl rings at the 3- and 4-positions are in close proximity to each other, steric and electronic effects counteract in this respect. With **T(Ph$_2$)**, for which crystals suitable for X-ray-structural analysis could be obtained, an insight into the nature of these influences was gained by comparing the results of the X-ray-structural analysis with those from quantum chemical calculations.[118]

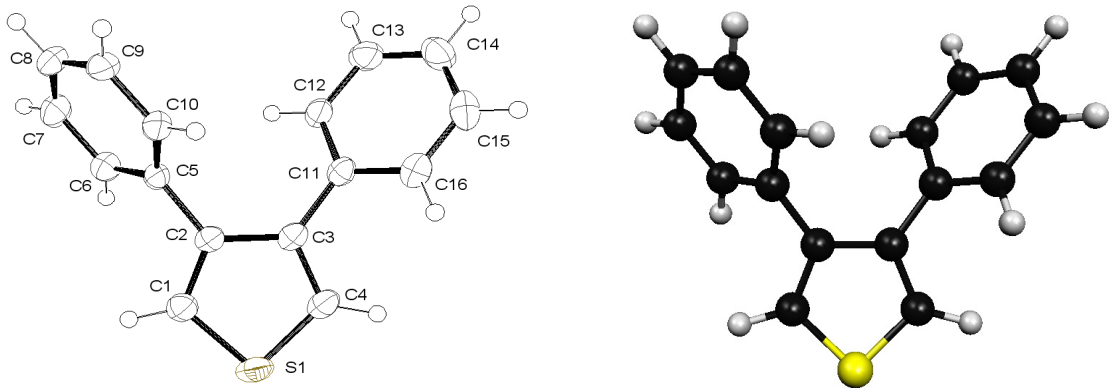

a) solid state structure **b)** calculated structure [B3LYP/6-31+G(d)]

Figure 67: Structures of T(Ph$_2$)[119]

Starting from the solid-state structure, energy optimisations of **T(Ph$_2$)** on the B3LYP/6-31+G(d) and MP2/6-31+G(d) levels were performed (figure 67b).[120,121] Here, almost identical torsion angles of 47.91° (B3LYP)/51.57° (MP2) for C10–C5–C2–C3, and 47.56° (B3LYP)/51.57° (MP2) for C12–C11–C3–C2 between the planar thiophene and phenyl systems were observed. Further quantum-chemical studies revealed no other conformers besides the energy-optimised structure of **T(Ph$_2$)**. Semiempiric calculations[122] had predicted structures closer to C_2 symmetry, but with torsion angles significantly smaller (44.90°/44.80°; AM1) or larger (52.86°/52.79°; PM3) than those from the more reliable ab initio calculations. The large twist of the phenyl rings results in non-ideal overlap of the π subsystems and is caused by the steric repulsion of the substituents, what can be shown by comparison with the calculated dihedral angle of only 28.3° (AM1) in 3-phenylthiophene.

In the crystal, packing effects cause a different structure compared to the calculated ones. The most significant parameters in the crystal structure (figure 67a) are the two different torsion angles of 33.5° (C2–C3–C11–C16) and 55.9° (C3–C2–C5–C6) of the phenyl substituents, which are, respectively, smaller or larger than the calculated values. Although the hydrogen atom at C12 exhibits a distance of only 3.22 Å to the centre of the adjacent phenyl ring and the C12–H12 axis is almost parallel to the neighbouring π system, this distance is too large for a significant intramolecular C_{phenyl}–H···π stabilisation, and no deviation of the C12–H12 bond parameters from other C_{phenyl}–H bonds in the molecule can be observed. Thus, intramolecular C–H···π interactions can only play a minor role in the surprisingly different twists of the phenyl rings, and a closer look at the crystal packing is necessary.

T(Ph$_2$) crystallised from petrol ether in a monoclinic crystal system, space group $P2_1/n$. One crystallographically independent molecule was found in the asymmetric unit. The unit cell has a dimension of 6.101 × 11.168 × 18.086 Å^3 with a monoclinic angle close to 90° (90.5°). It contains a layer of four molecules, two of which are arranged with the thiophene pointing in one and two with the thiophene pointing in the opposite direction. As a result of the slight twist of the molecules out of the *xy* plane, the phenyl groups point up- and downward in *z* direction. A principal scheme of the unit cell together with its crystal structure is presented in figure 68.

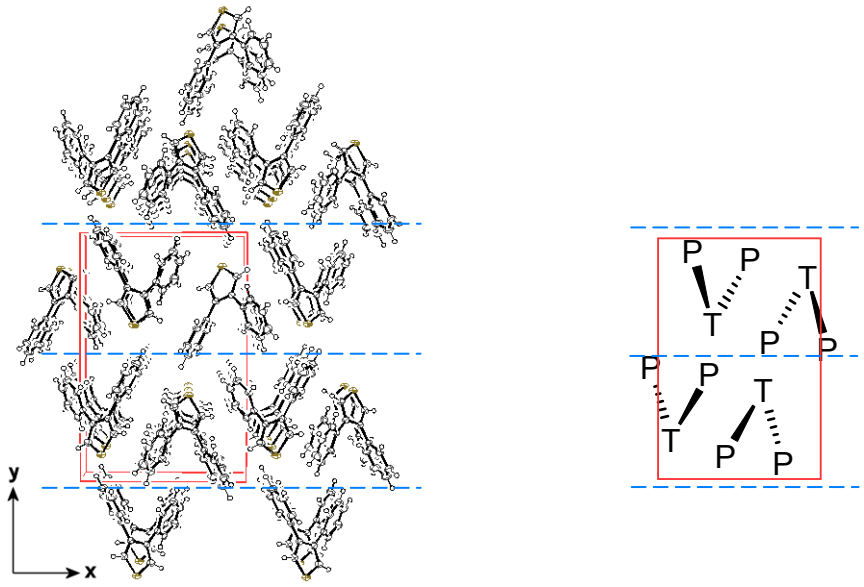

a) (100) view of the crystal structure; the red frame depicts the unit cell, the dotted blue lines depict borders between horizontal bands

b) scheme of the (100) view onto the unit cell (red); T = thiophene; P = phenyl substituent; the dotted blue lines depict borders between horizontal bands

Figure 68: Packing of T(Ph$_2$) in the crystal[118]

In the *z* direction the molecules form perfect stacks. However, the large translational distance of 6.10 Å between two molecules and the twisting of the aromatic moieties prevent the necessary π–π overlap to allow the expected π–π stacking. Instead, intermolecular interactions are restricted to interactions between hydrogen atoms and the phenyl π systems. Along the stacks, these interactions are within the upper limit of C–H···π distances, with 3.79 Å from the hydrogen centre at C6 and the phenyl-ring centroid of the adjacent molecule (figure 69a).

In the *xy* plane, the **T(Ph$_2$)** molecules form horizontal bands (separated by dotted blue lines in figure 68). Within one band, all molecules arrange side-by-side in an alternating up-and-down fashion. Each band is formed by molecules of only one chirality, with neighbouring bands possessing mirrored structures. Along one band, each molecule is involved into two $C_{thienyl}$–H···π interactions per side with an adjacent molecule (figure 69b). The $C_{thienyl}$···centroid distance of 3.47 Å here is smaller than the above-mentioned C_{phenyl}···centroid distance, i.e. interactions within the bands are stronger than in the stacks. The distances of the corresponding centroids of the aromatic systems are 4.719 Å and 5.054 Å, respectively, and thus significantly smaller than the distances of 5.052–5.986 Å for edge-to-face orientations in the benzene crystal.[123]

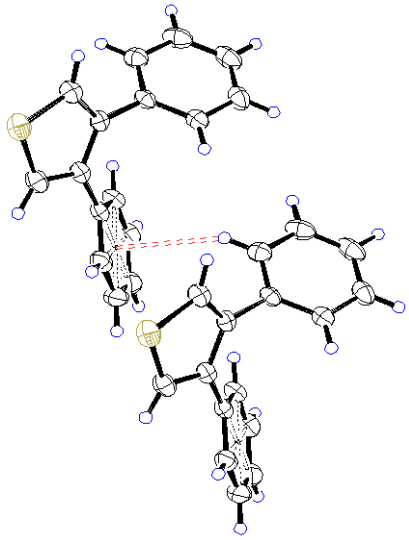

a) C_{phenyl}–H···π interactions (red) along the stacks

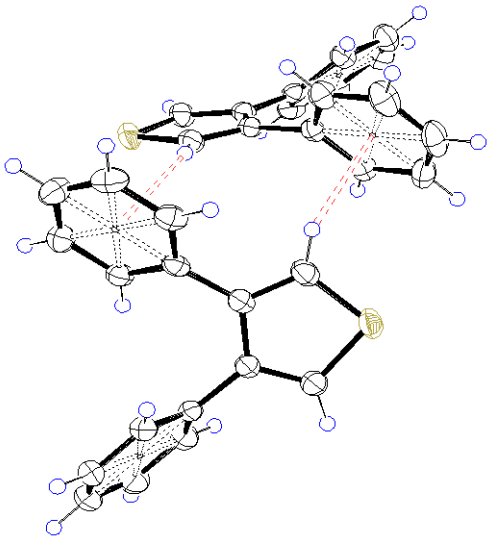

b) $C_{thienyl}$–H···π interactions (red) along the bands

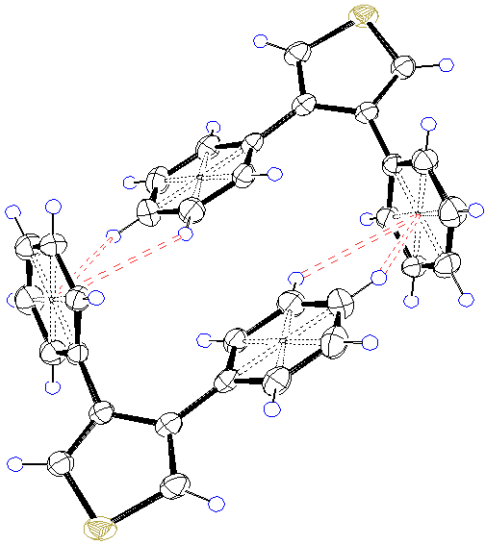

c) C_{phenyl}–H···π interactions (red) between the bands

Figure 69: Intermolecular C–H···π interactions of T(Ph_2) in the solid state[118]

The bands are interconnected by two edge-on C_{phenyl}–H···π contacts between paired molecules (figure 69c). Here the centroid···centroid distance of 5.32 Å still is in the range of such values for benzene,[123] but the distance is larger than for the $C_{thienyl}$–H···π connections along the bands.

In summary, the molecules arrange in the crystal by C–H···π interactions between either thienyl or phenyl hydrogen atoms and the phenyl π systems. Despite the weak nature of these bonds, they have a strong influence on the solid-state structure of **T(Ph_2)** and lead to different torsion angles of the two phenyl substituents, what allows the molecule to develop C–H···π interactions in all three dimensions. Furthermore, compared with the calculated minimum energy structure, this asymmetry allows for one of the phenyl substituents to build up a better conjugation with the thiophene core, what would be a benefit for the control of electronic properties by the substituents.

3.3 Preparation of Phenyl-Substituted Macrocycles

For the macrocyclisation, **TMSA–3T(Ph$_4$)–TMSA** was first deprotected by stirring with 10 eq of either KOH or CsF for ca. 4 h in methanol, until no starting material could be detected by TLC control (scheme 42). After aqueous workup, the dichloromethane solution of **A–3T(Ph$_4$)–A** was concentrated and applied in situ.

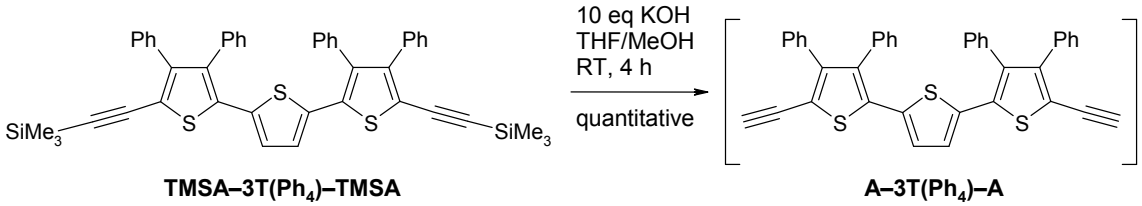

Scheme 42: Synthesis of A–3T(Ph$_4$)–A

A–3T(Ph$_4$)–A was added to a suspension of Pt(dppp)Cl$_2$ with ca. 10 mol% of CuI and 10 eq of triethylamine in toluene. After stirring for a few days at room temperature, the reddish-brown suspension was filtered, washed with methanol and dried. Yields ranged up to 88 %.

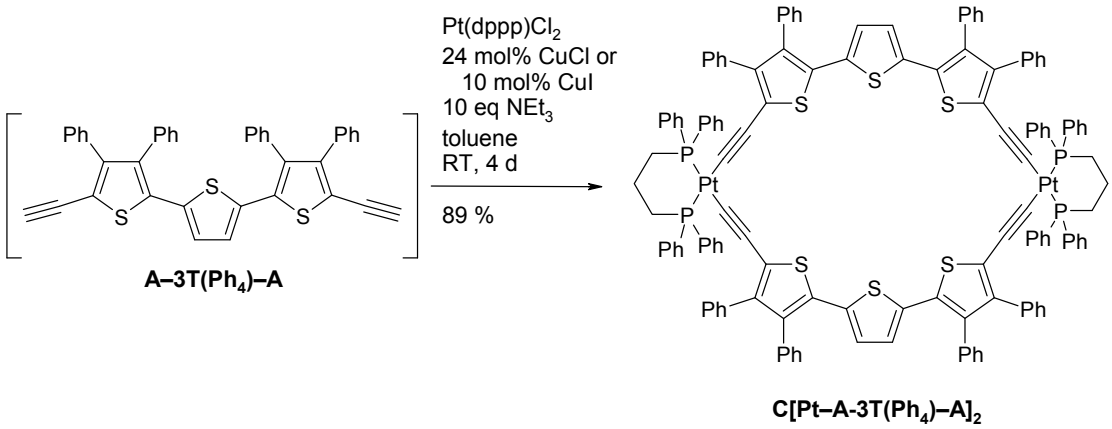

Scheme 43: Synthesis of C[Pt–A–3T(Ph$_4$)–A]$_2$

The product was completely insoluble in any common organic solvent, with the exception of benzonitrile and nitrobenzene. In the latter solvent, ^{1}H NMR spectroscopy was possible but gave bad results due to extremely broad signals. MALDI TOF mass spectrometry indicated the formation of the desired dimeric macrocycle (figure 70): only peaks for the product and its fragments were detected and no byproducts of higher masses could be seen, while for a comparative reaction with 24 mol% CuCl some impurity peaks arose.

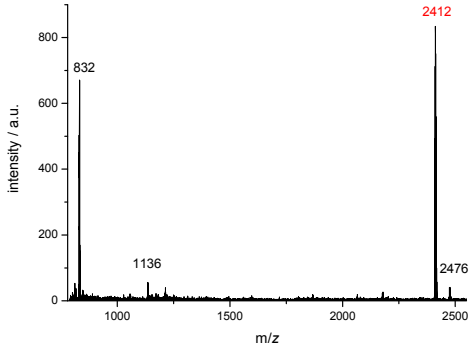

a) MALDI TOF mass spectrum;
m/*z* = 832 [Pt(dppp) + matrix]$^+$, 1136, 2412 [M]$^+$, 2476 [M + Cu]$^+$

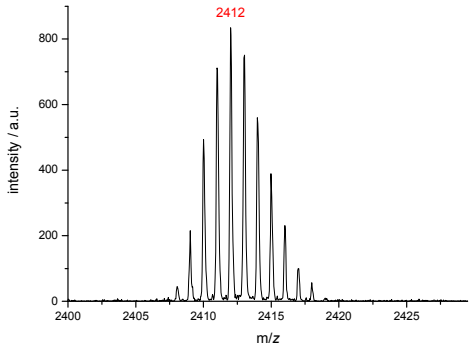

b) close-up view of the M^+ peak set

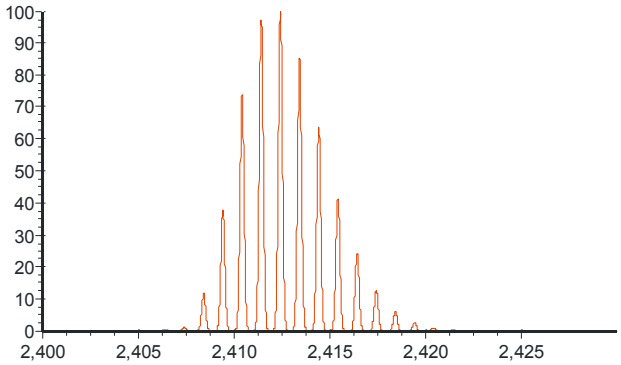

c) calculated mass spectrum

Figure 70: Mass spectra of C[Pt–A–3T(Ph$_4$)–A]$_2$

To check whether an Ag(I)-induced platinum elimination might be possible, silver(I) triflate was added to the macrocycle directly on the MALDI target plate. Unfortunately, the resulting mass spectrum showed a large number of new peaks which could not be attributed to any elimination products or Ag(I) adducts.

For several other platinamacrocycles, it had been possible to obtain NMR spectra by addition of the ligand trifurylphosphine P(fu)$_3$ to a suspension of the macrocycle in $CDCl_3$.[124] Apparently, the ligand helped to increase the solubility of the macrocycle. Unfortunately, for **C[Pt–A–3T(Ph$_4$)–A]$_2$** only the P(fu)$_3$ signals were visible in the ^{13}C NMR spectrum after the addition of trifurylphosphine. In the ^1H NMR spectrum, some additional aromatic signals were seen but could not be attributed. The ^{31}P NMR spectrum also showed, among the signal of P(fu)$_3$, seven more signals in the range from +5.2 to −15.82 ppm, what could either indicate a rapid decomposition, e.g. by ligand exchange, or a mixture of different Pt(II) compounds (e.g. macrocycles of different sizes).

Elimination of the Pt(II) centres from the diplatina-macrocycle was tried by stirring a THF suspension of **C[Pt–A–3T(Ph$_4$)–A]$_2$** with a slight excess of iodine over night at room temperature (scheme 44). The mixture was worked up with thiosulfate and filtered over celite.

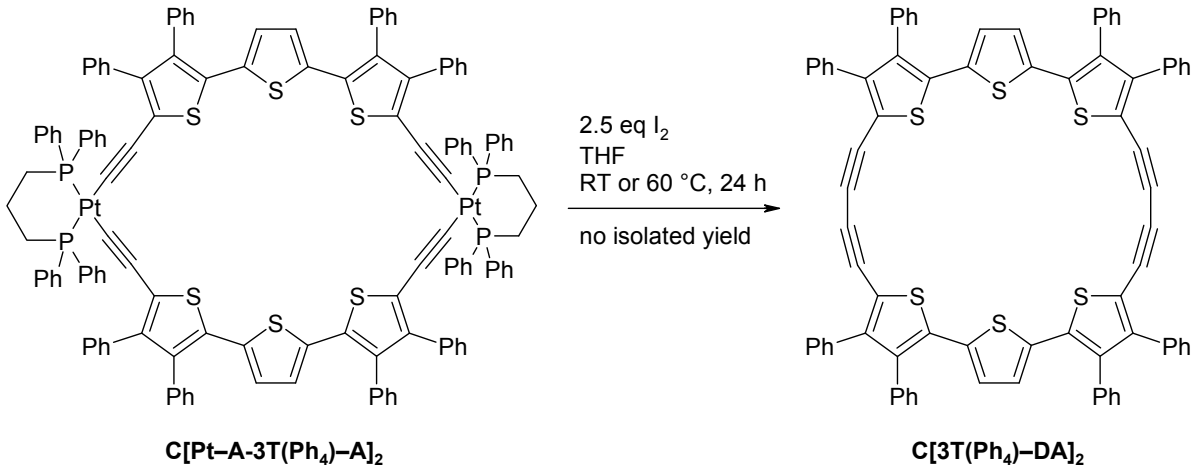

Scheme 44: Synthesis of C[3T(Ph$_4$)–DA]$_2$

After chromatography, fractions with a total yield of 35 % (with respect to the mass of the desired product) were isolated, but TLC still showed various different spots. Analytic HPLC detected several compounds with absorption spectra similar to the ones of the butyl-substituted macrocycles. Unfortunately, a baseline separation of the peaks in HPLC was not possible, so the different compounds could not be separated by preparative HPLC. MALDI TOF mass spectra clearly showed the presence of **C[3T(Ph$_4$)–DA]$_2$**, but also additional Pt(II) fragments that could not be separated off by column chromatography (figure 71).

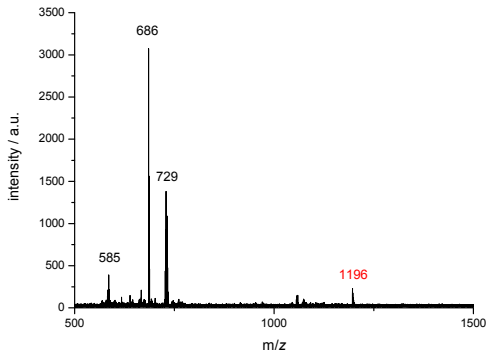

Figure 71: MALDI TOF mass spectrum of the crude product of reductive elimination
m/*z* = 585 [Pt$_3$]$^+$, 686, 729 [iodinated A–3T(Ph$_4$)–A/Pt(dppp)]$^+$, 1196 [cyclic dimer]$^+$

After an additional column chromatography step, the first fraction now indicated the clear formation of the cyclic dimer up to the pentamer:

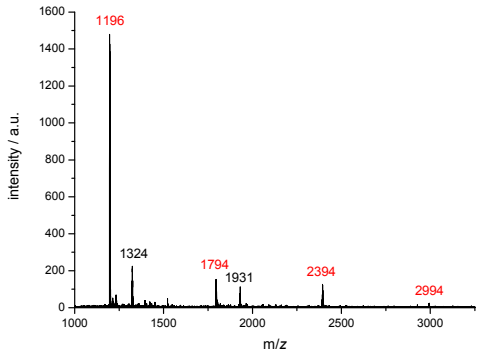

a) MALDI TOF mass spectrum;
m/*z* = 1196 [cyclic dimer]$^+$, 1324 [cyclic dimer + I]$^+$, 1794 [cyclic trimer]$^+$, 1931 [cyclic dimer + Pt(dppp) I]$^+$, 2394 [cyclic tetramer]$^+$, 2994 [cyclic pentamer]$^+$

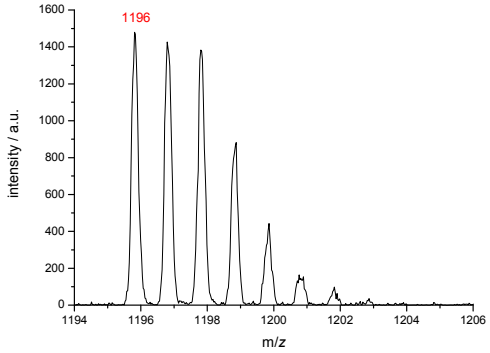

b) close-up view of the $[M]^+$ peak set for the cyclic dimer

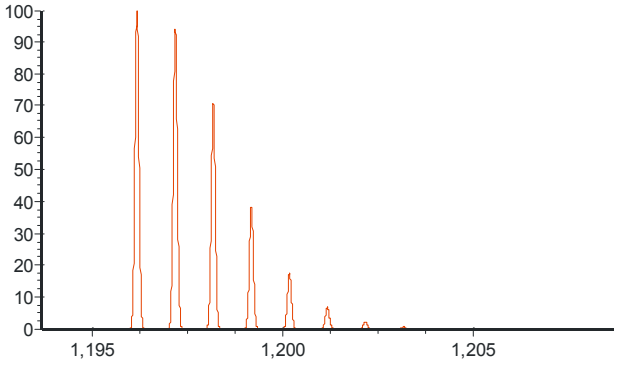

c) calculated mass spectrum for the cyclic dimer

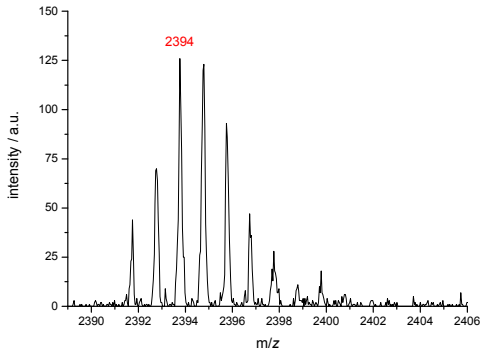

d) close-up view of the $[M]^+$ peak set for the cyclic tetramer

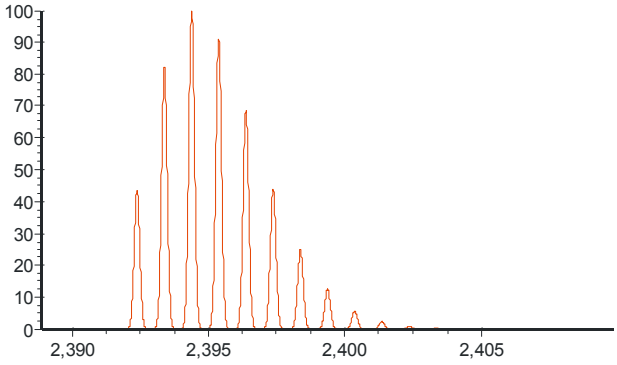

e) calculated mass spectrum for the cyclic tetramer

Figure 72: Mass spectrum of the first column chromatography fraction of reductive elimination

Although the dimer seems to be the dominating product, this conclusion has to be taken with care, as the different macrocycles probably have a different desorption behaviour in the MALDI TOF spectrometer, and larger macrocycles are expected to desorb not as easily as smaller ones. In contrast to the peaks for the larger macrocycles, the peak for the cyclic dimer was also found in the MALDI TOF spectra of all further chromatography fractions.

In another elimination reaction, the mixture of **C[Pt–A–3T(Ph$_4$)–A]$_2$** and iodine was stirred at 60 °C. In this case, like for the elimination at room temperature, **C[3T(Ph$_4$)–DA]$_2$** could be detected in the mass spectrum, but several additional peaks at higher masses up to m/z = 1600 appeared which could not be identified. Semipreparative HPLC separation of the crude product was tried, but while the resulting MALDI TOF spectra of the last fractions contained no more platinum fragments, impurities with higher masses were still visible and HPLC still showed a number of peaks which could not be baseline-separated.

3.4 Discussion of the Preparative Results

Adapting the preparation of alkyl-substituted building blocks for the synthesis of their phenyl-substituted counterparts only worked well to a certain extent, depending on the nature of the phenyl substituent. The preparation included as one of the first steps the coupling reaction of a phenyl Grignard compound with 3,4-dibromothiophene. In both cases — for the phenyl and 4-dodecylphenyl substitution — homocoupling to a symmetric biphenyl turned out to be a major side reaction which drastically lowered the yields compared to butyl substitution (32 % and 19 %, respectively, compared to 72 %[113]). Negishi coupling with 4-bromododecylbenzene **BrPh'** failed due to precipitation of this compound at low temperatures. X-ray structure analysis of **T(Ph'$_2$)** revealed various C–H···π interactions between aromatic moieties, which might be a reason for the inferior solubility of the phenyl-substituted thiophene compounds. Consequently, alkyl substitution of the phenyl moieties is necessary to achieve a higher solubility and, hence, better reactivity and possibilities of characterisation.

For the subsequent synthesis of the terthiophene **3T(Ph$_4$)**, Negishi coupling as a one-step reaction proved to be a valuable alternative to the Kumada coupling used for alkyl-substituted thiophenes. Terthiophene formation turned out to be the key reaction step for the synthesis of macrocycles, as an incomplete reaction is likely and leads to separation problems. The long dodecyl chains, e.g., seem to be sterically too demanding: a low yield of only 18 % was obtained for **3T(Ph'$_4$)**, while the mono-coupled bithiophene was the major product. Reactivity for the synthesis of both **T(Ph'$_2$)** and **3T(Ph'$_4$)** had decreased so much that a further conversion to macrocycles was discarded, since the separation of the pure product from reaction intermediates had already become an enormous task already for the terthiophene. For the following steps, it was expected to become even more extensive, probably resulting in similarly low yields. If the synthesis of phenyl-substituted macrocycles with alkyl moieties at the outer sphere should be persued further, a shorter alkyl chain (like C_6H_{13}) would be strongly recommended, along with an ether linkage between the alkyl chain and the benzene ring to provide a higher flexibility. 4-hexyloxyphenyl substituents, e.g., should provide an enhancement of solubility while retaining enough reactivity compared to benzene-substituted compounds.

Iodination of **3T(Ph$_4$)** to yield **I–3T(Ph$_4$)–I** was successful in up to 98 % yield by using the pivalylic acid salt of Hg(II) in chloroform for the mercuration step. Here, a clear enhancement was observed over $Hg(OAc)_2$ or the NIS route, the latter requiring a more extensive purification process. In similar high yields of up to 91 %, Sonogashira coupling to the trimethylsilyl-protected

diacetylide **TMSA–3T(Ph$_4$)–TMSA** was accomplished. Initial separation problems and low yields could be overcome by careful monitoring of the reaction by means of analytical HPLC and successive addition of relatively large amounts (up to 10 equivalents) of trimethylsilylacetylide.

The linear precursor could be smoothly deprotected and reacted with Pt(dppp)Cl$_2$ to dimeric macrocycles. Due to their extremely low solubility, characterisation of these complexes failed, with the exception of MALDI-TOF mass spectrometry which clearly indicated formation of the cyclic product **C[Pt–A–3T(Ph$_4$)–A]$_2$**. Efforts to remove the Pt corners by oxidatively induced reductive elimination reactions led to product mixtures which could not be fully characterised and which seemed to contain low yields of conjugated macrocycles of various sizes that could not be successfully separated off. Although an electrochemical attempt to selectively prepare the fully conjugated cyclic dimer indicated that the Pt(II) corners are eliminated in two steps (cf. section 5.4), the mechanism is not yet fully understood. Again, the inferior solubility of the phenyl derivatives compared to butyl-substituted oligothiophenes might be an important factor that a product mixture was obtained instead of a defined macrocyclic product.

In summary, phenyl substitution bears significant disadvantages compared with alkyl substitution. Its main drawback is the bad solubility of the platinum complexes, which does not allow reasonable characterisation other than mass spectrometry. Possibly, this is also the reason why the product mixture of the oxidatively induced elimination reactions could not be separated. An effort to enhance solubility by preparation of building blocks with longer alkyl chains at the phenyl rings failed due to the steric demand and the low reactivity of such compounds, what resulted in low yields already in the first reaction steps. Attachment of shorter alkyl chains, possibly in combination with an ether linkage to the phenyl rings, might solve this problem. However, the failure of reductive elimination experiments from Pt(II)–oligothienyl macrocycles with various alkyl substitutions[125] showed that the parameters for a controlled formation of fully conjugated macrocycles lie within a narrow range and are still not fully understood. Some critical requirements seem to be the following factors: a) a substituent at the outmost β position of the oligothiophene to promote reductive elimination by its steric demand; b) substituents at least at every second thiophene unit. In this respect, the search of alternative substituents and substitution patterns for the successful **3T(Bu$_4$)** precursor remains open.

3.5 Experimental Section

3.5.1 Materials and Methods

Chemicals and conditions

All solvents had been distilled or dried using standard procedures prior to use. Reactions involving reactive metal compounds were carried out under dry argon (Ar 4.6); the reagent mixtures were degassed and purged with argon several times before starting the reaction. All solutions (including acids and bases) used for washing of organic phases were prepared with deionised water.

The following reagents were prepared as described in the literature:

Tetrabromothiophene;[111a,126] 3,4-dibromothiophene;[111] 3,4-diphenylthiophene;[112] 2,5-diiodothiophene;[127] mercury(II) 2,2-dimethylpropanoic acid salt (mercury(II) pivalate; $Hg(OPiv)_2$);[128] $Pt(dppp)Cl_2$;[129] $Pd(PPh_3)_4$[130].

Commercially available reagents:

Aluminium chloride (Merck); bromobenzene (Fluka); *n*-butyllithium 1.59 M in hexane (Merck); cesium fluoride (ABCR); copper(I) iodide (Aldrich); 2,2-dimethylpropionic acid (pivalic acid; Merck); dodecanoyl chloride (lauroyl chloride, Aldrich); hydrazine hydrate 99 % (Fluka); iodine (Merck); *N*-iodosuccinimide (Merck); magnesium turnings (Merck); yellow mercury(II) ocide (Merck); $Ni(dppp)Cl_2$ (Aldrich); $Pd(dppp)Cl_2$ (Merck); triethylamine (Merck); triethylene glycol (Merck); trimethylsilylacetylene (ABCR); triphenylphosphine (Merck); zinc chloride (Merck).

Nuclear magnetic resonance

^1H and ^{13}C NMR spectra were recorded at room temperature in $CDCl_3$ on a Bruker AMX 400 spectrometer. The chemical shifts δ [ppm] are calibrated to the resonance signals of residual solvent protons ($CDCl_3$: $\delta_H = 7.26$ ppm; $\delta_C = 77.16$ ppm) or, if unapplicable, to TMS as the internal standard ($\delta_H = 0.00$ ppm). Calibration of ^{31}P NMR spectra was performed with H_3PO_4 as the external standard. Splitting patterns are denoted with s = singlet, d = doublet, dd = doublet of doublet, t = triplet, tt = triplet of triplet (appears as a quintuplet) and m = multiplet. If signals apply to different symmetric atoms, assignment is only denoted for one of these atoms, even if the other corresponding atoms are numbered in the structure due to clarification of connectivity. Different possible assignments are separated by a slash instead of a comma. If subsequent signals can only be correlated with a group of atoms rather than individual atoms, the corresponding group is denoted after the last signal of this group.

Gas chromatography

GC analyses were carried out using a Varian CP-3800 gas chromatograph equipped with a flame-ionisation detector and an 8 % phenyl-modified polydimethylsiloxane silica capillary (CP-SIL 8 CB) of 30 m length and 0.25 mm diameter. Helium 5.0 was used as carrier gas. For GC-MS analyses, a Varian Saturn 2000 EI (electron impact) mass spectrometer was used.

Analytical thin-layer chromatography

Thin-layer chromatography was carried out on TLC aluminium sheets coated with Silica Gel 60 F_{254} (Merck). Developed plates were dried and examined under a UV lamp (254 nm or 366 nm excitation) or developed in a TLC chamber with iodine-saturated silica gel.

Analytical chromatography

HPLC analysis was performed on a Shimadzu SPD-M10A VP detector connected to an SCL-10AVP controller and an LC-10AT pump, using a nucleosil column (NO_2; 4 mm × 250 mm; 5 μm corn size; Macherey–Nagel) at a flow rate of 1.3 mL min^{-1}.

Preparative chromatography

Preparative flash column chromatography (under elevated pressure) was carried out on glass columns of different length and diameters packed with Silica Gel 60 (particle size 40–63 μm; Merck).

Melting points

Melting points were determined with a Büchi B-540 melting point apparatus and are not corrected.

Mass spectrometry

Matrix-assisted laser desorption/ionisation time-of-flight (MALDI TOF) mass spectrometry was performed on a Bruker Daltonics Reflex III spectrometer with 1,8,9-trihydroxyanthracene (dithranol) as the matrix. Electron-spray ionisation (ESI) spectra were recorded on a Waters–Micromass ZMD spectrometer; samples were injected as an acetic acid solution with THF (15 %; spectroscopic grade, Merck) and water (millipore grade; 1 %). Chemical ionisation (CI) mass spectrometry was performed on a Finnigan MAT SSQ-7000 spectrometer. For all compounds, monoisotopic masses are listed.

Elemental analysis

CHN analyses were performed on an Elementar Vario EL with a 0.3 % limit of experimental error.

Nomenclature and conventions

IUPAC names were generated with the programs AutoNom 2000© or ACD/Name Pro. The platina-macrocycle was named according to IUPAC provisional recommendations for coordination compounds (draft march 2004). The shorter working names, which are used in the previous sections, are added.

Inorganic substances, in contrast to organic reagents, are usually denoted by their chemical formula.

Equivalents of reactands are given relative to the number of reacting sites.

In the structures, symmetric atoms are only numbered once. For clarification of the connectivity along oligothiophene chains, exceptions are made for atoms which are numbered as connecting points in the IUPAC name.

3.5.2 Preparation of Phenyl-Substituted Building Blocks

3,4-diphenylthiophene;

T(Ph$_2$)

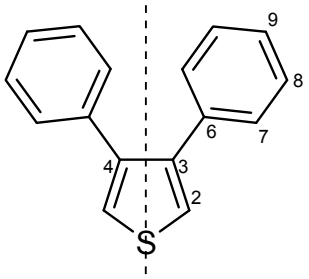

Molecular Weight = 236.34
Exact Mass = 236
Molecular Formula = C16H12S

In a three-neck flask with argon atmosphere, 28.1 g (1.16 mol) of Mg turnings were coated with 100 mL of diethyl ether. Of 110 mL (1.04 mol) of bromobenzene in a dropping funnel, ca. 10 mL were added quickly to start the Grignard reaction, then 100 mL of diethyl ether were added each to the dropping funnel and the reaction mixture. The bromobenzene solution was added slowly to keep the reaction at reflux, then heating to reflux was applied for another 4 h.

Under argon atmosphere, 400 mg (738 μmol; 0.15 mol%) of Ni(dppp)Cl_2 and 60.5 g (250 μmol) of 3,4-dibromothiophene were suspended in 100 mL of diethyl ether. To this mixture, the Grignard solution was added dropwise, then the whole mixture was heated to reflux for 4 d.

The reaction was cooled with an ice bath and quenched with 2 M HCl until intermediate precipitates dissolved again. The organic phase was separated, the aqueous phase was extracted with diethyl ether and the combined organic phases were washed with water. After drying over Na_2SO_4 and concentrating the solution, inorganic residues were removed by filtration over celite. The solid that precipitated from the dark brown solution was filtered and washed with petrol ether. Purification was performed by recrystallisation from petrol ether or ethanol to yield 18.9 g (80.0 μmol; 32 %) of **T(Ph$_2$)** as white crystals which were suitable for X-ray structure analysis.

Melting point: 112 °C

^{1}H NMR (400 MHz, $CDCl_3$): δ [ppm] = 7.24 (s, 2H, H^2), 7.19–7.10 (m, 10H, $H^{7–9}$).

^{13}C NMR (100 MHz, $CDCl_3$): δ [ppm] = 141.9 (C^3), 136.7, 129.2, 128.3, 127.0 ($C^{6–9}$), 124.2 (C^2).

Mass spectrometry (CI): m/*z* = 237 (M^+).

Elemental analysis: calcd. (%) C: 81.32, H: 5.12; found C: 80.98, H: 5.06.

3,4,3'',4''-tetraphenyl[2,2';5',2'']terthiophene;

3T(Ph$_4$)

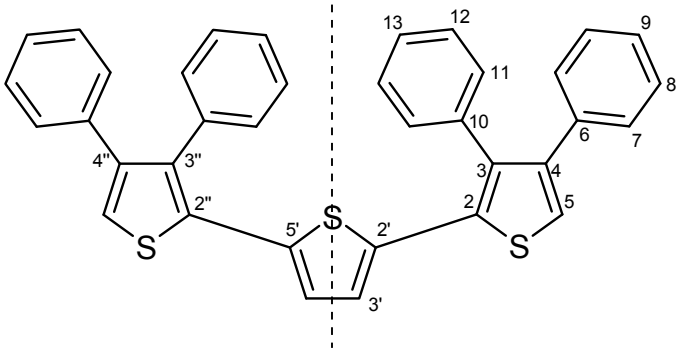

Molecular Weight = 552.78
Exact Mass = 552
Molecular Formula = C36H24S3

Under argon atmosphere, a solution of 2.35 g (9.94 mmol) of **T(Ph$_2$)** in THF was cooled to −78 °C. 6.3 mL (10 mmol) of a 1.59 M solution of *n*-butyllithium in hexane were added over a period of 1 h by a syringe with a perestaltic pump. Stirring was continued, and after 30 min a solution of 1.50 g (11.0 mmol; 1.1 eq) of $ZnCl_2$ was added within 5 min. The now yellow solution was kept at −78 °C for 30 min more, then the cooling bath was removed so that within another 30 min the mixture warmed up to room temperature.

The organozinc solution was added within 5 min to a solution of 1.67 g (4.97 mmol) of 2,5-diiodothiophene and 577 mg (499 μmol; 5 mol%) of $Pd(PPh_3)_4$ in 15 mL THF. While stirring at room temperature over night, a yellow solid precipitated. The suspension was quenched with 100 mL of a half concentrated NH_3 solution. The organic phase was separated and washed with H_2O. After evaporation of the solvent, the residue was purified by multiple recrystallisation from toluene. 1.67 g (3.02 mmol; 61 %) of pure **3T(Ph$_4$)** was obtained as a light yellow solid.

Melting point: 228 °C

^{1}H NMR (400 MHz, $CDCl_3$): δ [ppm] = 7.23–7.15 (m, 14H, $H^{5/7/8/9/11/12/13}$), 7.07–7.04 (m, 8H, $H^{5/7/8/9/11/12/13}$), 6.69 (s, 2H, $H^{3'}$).

^{13}C NMR (100 MHz, $CDCl_3$): δ [ppm] = 144.0 ($C^{2/4}$), 137.9 ($C^{2/4}$), 136.6, 136.6, 135.7, 133.8, 130.9, 128.9, 128.5, 128.1, 127.6, 126.9 ($C^{3,6–13,2'}$), 126.0 ($C^{3'}$), 121.4 (C^5).

Mass spectrometry (MALDI TOF): m/*z* = 552.1 (M^+).

Elemental analysis: calcd. (%) C: 78.22, H: 4.38; found C: 78.12, H: 4.27.

5,5''-Diiodo-3,4,3'',4''-tetraphenyl[2,2';5',2'']terthiophene;

I–3T(Ph$_4$)–I

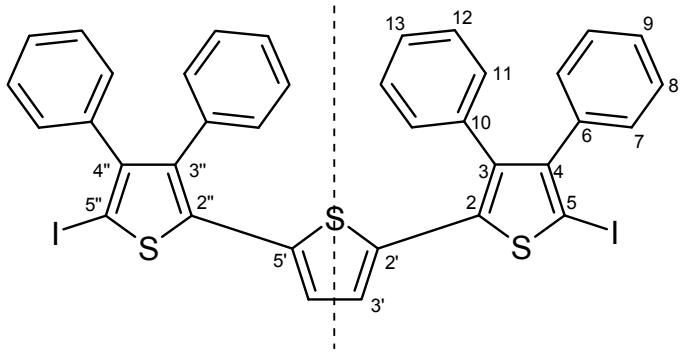

Molecular Weight = 804.58
Exact Mass = 804
Molecular Formula = C36H22I2S3

Preparation with Hg(OPiv)$_2$:

Under argon atmosphere, a solution of 353 mg (639 μmol) of **3T(Ph$_4$)** and 566 mg (1.41 mmol; 1.1 eq) of $Hg(OPiv)_2$ in 100 mL of chloroform was stirred at room temperature for 5 d. The yellow solution was then cooled to 0 °C, and over a period of 30 min a solution of 713 mg (2.18 mmol; 2.2 eq) of I_2 in 40 mL of chloroform was added. Initially, the yellow colour vanished, and after half of the addition the mixture turned red and an olive-coloured precipitation occurred. After further stirring for 4 h, the precipitate was filtered off. The filtrate was successively washed with 10 % aqueous solutions of $NaHCO_3$, $NaHSO_3$ (from $Na_2S_2O_5$) and KI, then with 2 M NaOH and finally with water. The solution was dried over $MgSO_4$, the solvent was removed and the product was dried in vacuo. 493 mg (613 μmol; 96 %) of **I–3T(Ph$_4$)–I** were obtained as a yellow powder.

Preparation with N-*iodosuccinimide:*

101 mg (183 μmol) **3T(Ph$_4$)** were dissolved in 50 mL chloroform and 10 drops of concentrated acetic acid were added. A solution of 123 mg (548 μmol; 1.5 eq) *N*-iodosuccinimide in 5 mL DMF was added within 5–10 min. The solution was stirred at room temperature and under exclusion of light for 5 d.

A saturated aqueous solution of Na_2CO_3 was added until the solution turned basic, then water was added to improve phase separation. The organic phase was washed with a 10 % $NaHSO_3$ solution (from $Na_2S_2O_5$), twice with water, and dried over $MgSO_4$. After removal of the solvent, the crude product was purified by column chromatography (SiO_2; petrol ether:dichloromethane 75:25). 107 mg (133 μmol; 73 %) of **I–3T(Ph$_4$)–I** were obtained.

Melting point: 269 °C

^{1}H NMR (400 MHz, $CDCl_3$): δ [ppm] = 7.21–7.10 (m, 14H, $H^{7/8/9/11/12/13}$), 7.04–7.01 (m, 4H, $H^{7/8/9/11/12/13}$), 6.93 (d, ^{3}J = 6.57 Hz, 4H, $H^{7/11}$), 6.68 (s, 2H, $H^{3'}$).

^{13}C NMR (100 MHz, $CDCl_3$): δ [ppm] = 149.1 (C^{4}), 138.8, 138.2, 136.9, 136.2, 135.3, 130.6, 130.3, 128.3, 127.9, 127.8, 127.6, 126.1 ($C^{2,3,6–13,2',3'}$), 75.0 (C^{5}).

Mass spectrometry (MALDI TOF): m/*z* = 552.1 ($M^+ - 2I$), 677.0 ($M^+ - I$), 803.9 (M^+), 1228.1 ($2M^+ - 3I$), 1354.0 ($2M^+ - 2I$), 1479.9 ($2M^+ - I$).

Elemental analysis: calcd. (%) C: 53.74, H: 2.76; found C: 53.98, H: 2.95.

3,4,3'',4''-Tetraphenyl-5,5''-bis(trimethylsilanylethynyl)[2,2';5',2'']terthiophene;

TMSA–3T(Ph$_4$)–TMSA

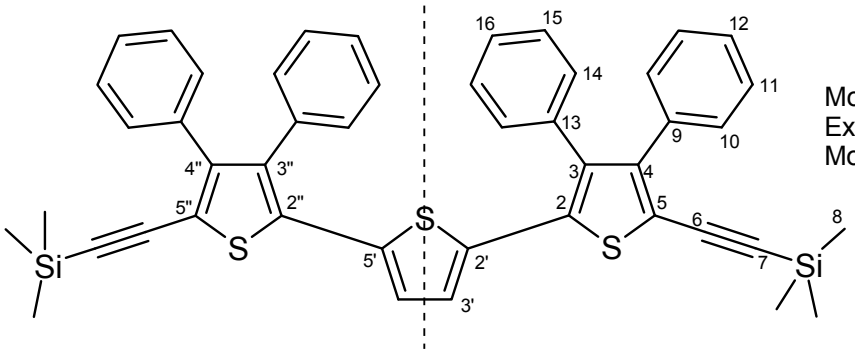

Molecular Weight = 745.20
Exact Mass = 744
Molecular Formula = C46H40S3Si2

In a thick-walled Schlenck tube with argon atmosphere, 500 mg (622 μmol) of **I–3T(Ph$_4$)–I**, 11 mL of triethylamine and 11 mL of pyridine were mixed and degassed several times. 30.6 mg (44.2 μmol; 7 mol%) of $Pd(PPh_3)_2Cl_2$, 5.90 mg (31.3 μmol; 5 mol%) of CuI, 11.4 mg (44.0 μmol; 7 mol%) of PPh_3 and 0.60 mL (4.4 mmol) of trimethylsilylacetylene were added, the tube was sealed and the mixture was stirred over night at 75 °C. With heating being continued, more of the acetylene compound was added in regular intervals of a few hours, until analytical HPLC indicated complete conversion of the iodinated sites at a total of 0.80 mL (5.9 mmol; 9.6 eq) of trimethylsilyl-acetylene.

The mixture was quenched with 50 mL of 2 M HCl and diluted with 100 mL of dichloromethane. The organic phase was separated and the aqueous phase was washed three times with dichloromethane. The organic phases were combined and washed with 2 M HCl until the smell of pyridine had vanished, then dried over Na_2SO_4. Column chromatography (SiO_2; petrol ether:dichloromethane 80:20) of the crude product yielded 462 mg (620 μmol; 99 %) of **TMSA–3T(Ph$_4$)–TMSA** as a yellow powder.

Melting point: 218 °C (decomposition)

^{1}H NMR (400 MHz, $CDCl_3$): δ [ppm] = 7.26–7.15 (m, 16H, $H^{10/11/12/14/15/16}$), 6.99 (d, ^3J = 6.82 Hz, 4H, $H^{10/14}$), 6.69 (2H, s, $H^{3'}$), 0.15 (18H, s, H^8).

^{13}C NMR (100 MHz, $CDCl_3$): δ [ppm] = 147.7, 138.1, 136.2, 135.3, 134.7 ($C^{2,2',3,3',4}$), 133.4 ($C^{9/10/11/12/13/14/15/16}$), 130.7, 129.9, 128.4, 127.4 ($C^{9/10/11/12/13/14/15/16}$), 127.8, 127.2, 126.2 ($C^{9/10/11/12/13/14/15/16}$), 117.9 ($C^5$), 101.9 ($C^6$), 97.8 ($C^7$), 0.0 ($C^8$).

Mass spectrometry (MALDI TOF): m/*z* = 744.2 (M^+).

Elemental analysis: calcd. (%) C: 74.14, H: 5.41; found C: 74.08, H: 5.77.

3.5.3 Preparation of *p*-Alkylphenyl-Substituted Building Blocks

1-(4-Bromophenyl)dodecan-1-one; p-bromododecanoylbenzene;

BrPh'(O)

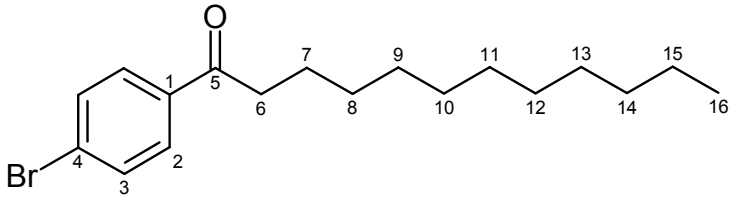

Molecular Weight = 339.32
Exact Mass = 339
Molecular Formula = C18H27BrO

Under argon atmosphere, 131 g (0.832 mol) of bromobenzene were mixed with 66.6 g (0.499 mol) of $AlCl_3$ in a three-neck flask and cooled to 0 °C. 90.8 g (0.415 mol) of lauroyl chloride were added within 1 h, then the suspension was stirred for 3 h at 80 °C. The mixture was allowed to cool to room temperature and then was poured onto 500 g of crushed ice, followed by addition of 150 mL of 5M HCl. The aqueous phase was extracted four times with diethyl ether; the ether phase then was washed with H_2O and a saturated $NaHCO_3$ solution, and finally was dried over Na_2SO_4.

The crude product was recrystallised from 500 mL of ethanol and washed with cold ethanol. From the mother liquor, additional fractions could be collected, yielding a total of 98.4 g (0.289 mol; 70 %) of **BrPh'(O)** as a white crystalline substance.

Melting point: 65 °C

^{1}H NMR (400 MHz, CDCl3): δ [ppm] = 7.81 (d, ^3J = 8.59 Hz, 2H, H^2), 7.59 (d, ^3J = 8.84 Hz, 2H, H^3), 2.91 (t, ^3J(H,H) = 7.32 Hz, 2H, H^6), 1.71 (tt, ^3J = 7.33 Hz, 2H, H^7), 1.38–1.24 (m, 16H, $H^{8–15}$), 0.88 (t, ^3J = 6.80 Hz, 3H, H^{16}).

^{13}C NMR (100 MHz, $CDCl_3$): δ [ppm] = 199.6 (C^5), 136.0 (C^1), 132.0 (C^3), 129.7 (C^2), 128.1 (C^4), 38.7 (C^6), 32.0, 29.7, 29.6, 29.6, 29.5, 24.4, 22.8 ($C^{7–15}$), 14.2 (C^{16}).

Mass spectrometry (CI): m/*z* = 339 (M^+), 198 ($M^+ - C_{10}H_{21}$), 183 ($M^+ - C_{11}H_{23}$).

Elemental analysis: calcd. (%) C: 63.72, H: 8.02; found C: 63.75, H: 7.98.

1-Bromo-4-dodecylbenzene; p-bromododecylbenzene;

BrPh'

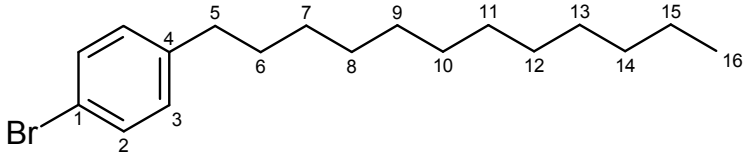

Molecular Weight = 325.34
Exact Mass = 325
Molecular Formula = C18H29Br

To a suspension of 96.6 g (0.285 mol) of **BrPh'(O)** in 500 mL of triethylene glycol, 64.0 g (1.14 mol) of KOH and 42.8 g (0.855 mol) of $N_2H_4 \cdot H_2O$ were added. The reaction mixture was heated to reflux for 2 h, then the resulting water and excess $N_2H_4 \cdot H_2O$ were distilled off at 230 °C for 7 h, until the gas development (N_2) had significantly decreased. The cooled mixture was poured onto 300 g of crushed ice, followed by addition of 150 mL of 6 M HCl. The aqueous phase was extracted twice with diethyl ether; the ether phase then was washed with H_2O and concentrated by vacuum evaporation. The remaining brown oil was filtered (SiO_2; petrol ether) and distilled twice. After taking up the crude product in diethyl ether, the solution was washed four times with 2 M HCl, filtered over acidic aluminum oxide using diethyl ether, evaporated and dried. 49.2 g (0.152 mol; 54 %) of **BrPh'** were obtained as a light yellow oil.

^{1}H NMR (400 MHz, $CDCl_3$): δ [ppm] = 7.40 (d, ^3J = 8.34 Hz, 2H, H^2), 7.06 (d, ^3J = 8.33 Hz, 2H, H^3), 2.57 (t, ^3J = 7.83 Hz, 2H, H^5), 1.60 (tt, ^3J = 7.33 Hz, 2H, H^6), 1.35–1.26 (m, 18H, $H^{7–15}$), 0.91 (t, ^3J = 7.07 Hz, 3H, H^{16}).

^{13}C NMR (100 MHz, $CDCl_3$): δ [ppm] = 142.0 (C^4), 131.4 (C^2), 130.3 (C^3), 119.4 (C^1), 35.5 (C^5), 32.1, 31.7, 31.5, 29.8, 29.8, 29.7, 29.6, 29.5, 29.3, 22.8 ($C^{6–15}$), 14.3 (C^{16}).

Mass spectrometry (CI): m/*z* = 169 ($M^+ - C_{11}H_{23}$), 325 (M^+).

Elemental analysis: calcd. (%) C: 66.45, H: 8.98; found C: 66.67, H: 9.14.

3,4-Bis(4-dodecylphenyl)thiophene;

T(Ph'$_2$)

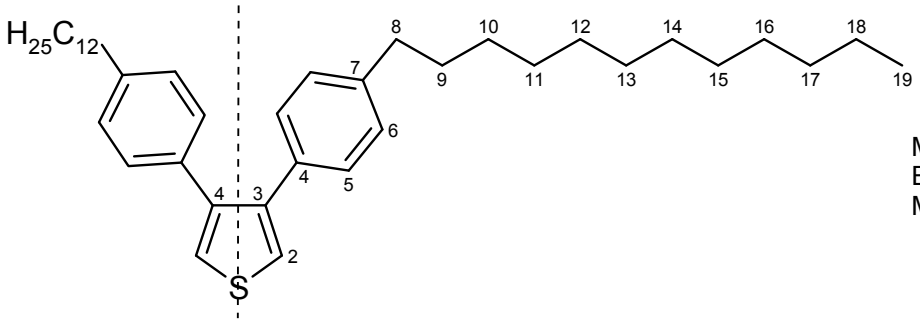

Molecular Weight = 572.99
Exact Mass = 572
Molecular Formula = C40H60S

Under argon atmosphere, 2.06 g (84.8 mmol) of dry Mg turnings were covered with 80 mL of diethyl ether. A solution of 25.0 g (76.8 mmol) of **BrPh'** in 40 mL of diethyl ether was added dropwise within 2 h, then the mixture was heated to reflux for 2 days. This Grignard solution was added dropwise to a mixture of 4.65 g (19.2 mmol) of 3,4-dibromothiophene and 31.2 mg (57.6 μmol; 1.5 mol%) of Ni(dppp)Cl_2 in 30 mL of diethyl ether under argon atmosphere. The mixture was refluxed again for 4 days, poured on crushed ice and quenched with 150 mL of 2 M HCl. The organic phase was separated and the aqueous phase was washed twice with diethyl ether. The combined organic phases were washed with H_2O, dried over Na_2SO_4 and filtered over SiO_2. After column chromatography (SiO_2; petrol ether) of the crude product, **T(Ph'$_2$)** was obtained in 4.47 g (7.80 mmol; 41 %) yield as a pale yellow solid.

Melting point: 47 °C

^{1}H NMR (400 MHz, $CDCl_3$): δ [ppm] = 7.27 (s, 2H, H^2), 7.11 (d, ^3J = 8.34 Hz, 4H, H^5), 7.06 (d, ^3J = 8.34 Hz, 4H, H^6), 2.59 (t, ^3J = 7.58 Hz, 4H, H^8), 1.61 (tt, ^3J = 7.32 Hz, 4H, H^9), 1.35–1.25 (m, 36H, $H^{10–18}$), 0.89 (t, ^3J = 6.56 Hz, 6H, H^{19}).

^{13}C NMR (100 MHz, $CDCl_3$): δ [ppm] = 141.9 (C^3), 141.7 (C^7), 134.1 (C^4), 128.9 (C^6), 128.2 (C^5), 123.6 (C^2), 35.8 (C^8), 32.1, 31.5, 29.9, 29.8, 29.8, 29.7, 29.6, 29.5, 22.8 ($C^{9–18}$), 14.3 (C^{19}).

Mass spectrometry (MALDI TOF): m/*z* = 572.4 (M^+).

Elemental analysis: calcd. (%) C: 83.85, H: 10.55; found C: 83.43, H: 10.33.

3,4,3'',4''-Tetrakis(4-dodecylphenyl)[2,2';5',2'']terthiophene;

3T(Ph'$_4$)

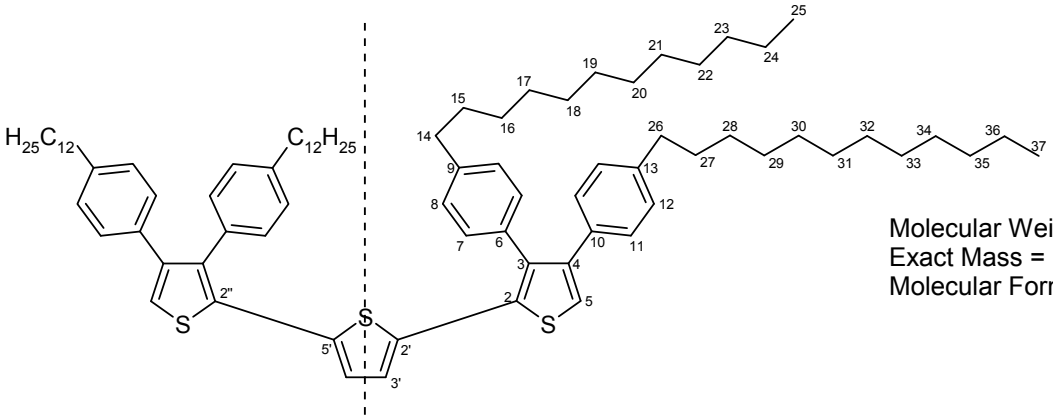

Under argon atmosphere, 4.30 g (7.50 mmol) of **T(Ph'$_2$)** were dissolved in 100 mL of THF and cooled to −78 °C. With a perestaltic pump, 5.20 mL (8.20 mmol) of a 1.59 M *n*-butyllithium solution in hexane were added from a syringe over a period of 1 h. The mixture was stirred for 2 h at −78 °C, then a solution of 1.12 g (8.20 mmol) of $ZnCl_2$ in 20 mL of THF, prepared under argon atmosphere, was added. After 30 min the cold bath was removed and the mixture was stirred for another 30 min at room temperature.

Also under argon atmosphere, a solution of 1.26 g (3.75 mmol) of 2,5-diiodothiophene and 433 mg (375 µmol; 5 mol%) of $Pd(PPh_3)_4$ in 20 mL of THF was prepared, and with a double canula the organozinc solution was added. After 4 days of stirring at room temperature, the mixture was quenched with 100 mL of half-concentrated NH_3. The organic phase was separated, concentrated, combined with a diethyl ether extract of the aqueous phase and successively washed with H_2O, a saturated $NaHSO_3$ solution and again H_2O. After drying the organic phase over Na_2SO_4 and filtration over SiO_2, the crude product was purified by column chromatography (SiO_2; petrol ether:dichloromethane 90:10) to yield 0.808 g (0.659 mmol; 18 %) of **3T(Ph'$_4$)** as a yellow solid.

Melting point: 94 °C

^{1}H NMR (400 MHz, $CDCl_3$): δ [ppm] = 7.14 (s, 2H, H^5), 7.05 (d, ^3J = 8.34 Hz, 4H, $H^{7/8/11/12}$), 7.00–6.96 (m, 12H, $H^{7/8/11/12}$), 6.65 (s, 2H, $H^{3'}$), 2.62 (t, 3J = 7.58, 4H, $H^{14/26}$), 2.53 (t, ^3J(H,H) = 7.71 Hz, 4H, $H^{14/26}$), 1.64–1.53 (m, 8H, $H^{15,27}$), 1.32–1.27 (m, 72H, $H^{16–24,28–36}$), 0.89 (t, ^3J = 7.08 Hz, 12H, $H^{25,37}$).

^{13}C NMR (100 MHz, $CDCl_3$): δ [ppm] = 144.0, 142.2 ($C^{2,4}$), 141.6, 138.0, 136.7, 134.0, 133.7, 133.2, 130.7, 128.7, 128.7, 128.0, 125.7 ($C^{3,6–13,2',3'}$), 120.7 (C^{5}), 35.9, 35.8 ($C^{14,26}$), 32.1, 32.1 ($C^{15,27}$), 31.4, 29.9–29.4 ($C^{16–23,28–35}$), 22.8 ($C^{24,36}$), 14.3 ($C^{25,37}$).

Mass spectrometry (MALDI TOF): m/*z* = 1224.8 (M^+).

Elemental analysis: calcd. (%) C: 82.29, H: 9.87; found C: 81.91, H: 9.59.

3.5.4 Preparation of Macrocyclic Compounds

Cyclo-bis{μ-[diyne-2,2′-(3,3′′,4,4′′-tetraphenyl[2,2′:5′,2′′]terthien-5,5′′-diyl)-1,1′-diyl-κC¹:κC¹¹]}bis{[propane-1,3-diylbis(diphenylphosphane)-κ²P]platinum(II)};

C[Pt–A–3T(Ph$_4$)–3T]$_2$

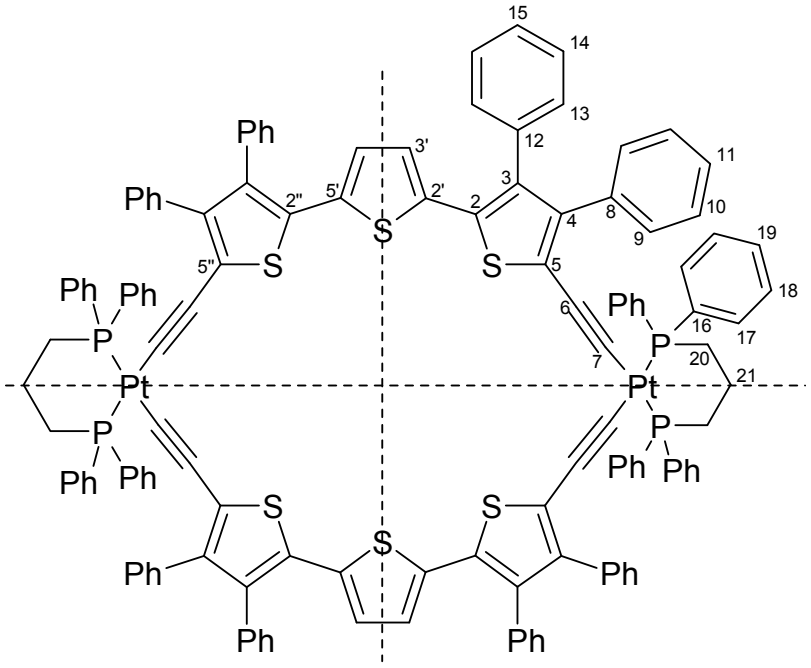

Molecular Weight = 2412.65
Exact Mass = 2410
Molecular Formula = C134H96P4Pt2S6

353 mg (474 μmol) of **TMSA–3T(Ph$_4$)–TMSA** were dissolved in 50 mL of THF. A solution of 266 mg (4.74 mmol; 10 eq) of KOH and 2 drops of H_2O in 20 mL of MeOH was added and the solution was stirred for 12 h at room temperature. At a bath temperature below 30 °C, the solvent was evaporated and the precipitate was taken up in 20 mL of dichloromethane. The solution was successively washed with H_2O, 2 M HCl, a saturated $NaHCO_3$ solution and H_2O, and then dried over $MgSO_4$. Again, the solvent was evaporated at a bath temperature below 30 °C. The diethynyl terthiophene was taken up in 10 mL of THF and used in situ without further characterisation.

Under argon atmosphere, 368 mg (543 μmol) of $PtCl_2$(dppp), 10 mg (54 mmol; 10 mol%) of CuI and 0.75 mL (5.4 mmol; 10 eq) of triethylamine were suspended in 100 mL of toluene and degassed. The diethynyl–terthiophene solution was added, then the mixture was degassed and purged with argon for 1 min. While stirring for 3 d, the colour of the suspension changed to brown. Finally, the mixture was filtered through a Büchner funnel and the residue was washed with methanol. 505 mg (209 μmol; 88 %) of **C[Pt–A–3T(Ph$_4$)–3T]$_2$** were obtained as a brown powder.

Melting point: 280–288 °C (decomposition)

Mass spectrometry (MALDI TOF): m/*z* = 831 [(Pt(dppp)+matrix)$^+$], 2409 (M^+).

7,8,15,16,23,24,31,32-octaphenyl-33,34,35,36,37,38-hexathiaheptacyclo-[28.2.1.1^{2,5}.1^{6,9}.1^{14,17}.1^{18,21}.1^{22,25}]octatriaconta-1(32),2,4,6,8,14,16,18,20,22,24,30-dodecaene-10,12,26,28-tetrayne;

Cyclo-bis[diyne-2,2′-(3,4,3′′,4′′-tetraphenyl-[2,2′:5′,2′′]terthien-5,5′′-diyl)-1,1′-diyl];

C[3T(Ph$_4$)–DA]$_2$

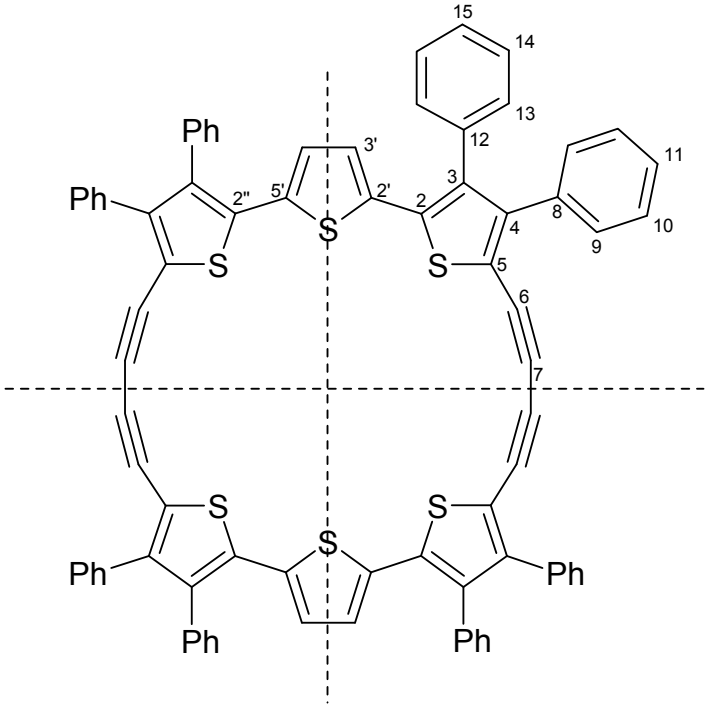

Molecular Weight = 1197.63
Exact Mass = 1196
Molecular Formula = C80H44S6

Under argon atmosphere, 50 mg (21 μmol) of **C[Pt–A–3T(Ph$_4$)–3T]$_2$** were dissolved in 10 mL of THF. In the absence of light, a solution of 13 mg (53 μmol; 2.5 eq) of I_2 in 5 mL of THF was added and the mixture was stirred for 24 h at room temperature.

Dichloromethane was added to obtain a better phase separation. The organic phase was washed successively with a saturated $NaHSO_3$ solution (from $Na_2S_2O_5$), 2 M HCl, H_2O, a saturated $NaHCO_3$ solution and again H_2O, then dried over $MgSO_4$. Column chromatography of the crude product yielded fractions of only a few milligrams, which still showed a number of broad, strongly overlapping peaks in analytic HPLC. Further separation or isolation of a pure product was not possible.

Mass spectrometry (MALDI TOF): m/*z* = 1196 (M^+), 1324 [$(M+I)^+$], 1794 {C[3T(Ph$_4$)–DA]$_3^+$}, 1931 {[M+Pt(dppp)I]$^+$}, 2394 {C[3T(Ph$_4$)–DA]$_4^+$}, 2994 {C[3T(Ph$_4$)–DA]$_5^+$}.

3.5.5 Details for the Structure Discussion of 3,4-Diphenylthiophene

Structural Refinement

The diffraction data of 3,4-diphenylthiophene **T(Ph$_2$)** was collected on a Bruker APEX-CCD (D8 three-circle goniometer). Data was collected and processed with the following software: Smart v5.622 (Bruker AXS, 2001; data collection, cell determination and refinement), SaintPlus v6.02 (Bruker AXS, 1999; integration), Sadabs v2.01 (Bruker AXS, 1999; empirical absorption correction). The structure was solved with the program SHELXS90[131a] with direct methods and was refined with the program SHELXL97[131b]. All non-hydrogen atoms were refined anisotropically. The hydrogen atoms were refined on a riding model in their ideal geometric positions.

parameter	value(s)	
empirical formula	$C_{16}H_{12}S$	
formula weight	236.32	
temperature	173(2) K	
wavelength	0.71073 Å	
crystal system	monoclinic	
space group	$P2_1/n$	
unit cell dimensions	a = 6.1007(9) Å b = 11.1679(16) Å c = 18.086(3) Å	β = 90.459(2)°
volume	1232.2(3) Å^3	
Z	4	
density (calculated)	1.274 g cm^{-3}	
absorption coefficient	0.235 mm^{-1}	
F(000)	496	
crystal size	0.1 × 0.1 × 0.2 mm^3	
2θ range for data collection	4.28 to 50.00°	
index ranges	$-7 \le h \le 7$, $-13 \le k \le 13$, $-21 \le l \le 21$	
reflections collected	22940	
independent reflections	2181 (R_{int} = 0.1580)	
completeness to 2θ = 50.00°	100.0 %	
refinement method	full-matrix least-squares on F^2	
data / restraints / parameters	2181 / 0 / 154	
goodness-of-fit on F^2	0.561	
final *R* indices [$I > 2\sigma(I)$]	R1 = 0.0414, wR2 = 0.1140	
***R* indices (all data)**	R1 = 0.0454, wR2 = 0.1191	
largest diff. peak and hole	0.394 and −0.389 e.Å^{-3}	

Table 2: Crystal data and structure refinement for T(Ph$_2$)

atom	x	y	z	U(eq)
C(1)	8909(3)	2261(2)	2184(1)	31(1)
C(2)	7578(2)	1893(1)	2743(1)	25(1)
C(3)	6073(3)	973(1)	2509(1)	26(1)
C(4)	6363(3)	693(2)	1779(1)	32(1)
C(5)	7711(3)	2442(1)	3490(1)	26(1)
C(6)	9676(3)	2428(2)	3883(1)	34(1)
C(7)	9821(3)	2976(2)	4574(1)	43(1)
C(8)	8024(4)	3541(2)	4870(1)	44(1)
C(9)	6063(3)	3557(2)	4486(1)	39(1)
C(10)	5902(3)	3006(2)	3797(1)	31(1)
C(11)	4474(3)	338(1)	2977(1)	26(1)
C(12)	4967(3)	25(2)	3710(1)	30(1)
C(13)	3481(3)	−629(2)	4123(1)	40(1)
C(14)	1501(3)	−982(2)	3817(1)	44(1)
C(15)	997(3)	−681(2)	3098(1)	41(1)
C(16)	2466(3)	−27(2)	2680(1)	33(1)
S(1)	8383(1)	1518(1)	1376(1)	37(1)

Table 3: **Atomic coordinates (× 10^{-4}) and equivalent isotropic displacement parameters (Å^2 × 10^3) for T(Ph_2)**
U(eq) is defined as one third of the trace of the orthogonalised U_{ij} tensor

atom	x	y	z	U(eq)
H(1)	10002	2861	2238	37
H(4)	5529	103	1524	39
H(6)	10924	2043	3681	41
H(7)	11166	2961	4842	52
H(8)	8136	3920	5339	53
H(9)	4822	3944	4691	46
H(10)	4547	3016	3535	37
H(12)	6326	261	3925	36
H(13)	3826	−835	4620	48
H(14)	492	−1432	4102	52
H(15)	−363	−923	2887	49
H(16)	2099	176	2184	39

Table 4: **Hydrogen coordinates (× 10^{-4}) and isotropic displacement parameters (Å^2 × 10^3) for T(Ph_2)**
U(eq) is defined as one third of the trace of the orthogonalised U_{ij} tensor

involved atoms	bond length [Å]	involved atoms	bond length [Å]
C(1)–C(2)	1.364(2)	**C(7)–C(8)**	1.376(3)
C(1)–S(1)	1.7095(17)	**C(8)–C(9)**	1.378(3)
C(2)–C(3)	1.440(2)	**C(9)–C(10)**	1.392(2)
C(2)–C(5)	1.486(2)	**C(11)–C(16)**	1.394(2)
C(3)–C(4)	1.369(2)	**C(11)–C(12)**	1.402(2)
C(3)–C(11)	1.478(2)	**C(12)–C(13)**	1.387(2)
C(4)–S(1)	1.7069(18)	**C(13)–C(14)**	1.383(3)
C(5)–C(6)	1.389(2)	**C(14)–C(15)**	1.376(3)
C(5)–C(10)	1.391(2)	**C(15)–C(16)**	1.385(3)
C(6)–C(7)	1.393(2)		
involved atoms	**angle [°]**	**involved atoms**	**angle [°]**
C(2)–C(1)–S(1)	112.23(13)	**C(7)–C(8)–C(9)**	120.04(17)
C(1)–C(2)–C(3)	112.30(14)	**C(8)–C(9)–C(10)**	119.98(18)
C(1)–C(2)–C(5)	121.38(14)	**C(5)–C(10)–C(9)**	120.50(16)
C(3)–C(2)–C(5)	126.30(14)	**C(16)–C(11)–C(12)**	118.16(15)
C(4)–C(3)–C(2)	111.05(15)	**C(16)–C(11)–C(3)**	120.12(14)
C(4)–C(3)–C(11)	122.27(15)	**C(12)–C(11)–C(3)**	121.62(14)
C(2)–C(3)–C(11)	126.61(14)	**C(13)–C(12)–C(11)**	120.32(15)
C(3)–C(4)–S(1)	112.81(13)	**C(14)–C(13)–C(12)**	120.46(17)
C(6)–C(5)–C(10)	118.97(15)	**C(15)–C(14)–C(13)**	119.81(17)
C(6)–C(5)–C(2)	120.17(15)	**C(14)–C(15)–C(16)**	120.25(17)
C(10)–C(5)–C(2)	120.84(14)	**C(15)–C(16)–C(11)**	121.01(16)
C(5)–C(6)–C(7)	120.17(17)	**C(4)–S(1)–C(1)**	91.60(8)
C(8)–C(7)–C(6)	120.33(17)		
involved atoms	**torsion angle [°]**	**involved atoms**	**torsion angle [°]**
C(2)–C(3)–C(11)–C(16)	146.49 (0.16)	**C(6)–C(5)–C(2)–C(3)**	124.11 (0.18)

Table 5: Bond lengths, angles and selected torsion angles for T(Ph_2)

atom	U_{11}	U_{22}	U_{33}	U_{23}	U_{13}	U_{12}
C(1)	38(1)	27(1)	28(1)	2(1)	0(1)	0(1)
C(2)	30(1)	22(1)	23(1)	1(1)	−1(1)	3(1)
C(3)	32(1)	23(1)	24(1)	0(1)	−4(1)	4(1)
C(4)	43(1)	30(1)	24(1)	−2(1)	−4(1)	2(1)
C(5)	34(1)	21(1)	23(1)	1(1)	0(1)	−5(1)
C(6)	36(1)	35(1)	31(1)	−1(1)	−2(1)	−4(1)
C(7)	48(1)	52(1)	30(1)	−1(1)	−11(1)	−15(1)
C(8)	64(1)	43(1)	24(1)	−8(1)	1(1)	−18(1)
C(9)	52(1)	32(1)	32(1)	−6(1)	13(1)	−7(1)
C(10)	35(1)	28(1)	29(1)	−1(1)	0(1)	−4(1)
C(11)	33(1)	19(1)	27(1)	−3(1)	−3(1)	2(1)
C(12)	37(1)	26(1)	27(1)	−2(1)	−5(1)	−4(1)
C(13)	55(1)	34(1)	30(1)	3(1)	4(1)	−6(1)
C(14)	45(1)	36(1)	50(1)	1(1)	10(1)	−10(1)
C(15)	33(1)	33(1)	57(1)	−6(1)	−5(1)	−4(1)
C(16)	36(1)	27(1)	36(1)	−2(1)	−8(1)	3(1)
S(1)	50(1)	39(1)	21(1)	1(1)	4(1)	2(1)

Table 6: **Anisotropic displacement parameters ($Å^2 \times 10^3$) for T(Ph_2)**
The anisotropic displacement factor exponent takes the form: $-2\,\pi^2\,[h^2\,a^{*2}\,U_{11} + ... + 2\,h\,k\,a^*\,b^*\,U_{12}]$

Quantum-Chemical Calculations

The structure optimisation for **T(Ph_2)** was performed with the program *Gaussian98 Revision A.7* on the B3LYP/6-31+G(d) and MP2/6-31+G(d) levels,[120,121] starting from the structural parameters of the crystal structure. A subsequent frequency calculation for determination of the type of the stationary point revealed no negative frequencies.

A search for other possible conformers was performed on the HF/3-21+G(d) level by energy optimisation of selected geometries with different torsion angles of the phenyl groups. The obtained stationary points were identical in their conformation to the structure obtained by the above described B3LYP optimisation.

atom	x	Y	z
S	0.37925	−3.50911	−0.15851
C	−1.51476	0.98648	0.97487
H	−0.68152	0.97840	1.67159
C	−0.60726	−1.11158	−0.08205
C	1.58424	0.32456	−0.04507
C	1.47751	−2.17461	−0.08555
H	2.54513	−2.34750	−0.12737
C	−1.60907	−0.01852	−0.00394
C	2.00566	2.54280	−0.95794
H	1.74698	3.32792	−1.66416
C	−2.70253	0.00971	−0.88699
H	−2.77901	−0.74936	−1.66162
C	1.26804	1.35812	−0.94426
H	0.44564	1.22715	−1.64144
C	0.83647	−0.95812	−0.05373
C	−0.97675	−2.43500	−0.14363
H	−1.98349	−2.83192	−0.12288
C	2.65922	0.51563	0.84059
H	2.90407	−0.26614	1.55543
C	−2.48493	1.98534	1.06789
H	−2.39530	2.75112	1.83446
C	3.07445	2.71962	−0.07365
H	3.64738	3.64337	−0.08493
C	−3.67482	1.00847	−0.79282
H	−4.51054	1.01348	−1.48835
C	−3.56921	2.00124	0.18487
H	−4.32337	2.78074	0.25767
C	3.39910	1.70045	0.82547
H	4.22457	1.82872	1.52145

Table 7: XYZ table of the energy minimum structure of T(Ph_2), calculated on a B3LYP/6-31+G(d) level

atom	x	Y	z
S	0.38339	−3.55214	−0.16283
C	−1.42355	0.91934	1.03448
H	−0.61578	0.83367	1.75961
C	−0.59202	−1.16583	−0.06372
C	1.53449	0.28367	−0.07571
C	1.48350	−2.23630	−0.12490
H	2.55158	−2.40918	−0.20319
C	−1.55079	−0.04926	0.02303
C	1.86195	2.50434	−1.01125
H	1.59442	3.26382	−1.74367
C	−2.60104	0.06400	−0.90323
H	−2.68748	−0.67080	−1.70304
C	1.19787	1.27529	−1.01421
H	0.42061	1.07472	−1.74993
C	0.83333	−1.01317	−0.07876
C	−0.96952	−2.49849	−0.11258
H	−1.97655	−2.89780	−0.05551
C	2.54463	0.54740	0.86442
H	2.79046	−0.20943	1.60865
C	−2.33188	1.97752	1.11656
H	−2.22484	2.72038	1.90494
C	2.86953	2.75965	−0.07275
H	3.38454	3.71829	−0.07114
C	−3.51204	1.12185	−0.81663
H	−4.32051	1.20035	−1.54133
C	−3.37790	2.08294	0.19141
H	−4.08347	2.90889	0.25619
C	3.21136	1.77700	0.86288
H	3.99086	1.97074	1.59760

Table 8: XYZ table of the energy minimum structure of T(Ph_2), calculated on an MP2/6-31+G(d) level

method of determination	absolute energy [a.u. (Hartree)]
without zero-point correction	−1015.137998
with zero-point correction	−1014.909249

Table 9: Absolute energy of the energy minimum structure of T(Ph_2), calculated on a B3LYP/6-31+G(d) level

4 Photophysical Properties of Oligothienyl Macrocycles

4.1 Theoretical Model and Selection Rules for Conjugated Macrocycles

4.1.1 Properties of Linear Oligothiophenes

Among the best-known conjugated polymers, with properties superior to the initial polyacetylene reported by the Nobel laureates *Heeger, Shirakawa and MacDiarmid* in 1977,[132] are polythiophenes. But also their shorter analogues, the oligothiophenes, gained much interest: Not only can they be regarded as well-defined model systems for polythiophenes, but they already show intriguing electronic properties similar to those of their polymeric pendants.[133] Together with their inherent stability in a number of redox states, this renders them good candidates for application in molecular electronic devices such as organic light-emitting diodes[134], as in field effect transistors[135] or in solar cells[134e,136].

Along with research for the application of oligothiophenes in nanotechnology, structure–property investigations became necessary to gain a deeper understanding of the electronic nature and the change of properties upon variation of the molecular structure. In this respect, homologue series of oligothiophenes have been synthesised to provide basic motifs with a broad range of π-conjugation lengths, up to a region that already corresponds to polymer systems.[137] Alkyl substituents at the β positions helped to improve the solubility of such long oligomers, and so far the longest oligomer reported in literature (by *Otsubo et al.*) contains no less than 96 thiophene rings.[137a] With such series, systematic studies of the photophysical properties of oligothiophenes could be realised. Certainly, one of the most important parameters is the effective conjugation length. This value describes the number of thiophene/momomer units after which the π–π^* absorption no longer shifts to the red: For a small number of aromatic rings in the oligomer, the absorption maxima linearly progress to longer wavelengths, but this behaviour changes for longer oligomers. Causes for this "saturation" of the absorption maxima can be found in the deviation from planarity (e.g., by rotation around single bonds) for longer chains, the reduced electron mobility due to resonance stabilisation of the aromatic rings within the oligomers, increasing effects of the electron–electron correlation, or alternating bond lengths as error potentials.[138] While earlier studies suggested that saturation for the effective conjugation length is almost approached with 11 repeating units,[139] the experiments of *Otsubo et al.* proved that the progressive bathochromic shift of absorption and emission does not

even stop at the 96mer. Absorption of this long oligomer shows maxima at 527.7 and 556.5 nm, which is even at longer wavelengths than the values of 500–526 nm for regioregular poly(alkylthiophene)s.[137a]

A thorough investigation was performed for a series of butyl-substituted oligothiophenes by *Bäuerle et al.*: By dimerisation of acetylene-substituted (oligo)thiophenes and subsequent rendering of the diethynyl units into thiophenes, the linear chain could be prolonged in bithienyl steps from the trimer to the 19mer (figure 73).[137e]

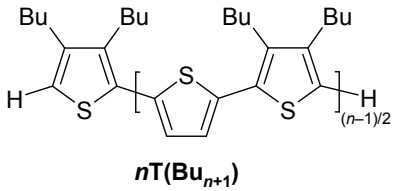

***n*T(Bu$_{n+1}$)**

Figure 73: Homologue series of butyl-substituted linear oligomers investigated by *Bäuerle et al.* (*n* = 3, 5, 7, 9, 11, 13, 15, 17, 19)

compound	*n* = 3	*n* = 5	*n* = 7	*n* = 9	*n* = 11	*n* = 13	*n* = 15	*n* = 17	*n* = 19
absorption λ_{max} / nm	342	386	409	418	422	425	427	429	430
extinction coeff. ε_{max} / L mol^{-1} cm^{-1}	18500	26600	41000	55700	71500	88000	100500	115000	125000

Table 10: Summary of spectroscopic data of the *n*T(Bu$_{n+1}$) series

As can be seen in table 10 and the left graph of figure 74, the energy of the longest wavelength π–π^* transition decreases and the maximum extinction coefficient increases with growing chain length. By plotting the inverse chain length 1/*n* against the transition energy (figure 74, right graph), both the region of linear dependence (for $n \leq 7$) and the region of saturation (for $n \geq 9$) are clearly visible:

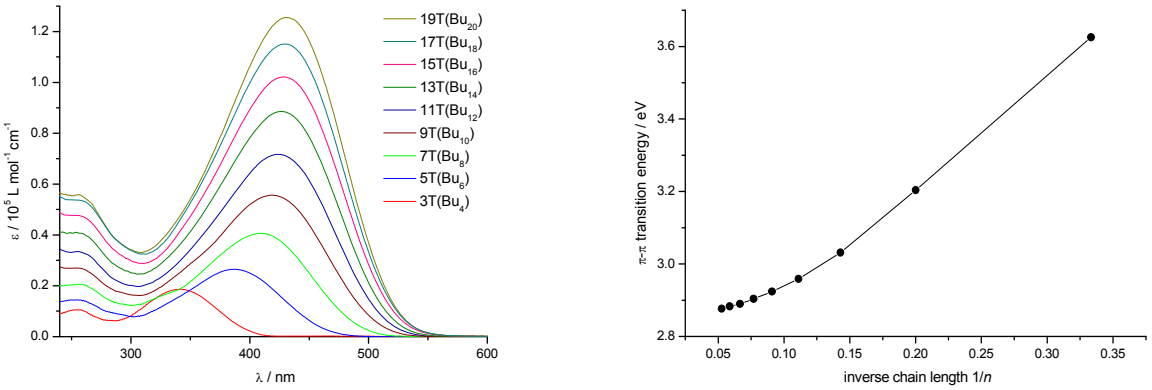

Figure 74: **Absorption spectra of the *n*T(Bu$_{n+1}$) series and correlation with the lengths of the oligomers**
left graph: absorption spectra of ***n*T(Bu$_{n+1}$)**;
measured in CH_2Cl_2 at a concentration of 1×10^{-5} mol L^{-1}
right graph: correlation of the transition energy of the longest wavelength absorption maxima with the inverse chain length $1/n$ (n = number of thiophene units)

According to these results, a mathematical model[138d] could be successfully applied which describes the behaviour by an exponential function (eq. 1).[137e]

$$\lambda_{i,n} = \lambda_{i,\infty} + (\lambda_{i,1} - \lambda_{i,\infty})e^{-a_i(n-1)} \qquad (\text{Eq. 1})$$

$\lambda_{i,n}$: longest wavelength absorption maximum for an oligomer consisting of n units

$\lambda_{i,\infty}$: longest wavelength absorption maximum for an ideal, fully conjugated oligomer of infinite length

$\lambda_{i,1}$: longest wavelength absorption maximum for the shortest oligomer of a series (n = 1)

a_i: determines how fast saturation of the values will occur for growing chain length

n: number of monomer units

Especially a_i reflects the influence of the structure: the higher value of 0.333 for the ***n*T(Bu$_{n+1}$)** series, where every second thiophene has two butyl side chains, compared to 0.287 for an oligothiophene series in which every third thiophene has one dodecyl substituent, is a result of the higher steric demand of the substitution pattern in ***n*T(Bu$_{n+1}$)**.

4.1.2 The Frenkel Exciton Model for Linear and Cyclic Oligothiophenes

By comparison of the absorption maxima of the cyclo[*n*]thiophenes **C[12]T**, **C[16]T** and **C[18]T** (cf. figure 2 on p. 10), which are discussed more in detail in section 4.8.3, with those of the linear analogues presented above, a remarkable discovery was made:[140]

Although, as expected, the absorptions of the macrocycles are progressively red-shifted, linear oligomers comprising the same number of thiophenes absorb at even longer wavelengths. In fact, the transition energy of the cyclothiophenes rather corresponds to linear oligothiophenes with *half* the number of thiophenes, while the extinction is in the range of oligomers with the same length. E.g., **C[18]T** absorbs at 419 nm (2.96 eV) with an extinction coefficient of 123 900 L mol^{-1} cm^{-1}. The absorption maximum is close to the 418 nm (2.94 eV) of the linear nonamer **9T(Bu$_{10}$)**, but the extinction rather fits the value of 125 000 L mol^{-1} cm^{-1} for **19T(Bu$_{20}$)**.

Therefore, a new model was worked out in which describes the electronic transitions with a Frenkel exciton model, i.e. the superposition of local excitations of the monomers defined by the thiophene units.[140] By transformation of the corresponding Hamiltonian for the transition energy with a different basis each for linear and for cyclic geometry, different equations for the eigenvalues $E^{\text{lin}}_{k_{\text{lin}}}$ and $E^{\text{cyc}}_{k_{\text{cyc}}}$ of linear and cyclic oligomers can be derived (eq. 2 and eq. 3):

$$E^{\text{lin}}_{k_{\text{lin}}} = \omega_0 - 2J\cos\left(\frac{\pi k_{\text{lin}}}{N_{\text{lin}}+1}\right) \qquad \text{(Eq. 2)}$$

$$E^{\text{cyc}}_{k_{\text{cyc}}} = \omega_0 - 2J\cos\left(\frac{2\pi k_{\text{cyc}}}{N_{\text{cyc}}}\right) \qquad \text{(Eq. 3)}$$

ω_0: excitation energy of a monomer

J: parameter for the nearest-neighbour coupling; the sign (which depends on the angle between the transition dipole moment and the chain axis) is assumed to be positive, i.e. the states coupling to the light are those at the bottom of the exciton band

k_{lin}, k_{cyc}: selection rule parameters for linear/cyclic oligomers

N_{lin}, N_{cyc}: length of the linear/cyclic oligomer

For linear oligomers, k_{lin} can adopt the values 1, 2, …, N_{lin}; where the energy state for $k_{\mathrm{lin}} = 1$ lies at the bottom of the excitation band. For a macrocyclic geometry, periodic boundary conditions have to be applied and, as a consequence, N_{cyc} only adopts even values. Here, the selection rule is $k_{\mathrm{cyc}} = 0, \pm 1, \pm 2, \ldots, \pm\frac{N_{\mathrm{cyc}}}{2}$, with degenerate eigenstates for each pair $\pm k_{\mathrm{cyc}}$.

An important difference between the two geometries is that for the linear model the energy always depends on the size N_{lin}, whereas the energy of the lowest state for cyclic systems is independent of N_{cyc} (due to the lowest possible k_{cyc} value of zero in the cosinus part of eq. 3) and has a value of

$$E_0^{\mathrm{cyc}} = \omega_0 - 2J \qquad (\text{Eq. 4})$$

A comparison of the terms for linear and cyclic energies (eq. 2 and eq. 3) finally shows that they are related according to

$$N_{\mathrm{cyc}} = 2(N_{\mathrm{lin}} + 1) \qquad (\text{Eq. 5})$$

which confirms the experimental finding that the absorption maxima of the macrocycles are near the values of linear analogues of half the size.

Similar to the energy states, the oscillator strengths O_k of the transitions differ for linear and cyclic oligomers, because in cyclic oligomers in-plane dipole rotation around the ring has to be considered. The values can be calculated according to eq. 6 and eq. 7:

$$O_{k_{\mathrm{lin}}}^{\mathrm{lin}} = \frac{1-(-1)^{k_{\mathrm{lin}}}}{2} \times \frac{2\mu^2}{N_{\mathrm{lin}}+1} \times \left(\cot^2 \frac{\pi k_{\mathrm{lin}}}{2(N_{\mathrm{lin}}+1)} \right) \qquad (\text{Eq. 6})$$

$$O_{k_{\mathrm{cyc}}}^{\mathrm{cyc}} = N_{\mathrm{cyc}}\mu^2 \left[\sin^2\beta\,\delta_{k_{\mathrm{cyc}},0} + \frac{1}{2}\cos^2\beta\left(\delta_{k_{\mathrm{cyc}},-1} + \delta_{k_{\mathrm{cyc}},1}\right) \right] \qquad (\text{Eq. 7})$$

μ: transition dipole

β: angle between the monomer dipoles and the ring plane

δ_k: parameter regarding selection rules

For linear oligothiophenes, using eq. 2 and eq. 6, a perfect fit of a calculated curve to the experimental absorption maxima was possible. Furthermore, with the values for ω_0 and J obtained from this fit, even theoretical values for the macrocycles **C[12]T**, **C[16]T** and **C[18]T**, derived from eq. 3 and eq. 7, agreed well with the experimental data, like shown in table 11:

compound	**C[12]T**	**C[16]T**	**C[18]T**
experimental absorption maximum λ_{max} / eV (nm)	3.171 (391)	2.987 (415)	2.959 (419)
calculated extinction maximum λ_{max} / eV (nm)	3.196 (388)	3.043 (407)	3.004 (413)

Table 11: **Comparison between experimental and calculated absorption maxima for the C[*n*]T series**
the values of ω_0 = 5.5 eV and J = 1.3 eV were derived from the linear oligomer series

4.2 Absorption and Emission of Cyclic Oligo(thienylene-butadiinylene)s

4.2.1 Macrocycles with terthiophene (3T) units

From the family of macrocyclic oligo(terthienylene–diethynylene)s **C[3T(Bu$_4$)–DA]$_m$**, the compounds ranging from m = 2 (cyclic dimer) up to m = 9 (cyclic nonamer) were investigated, from which the values for **C[3T(Bu$_4$)–DA]$_2$** had been reported before.[141] On the following pages, absorption as well as emission and excitation spectra of these compounds are presented (figure 75 and table 12) and will be discussed in section 4.8. For m = 2–6, extinction coefficients were obtained from concentration rows with three or four concentrations between 10^{-4} and 10^{-8} mol L^{-1}. For m = 7–9, not enough substance was available to determine these values.

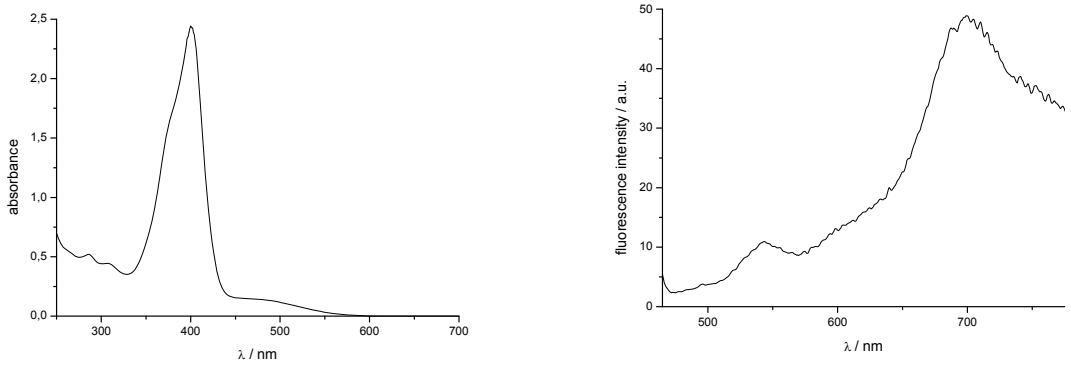

a) C[3T(Bu$_4$)–DA]$_2$
left graph: absorption spectrum: λ_{max} = 400 nm; ε_{max} = 129000 L mol^{-1} cm^{-1}
right graph: emission spectrum: λ_{ecx} = 400 nm; λ_{max} = 545 nm and 699 nm; Φ_{fl} << 1 %

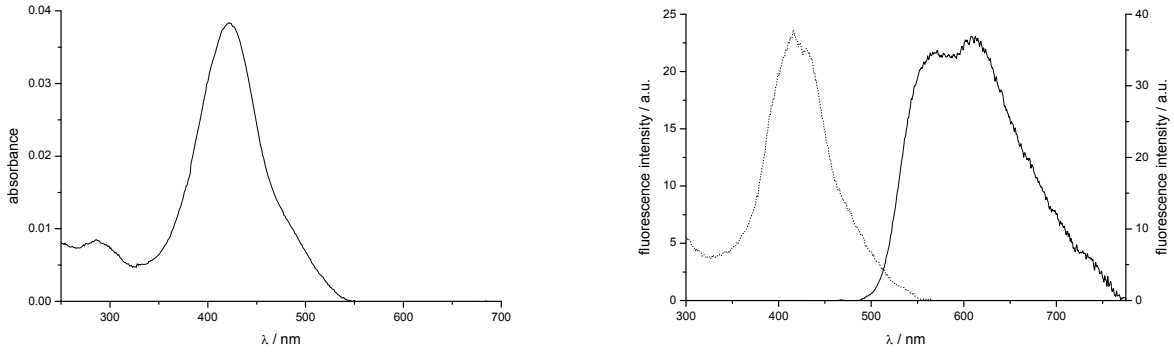

b) C[3T(Bu$_4$)–DA]$_3$
left graph: absorption spectrum: λ_{max} = 422 nm; ε_{max} = 133500 L mol^{-1} cm^{-1}
right graph: excitation spectrum (dotted line);
emission spectrum (solid line): λ_{ecx} = 422 nm; λ_{max} = 571 nm and 612 nm; Φ_{fl} = 7.2 (± 0.7) %

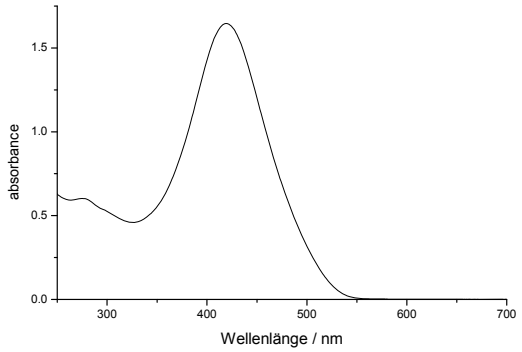

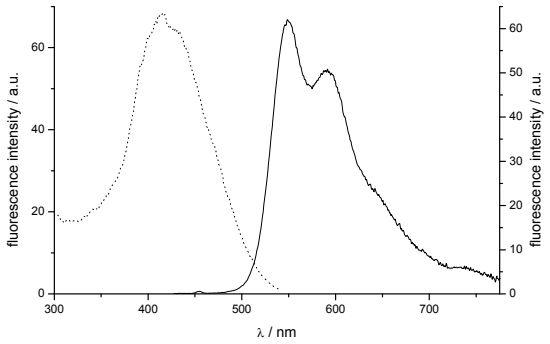

c) C[3T(Bu$_4$)–DA]$_4$

left graph: absorption spectrum: λ_{max} = 420 nm; ε_{max} = 162800 L mol^{-1} cm^{-1}
right graph: excitation spectrum (dotted line);
emission spectrum (solid line): λ_{ecx} = 420 nm; λ_{max} = 549 nm and 594 nm; Φ_{fl} = 13.6 (± 1.3) %

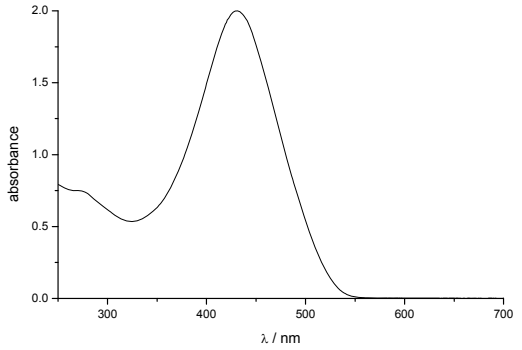

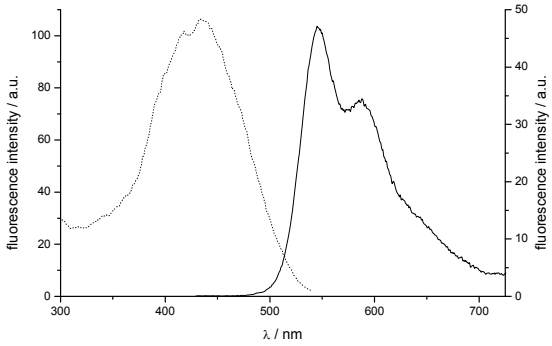

d) C[3T(Bu$_4$)–DA]$_5$

left graph: absorption spectrum: λ_{max} = 431 nm; ε_{max} = 211300 L mol^{-1} cm^{-1}
right graph: excitation spectrum (dotted line);
emission spectrum (solid line): λ_{ecx} = 431 nm; λ_{max} = 546 nm and 588 nm; Φ_{fl} = 15.5 (± 1.2) %

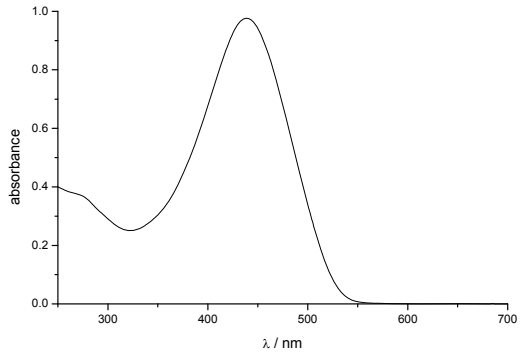

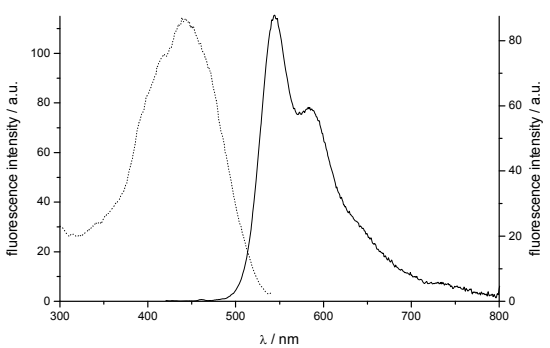

e) C[3T(Bu$_4$)–DA]$_6$

left graph: absorption spectrum: λ_{max} = 439 nm; ε_{max} = 212900 L mol^{-1} cm^{-1}
right graph: excitation spectrum (dotted line);
emission spectrum (solid line): λ_{ecx} = 439 nm; λ_{max} = 545 nm and 587 nm; Φ_{fl} = 18.2 (± 1.2) %

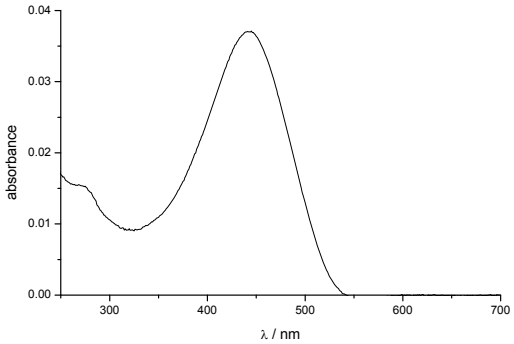

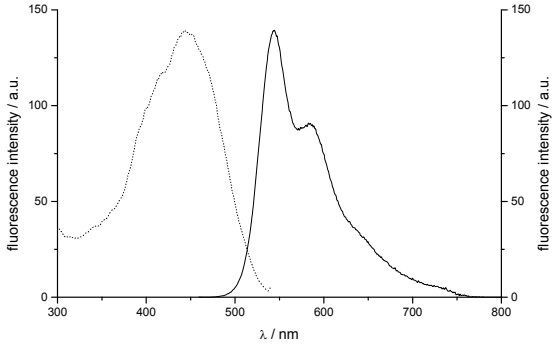

f) C[3T(Bu$_4$)–DA]$_7$
left graph: absorption spectrum: λ_{max} = 443 nm
right graph: excitation spectrum (dotted line);
emission spectrum (solid line): λ_{ecx} = 443 nm; λ_{max} = 544 nm and 585 nm; Φ_{fl} = 24.0 (± 1.2) %

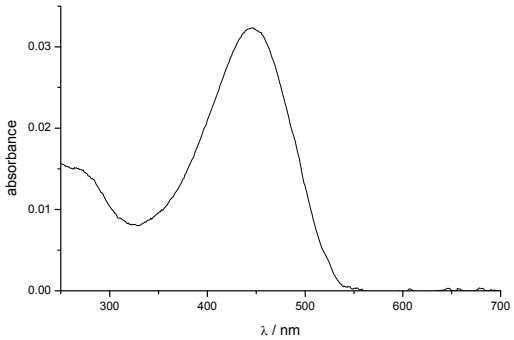

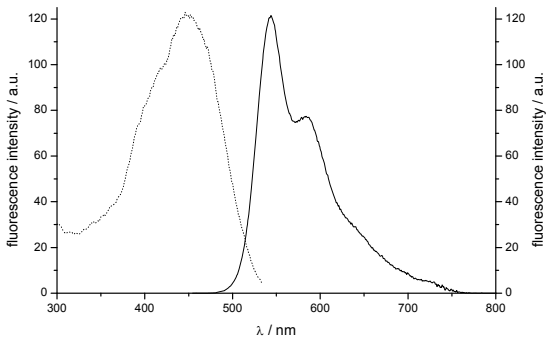

g) C[3T(Bu$_4$)–DA]$_8$
left graph: absorption spectrum: λ_{max} = 445 nm
right graph: excitation spectrum (dotted line);
emission spectrum (solid line): λ_{ecx} = 445 nm; λ_{max} = 544 nm and 584 nm; Φ_{fl} = 23.5 (± 0.9) %

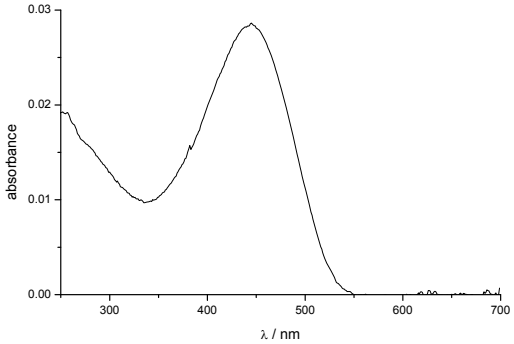

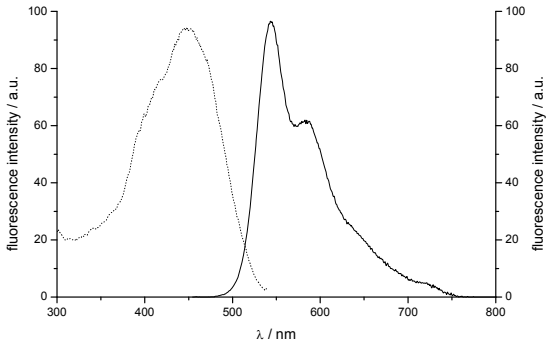

h) C[3T(Bu$_4$)–DA]$_9$
left graph: absorption spectrum: λ_{max} = 445 nm
right graph: excitation spectrum (dotted line);
emission spectrum (solid line): λ_{ecx} = 445 nm; λ_{max} = 544 nm and 584 nm; Φ_{fl} = 20.4 (± 1.4) %

Figure 75: Optical spectra of the C[3T(Bu$_4$)–DA]$_m$ series (m = 2–9)
further details are shown in table 12

compound	absorption λ_{max} / nm	further abs. λ_{max} / nm	extinction coeff. ε_{max} / L mol^{-1} cm^{-1}	fluorescence λ_{max} / nm	quantum yield $\Phi_{Fl.}$ / %[a]
C[3T(Bu$_4$)–DA]$_2$	400; ≈490	285; 308	129000	545; 584	<< 1 [b]
C[3T(Bu$_4$)–DA]$_3$	422	287; ≈ 302	133500	571; 612	7.2 (0.7)[b]
C[3T(Bu$_4$)–DA]$_4$	420	276; ≈ 295	162800	549; 594	13.6 (1.3)[b]
C[3T(Bu$_4$)–DA]$_5$	431	≈ 273	211300	546; 588	15.5 (1.2)[b]
C[3T(Bu$_4$)–DA]$_6$	439	≈ 272	212900	545; 587	18.2 (1.2)[b]
C[3T(Bu$_4$)–DA]$_7$	443	≈ 273	--[c]	544; 585	24.0 (1.2)[d]
C[3T(Bu$_4$)–DA]$_8$	445	≈ 267	--[c]	544; 584	23.5 (0.9)[d]
C[3T(Bu$_4$)–DA]$_9$	445	≈ 274	--[c]	544; 584	20.4 (1.4)[d]

Table 12: **Summary of spectroscopic data of the C[3T(Bu$_4$)–DA]$_m$ series (m = 2–9)**
[a] mean value for different wavelengths; maximum deviation of a single value is given in parentheses
[b] quantum yield standard: 9,10-diphenylanthracene (dpa)
[c] not enough substance for measurement
[d] quantum yield standard: fluoresceine

The absorption curves of the substances all look rather similar, with a small maximum in the region of 270–285 nm (originating from the n–π^* transition of the thiophenes) and a relatively broad longest wavelength absorption between 400 and 445 nm. The emission spectra typically possess a large (yet decreasing) Stokes shift and show two peaks between 544 and ca. 600 nm, of which the first one is higher in intensity. Towards longer wavelengths, usually one or two shoulders are visible. Excitation spectra are congruent to the absorption spectra, except for a fine structure resolved in the main peak.

As can be seen in table 12, the longest wavelength absorption maxima expectedly shift to the red (from 400 to 445 nm) with increasing ring size, while the first and second emission maxima shift to the blue (from 571 to 544 nm and from 612 to 584 nm).

The values for **C[3T(Bu$_4$)–DA]$_2$**, which do not obey these trends, will be discussed in section 4.8.

4.2.2 Macrocycles with quinquethiophene (5T) units

Of the cyclic oligo(quinquethienylene–diethynylene)s series, pure **C[5T(Bu$_6$)–DA]$_m$** with m = 2–4 were available for spectroscopic investigations.[141] Only from the smallest macrocycles (m = 3 and m = 4) extinction coefficients could be measured, due to only very small substance quantities. For the latter (m = 4), the variation of the coefficients at different concentrations was rather large (± 15000 L mol^{-1} cm^{-1}). The optical spectra of these compounds and some key values are given in figure 76 and table 13:

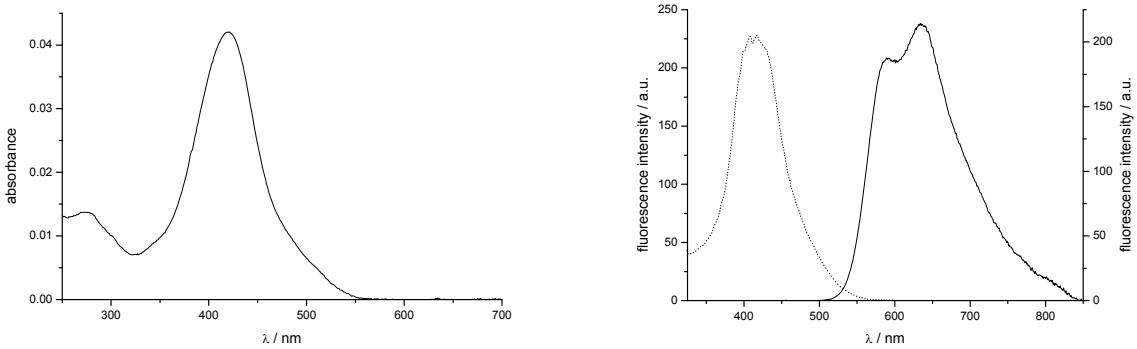

a) C[5T(Bu$_6$)–DA]$_2$
left graph: absorption spectrum: λ_{max} = 421 nm; ε_{max} = 118800 L mol^{-1} cm^{-1}
right graph: excitation spectra (dotted line);
emission spectrum (solid line): λ_{ecx} = 421 nm; λ_{max} = 592 nm and 635 nm; Φ_{fl} = 7.8 (± 0.7) %

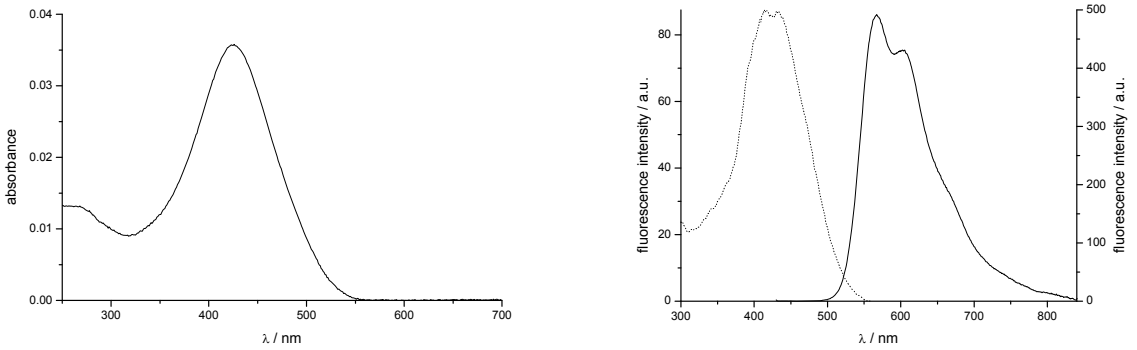

b) C[5T(Bu$_6$)–DA]$_3$
left graph: absorption spectrum: λ_{max} = 425 nm; ε_{max} = 205200 L mol^{-1} cm^{-1}
right graph: excitation spectrum (dotted line);
emission spectrum (solid line): λ_{ecx} = 425 nm; λ_{max} = 567 nm and 603 nm; Φ_{fl} = 17.4 (± 1.4) %

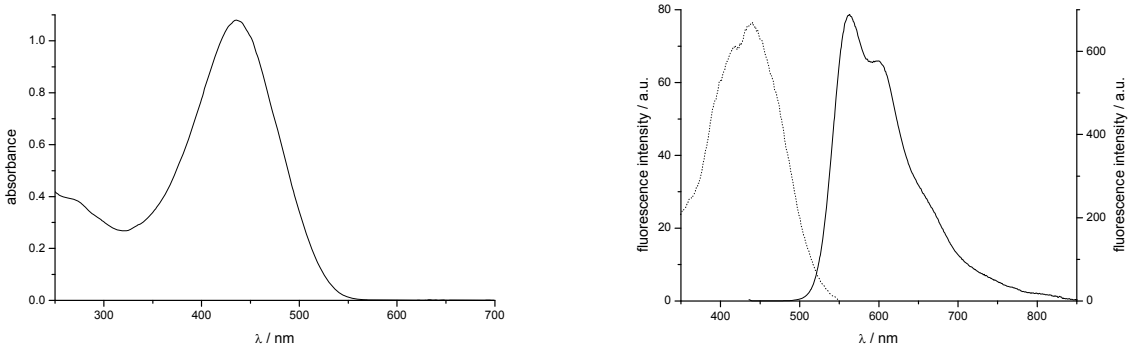

c) C[5T(Bu$_6$)–DA]$_4$
left graph: absorption spectrum: λ_{max} = 436 nm; ε_{max} = 235200 L mol^{-1} cm^{-1}
right graph: excitation spectrum (dotted line);
emission spectrum (solid line): λ_{ecx} = 436 nm; λ_{max} = 563 nm and 599 nm; Φ_{fl} = 14.8 (± 1.4) %

Figure 76: Optical spectra of the C[5T(Bu$_6$)–DA]$_m$ series (m = 2–4)
further details are shown in table 13

compound	absorption λ_{max} / nm	further abs. λ_{max} / nm	extinction coeff. ε_{max} / L mol^{-1} cm^{-1}	fluorescence λ_{max} / nm	quantum yield $\Phi_{Fl.}$ / %
C[5T(Bu$_6$)–DA]$_2$	421	275	118800	592; 635	7.8 (± 0.7)[a]
C[5T(Bu$_6$)–DA]$_3$	425	≈ 266	205200	567; 603	17.4 (± 1.4)[a]
C[5T(Bu$_6$)–DA]$_4$	436	≈ 266	235200[b]	563; 599	14.8 (± 1.4)[a]

Table 13: **Summary of spectroscopic data of the C[5T(Bu$_6$)–DA]$_m$ series (m = 2–4)**
[a] quantum yield standard: dpa
[b] large single deviations from mean value (> 5 %)

In general, the absorption, emission and excitation spectra look similar to those of the 3T series, with the slight difference that the emission spectra the two vibronic bands are of almost the same intensity. Like **C[3T(Bu$_4$)–DA]$_3$**, the smallest quinquethiophene macrocycle **C[5T(Bu$_6$)–DA]$_2$** shows a shoulder in the relatively narrow absorption spectra. With growing size, the longest wavelength absorption again shifts to the blue, while the first emission maximum becomes shifted to the red.

The energy difference between the two emission maxima for **C[5T(Bu$_6$)–DA]$_2$**, **C[5T(Bu$_6$)–DA]$_3$** and **C[5T(Bu$_6$)–DA]$_4$** is 0.142, 0.131 and 0.132 eV, respectively. Thus, the energetic splitting of these bands is weaker than for the **C[3T(Bu$_4$)–DA]$_m$** series (0.156–0.168 eV). Similarly, this energy difference seems to become smaller, but for this series saturation not yet seems to be reached with the cyclic tetramer. Like for the terthiophene series, further emission maxima could only be estimated, as only the first two peaks are separated while the others appear as shoulders in the emission spectra. For the smallest macrocycle **C[5T(Bu$_6$)–DA]$_2$** there is even no such shoulder visible. Nevertheless, the approximate values of ca. 0.19 eV for the energy gap between the second and third emission maxima are significantly larger than the difference between the first and second emission maxima.

The quantum yield seems to reach its maximum faster than for the terthiophene series: Already for **C[5T(Bu$_6$)–DA]$_4$**, the quantum yield drops as an effect of the higher number of thiophene units (cf. section 4.8.2).

4.2.3 Macrocycles with undecithiophene (11T) units

In a different synthetic approach to oligothiophene macrocycles, the longer undecithiophene–diacetylide monomers had been synthesised and cyclised to **C[11T(Bu$_{12}$)–DA]$_m$** macrocycles (m = 1, 2). Their spectra are shown in figure 77 and summarised in table 14:

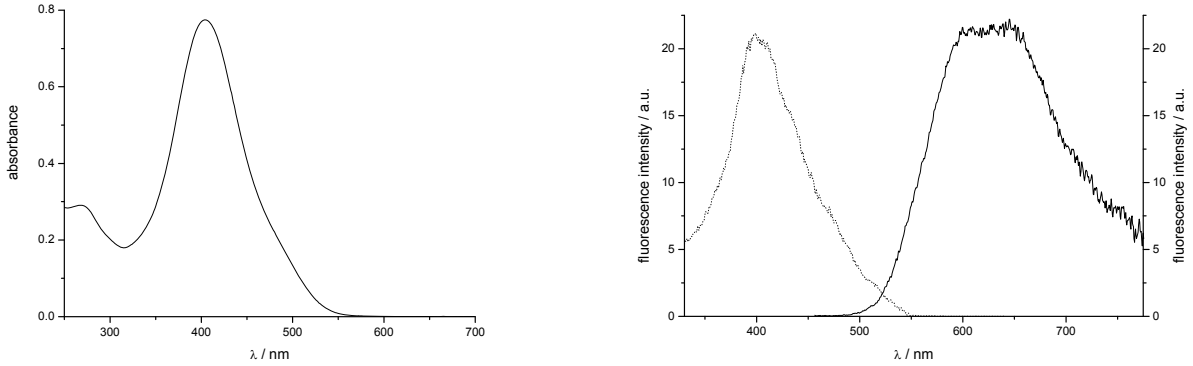

a) C[11T(Bu$_{12}$)–DA]$_1$
left graph: absorption spectrum: λ_{max} = 406 nm; ε_{max} = 87700 L mol^{-1} cm^{-1}
right graph: excitation spectrum (dotted line);
emission spectrum (solid line): λ_{ecx} = 406 nm; λ_{max} = 605 nm and 647 nm; Φ_{fl} = 7.7 (± 0.8) %

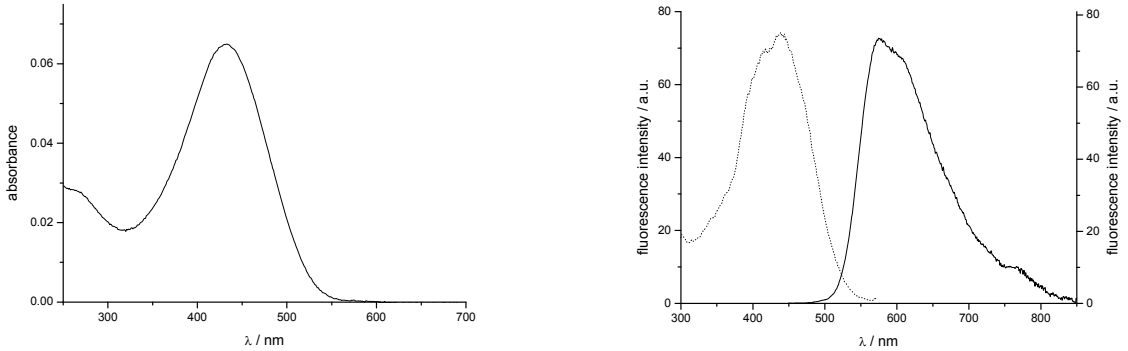

b) C[11T(Bu$_{12}$)–DA]$_2$
left graph: absorption spectrum: λ_{max} = 433 nm; ε_{max} = 69100 L mol^{-1} cm^{-1}
right graph: excitation spectrum (dotted line);
emission spectrum (solid line): λ_{ecx} = 433 nm; λ_{max} = 578 nm and ≈ 601 nm; Φ_{fl} = 20.5 (± 0.6) %

Figure 77: Optical spectra of the C[11T(Bu$_{12}$)–DA]$_m$ series (m = 1, 2)
further details are shown in table 14

compound	absorption λ_{max} / nm	further abs. λ_{max} / nm	extinction coeff. ε_{max} / L mol^{-1} cm^{-1}	fluorescence λ_{max} / nm	quantum yield $\Phi_{Fl.}$ / %
C[11T(Bu$_{12}$)–DA]	405	≈ 268	87700	605; 647	7.7 (± 0.6) [a]
C[11T(Bu$_{12}$)–DA]$_2$	433	≈ 263	69100	578; ≈ 601	20.5 (± 0.6) [a]

Table 14: Summary of spectroscopic data of the C[11T(Bu$_{12}$)–DA]$_m$ series (m = 1, 2)
[a] quantum yield standard: dpa

In general, the shapes of the spectra are similar to the previous series. The spectroscopic values of **C[11T(Bu$_{12}$)–DA]$_2$** seamlessly fit to those of the macrocycles **C[3T(Bu$_4$)–DA]$_6$** and **C[5T(Bu$_6$)–DA]$_4$** which have the same size (i.e., the same number of carbon atoms): The longest wavelength absorption is at 434 nm (439 and 436 nm for the other macrocycles), and the quantum yield of 20 % is also in the same region as for the other two cycles (18 and 15 %).

In contrast, the values for the extinction coefficients of the cyclic oligo(undecithienylene-diethynylene)s are somewhat unusual: the dimer not only has a lower extinction maximum than the monomer, but also the value of 69100 L mol^{-1} cm^{-1} is extremely low for an oligothiophene macrocycle of this size.

In the emission spectra, the first two maxima of **C[11T–DA]$_2$** are merged to almost a single, broad band that “peaks” at a longer wavelength than the 3T and 5T analogues.

4.3 Pt(II) Macrocycles with Oligothienyl Monomers

4.3.1 C[Pt–A–3T(Bu_4)–A]$_2$ ("butyl series")

For the preparation of the conjugated oligothiophene macrocycles, a metal template route had been worked out.[141,142] Instead of coupling the monomers in a statistic way by a Glaser-type reaction under pseudo-high-dilution conditions, which resulted in a variety of macrocycles with different sizes, the monomer acetylide precursors were brought to reaction with Pt(dppp)Cl_2. The resulting intermediate diplatina-macrocycle **C[Pt–A–3T(Bu_4)–A]$_2$** (figure 78), which was obtained pure and with good yields, could be converted to the desired conjugated system by oxidatively induced reductive elimination with the aid of iodine as an oxidant. A more detailed description of the synthesis is presented in sections 2.3 and 3.3.

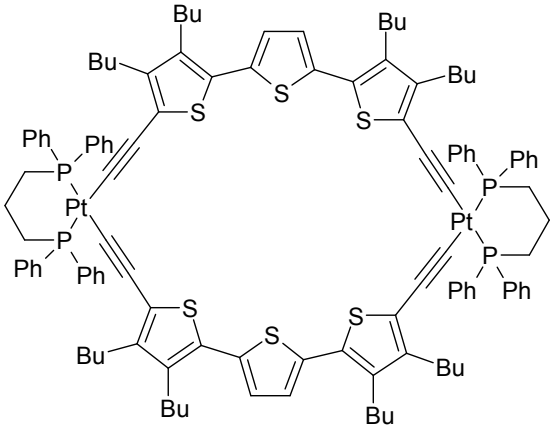

Figure 78: Diplatina-macrocycle C[Pt–A–3T(Bu_4)–A]$_2$

The incorporation of a transition metal into the cyclic organic array was expected to lead to a disruption of the conjugation and should have a major influence on the appearance of the optical spectra. However, measurement of these spectra was complicated by the extremely low solubility of this compound. In chlorinated solvents like dichloromethane (in which the spectra for all the conjugated macrocycles had been measured) decomposition of the platina-macrocycle occurred (figure 79), like reported for other platinum-containing macrocycles.[143]. Nonetheless, the spectroscopic values for **C[Pt–A–3T(Bu_4)–A]$_2$** and larger homologues that had been obtained in dichloromethane before[141] will be regarded in the discussion in section 4.8.5.

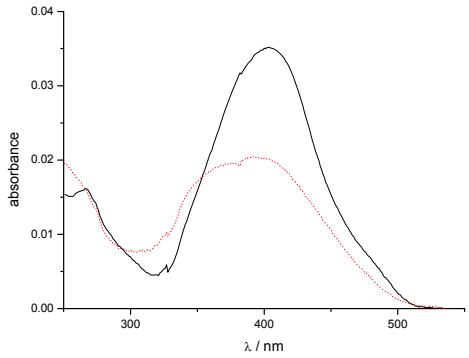

Figure 79: **Absorption spectra of a freshly prepared CH_2Cl_2 solution of C[Pt–A–3T(Bu_4)–A]$_2$ (solid line) and after 4 h (dotted red line)**
initial λ_{max} = 410 nm

The broad shape of the new absorption band in figure 79 makes a formation of fully conjugated macrocycles by Pt(II) elimination unlikely, and also in mass spectra of the solution no hint was found for such a reaction. Using other solvents, solubility was only sufficient in DMSO (but with broad and unstructured spectra) and THF. In the latter, no decomposition could be monitored and absorption and emission spectra were recorded (figure 80):

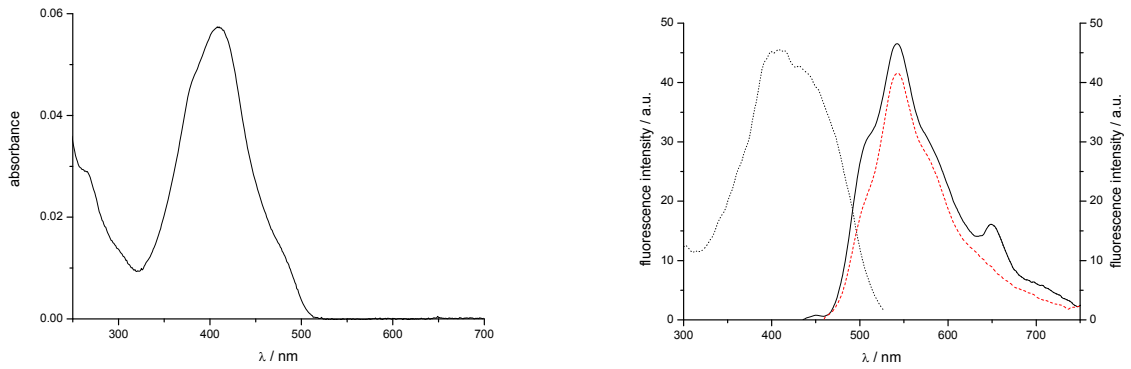

Figure 80: **Optical spectra of C[Pt–A–3T(Bu_4)–A]$_2$ in THF**
left graph: absorption spectrum: λ_{max} = 410 nm; ε_{max} = 52200 L mol^{-1} cm^{-1}
right graph: excitation spectrum (dotted line);
emission spectra upon excitation at 410 (solid line) and 440 nm (dashed red line):
λ_{max} = 543 and 650 nm
the values are summarized together with those of further platinacycles in table 15 (next section)

The platina macrocycle **C[Pt–A–3T(Bu_4)–A]$_2$** shows several differences to the "typical" cyclo(oligothiophene) spectra. Its longest wavelength absorption maximum of 410 nm is lower than that of **C[3T(Bu_4)–DA]$_3$** (422 nm), but unexpectedly higher than that of **C[3T(Bu_4)–DA]$_2$** (400 nm).

Even more interesting, the absorption spectrum of **C[Pt–A–3T(Bu$_4$)–A]$_2$** shows a shoulder at ca. 490 nm which corresponds to the first electronic transition seen for **C[3T(Bu$_4$)–DA]$_2$**. For **C[Pt–A–3T(Bu$_4$)–A]$_2$**, these shoulders have a strong influence on the emission values: Upon excitation at the absorption maximum of 410 nm, an emission peak at 650 nm appears, which is not visible when exciting at 440 nm.

The corresponding excitation spectrum (not shown here) of the 650 nm emission shows a more narrow maximum at 410 nm than the excitation spectrum for the 543 nm emission: the latter incidates a significant influence in the longer wavelength region of 440–460 nm for which, as mentioned above, no peak can be seen at 650 nm.

4.3.2 Pt(II) macrocycles with other oligothienyl monomers

In the course of the optical measurements, three other Pt(II) oligothienyl macrocycles with monomers differing in length and substitution pattern had been available (figure 81).[144]

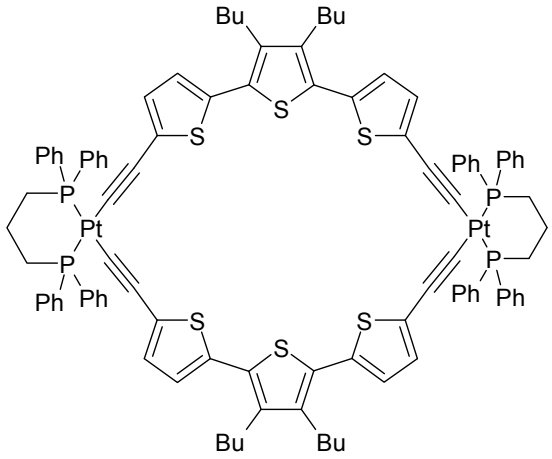

a) C[Pt–A–3T(Bu$_2$)–A]$_2$

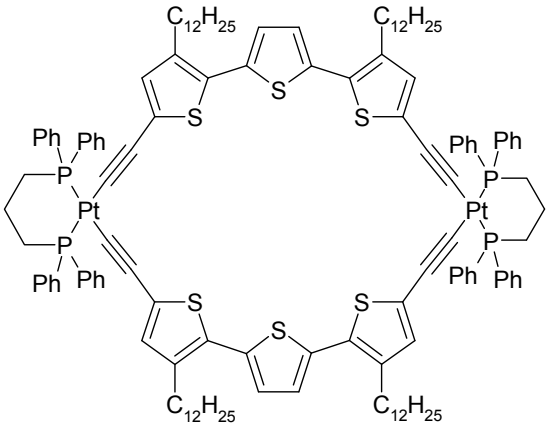

b) C[Pt–A–3T(Dodec$_2$)–A]$_2$

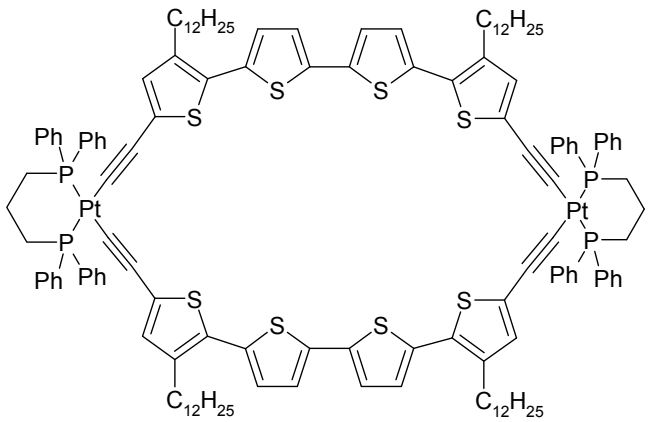

c) C[Pt–A–4T(Dodec$_2$)–A]$_2$

Figure 81: Pt(II) macrocycles with different oligothienyl monomer units

As the first macrocycle of this family, **C[Pt–A–3T(Bu$_4$)–A]$_2$**, had shown decomposition in chlorinated solvents, the spectra were all recorded in THF. Unfortunately, **C[Pt–A–3T(Bu$_2$)–A]$_2$** and **C[Pt–A–4T(Dodec$_2$)–A]$_2$** were only weakly soluble in this solvent, so the absorption spectra had to be taken in high dilution (like for the emission spectra). The spectra are shown in figure 82 and are summarised in table 15:

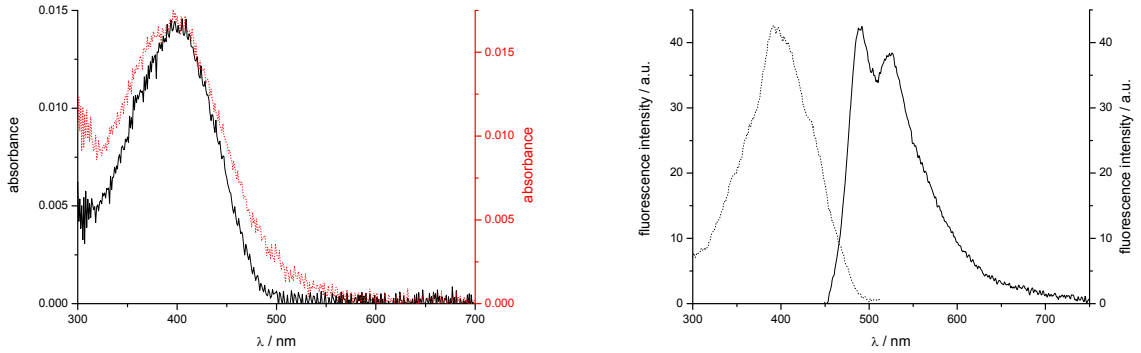

a) C[Pt–A–3T(Bu$_2$)–A]$_2$
left graph: absorption spectrum before (solid line) and after 6 h (dotted red line); λ_{max} = 400 nm; the *y* axis have been adjusted to make any differences more apparent
right graph: excitation spectrum (dotted line);
emission spectrum (solid line): λ_{ecx} = 400 nm; λ_{max} = 489 and 523 nm; Φ_{fl} << 1 %

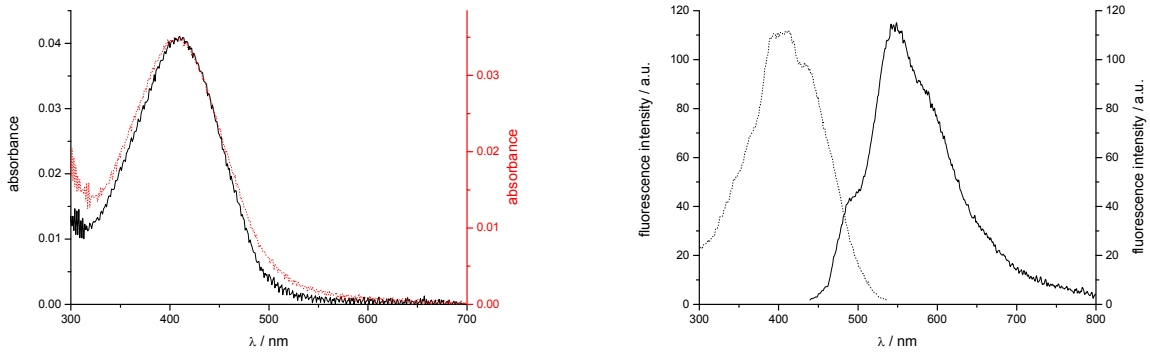

b) C[Pt–A–3T(Dodec$_2$)–A]$_2$
left graph: absorption spectrum before (solid line; λ_{max} = 410 nm) and after 16 h (dotted red line; λ_{max} = 407 nm); the *y* axis have been adjusted to make any differences more apparent
right graph: excitation spectrum (dotted line);
emission spectrum (solid line): λ_{ecx} = 410 nm; λ_{max} = 545 nm; Φ_{fl} = 2.2 (± 2.0) %

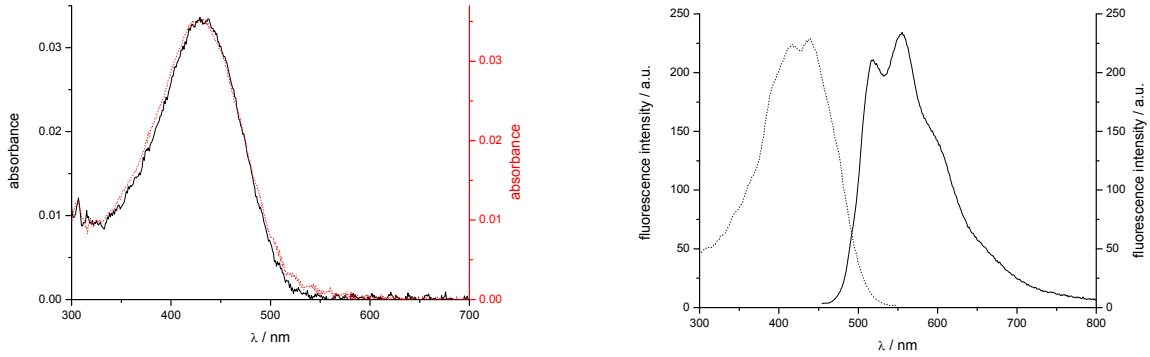

c) **C[Pt–A–4T(Dodec$_2$)–A]$_2$**
left graph: absorption spectrum before (solid line) and after 4 h (dotted red line); λ_{max} = 430 nm; the *y* axis have been adjusted to make any differences more apparent
right graph: excitation spectrum (dotted line); emission spectrum (solid line): λ_{ecx} = 430 nm; λ_{max} = 517 and 555 nm; Φ_{fl} = 3.2 (± 1.2) %

Figure 82: **Optical spectra of other oligothienyl platinacycles**
further details are shown in table 15

compound	absorption λ_{max} / nm	further abs. λ_{max} / nm	extinction coeff. ε_{max} / L mol^{-1} cm^{-1}	fluorescence λ_{max} / nm	quantum yield $\Phi_{Fl.}$ / %
C[Pt–A–3T(Bu$_4$)–A]$_2$	410	263; ≈ 384; ≈ 470	52200	543; ≈511; ≈581	<< 1 %
C[Pt–A–3T(Bu$_2$)–A]$_2$	400	--[a]	--[a]	489; 523	<< 1 %
C[Pt–A–3T(Dodec$_2$)–A]$_2$	410	--[a]	--[a]	545; ≈485; ≈590	2.2 (± 2.0) [b]
C[Pt–A–4T(Dodec$_2$)–A]$_2$	430	--[a]	--[a]	517; 555	3.2 (± 1.2) [b]

Table 15: **Summary of spectroscopic data of the oligothienyl platinacycles**
[a] not measured
[b] quantum yield standard: dpa

While the shape of the absorption spectra of the platinacycles is almost similar in all cases, the absorption maximum, which was at 410 nm for **C[Pt–A–3T(Bu$_4$)–A]$_2$**, shifts to 400 nm for **C[Pt–A–3T(Bu$_2$)–A]$_2$**, which has its alkyl side chains attached to the centre thiophene.

At the same time, the shape of the emission spectrum differs: **C[Pt–A–3T(Bu$_4$)–A]$_2$** and **C[Pt–A–3T(Dodec$_2$)–A]$_2$** possess only one main emission peak with two shoulders to the blue and to the red, whereas for **C[Pt–A–3T(Bu$_2$)–A]$_2$** and **C[Pt–A–4T(Dodec$_2$)–A]$_2$** the "blue" shoulder appears as a distinct second peak (like the typical emission spectra of the fully conjugated 3T series). However, an additional emission band — like it had been seen for **C[Pt–A–3T(Bu$_4$)–A]$_2$** when exciting at a wavelength higher than the absorption maximum — did not show up for the other platinacycles.

In all cases, excitation spectra for the emission maxima correspond to the absorption spectra, with a clearly visible structure especially for **C[Pt–A–3T(Dodec$_2$)–A]$_2$** and **C[Pt–A–4T(Dodec$_2$)–A]$_2$**.

A significant observation is the slight change in the absorption spectra of **C[Pt–A–3T(Bu$_2$)–A]$_2$** and **C[Pt–A–3T(Dodec$_2$)–A]$_2$**. Apparently for this type of compounds, decomposition takes place also in non-chlorinated solvents, although the change was much less pronounced. The absorption spectrum of **C[Pt–A–4T(Dodec$_2$)–A]$_2$** did not change, but its emission spectrum decreased by 25 % in the course of the measurements. This might either indicate a fluorescence quenching for the 4T compound that is not possible for the 3T macrocycle due to the smaller π system, or — more probably — indicate again a decomposition, as free 4T-diacetylide units would absorb around 370 nm and thus the absorption spectrum would hardly change, in contrast to a 3T unit which absorbs around 340 nm.[137e]

4.4 Cyclo[*n*]thiophenes

Of the all-thiophene series, **C[12]T**, **C[16]T** and **C[18]T** had been prepared from their macrocyclic terthiophene precursors discussed in section 4.2.1. The spectroscopic values of **C[8]T**, which was synthesised using the metal-template route, have already been reported by others.[141] Due to a lack of enough substance, only for **C[18]T** an extinction value could be determined. The results of the spectroscopic measurements are shown in figure 83 and table 16 and will be discussed in section 4.8.3:

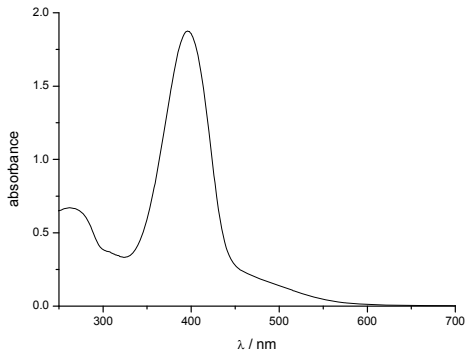

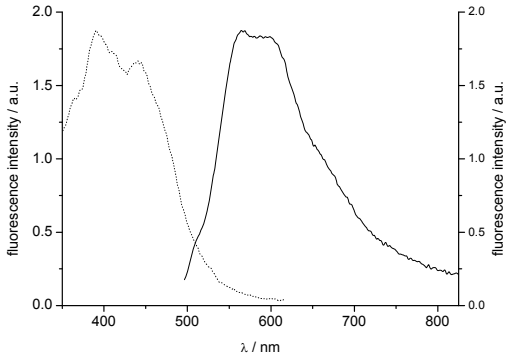

a) C[8]T[141]
left graph: absorption spectrum: λ_{max} = 396 nm; ε_{max} = 51300 L mol^{-1} cm^{-1}
right graph: excitation spectrum (dotted line);
emission spectrum (solid line): λ_{ecx} = 396 nm; λ_{max} = 566 nm and 598 nm

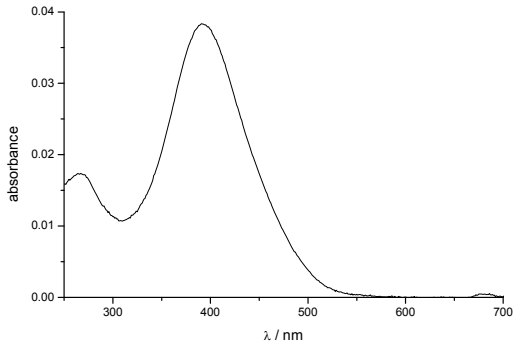

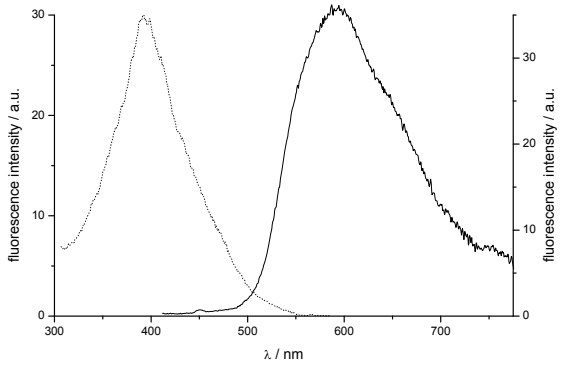

b) C[12]T
left graph: absorption spectrum: λ_{max} = 392 nm
right graph: excitation spectrum (dotted line);
emission spectrum (solid line): λ_{ecx} = 392 nm; λ_{max} = 594 nm; Φ_{fl} = 7.9 (± 2.0) %

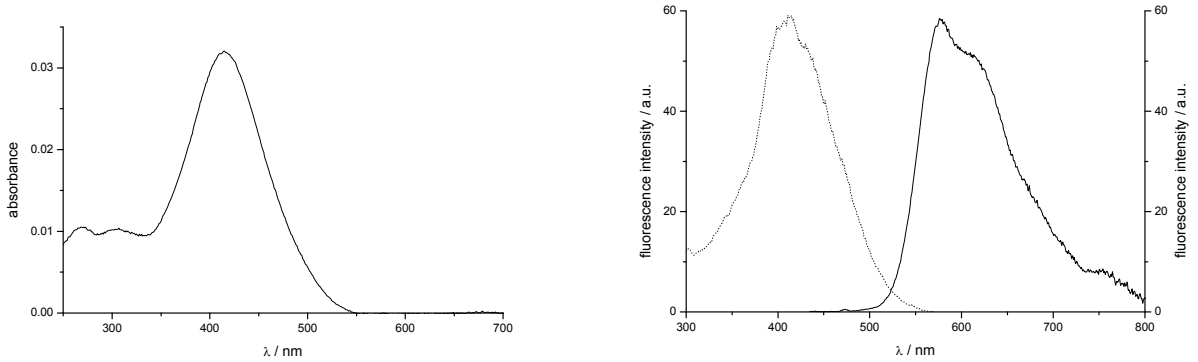

c) C[16]T

left graph: absorption spectrum: λ_{max} = 414 nm
right graph: excitation spectrum (dotted line);
emission spectrum (solid line): λ_{ecx} = 414 nm; λ_{max} = 577 and ≈ 613 nm; Φ_{fl} = 16.3 (± 2.3) %.

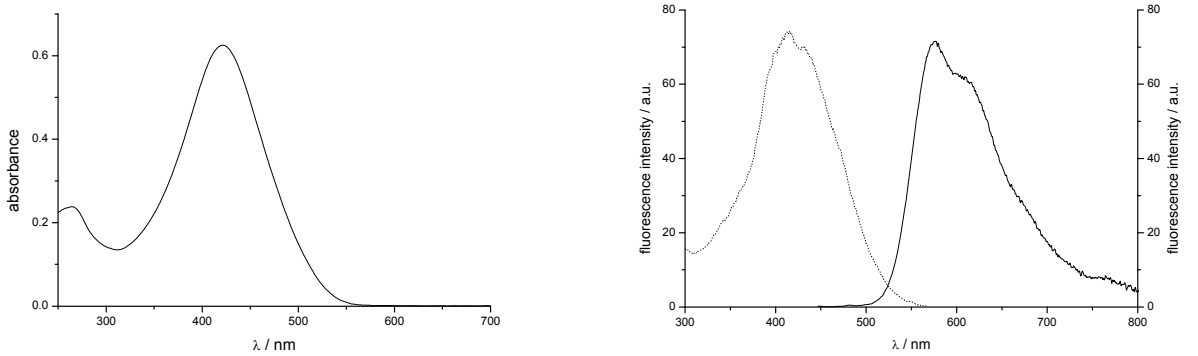

d) C[18]T

left graph: absorption spectrum: λ_{max} = 421 nm; ε_{max} = 132000 L mol^{-1} cm^{-1}
right graph: excitation spectrum (dotted line);
emission spectrum (solid line): λ_{ecx} = 421 nm; λ_{max} = 575 and ≈ 615 nm; Φ_{fl} = 18.5 (± 1.3) %.

Figure 83: Optical spectra of the C[*n*]T series (*n* = 12, 16, 18)
further details are shown in table 16

compound	absorption λ_{max} / nm	further abs. λ_{max} / nm	extinction coeff. ε_{max} / L mol^{-1} cm^{-1}	fluorescence λ_{max} / nm	quantum yield $\Phi_{Fl.}$ / %
C[8]T[141]	396 ; ≈460	265	51300	566; 598	< 1[a]
C[12]T	392	267	--[a]	594	7.9 (± 2.0)[b]
C[16]T	414	269; 305	--[a]	577; ≈ 613	16.3 (± 2.3)[b]
C[18]T	421	265	132000	575; ≈ 615	18.5 (± 1.3)[b]

Table 16: Summary of spectroscopic data of the C[*n*]T series (*n* = 12, 16, 18).
[a] not enough substance for measurement
[b] quantum yield standard: dpa

While the absorption spectra and most of the emission spectra show the usual shape for oligothiophene macrocycles, there are two differences that catch one's eye: First, in the case of **C[8]T**, the band for the absorption maximum is unusually sharp, with a tail of low intensity between 450 and 550 nm like it was found for **C[3T(Bu$_4$)-DA]$_2$** (cf. section 4.2.1, p. 131). The second particularity is that the emission spectrum for **C[12]T** consists of one broad emission band instead of two resolved peaks. Its maximum of 594 nm stands out of the other values of 566–577 nm for the first emission maximum, although a shoulder at ca. 557 nm is clearly visible. Generally, the emission maxima do not seem to follow a trend to lower values like it is the case for the 3T, 5T and 11T series. In contrast, the values rise from **C[12]T** to **C[16]T**, going along with a large gap from 392 nm to 414 nm in the absorption maxima.

4.5 Fluorescence Correlation Spectroscopy (FCS)

4.5.1 Theory and Experimental Setup

Fluorescence correlation spectroscopy (FCS), as a special application of laser spectroscopy, works with highly diluted solutions in the nanomolar range which are put into a sample holder with transparent bottom.[145] The laser beam, which is applied from below the sample, is focused on a very small volume of the solution, allowing observation of single molecules from the top. The count rate of emission is detected by an avalanche detector and converted by a correlation function to gain insight into the dynamics of emission. By this method, factors like fluorophore concentration, diffusion times and the triplet ratio of the excitation can be determined. The latter is of special importance and should be low to allow an effective charge transfer in supramolecular aggregates.

As the macrocyclic oligothiophenes are not soluble in, water and commercially available sample carriers are not stable towards organic solvents like chloroform, a special cell had to be developed: In a teflon tube, a cover slip of 0.17 nm thickness was clamped by a teflon screw and thus served as a bottom glass. The macrocycle solution was then dropped into the cylindrical well of the screw.

Due to the apparative setup, excitation occurred at the fix wavelength of 454 nm by an argon ion laser, above the typical absorption maximum of the macrocycles of around 420–430 nm. To avoid reflection of the laser beam, a bandpass emission filter was used (582 nm, width 50 nm; characteristics are shown in figure 84).

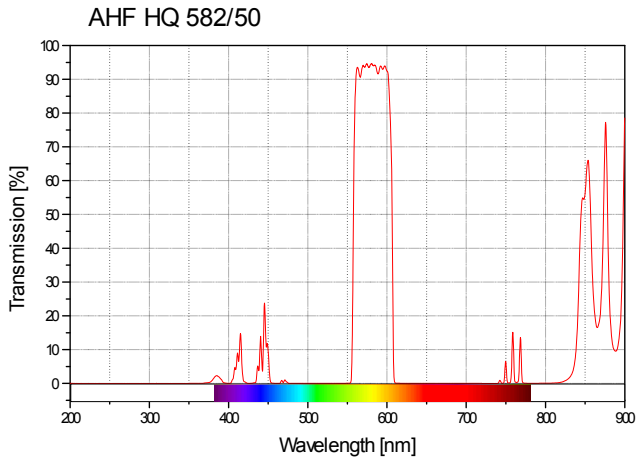

Figure 84: Transmission curve of the bandpass emission filter

The laser power was varied from 5 to 200 μW for each solution. For every new setting, an average of ten measurements (each of one minute duration) was recorded. As a reference, an aqueous solution of rhodamine-6G at an excitation wavelength of 454 nm and 150 μW laser power was used. With the diffusion coefficient of this reference ($D = 2.8\times10^{-6}$ cm^2 s^{-1}) and the experimentally determined correlation time, the structure parameter r_0 of the confocal volume could be calculated by eq. 8:

$$\tau = \frac{r_0^2}{4D} \qquad \text{(Eq. 8)}$$

A more detailed description of the correlation function can be found in literature.[145] Of special importance is the consideration of two time domains (for fluorescence and phosphorescence) with separate amplitude and diffusion time in the correlation function.

4.5.2 Results for [3T(Bu$_4$)–DA]$_2$–3T(Bu$_4$), C[3T(Bu$_4$)–DA]$_3$ and C[12]T

To evaluate the general application of FCS for the oligothiophene systems and to reveal differences between the linear diacetylide-bridged **[3T(Bu$_4$)–DA]$_2$–3T(Bu$_4$)**, the cyclic diacetylide-bridged **C[3T(Bu$_4$)–DA]$_3$** and the cyclic full-thiophene compound **C[12]T** were investigated by this method.

The structure parameter r_0 was determined to be 0.28 μm for **[3T(Bu$_4$)–DA]$_2$–3T(Bu$_4$)** (with $\tau = 68$ μs) and 0.31 μm for **C[12]T** und **C[3T(Bu$_4$)–DA]$_3$**, respectively ($\tau = 86$ μs). Figure 85 to figure 87 show the correlation functions at different laser powers.

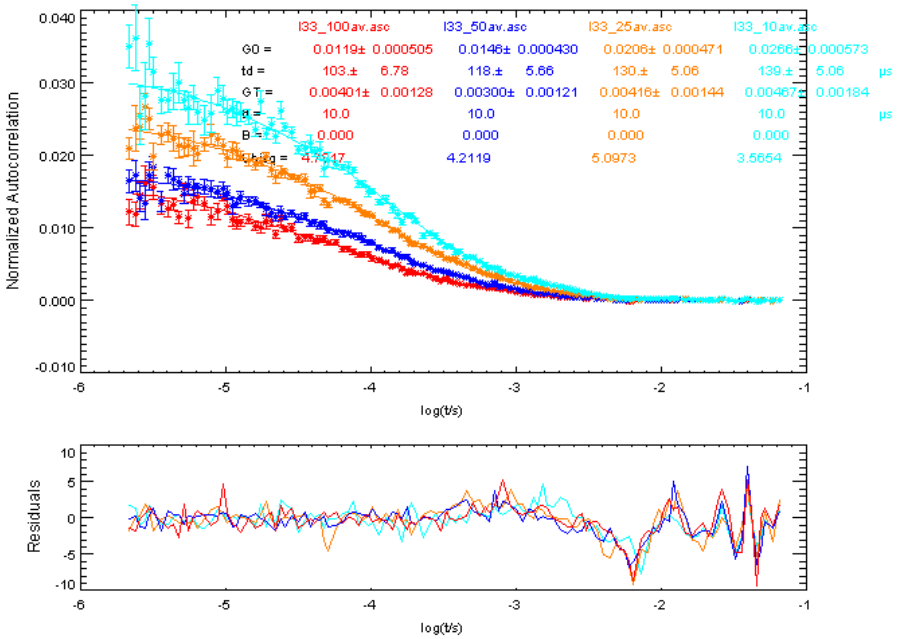

Figure 85: **FCS of [3T(Bu$_4$)–DA]$_2$–3T(Bu$_4$) (excitation at 454 nm with 10, 25, 50 and 100 µW laser power)**
upper graph: normalised correlations
lower graph: deviations from the fitting curve, weighted with the reciprocal standard deviations; triplet lifetimes (tt) were manually set to 10 µs to obtain a better fit.

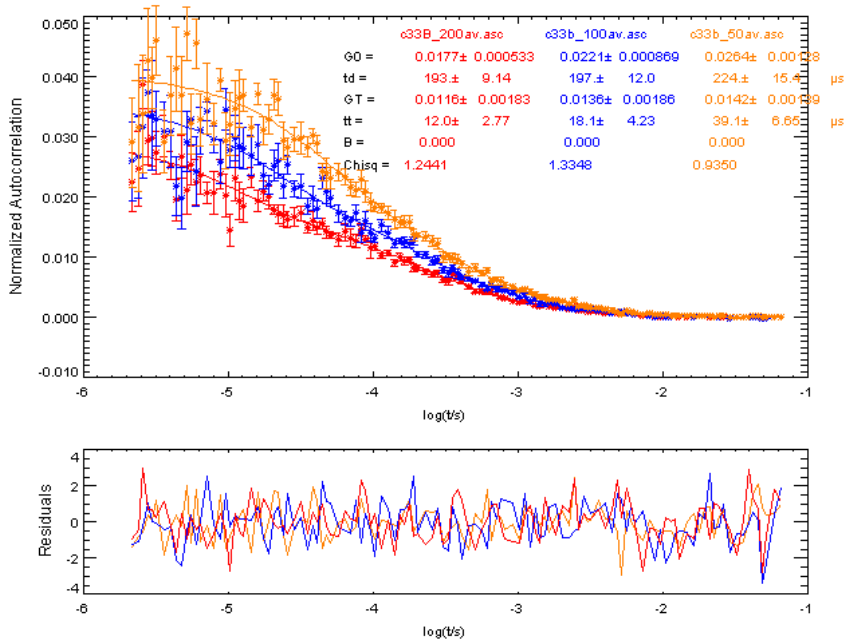

Figure 86: **FCS of C[3T(Bu$_4$)–DA]$_3$ (excitation at 454 nm with 50, 100 and 200 µW laser power)**
upper graph: normalised correlations
lower graph: deviations from the fitting curve, weighted with the reciprocal standard deviations

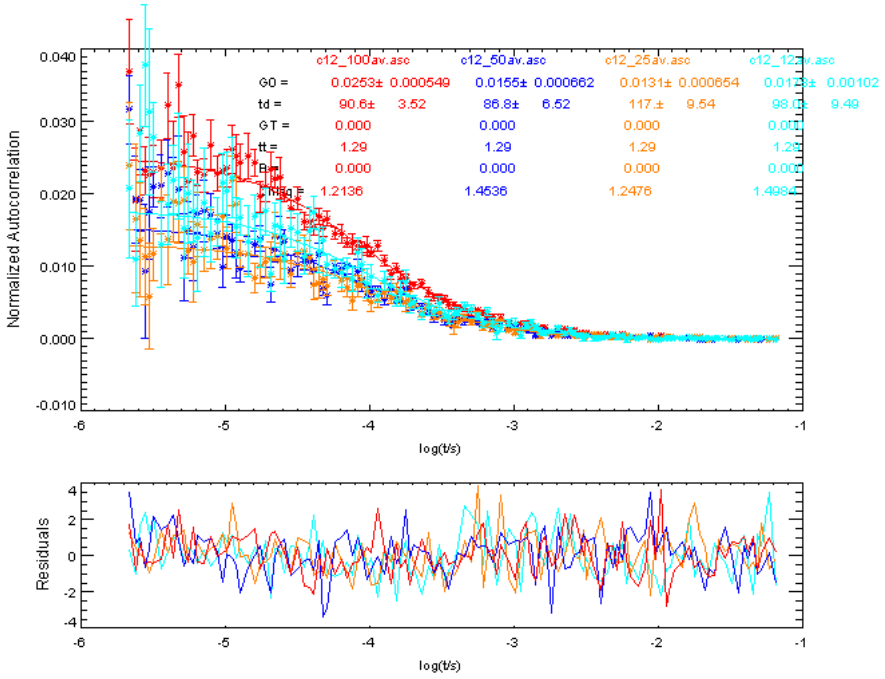

Figure 87: **FCS of C[12]T (excitation at 454 nm with 12, 25, 50 and 100 µW laser power)**
upper graph: normalised correlations
lower graph: deviations from the fitting curve, weighted with the reciprocal standard deviations

Due to the strong noise, the values of the measurements (especially those for the triplet values) cannot be taken quantitatively. One reason for this noise is the low quantum yield of the oligothiophene compounds. For **C[12]T** the problem of the excitation wavelength adds to this: 454 nm is already the lower limit for the Ar ion laser, while the absorption maximum for **C[12]T** is at 392 nm.

The correlation curves for higher laser powers are beneath those of low intensities, what indicates strong bleaching of the molecules. This bleaching also leads to a broadening of the wavelength profile and a deviation from a Gaussian wave packet. Together with the noise of measurements with low count rate, this has a negative influence on the normalisation of the curves.

The diffusion times of the fluorescence regime are for all compounds in the same range: ca. 100 ns for **[3T(Bu$_4$)–DA]$_2$–3T(Bu$_4$)** and **C[12]T**, and ca. 200 ns for **C[3T(Bu$_4$)–DA]$_3$**. An interesting parameter which can be derived from this value is the hydrodynamic radius, i.e., the hypothetic radius of a spherical particle with the same diffusion properties. Taken into account the different viscosities of chloroform and water, the hydrodynamic radius is ca. 2 nm for all three molecules (about 2.5 times the value of rhodamine-6G), which is a realistic value that agrees very well with the size of the compounds.

As expected, at higher laser intensities the ratio of the singlet and triplet amplitudes (GO : GT in figure 85–figure 87) shifts towards the triplet state. While the correlation curves indicate that the triplet ratio of **[3T(Bu$_4$)–DA]$_2$–3T(Bu$_4$)** is lower than that of **C[3T(Bu$_4$)–DA]$_3$**, the triplet correlation time (GT) indicates the opposite situation.

As the photobleaching of the macrocycles prevents access to more qualitative and useful quantitative values, FCS measurements were not continued.

4.6 Low Temperature Spectroscopy of C[3T(Bu$_4$)–DA]$_3$

4.6.1 Experimental Setup

The spectra of the macrocycles, especially those of the smallest ones, show interesting properties (cf. section 4.2.1), but usually have broad absorption and emission bands. By embedding these macrocycles in a glass-forming matrix, it is possible to cool down the samples to a few Kelvin, what should result in a higher resolution of the spectra. To gain such additional information, experiments were conducted with a SPEX Fluorolog II fluorescence spectrometer with a probe head for low temperature measurements (Cold Head CTI 22 with Closed Cycle Refrigerator, shown in figure 88).[146]

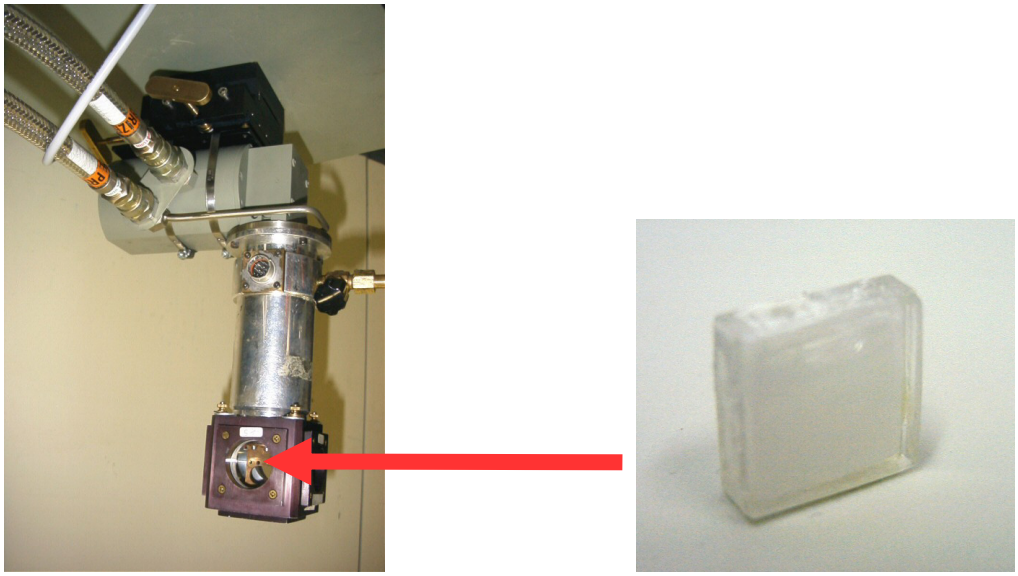

a) Cold Head CTI 22 probe head, connected to a cooling pump

b) PMMA cell

Figure 88: Experimental setup for low temperature measurements

As a container for the matrix, PMMA cells had to be employed, as quartz cells were not suitable for the strong temperature gradient. The cuvette with dimension of $10 \times 10 \times 2$ mm^3 was self-made from PMMA windows (that were glued to the PMMA frame) and was sealed after injection of the sample solution.

Due to the resulting restriction to materials which are compatible to PMMA, the widely used methyl cyclohexane (MCH; glass transition temperature $T_g \approx 100$ K; melting point $\upsilon_m = 147$ K) was taken as the matrix. Experiments with alternative matrices *o*-terphenyl (OTP; $T_g = 240$ K; melting point $\upsilon_m = 329$ K)[147] and 2-methyl tetrahydrofurane resulted in wrong results due to fluorescence emission of the matrix, or in destruction of the cell, respectively.

C[3T(Bu$_4$)–DA]$_3$, as a small macrocycle which has geometrical restrictions due to its size, was chosen as target for the low temperature investigations. The samples were prepared as follows:

C[3T(Bu$_4$)–DA]$_3$ was dissolved in optically pure, degassed MCH (distilled over $LiAlH_4$), so that the optical density was below 0.05. 0.2 mL of this solution were injected into the PMMA cell and mounted onto the probe head. By carefully cooling the sample with the cryostat, the glass transition temperature could be reached without crystallisation. During this cooling process (which took about 2 h) various spectra were taken between 150 and ca. 10 K. All spectra were corrected automatically.

4.6.2 PMMA cell restrictions

In the course of the measurements, emission bands between 400 and 550 nm appeared that initially could not be explained and were assigned to the matrix. Control experiments with pure MCH in a PMMA cell clearly showed emission peaks between 430 and 490 nm, although MCH does not absorb in the range of 340–700 nm when a quartz cell is used. Consequently, the band were found in measurements with an empty PMMA cell (figure 89), what proved that the emissions arose from the cell itself, either from the PMMA material or from the glue. Hence, emission peaks below 500 nm should be considered artefacts of the PMMA cuvette. Unfortunately, these artefacts are worst for excitation at lower wavelength, what makes an investigation of the smallest (yet most interesting) macrocycles, which absorb at 400 nm or even below, virtually useless.

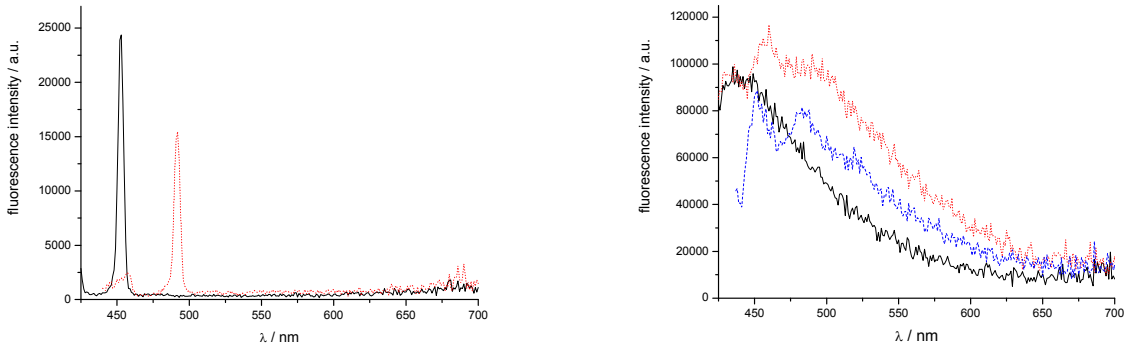

Figure 89: Comparison of the emission spectra of MCH and the PMMA cell
left graph: emission spectrum of MCH in a quartz cuvette at 298 K; λ_{exc} = 400 (solid line) and 430 nm (dotted red line); peaks correspond to Raman bands
right graph: emission spectrum of an empty PMMA cell at 298 K (λ_{exc} = 400 nm, solid line) and 11 K (λ_{exc} = 400, dotted red line; λ_{exc} = 420 nm, dashed blue line).

4.6.3 Emission at Room Temperature

First, an absorption spectrum (figure 90) of **C[3T(Bu$_4$)–DA]$_3$** in MCH was taken to detect the absorption maximum in this solvent and to adjust the concentration:

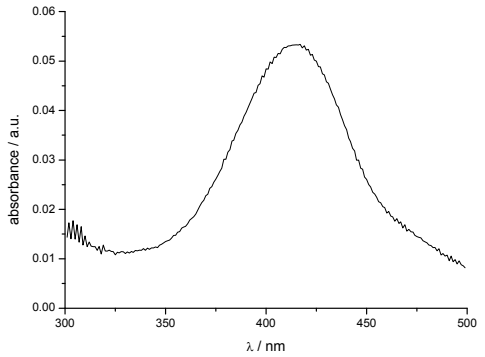

Figure 90: Absorption spectrum of C[3T(Bu$_4$)–DA]$_3$ in MCH in a quartz cuvette at 298 K
λ_{max} = 415 nm

The longest wavelength absorption, which was 422 nm in dichloromethane, shifted to the blue by 7 nm in MCH, so obviously MCH has a weaker interaction with the molecules due to its reduced polarity. For this absorption maximum at 415 nm, the emission spectrum was recorded as well as the excitation spectrum for the emission maxima (552 and 600 nm; figure 91).

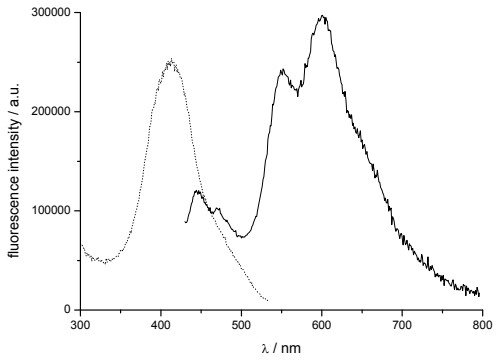

Figure 91: Fluorescence spectra of C[3T(Bu$_4$)–DA]$_3$ in MCH in a PMMA cell at 298 K
excitation spectrum (dotted line);
emission spectrum (solid line): λ_{exc} = 415 nm; λ_{max} = 552 and 600 nm

A comparison of the emission spectrum in the PMMA cell with a solution in a quartz cell identified the peaks below 500 nm as artefacts of the cell, in agreement with the results presented in section 4.6.2. The shapes of the spectra correspond to those of the spectra taken in dichloromethane (cf. section 4.2.1); the values for the emission maxima are blue shifted by 12–19 nm.

4.6.4 Emission Spectra at Low Temperatures

During the cooling process, emission spectra were taken continuously. While the spectra in-between 150 K (melting point of MCH) and 298 K stayed almost constant, the maxima started shifting to the blue at temperatures below the melting point of MCH (figure 92) when the glass transition took place. In this temperature region, also an intensity drop of the emission was noticed.

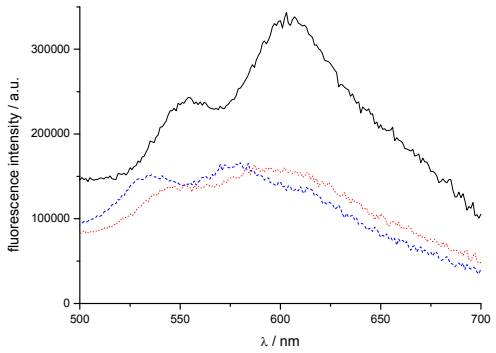

Figure 92: Emission spectra (λ_{exc} = 415 nm) of C[3T(Bu_4)–DA]$_3$ in MCH in a PMMA cell at low temperatures
150 K (solid line): λ_{max} = 554 and 602 nm;
140 K (dotted red line): λ_{max} = 544 and 594 nm;
11 K (dashed blue line): λ_{max} = 535 and 577 nm;
spectra are cut off at 500 nm, as emission maxima below this value result from the cell material

At the lowest temperature of 11 K, several emission and excitation spectra of corresponding peaks were taken and are shown in figure 93. Most noticeable in the excitation spectrum is the broad peak around the maximum at 415 nm, since a narrowing of the bands was expected instead. On the other hand, the part that was only seen as a shoulder in the absorption spectrum at room temperature became more structured and showed contributions of bands at ca. 460 and 485 nm to the excited state. Excitation at such a higher wavelength led to a more structured emission spectrum, where a third emission peak at 626 nm could be clearly seen. This peak was only noticed as a shoulder upon excitation at 415 nm.

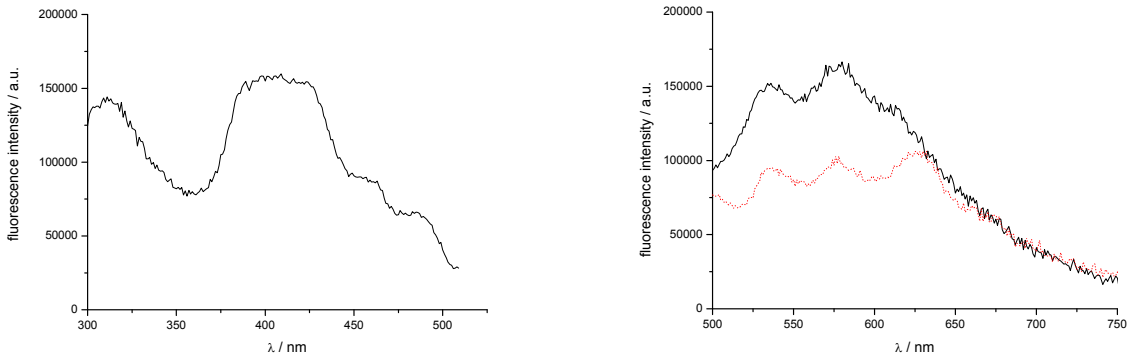

Figure 93: Spectra of C[3T(Bu$_4$)–DA]$_3$ in MCH in a PMMA cell at 11 K
left graph: excitation spectrum for emission at 535 nm. $\lambda_{max} \approx$ 390–425 nm
right graph: emission spectra with excitation at 415 nm (solid line; λ_{max} = 535 and 577 nm) and 460 nm (dashed red line; λ_{max} = 534, 579 and 626 nm); spectra are cut off at 500 nm, as emission maxima below this value result from the cell material

As the conclusions from the experiments at low temperatures support those derived from room temperature spectroscopy regarding the nature of the excited state, they are discussed later in section 4.8.2.

4.7 Calculations on the Ring Strain of Cyclic Oligo(terthienyldiacetylide)s

4.7.1 Method of Strain Determination

To determine the ring strain of the macrocyclic oligothiophenes, a comparison with the energy of linear pendants was necessary. As these linear analogues possess hydrogen atoms at the ends, the key parameter is the incremental energy increase when inserting additional monomer units (figure 94).

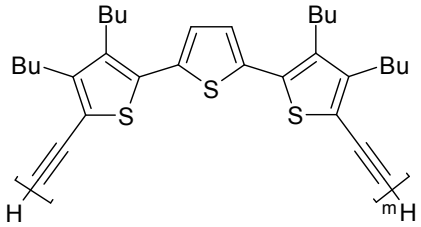

Figure 94: Linear [A–3T(Bu$_4$)–A]$_m$ structures
m = 1–6

Thus, geometry was optimised by semiempiric AM1-level calculations for linear oligo-(terthienyldiacetylide)s with 1–6 monomer units and for corresponding macrocycles built up from 2–6 units.[148,149] Also with the AM1 method, the energy content was calculated. The value to which the energy differences of the linear series converged was considered the "strain-free" enlargement and would be the idealised incremental value for linear oligothiophenes and strain-free macrocycles. Deviations from this value for the cyclic compounds can therefore be taken as the strain energy.

The energy values resulting from the calculations match the total energy of the molecules relative to the energy of the free, non-interacting atoms. Due to this method, positive energy values may occur even if the molecule is stable. (For comparison, the enthalpy of formation of benzene from the elements also has a positive value.) All values contain uncertainties, as one cannot be absolutely sure whether the calculated energy minima are local or global. Nevertheless, these errors presumably do not exceed a value of 2 kcal mol^{-1} (ca. 1 %).

4.7.2 Energies of the Linear Compounds

For the linear oligomers, the terthienyl units can be connected by the diacetylide bridges either in a "*cis*" or in a "*trans*" fashion (cf. Figure 95), while for the macrocycles only "*cis*" is possible to obtain a cyclic array.

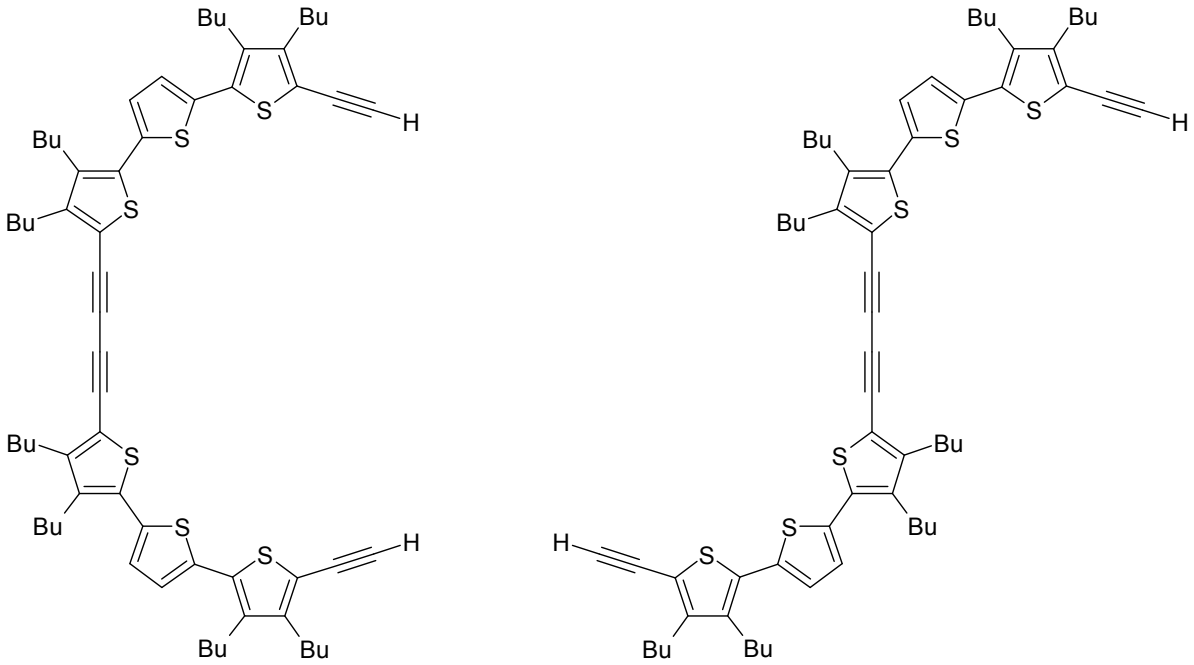

a) "*cis*" arrangement **b)** "*trans*" arrangement

Figure 95: "*Cis*" and "*trans*" arrangement for $[A–3T(Bu_4)–A]_2$

Already for the linear pentamer, nine different conformations exist that have to be considered. However, conformations with several subsequent "*cis*" connections would result in a helical stacking of different parts of the molecule and would therefore falsify the results due to energy interactions which are not applicable in the macrocycles. Hence, conformations that are not reasonable have been neglected. The results of the calculations for the linear series are presented in table 17.

	number of repeating units in [A–3T(Bu$_4$)–A]$_m$					
	***m* = 1**	***m* = 2**	***m* = 3**	***m* = 4**	***m* = 5**	***m* = 6**
energy / kcal mol^{-1}	89.378	173.911 (c)	259.154 (cc)	342.714 (ccc)	427.497 (ctcc)	512.328 (ctctc)
		173.956 (t)	258.555 (ct)	343.680 (cct)	427.719 (cttc)	512.369 (cctct)
			258.710 (tt)	343.079 (ctc)	427.714 (ctct)	
				343.763 (ctt)	427.191 (tcct)	
				343.320 (tct)	427.965 (cttt)	
				343.835 (ttt)	427.967 (tctt)	
					428.220 (tttt)	

Table 17: **AM1 energies of the linear [A–3T(Bu$_4$)–A]$_m$ series**
"c" and "t" depict the conformational order in which the monomer units are connected ("*cis*"/"*trans*"); the conformers taken as a reference for the strain calculations are underlined and in red

For the calculation of the increment, different models are possible, e.g. average values of all conformations, average values of all "*cis*" increments, or values for alternate "*cis*"/"*trans*" increments (figure 96). The latter method was considered the most useful, as alternate "*cis*"/"*trans*" increments result in a prolonged chain (of a zigzag pattern). Of all three methods, here, the deviations from the average value are smallest. Hence, the average energy increment for this method (which is practically the same for all methods) is 84.59 kcal mol^{-1}, with a variance of ca. 0.06.

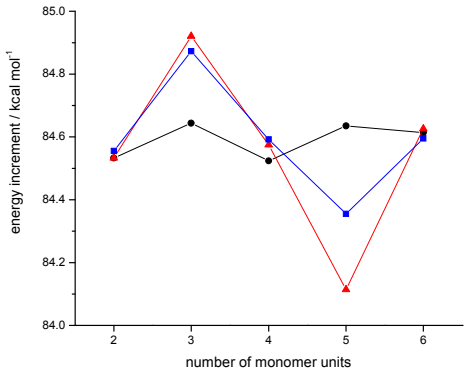

Figure 96: **Incremental energy change for the formation of linear [A–3T(Bu$_4$)–A]$_m$ oligomers**
black line (●): values for alternate "*cis*"/"*trans*" increments
red line (▲): average values of all "*cis*" increments
blue line (■): average values of all conformations

4.7.3 Ring Strain Energies of the Macrocycles

For the macrocyclic compounds, AM1 calculations of energy minimised geometries gave total energies of ca. 200–500 kcal mol^{-1} (table 18):

	C[3T(Bu_4)–DA]$_2$	**C[3T(Bu_4)–DA]$_3$**	**C[3T(Bu_4)–DA]$_4$**	**C[3T(Bu_4)–DA]$_5$**	**C[3T(Bu_4)–DA]$_6$**
total energy / kcal mol^{-1}	195.398	258.628	339.61	424.411	507.814
energy increment / kcal mol^{-1}	0	63.23	80.982	84.801	83.403

Table 18: AM1 energies of the terthienyl macrocycles C[3T(Bu_4)–DA]$_m$

A high incremental value close to the "ideal" value of 84.59 kcal mol^{-1} is an indication that at this stage the size change of the macrocycle occurs without strain. Therefore, **C[3T(Bu_4)–DA]$_5$** seems to be practically strain free and was taken as the basis for the strain calculations. For this macrocycle the many conformational degrees of freedom, especially the possibility of the thiophene units to twist, allows a strain free cyclic array. As the increments to both **C[3T(Bu_4)–DA]$_4$** and **C[3T(Bu_4)–DA]$_6$** are near the idealised value (within the tolerance that has to be conceded to semiempiric calculations), both neighboured macrocycles should also be strain free. The ring strain of the smaller macrocycles can be calculated by incremental subtraction of 84.59 kcal mol^{-1} from the energy value of **C[3T(Bu_4)–DA]$_5$** and by comparison with the calculated energy of the macrocycle. The results are shown in table 19.

	C[3T(Bu_4)–DA]$_2$	**C[3T(Bu_4)–DA]$_3$**	**C[3T(Bu_4)–DA]$_4$**	**C[3T(Bu_4)–DA]$_5$**	**C[3T(Bu_4)–DA]$_6$**
ring strain / kcal mol^{-1}	24.8	3.4	≈ 0	≈ 0	≈ 0

Table 19: Calculated ring strain for the C[3T(Bu_4)–DA]$_m$ macrocycles

The values for m = 4–6 are zero within the uncertainty range of the method, what agrees with the intuitive picture of a geometry with approximately 90° angles of the monomer units. (For the higher macrocycles, strain can be released by twisting of the monomer units against each other.) The strain energy for **C[3T(Bu_4)–DA]$_3$** (3.4 kcal mol^{-1} ≈ 15 kJ mol^{-1}) is in the same low region as, e.g., cyclopentane, while the strain for **C[3T(Bu_4)–DA]$_2$** (24.8 kcal mol^{-1} ≈ 105 kJ mol^{-1}) is rather high, like for cyclopropane. These values explain why in the statistical coupling method no **C[3T(Bu_4)–DA]$_2$** could be isolated, in contrast to **C[3T(Bu_4)–DA]$_3$** which was one of the main products.

4.8 Discussion of the Photophysical Properties of Oligothiophene Macrocycles

4.8.1 Correlation of the UV/Vis Spectra with the Frenkel Exciton Model

For the smallest macrocycle of the **C[3T(Bu$_4$)–DA]$_m$** family, **C[3T(Bu$_4$)–DA]$_2$**, the difference to its larger homologues is visible at first glance in the optical spectra. Figure 97 again shows the spectrum of **C[3T(Bu$_4$)–DA]$_2$**, compared to **C[3T(Bu$_4$)–DA]$_5$** a typical representative of the **C[3T(Bu$_4$)–DA]$_m$** series. Most obvious in the spectrum is the narrow shape of the absorption peak at 400 nm. Furthermore, a small band around 490 nm is visible which reminds of the shoulder in the spectra of other small macrocycles like **C[3T(Bu$_4$)–DA]$_3$**.

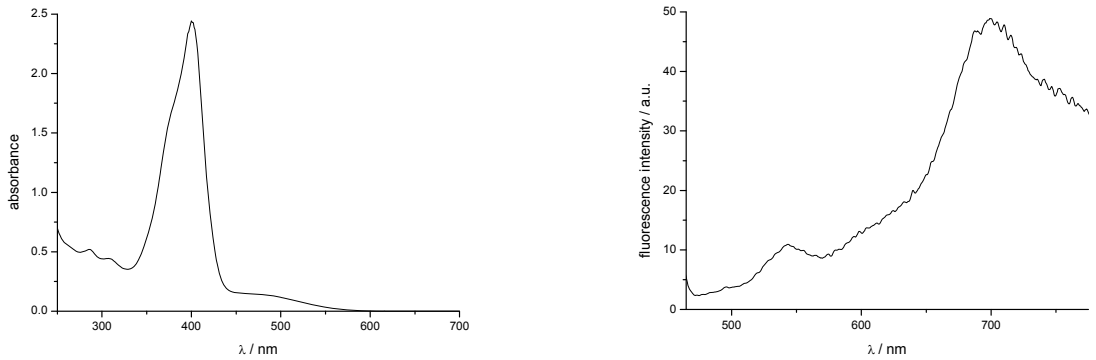

a) C[3T(Bu$_4$)–DA]$_2$
left graph: absorption spectrum: λ_{max} = 400 nm; ε_{max} = 129000 L mol^{-1} cm^{-1}
right graph: emission spectrum: λ_{max} = 545 nm and 699 nm; Φ_{fl} << 1 %

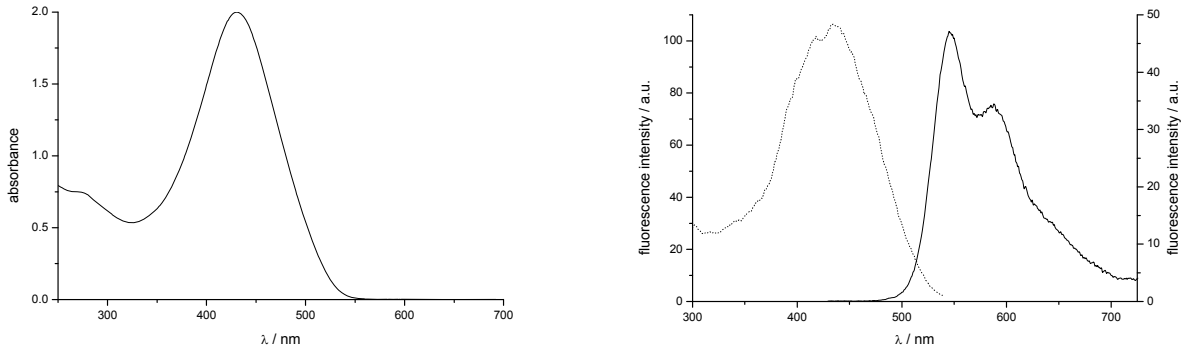

b) C[3T(Bu$_4$)–DA]$_5$
left graph: absorption spectrum: λ_{max} = 431 nm; ε_{max} = 211300 L mol^{-1} cm^{-1}
right graph: excitation spectrum (dotted line);
emission spectrum (solid line): λ_{max} = 546 nm and 588 nm; Φ_{fl} = 15.5 (± 1.2) %

Figure 97: Comparison between the optical spectra of C[3T(Bu$_4$)–DA]$_2$ and C[3T(Bu$_4$)–DA]$_5$

An explanation for these findings can be given by the Frenkel exciton model, which was applied successfully to the **C[*n*]T** macrocycles (cf. section 4.1.2). Although here several thiophene units are replaced by diacetylide moieties, the theory can be adopted at least for a qualitative picture. Figure 98 gives a graphical presentation of the energy states and transitions discussed in the model:

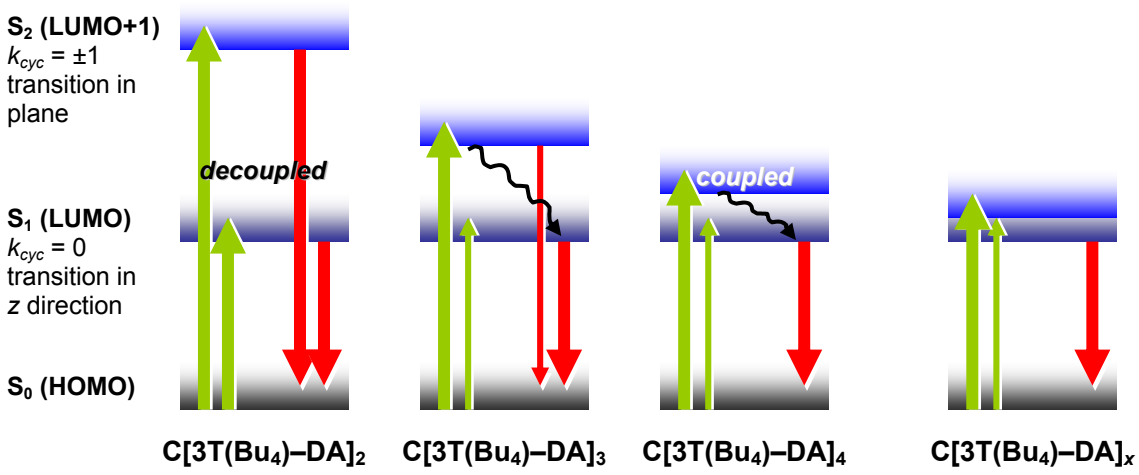

Figure 98: **Energetic model and transition diagram for the [3T(Bu$_4$)-DA]$_m$ family**
x represents any higher number;
absorption pathways are shown in green while those for the emission are in red.

According to eq. 4 (p. 129), the position of the LUMO is independent of the ring size and remains constant at $E^{cyc}_{k_{cyc}=0} = \omega_0 - 2J$. For $k_{cyc} = 0$ the transition dipoles of the thiophene moieties are more or less in the molecular plane, while the transition itself is positioned in *z* direction; hence the oscillator strength is almost zero for the HOMO–LUMO transition. Transition from the HOMO to the LUMO+1, on the other hand, is allowed and leads to the large absorption band between 400 and 445 nm. In praxis, the HOMO–LUMO transition can only be seen separately when the energy difference between LUMO and LUMO+1 is large enough, like it is the case for **C[3T(Bu$_4$)–DA]$_2$**: For this small macrocycle, the first transition shows a small, separate band at approx. 490 nm. As in bigger macrocycles the LUMO+1 approaches the LUMO and the transitions get close enough to couple, the band only appears as a shoulder at this position already for the next larger macrocycles **C[3T(Bu$_4$)–DA]$_3$**, **C[5T(Bu$_6$)–DA]$_2$** and **C[11T(Bu$_{12}$)–DA]**. For even larger rings the band cannot be seen any more at all. (This might also be due to the stronger distortion of the small, strained cycles, that leads to an increased transition dipole component in *z* direction.) Low temperature measurements of **C[3T(Bu$_4$)–DA]$_3$**, however, revealed a more distinct peask at ca. 485 nm (cf. section 4.6.4).

4.8.2 Trends and Particularities of the Experimental Values

Absorption and general effects of the ring size

While the optical spectra of the smallest macrocycles significantly differ from the spectra of their larger homologues (vide ultra), a common shape is apparent for most of the curves, and general trends can be determined.

The peak values of the absorption spectra of **C[3T(Bu$_4$)–DA]$_m$**, as well as those of the emission spectra, converge asymptotically to a limit. A graphical representation of the corresponding transition energy values, plotted against the reciprocal number of monomer units within the rings, is given in figure 99. According to the Frenkel exciton model discussed in the previous section, the absorption maxima correspond to the $S_0 \rightarrow S_2$ transition, while the $S_0 \rightarrow S_1$ transition appears only as a shoulder at a constant wavelength of approx. 490 nm.

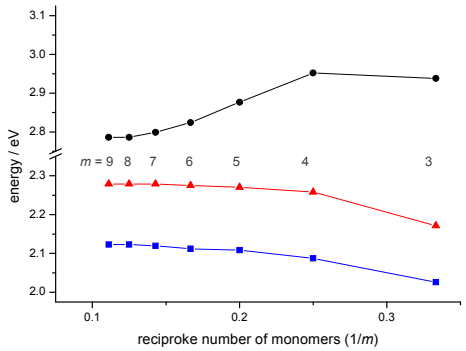

Figure 99: **Plot of absorption/emission maxima vs. reciprocal number of 3T(Bu$_4$)–DA units in the C[3T(Bu$_4$)–DA]$_m$ series (m = 3–9)**
black line (●): absorption maxima ($S_0 \rightarrow S_2$ transition)
red (▲) and blue (■) line: first and second emission maxima (vibronic splitting)

While in this 1/m plot (where m equals the number of terthienyl–diethynylene units) the absorption maxima have a linear dependence in the range m = 4–6, the energy values hardly change any more for $m \geq 7$. The same behaviour is known for linear oligomers.[137e] An explanation for this finding is that, due to the curvature of the building blocks, a size increase has to go along either with a twist or with a "*trans*" conformation of parts of the macrocycle.

As expected, the values of the **C[5T(Bu$_6$)–DA]$_m$** series do not yet show such a stagnation for the largest cycle (m = 4): A stand-still of the peak shifts should not appear until the still unknown **C[5T(Bu$_6$)–DA]$_5$**, which would correspond in size to **C[3T(Bu$_4$)–DA]$_8$**. This is reasonable, as the spectroscopic values are determined by the opposing effects of an expanding π-electronic system

(increasing ring size) and a decrease in planarity, of which the ring size should have the major influence.

Emission spectra

In contrast to only one large absorption maximum, the emission usually shows two peaks. Such a splitting is well-known for oligothiophenes, and is commonly assigned to a vibrational fine structure in the emission which indicates a significant change of shape, i.e., the macrocycles become more rigid in the excited state.[150] This is in full accordance with the expectations, as calculations predict a chinoidal structure upon excitation that flattens the π system. Related to this result is the finding that emission maxima for the 5T series are at longer wavelengths than for comparable cycles of the 3T series, i.e. that they have a larger Stokes shift (cf. table 20).

compound	absorption λ_{max} / nm	emission λ_{max} / nm	Stokes shift cm^{-1}
C[3T(Bu$_4$)–DA]$_2$	400 (≈ 490)	545	6651 (2060)
C[3T(Bu$_4$)–DA]$_3$	422	571	6184
C[3T(Bu$_4$)–DA]$_4$	420	549	5595
C[3T(Bu$_4$)–DA]$_5$	431	546	4887
C[3T(Bu$_4$)–DA]$_6$	439	545	4430
C[3T(Bu$_4$)–DA]$_7$	443	544	4191
C[3T(Bu$_4$)–DA]$_8$	445	544	4090
C[3T(Bu$_4$)–DA]$_9$	445	544	4090
C[5T(Bu$_6$)–DA]$_2$	421	592	6861
C[5T(Bu$_6$)–DA]$_3$	425	567	5893
C[5T(Bu$_6$)–DA]$_4$	436	563	5174
C[11T(Bu$_{12}$)–DA]	405	605	8162
C[11T(Bu$_{12}$)–DA]$_2$	433	578	5794
C[8]T	396 (≈ 460)	566	7585 (4071)
C[12]T	392	594	8675
C[16]T	414	577	6824
C[18]T	421	575	6362

Table 20: Stokes shifts of oligothiophene macrocycles

Obviously, larger structural rearrangements seem to take place at a higher thiophene ratio, correlating with a higher number of conformational degrees of freedom, as for the 5T series more oligothiophene subunits than for the 3T series have to twist back to a planar, quinoidal structure.

The trend is followed by the 11T macrocycles with an emission even more in the red region (cf. table 22 on page 168 and table 25 on page 169). The results from the low temperature investigations support the picture of a chinoidal excited state for the macrocycles (cf. section 4.6.4): A conformational change towards planarity is hindered in the matrix, leading to a smaller conformational change and an emission that is blue-shifted by 17–22 nm. Hence, the Stokes shift is smaller than at room temperature.

The energy difference between the first and second emission maximum is in the range of 0.13–0.16 eV, depending on the monomer unit of the macrocycle series, and slightly decreases with increasing ring size (starting from **C[3T(Bu$_4$)–DA]$_4$** in case of the 3T series). The reason of this trend is an increasing contribution from the more intensive first peak to the second emission peak, which causes a distinct and increasing blue shift of the second emission peak compared to the true position of the transition. While already the emission spectra of the 5T macrocycles have their two maxima closer together than the 3T series, the maxima are hardly separated at all for the 11T cycles. Here, the increased number of degrees of freedom and the chinoidal excited state can be taken as an additional explanation, as both of then would require a bigger rearrangement in the excited state (leading to a larger Stokes shift, i.e. a more distinct red shift of the first emission maximum).

A discussion of energy differences to further emission maxima is not practical because of the vague position of the shoulders. Principally, they could arise from transition of higher electronic states to the ground state as well as from further vibronic splitting.

Quantum yields and extinction coefficients

A noticeable behaviour, which gives hints on the structural nature of the macrocycles, was found for the quantum yields: In the 3T series, they reach a maximum of 24 % for **C[3T(Bu$_4$)–DA]$_7$** and then decrease slightly. Obviously, with increasing size — hence, increasing number of degrees of freedom — the channels for non-radiative energy decay gain importance, what could mean that the ground-state geometry of larger cycles becomes more and more different from a planar chinoidal excited structure, i.e. the macrocycles become wavier with size. The fact that for the 5T series the quantum yield already drops with **C[5T(Bu$_6$)–DA]$_4$**, which is equivalent in its size to **C[3T(Bu$_4$)–DA]$_6$** (where the quantum yield is still increasing), fits the picture: The higher number of thiophene units, which can be twisted against each other, leads to a comparably larger number of channels for non-radiative deactivation.

A surprise in this respect had been the intensity drop upon cooling (cf. section 4.6.4), as the "frozen" conformation should have less pathways for a non-radiative relaxation and therefore be more fluorescent. A drop in intensity could mean that light emission is unfavourable from a conformation where the thiophene units are strongly twisted against each other. This might also be an explanation for the extremely weak fluorescence of the smallest macrocycle **C[3T(Bu$_4$)–DA]$_2$**, for which it is virtually impossible to obtain a planar, chinoidal structure.

While the extinction coefficients expectedly rise with increasing ring size, this is not the case for the **C[11T(Bu$_{12}$)–DA]$_m$** macrocycles. There, the cyclic dimer ($m = 2$) has a low extinction coefficient of only 69100 L mol^{-1} cm^{-1}. For comparison, the values for **C[3T(Bu$_4$)–DA]$_6$** and **C[5T(Bu$_6$)–DA]$_4$**, which are similar in size, are 212900 and 235200 L mol^{-1} cm^{-1}. The shapes of the absorption and emission spectra give no hint why **C[11T(Bu$_{12}$)–DA]$_2$** should absorb worse than other macrocycles of comparable size; possibly a special conformation or geometry is effective here.

Excitation spectra

As emission — in contrast to absorption — was structured, it was interesting to look at the excitation spectra, which show the contribution of excitation wavelengths to a fixed emission band. Excitation spectra thereby reflect the energy pathways upon excitation, and, if the fluorescence quantum yields are independent from the excitation wavelength, correspond in shape to the absorption spectra. For the macrocycles, however, the emission spectra already showed a vibrational fine structure due to the chinoidal structure of the LUMO, which was expected to be mirrored in the excitation spectra. Indeed, the excitation spectra generally show a slight splitting.

Particularities for small cycles

An exception to most of the trends described above is **C[3T(Bu$_4$)–DA]$_2$**: Apart from the unique UV/Vis spectrum discussed in the previous section, it hardly shows any emission upon excitation at the absorption maximum of 400 nm. In fact, the slit widths of the spectrometer had to be adjusted to high values where the low fluorescence shows much noise, and where a reasonable comparison with quantum yield standards was neither possible nor useful, as the value is close to 0 %. Although this contrasts the high extinction of 129 000 L mol^{-1} cm^{-1}, reabsorption might be the explanation, as for this small macrocycle a separate band at 490 nm exists (corresponding to the $S_0 \rightarrow S_1$ absorption, cf. section 4.8.1).

A better resolved emission spectrum for **C[3T(Bu$_4$)–DA]$_2$**, obtained upon excitation at 460 nm, has been reported before.[141] Both the first and the second emission maximum of 545 and 584 nm do not fit into the trend for this series' fluorescence data. In contrast, they oppose the trend and are blue-shifted compared to **C[3T(Bu$_4$)–DA]$_3$** (571 and 612 nm), probably due to the higher ring strain. Interestingly, the values are virtually identical to the limit values that are reached by the larger homologues.

4.8.3 Comparison of the Diethynylene-Containing Macrocycles with Cyclo[*n*]thiophenes

Comparing the spectra of cyclo[*n*]thiophenes (section 4.4) with those of the terthienylene–diethynylene macrocycles (section 4.2.1), the **C[*n*]T** series bears some analogies regarding the smallest members: Like its precursor **C[3T(Bu$_4$)–DA]$_2$**, **C[8]T** shows a narrow absorption band with a weak shoulder to the red (which has been discussed in the previous section); and like for the precursor **C[3T(Bu$_4$)–DA]$_3$**, the results of **C[12]T** stand out of the other values for the series. While for the 3T series the absorption of the second smallest cycle **C[3T(Bu$_4$)–DA]$_3$** is red-shifted compared to the next larger one, it is here the smallest compound **C[8]T** which shows this unusual behaviour.

In the following tables, the values for macrocycles of the same size (i.e., the same number of carbon atoms in the perimeter) are arranged:

compound	absorption λ_{max} / nm	further abs. λ_{max} / nm	extinction ε / L mol^{-1} cm^{-1}	fluorescence λ_{max} / nm	quantum yield $\Phi_{Fl.}$ / %
C[3T(Bu$_4$)–DA]$_2$	400; ≈490	285; 308	129000	545; 584	<< 1 [a]
C[8]T	396	265	51300	566; 598	--[b]

Table 21: **Summary of spectroscopic data of oligothiophene macrocycles bearing 32 ring carbon atoms**[141]
[a] quantum yield standard: dpa
[b] not enough substance for measurement

compound	absorption λ_{max} / nm	further abs. λ_{max} / nm	extinction ε / L mol^{-1} cm^{-1}	fluorescence λ_{max} / nm	quantum yield $\Phi_{Fl.}$ / %
C[3T(Bu$_4$)–DA]$_3$	422	287; ≈ 302	133500	571; 612	7.2 (± 0.7)[a]
C[5T(Bu$_6$)–DA]$_2$	421	275	118800	592; 635	7.8 (± 0.7)[a]
C[11T(Bu$_{12}$)–DA]	405	≈ 268	87700	605; 647	7.7 (± 0.6) [a]
C[12]T	392	267	--[b]	≈ 557; 594	7.9 (± 2.0) [a]

Table 22: **Summary of spectroscopic data of oligothiophene macrocycles bearing 48 ring carbon atoms**
[a] quantum yield standard: dpa
[b] not enough substance for measurement

compound	absorption λ_{max} / nm	further abs. λ_{max} / nm	extinction ε / L mol^{-1} cm^{-1}	fluorescence λ_{max} / nm	quantum yield $\Phi_{Fl.}$ / %
C[3T(Bu$_4$)–DA]$_4$	420	276; ≈ 295	162800	549; 594	13.6 (± 1.3)[a]
C[16]T	414	269; 305	--[b]	577; ≈ 613	16.3 (± 2.3)[a]

Table 23: **Summary of spectroscopic data of oligothiophene macrocycles bearing 64 ring carbon atoms**
[a] quantum yield standard: dpa
[b] not enough substance for measurement

compound	absorption λ_{max} / nm	further abs. λ_{max} / nm	extinction ε / L mol^{-1} cm^{-1}	fluorescence λ_{max} / nm	quantum yield $\Phi_{Fl.}$ / %
C[5T(Bu$_6$)–DA]$_3$	425	≈ 266	205200	567; 603	17.4 (± 1.4)[a]
C[18]T	421	265	132000	575; ≈ 615	18.5 (± 1.3)[a]

Table 24: **Summary of spectroscopic data of oligothiophene macrocycles bearing 72 ring carbon atoms**
[a] quantum yield standard: dpa

compound	absorption λ_{max} / nm	further abs. λ_{max} / nm	extinction ε / L mol^{-1} cm^{-1}	fluorescence λ_{max} / nm	quantum yield $\Phi_{Fl.}$ / %
C[3T(Bu$_4$)–DA]$_6$	439	≈ 272	212900	545; 587	18.2 (± 1.2)[a]
C[5T(Bu$_6$)–DA]$_4$	436	≈ 266	235200[b]	563; 599	14.8 (± 1.4)[a]
C[11T(Bu$_{12}$)–DA]$_2$	433	≈ 263	69100	578; ≈ 601	20.5 (± 0.6)[a]

Table 25: **Summary of spectroscopic data of oligothiophene macrocycles bearing 96 ring carbon atoms**
[a] quantum yield standard: dpa
[b] large single deviations from mean value (> 5 %)

If one compares **C[3T(Bu$_4$)–DA]$_3$**, **C[5T(Bu$_6$)–DA]$_2$**, **C[11T(Bu$_{12}$)–DA]** and **C[12]T** (table 22), a trend is visible for the longest wavelength absorption maxima: With progressive substitution of thiophene with diacetylide units, the absorption shifts to longer wavelengths (lower energy). The same principle applies to **C[3T(Bu$_4$)–DA]$_6$**, **C[5T(Bu$_6$)–DA]$_4$ and C[11T(Bu$_{12}$)–DA]$_2$** (table 25). Obviously, replacement of diacetylides by thiophene units reduces the conjugation, what can be caused by two effects: the aromatic nature of the thiophenes and their possibility to twist against each other, what results in more conformational degrees of freedom; and a rearrangement of the sp carbon atoms to sp^2, what leads to a smaller perimeter. In the same manner, the extinction values decrease with the number of diacetylide units; with the only exception of **C[3T(Bu$_4$)–DA]$_6$** which has a slightly lower extinction than **C[5T(Bu$_6$)–DA]$_4$** (table 25).

C[12]T deviates from the trend that emission takes place at higher wavelengths with cumulative thiophene units: The **C[11T(Bu$_{12}$)–DA]** emission maxima are at longer wavelengths than for **C[5T(Bu$_6$)–DA]$_3$** *and* **C[12]T**. Nevertheless **C[12]T** possesses the largest Stokes shift of 8675 cm^{-1}

(cf. table 20 on page 165) due to its absorption maximum at a significantly lower wavelength. Interesting though, the emission bands becomes less structured while moving from macrocycle **C[3T(Bu$_4$)–DA]$_3$** (two well resolved peaks) to **C[12]T** (one broad peak). This may again result from a greater flexibility of the thiophene–thiophene units, which can adopt a wide range of dihedral angles compared to thiophene–acetylide bonds.

While for the emission maxima **C[12]T** seems to be an exception, all the structures are in compliance regarding the emission intensity: The quantum yields of comparable macrocycles is always in the same range: About 8 % for substances with 48 ring carbon atoms, 17–18 % for those with 72, and 15–18 % for those with 96.

4.8.4 Differences between Corresponding Cyclic and Linear Oligomers

If one wants to compare cyclic and linear compounds regarding their spectroscopic propreties, the acyclic substances are somewhat crucial, as acetylide-terminated oligothiophenes are rather instable. Instead, oligothiophenes with intermittent diethynylene units were investigated: the linear compounds **[3T(Bu$_4$)–DA]$_m$–3T(Bu$_4$)** (with m = 1–3) and **5T(Bu$_6$)–DA–5T(Bu$_6$)**[137e] differ from their cyclic analogues by the lack of terminal acetylide groups, i.e. they possess one acetylide group less than the macrocycles (figure 100). For further comparison, the stable linear oligothiophene **[A–5T(Bu$_6$)–A]$_2$**[137e] with terminal acetylide units was also investigated.

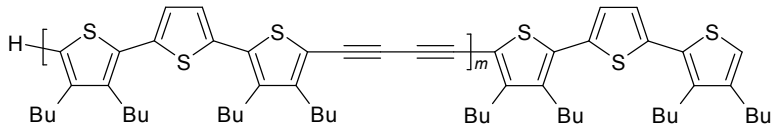

a) [3T(Bu$_4$)–DA]$_m$–3T(Bu$_4$)
m = 1–3

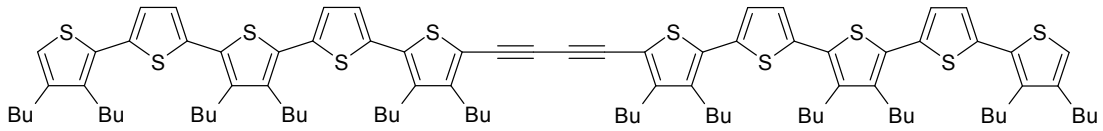

b) 5T(Bu$_6$)–DA–5T(Bu$_6$)

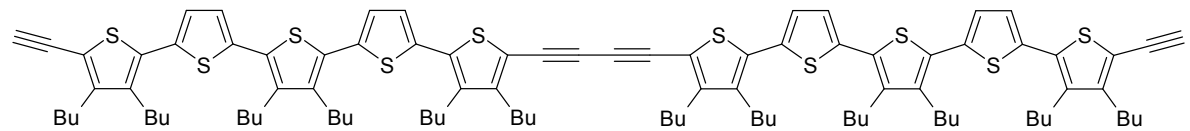

c) [A–5T(Bu$_6$)–A]$_2$

Figure 100: Structures of the linear oligothiophenes investigated for comparison

Of those substances, absorption and emission spectra were recorded and extinction coefficients were determined by variation of the concentration in the range of 10^{-4}–10^{-6} mol L^{-1} (figure 101/ table 26):

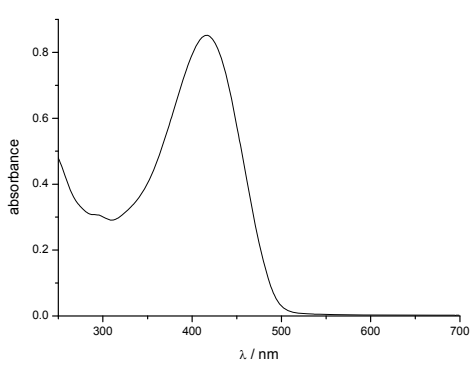

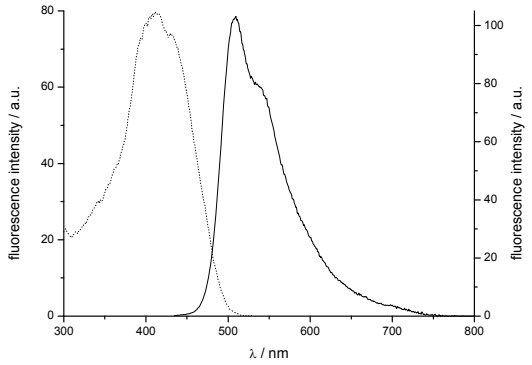

a) 3T(Bu_4)–DA–3T(Bu_4)
left graph: absorption spectrum: λ_{max} = 417 nm; ε_{max} = 48600 L mol^{-1} cm^{-1}
right graph: excitation spectrum (dotted line);
emission spectrum (solid line): λ_{max} = 509 nm and ≈ 540 nm

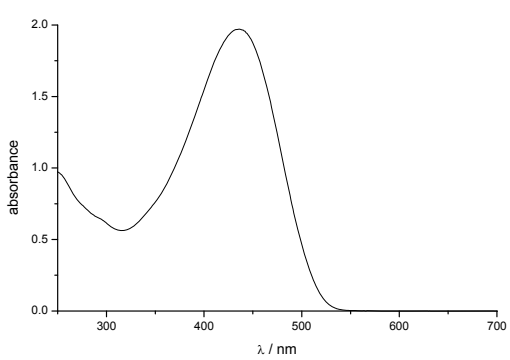

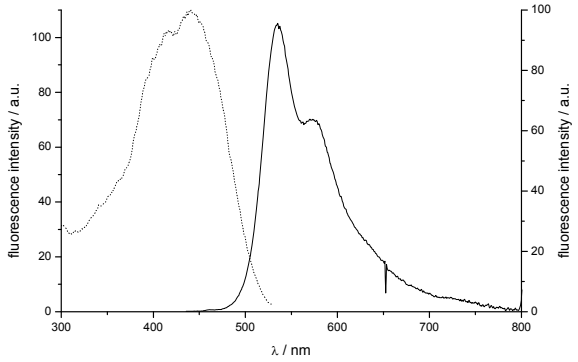

b) [3T(Bu_4)–DA]$_2$–3T(Bu_4)
left graph: absorption spectrum: λ_{max} = 436 nm; ε_{max} = 98500 L mol^{-1} cm^{-1}
right graph: excitation spectrum (dotted line);
emission spectrum (solid line): λ_{max} = 535 nm and 573 nm; Φ_{fl} = 19.0 (± 1.4) %.

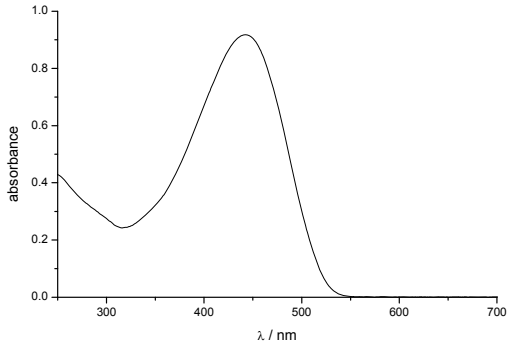

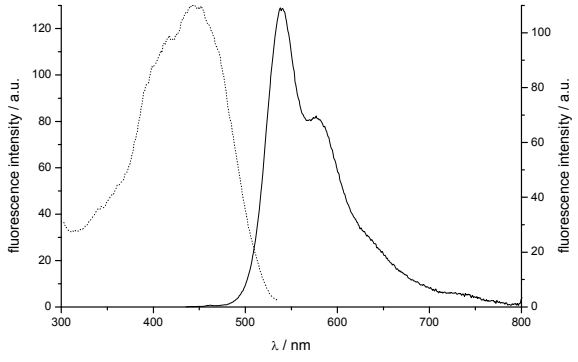

c) [3T(Bu_4)–DA]$_3$–3T(Bu_4)
left graph: absorption spectrum: λ_{max} = 442 nm; ε_{max} = 145500 L mol^{-1} cm^{-1}
right graph: excitation spectrum (dotted line);
emission spectrum (solid line): λ_{max} = 540 nm and 577 nm; Φ_{fl} = 24.5 (± 1.3) %.

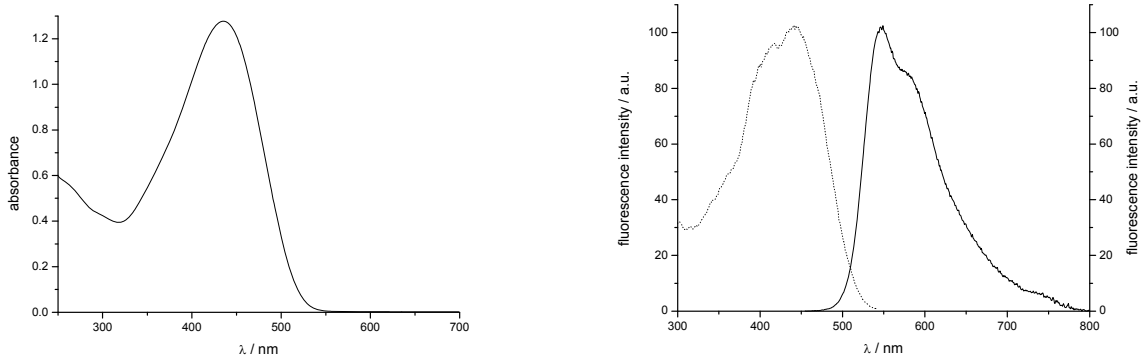

d) 5T(Bu_6)–DA–5T(Bu_6)
left graph: absorption spectrum: λ_{max} = 435 nm
right graph: excitation spectrum (dotted line);
emission spectrum (solid line): λ_{max} = 548 nm and ≈ 579 nm

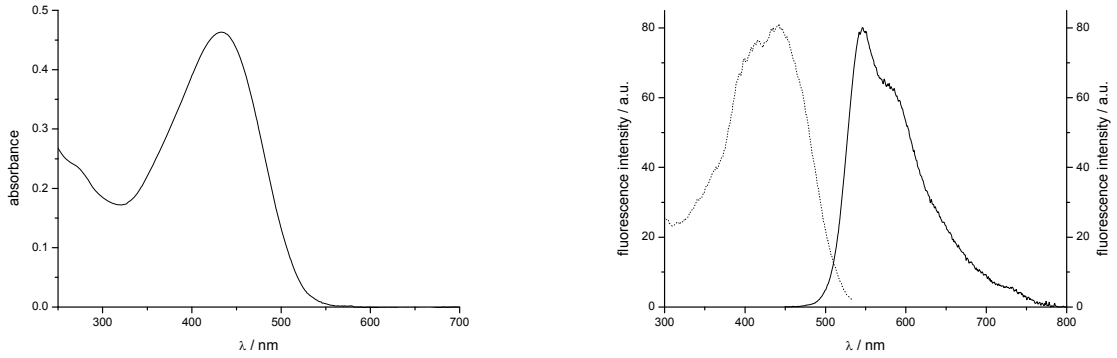

e) [A–5T(Bu_6)–A]$_2$
left graph: absorption spectrum: λ_{max} = 432 nm; ε_{max} = 32400 L mol^{-1} cm^{-1}
right graph: excitation spectrum (dotted line);
emission spectrum (solid line): λ_{max} = 546 nm and ≈ 580 nm

Figure 101: Optical spectra of the linear oligothiophenes
further details are shown in table 26

compound	absorption λ_{max} / nm	further abs. λ_{max} / nm	extinction ε / L mol^{-1} cm^{-1}	fluorescence λ_{max} / nm	quantum yield $\Phi_{Fl.}$ / %
3T(Bu_4)–DA–3T(Bu_4)	417	295	--[a]	509; ≈540	--[a]
[3T(Bu_4)–DA]$_2$–3T(Bu_4)	436	≈292	98500	535; 573	19.0 (± 1.4) [b]
[3T(Bu_4)–DA]$_3$–3T(Bu_4)	442	≈280	145500	540; 577	24.5 (± 1.3) [b]
5T(Bu_6)–DA–5T(Bu_6)	435	295	--[a]	548; ≈579	--[a]
[A–5T(Bu_6)–A]$_2$	432	271	32400	546; ≈580	--[a]

Table 26: Summary of spectroscopic data of the linear oligothiophenes
[a] not measured
[b] quantum yield standard: dpa

Compared to the cyclic compounds, a strong red-shift of the absorption maxima can be noticed: Even though the linear 3T series is missing terminal acetylide units, the absorption is at 417, 436 and 442 nm (compared to 400, 422 and 420 nm for the corresponding macrocycles), i.e. close to the values for the macrocycles with twice as much monomer units (which absorb at 420, 439 and 445 nm). This exactly fits the theoretical model presented in the sections 4.1.2 and 4.8.1, according to which the first electronic transition — for the cycles at ca. 490 nm — is only allowed for the linear compounds.

The difference to the macrocyclic systems can also be observed in the Stokes shift, which is here comparably small, e.g. 4334 cm^{-1} (417 → 509 nm) for **3T(Bu$_4$)–DA–3T(Bu$_4$)** instead of 6651 cm^{-1} (400 → 545 nm) for **C[3T(Bu$_4$)–DA]$_2$**. Like mentioned in the previous paragraph, absorption takes place using different transitions: For the macrocycles, the state that absorbs does not equal the states that emits, as the first electronic transition is forbidden.

4.8.5 Photophysical Properties of Pt(II)-Containing Macrocycles

A value which is unexpected at first glance is the relatively high absorption maximum of 410 nm for **C[Pt–A–3T(Bu$_4$)–A]$_2$** compared to 400 nm for the platinum-free cycle. The Pt–acetylide bond, due to its predominant σ character, should rather isolate[151] the two halves of **C[3T(Bu$_4$)–DA]$_2$** and result in a blue-shift of the absorption maximum. An explanation can be found using the Frenkel exciton model (cf. section 4.1.2), according to which the transition is already only located on half the cycle.[140] Upon "insertion" of Pt(II), however, this half is slightly extended towards the metal centre, what may well cause the red shift from 400 to 410 nm. The same applies to the larger homologues **C[Pt–A–5T(Bu$_6$)–A]$_2$**, **C[Pt–A–7T(Bu$_8$)–A]$_2$** and **C[*trans*-Pt–A–7T(Bu$_8$)–A]$_2$**, for which the absorption maxima move to 423, 428 and 436 nm, respectively (table 27).[141] Noticeable is the bathochromic shift from 428 to 436 nm when the *cis*-Pt(II) centres are replaced by *trans*-Pt(II) moieties, a feature which has been reported before for other systems.[152] The emission maxima, however, remain almost constant at 564 and 595 nm.

compound	absorption λ_{max} / nm	extinction ε / L mol^{-1} cm^{-1}	fluorescence λ_{max} / nm	quantum yield $\Phi_{Fl.}$ / %
C[Pt–A–3T(Bu$_4$)–A]$_2$	409	70800	508; 541	<< 1
C[Pt–A–5T(Bu$_6$)–A]$_2$	423	95500	555; 584	2
C[Pt–A–7T(Bu$_8$)–A]$_2$	428	123000	563; 595	10
C[*trans*-Pt–A–7T(Bu$_8$)–A]$_2$	436	141300	564; 595	9

Table 27: **Summary of spectroscopic data of the oligothienyl platinacycles obtained in CH_2Cl_2 before** [141] c = 1×10^{-6} mol L^{-1}; quantum yield standard: dpa

Another particularity of the **C[Pt–A–3T(Bu$_4$)–A]$_2$** spectra is the peak at 650 nm, which appears upon excitation at 410 nm. Such behaviour is known in literature: in a quite extensive study on *trans*-Pt(II) complexes, a strong dependency of the emission spectra on the excitation wavelength had been revealed.[153] There, it was found that the emission bands at 440–500 nm all emitted by triplet transitions and could be characterised by a significant charge transfer. The absorption values of such compounds had typically been in the range from 320 to 400 nm and could be assigned to intramolecular charge transfer as well as π–π^* transitions. As can be seen by comparing the excitation spectra of the 650 and 543 nm emissions, the excitation of the 650 nm band is rather narrow, which is in contrast to the typical spectra of oligothiophene macrocycles. Probably the metal centres play an important role for this transition, providing a charge transfer channel.

Also for the other platinacycles the emission spectra differ by showing more or less structured emission bands. An explanation for this finding might be the steric demand of the alkyl side chains in **3T(Bu$_4$)** and **3T(Dodec$_2$).** As they are — fully or partly — located next to the centre thiophene, they do not allow a strong planarisation in the excited state (what is usually a condition for a more structured emission). This behaviour is mirrored in the excitation spectrum, which for **C[Pt–A–4T(Dodec$_2$)–A]$_2$**, with at least two neighboured thiophene moieties that do not interfere sterically, shows a more resolved structure than the other macrocycles.

4.9 Experimental Section

UV/Vis absorption

UV/Vis absorption spectra were recorded in quartz cuvettes of 2–10 mm light path with a PerkinElmer Lambda 19 spectrometer. If not noted otherwise, optically pure dichloromethane (Aldrich; Merck [Uvasol®]) was used as the solvent.

Fluorescence emission

Fluorescence spectra were recorded in fluorescence quartz cuvettes of 10 mm light path with a PerkinElmer LS 55B luminescence spectrometer in a 90° setup. All spectra were corrected automatically. If not noted otherwise, optically pure dichloromethane (Aldrich; Merck [Uvasol®]) was used as the solvent. The samples were diluted so that the optical density of the corresponding absorption spectrum was slightly lower than 0.04 (optically dilute measurements).[154]

Calculation of quantum yields[154]

Quantum yields were calculated by comparing the integrals of the emission spectra at different wavelengths with those of fluorescence standards. The results were corrected according to eq. 9 by the optical densities at the corresponding wavelengths and by the refraction indices of the solvents. Finally, average values for different wavelengths were calculated.

$$\Phi_{\text{substance}} = \Phi_{\text{reference}} \frac{A(\lambda)_{\text{substance}}}{A(\lambda)_{\text{reference}}} \times \frac{n^2_{\text{substance}}}{n^2_{\text{reference}}} \times \frac{OD(\lambda)_{\text{reference}}}{OD(\lambda)_{\text{substance}}} \qquad \text{(Eq. 9)}$$

Φ : fluorescence quantum yield

$A(\lambda)$: area integral of emission curve (excitation at wavelength λ) with subtracted curves for pure solvent spectra.

n : refractive index of the solvent

$OD(\lambda)$: optical density at wavelength λ

The primarily used fluorescence standard was 9,10-diphenylanthracene ("dpa"; Aldrich) in optically pure *n*-hexane (Aldrich) with a fluorescence quantum yield of 0.90 ± 0.02.[155] As a further standard, a solution of fluoresceine in 0.1 M aqueous NaOH (prepared with millipore grade water; R > 15.0 MΩ) with a reference quantum yield of 0.93 was used.[156]

5 Electrochemical Properties of Oligothienyl Macrocycles

5.1 Electrochemical Features of Shape-Persistent Macrocycles

5.1.1 Electrochemical Demands on Shape-Persistent Macrocycles

Research in the field of shape-persistent macrocycles still means basic research, and characterisation is often reduced to the identification and the aggregation behaviour of the molecules; further — if applicable — to host–guest chemistry, photophysical properties, and studies on aromaticity. The redox properties usually come into play when there is interest in using these materials in molecular devices or "nanoelectronics". Macrocycles for such applications have to bring along unique properties with respect to their physicochemical performance, including their electrochemical behaviour.

Probably the most common way to realise this goal are specially designed functional groups that account for the functionality of the macrocycle. Prominent examples are of course the "Stoddart-type" cycles based on viologene: By changing the redox state, the molecule's charge is altered, leading to a different preference for the site of interaction with other molecules. This principle has already been applied to various molecular devices such as sensors, switches or shuttles,[157,158] and examples for this type of electrochemical response are so numerous that only one application by *Stoddart, Heath and coworkers* shall be presented here (figure 102): In the rotaxane **StoddartHeath1**, the viologene-containing ring "shuttles" between two different receptor sites on the axis, depending on the redox state. With cyclic voltammetry at various temperatures and different scan speeds, the kinetics of this movement could be determined.

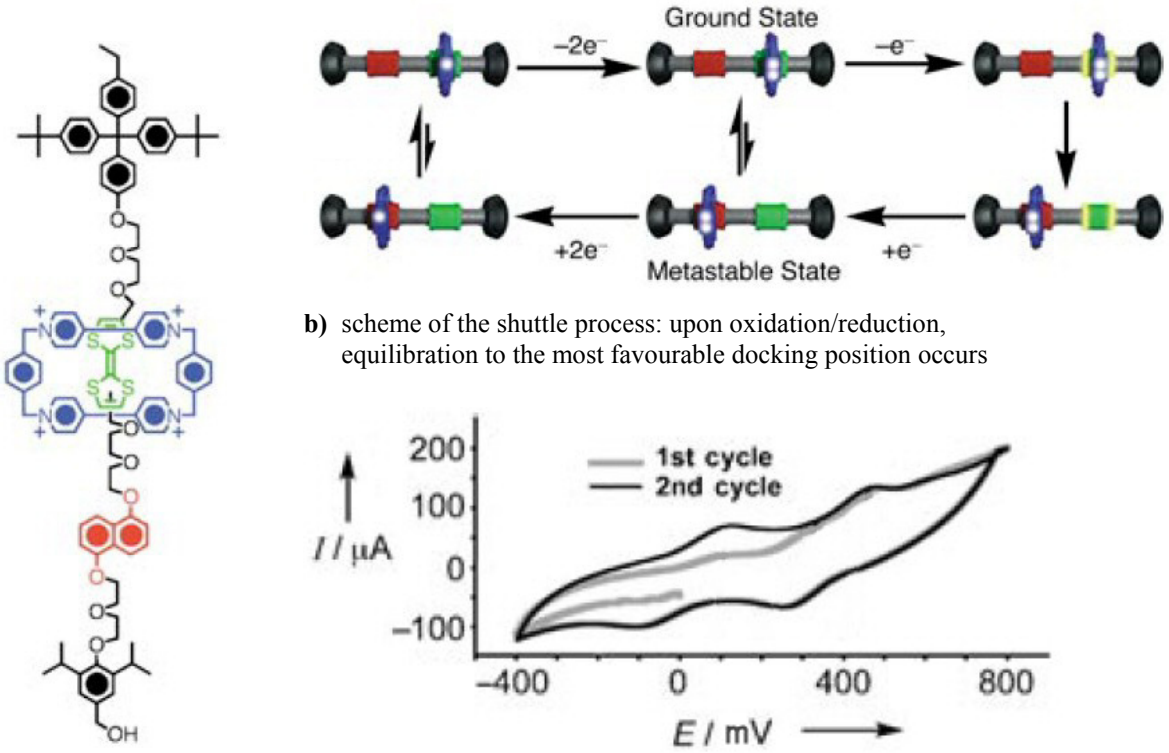

a) molecular structure of **StoddartHeath1**; the shuttle unit and the docking stations are highlighted by colours

b) scheme of the shuttle process: upon oxidation/reduction, equilibration to the most favourable docking position occurs

c) cyclic voltammogram of a polymer device containing the molecular shuttle: after the first cycle, the features for the metastable and ground-state co-conformers have shifted to the main oxidation peaks

Figure 102: A viologene-containing macrocycle as a molecular "shuttle" in rotaxane StoddartHeath1 with different docking stations on the dumbbell component[157a]

Fewer examples of electrochemical response are based directly on a structural change of the molecules. Oxidation (or reduction) in this case affects the constitution of the macrocycle, thereby changing its physicochemical properties. Scheme 45 shows an example by *Ono*, *Uno*, *Osuka et al.*, who were able to rearrange the N-fused benzohexaphyrin **OnoUnoOsuka1** by oxidation with DDQ.[159] While the initial molecule was non-fluorescent, the resulting macrocycle **OnoUnoOsuka2** includes a diindomethene subunit with a decent fluorescence in the near-IR region. Such behaviour might be considered similar to the ring-closure reaction of dithienylethenes.[160]

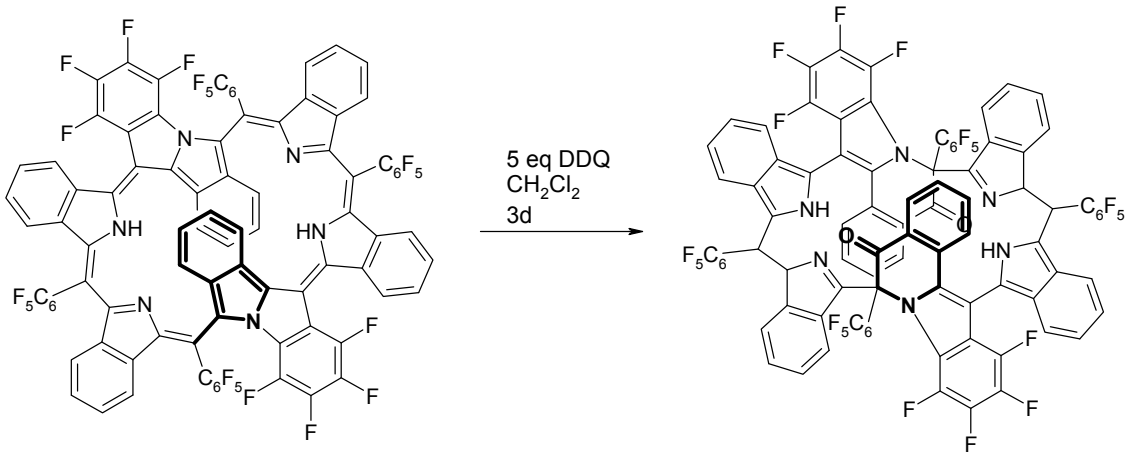

OnuUnoOsuka1 **OnuUnoOsuka2**

Scheme 45: Oxidation of OnoUnoOsuka1, yielding the fluorescent macrocycle OnoUnoOsuka2
parts of the molecules (which coincide with the reacting moieties) are marked in bold for a better differentiation of superimposed structures

In another case, *Sessler and coworkers* performed a reductive *N* alkylation of the cyclo[8]pyrroles **Sessler1a–b** (scheme 46).[161] Like in the previous example, the compound gives up its extended (even aromatic) conjugation and, due to the inner alkyl parts, twists away from planarity to a bowl-shaped conformation.

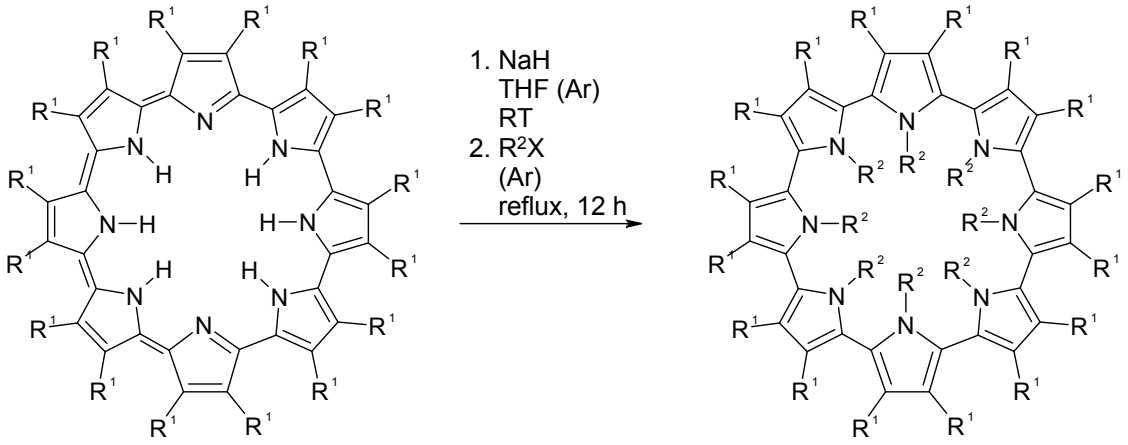

Sessler1a–b **Sessler1c–e**

Scheme 46: *N* alkylation of cyclo[8]pyrroles Sessler1a–b to Sessler1c–e
Sessler1a: R^1 = Et;
Sessler1b: R^1 = Me;
Sessler1c: R^1 = Et, R^2 = Me;
Sessler1d: R^1 = Me, R^2 = Et;
Sessler1e: R^1 = Me, R^2 = Bn (benzyl)

While functional groups or reactive sites are valuable for applications like sensors, they are often of disadvantage in molecular electronics, as they typically decrease the long-term stability of a device. Hence, oxidations/reductions should not lead to a complete change of the chemical nature, but

rather influence the geometry[162] and the aromatic character[163] of the ring system, or provoke intermolecular interactions, e.g. π-dimer formation[164]. A cyclic array can offer the advantage of a higher stability due to non-existing end groups. Therefore, the cyclic oligothiophenes discussed here are ideal targets for electrochemical investigations, as linear oligothiophenes are commonly used materials in organic transistors or solar cells (cf. introduction in section 1.1),[165,166] and cyclic voltammetry is a typical means of characterisation, either for the compounds themselves or for device setups. While the results of cyclic voltammetry measurement with oligothiophene macrocycles are presented in the sections 5.1.3–5.4, these macrocycles even meet further requirements for materials in applications, such as self-assembly on a graphite surface[167] and a (yet weak) interaction with fullerene C_{60} (cf. section 6), a corresponding electron acceptor material for photovoltaic devices.[168]

5.1.2 Influence of Pt(II) on the Electrochemical Properties

In the context of shape-persistent macrocycles, one focus of this thesis is Pt(II)-containing rings which can be used as intermediates in the synthesis of fully conjugated macrocycles. The electrochemical properties of platinum macrocycles are highly influenced by the metal centres, since the Pt(II) orbitals are contributing to both HOMO and LUMO of the molecule (cf. scheme 8, p. 25). Electron transport properties in molecular wires with platinum complexes have been studied,[169] and there is evidence that Pt(II) moieties can on one hand support conjugation and delocalisation in organic polymers[170], *and* on the other hand can also act as insulators[171]. In general, electronic transitions are dominated by metal-to-ligand charge transfer, with rather wide band gaps. Exceptions exist where the Pt(II) corners do not seem to be much involved in the redox processes of the macrocycle.[172] However, the band gaps can be significantly lowered by creating strong donor–acceptor systems, like in the example **Wong1** reported by *Wong and coworkers* (figure 103).[173] The acceptor character of Pt(II) moieties may also lead to a small or medium red-shift of the absorption maximum.[174]

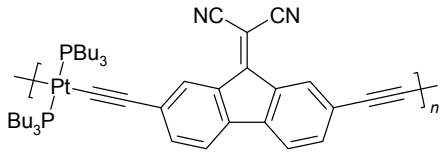

Figure 103: Low-bandgap donor–acceptor polymer comprising *trans*-Pt(II) moieties

To use Pt(II) macrocycles as intermediates, their electrochemical properties are vital for the success of the reductive elimination. As a result of various studies on this reaction type, it was shown that elimination usually occurs via a five-coordinated intermediate, like it is known for octahedral Pt(IV) complexes.[175,176] Hence, the reductive elimination has to be oxidatively induced. This can be achieved by addition of electron donors like iodine which add to the Pt(II) centre (cf. sections 2.3 and 3.3),[177,178] but an electron-transfer process is also possible: E.g., *Sato et al.* successfully eliminated a Pt(II)–diphosphine corner from the *cis*-Pt(II)(aryl)(alkynyl) complexes **Sato1a–f** by means of DDQ or $AgBF_4$.[179]

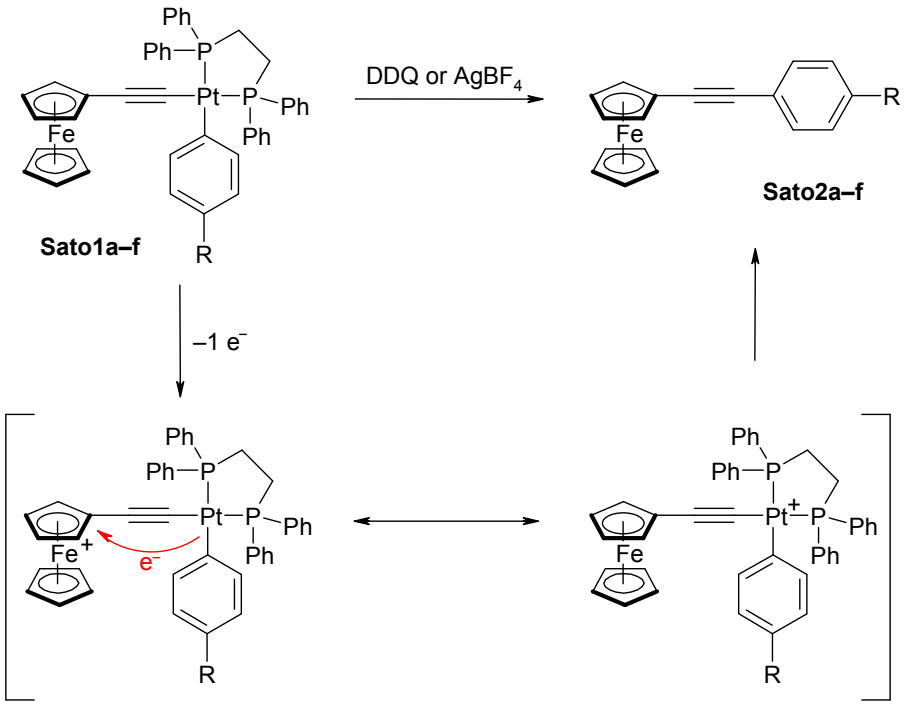

Scheme 47: Reductive Pt(II) elimination with Sato1a–f, induced by electron transfer via DDQ or $AgBF_4$
Sato1a/Sato2a: R = H;
Sato1b/Sato2b: R = Me;
Sato1c/Sato2c: R = Cl;
Sato1d/Sato2d: R = OMe;
Sato1e/Sato2e: R = CO_2Et;
Sato1f/Sato2f: R = COMe

Cyclic voltammetry investigations showed the same behaviour for the phenanthroline-containing oligothiophene–Pt(II) macrocycles **C[Pt–A–*n*T–phen–*n*T–A]** (figure 104, see also p. 73): In comparison to the Pt(II)-free linear precursors, the first oxidation peak shifted to a significantly lower potential, indicating an (irreversible) oxidation at the Pt(II) centre.[178b,180] However, as the CV diagram changes after the first scan and further oxidation peaks cannot be clearly separated, follow-up reactions are rather complex. The reaction products could not be identified, so probably polymerisation took place to some extent.

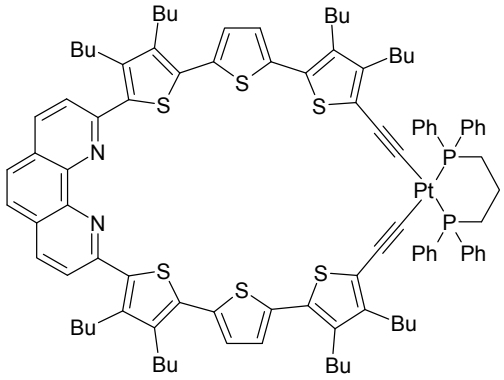

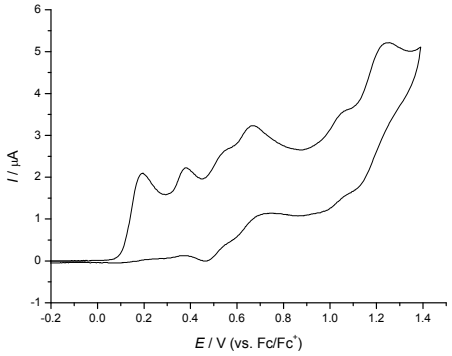

a) C[Pt–A–3T(Bu$_4$)–phen–3T(Bu$_4$)–A]
E^0_1 = +0.17 V (corresponds to oxidation of Pt(II) centre),
E^0_2 = +0.34 V, E^0_3 = +0.50 V,
E^0_4 = +0.59 V, E^0_5 = +0.99 V, E^0_6 = +1.17 V

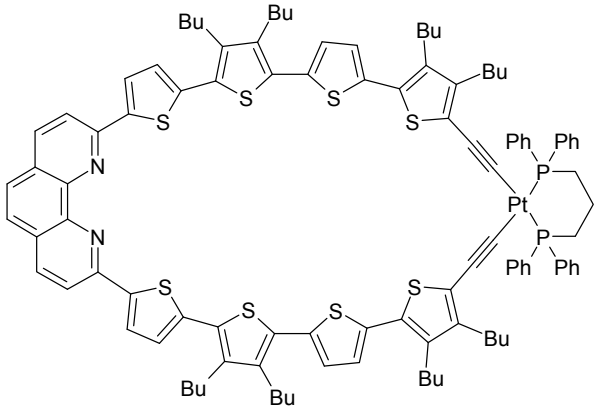

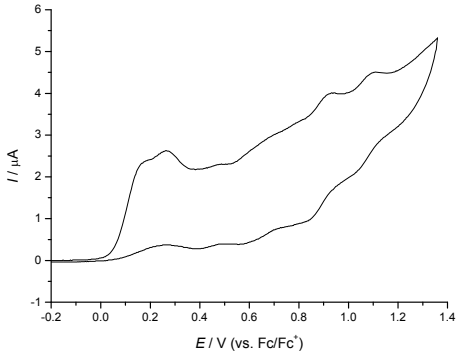

b) C[Pt–A–4T(Bu$_4$)–phen–4T(Bu$_4$)–A]
E^0_1 = +0.14 V (corresponds to oxidation of Pt(II) centre)

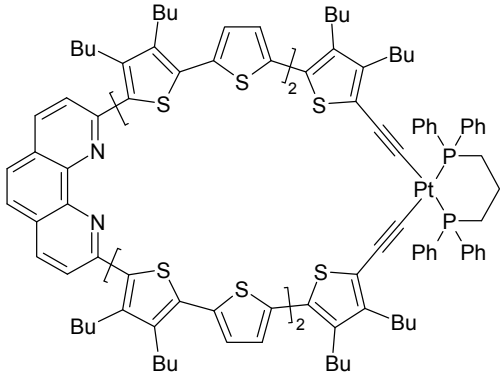

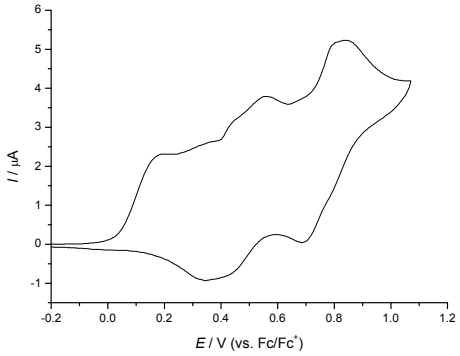

c) C[Pt–A–5T(Bu$_6$)–phen–5T(Bu$_6$)–A]
E^0_1 = +0.14 V (corresponds to oxidation of Pt(II) centre)

Figure 104: Structures and cyclic voltammograms of the phenanthroline-containing macrocycles C[Pt-A-*n*T-phen-*n*T-A][180]
10^{-3} M solutions in CH_2Cl_2; all spectra were recorded at 295 K at a scan rate of v = 100 mV s^{-1}, using 0.1 M Bu_4NPF_6 as supporting electrolyte; the values of the potentials are reported vs. Fc/Fc^+; potentials of irreversible peaks were calculated approximatively from the current I_p of the oxidative peak ($I^0 = 0.855 \times I_p$[181])

5.1.3 Electrochemical Data of Oligothiophene Macrocycles and Their Pt(II) Precursors

In order to prove the feasibility of such a one-electron transfer for the reductive elimination to **C[*n*T–DA]*m*** macrocycles (cf. section 2.3), cyclic voltammetry has been performed for the platinum precursor **C[A–Pt–A–3T(Bu$_4$)]$_2$** in dichloromethane.[177] Figure 105a shows that after an initial, irreversible oxidation at +0.06 V vs. Fc/Fc$^+$ two reversible oxidations at +0.44 V and +0.57 V appear, followed by a fourth irreversible wave at +0.72 V. Comparison with the cyclic voltammogram of **C[3T(Bu$_4$)–DA]$_2$** (figure 105c, cf. also figure 106 on page 187), which shows two reversible oxidation waves at +0.39 V (E^0_1 = 0.35 V) and +0.59 V(E^0_2 = 0.56 V), indicates that the second and third wave of figure 105a correspond to the waves in figure 105c, i.e. the metal centres are indeed eliminated and the desired Pt-free cycle was formed (cf. also table 28).

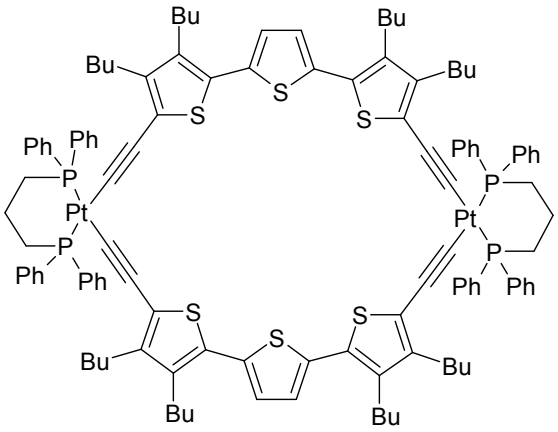

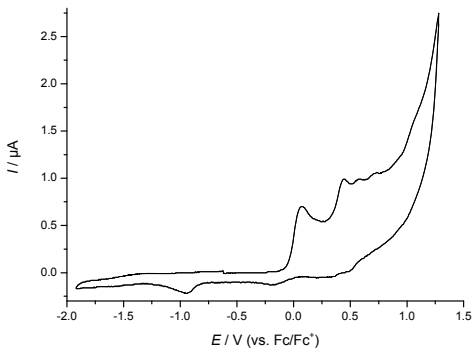

a) C[Pt–A–3T(Bu$_4$)–A]$_2$
c = 1×10^{-4} M in CH_2Cl_2;
E^{ox}_1 = +0.06 V, E^{ox}_2 = +0.44 V, E^{ox}_3 = +0.57 V,
E^{ox}_4 = +0.72 V

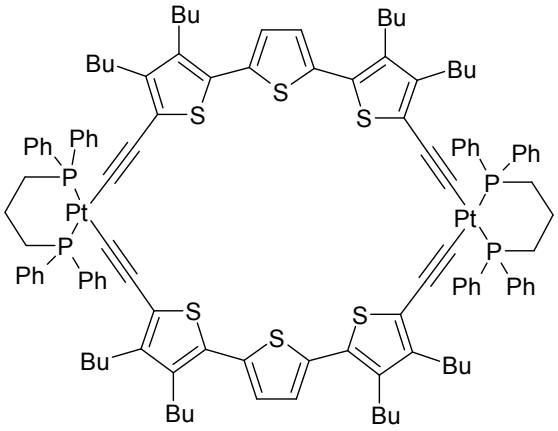

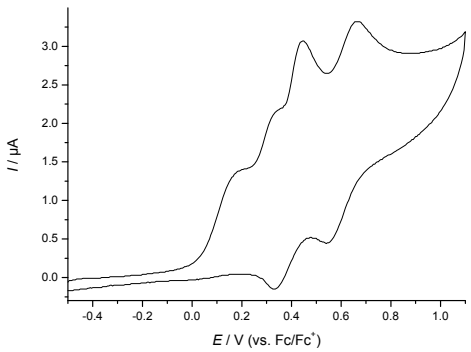

b) C[Pt–A–3T(Bu$_4$)–A]$_2$
c = 1×10^{-4} M in benzonitrile;
E^{ox}_1 = +0.19 V, E^{ox}_2 = +0.34 V, E^{ox}_3 = +0.45 V
(E^0_3 = +0.39 V), E^{ox}_4 = +0.66 V (E^0_4 = +0.61 V)

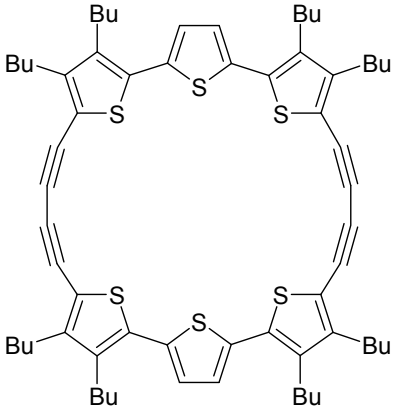

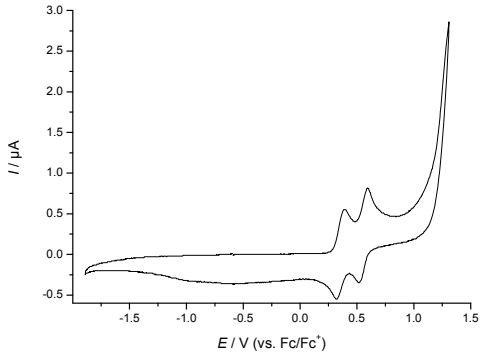

c) C[3T(Bu$_4$)–DA]$_2$
$c = 1\times10^{-3}$ M in CH_2Cl_2;
$E^{ox}_1 = +0.39$ V ($E^0_1 = +0.35$ V), $E^{ox}_2 = +0.59$ V
($E^0_2 = +0.56$ V)

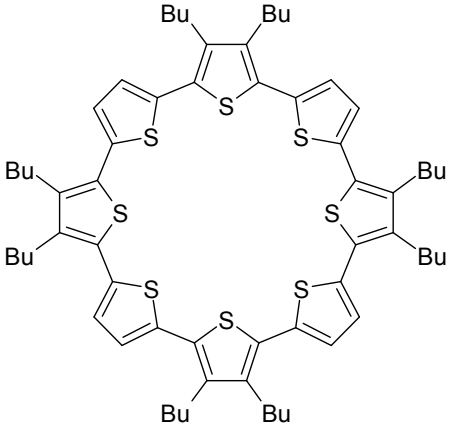

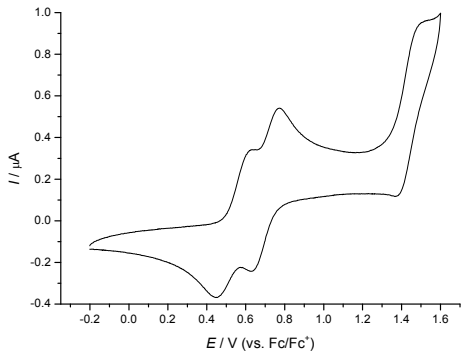

d) C[8]T
$c = 1\times10^{-4}$ M in CH_2Cl_2;
$E^0_1 = +0.54$ V, $E^0_2 = +0.70$ V, $E^0_3 = +1.45$ V

Figure 105: Structures and cyclic voltammograms of the smallest butyl-substituted macrocycles and their Pt(II) precursor[177]
all spectra were recorded at 295 K at a scan rate of $v = 100$ mV s^{-1}, using 0.1 M Bu_4NPF_6 as supporting electrolyte; the values of the potentials are reported vs. Fc/Fc$^+$

compound	E^{ox}_1 (E^0_1) / V	further E^{ox} (E^0) / V
C[Pt–A–3T(Bu$_4$)–A]$_2$	+0.06	+0.44, +0.57, +0.72
C[3T(Bu$_4$)–DA]$_2$	+0.39 (+0.35); fully reversible	+0.59 (+0.56); fully reversible
C[8]T	+0.54; fully reversible	+0.70, +1.45; fully reversible

Table 28: Summary of electrochemical data of of the smallest butyl-substituted macrocycles and their Pt(II) precursor[177]
all potentials are reported vs. Fc/Fc$^+$

The practical transfer of these results to prepare **C[3T(Bu$_4$)–DA]$_2$** by preparative electrolysis of **C[A–Pt–A–3T(Bu$_4$)]$_2$**, however, pointed out the limits of this method: To provide an adequate

solubility, the solvent had to be changed to benzonitrile, in which the cyclic voltammogram looked significantly different (figure 105b): The initial oxidation wave shifted to a more positive value of +0.19 V, and an unknown second (irreversible) oxidation at +0.34 V showed up. Still, in an electrolysis experiment in a CV cell at 80 °C and a constant potential of +0.85 V vs. Ag/AgCl (i.e., ca. +0.50 V vs. Fc/Fc^+) the two initial peaks had disappeared after 48 h. After work-up and chromatographic purification, pure **C[3T(Bu$_4$)–DA]$_2$** was obtained in 6 % yield. The low yield was mainly attributed to the weak solubility of the Pt(II) macrocycle, which was likely to precipitate and cover the electrodes during the electrosynthesis.

Besides **C[3T(Bu$_4$)–DA]$_2$**, also the all-thiophene macrocycle **C[8]T** was characterised by CV. While for **C[3T(Bu$_4$)–DA]$_2$** only two reversible waves could be seen, **C[8]T** allows for three one-electron oxidations at E^0 values of +0.54 V, +0.76 V and +1.45 V (figure 105d). As discussed in section 4.8, the radical cation should adopt a fully quinoidal structure (scheme 48). Upon the second electron removal, the molecular state likely corresponds to a bipolaronic structure, in which the two charges reside on the half of the ring that still maintains a quinoid structure. In the radical trication, there have to be two quinoidal regions with the charges being as far apart as possible.

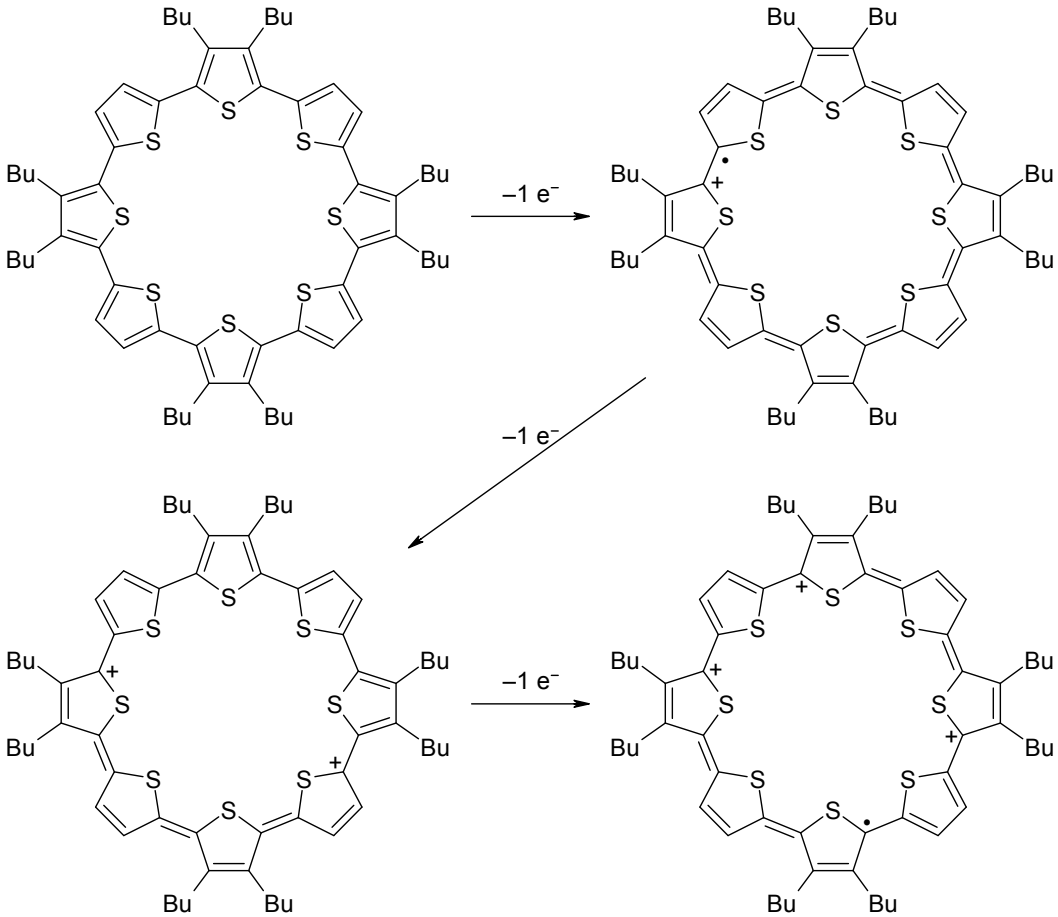

Scheme 48: Proposed structures and charge distributions of C[8]T upon oxidation

5.2 Cyclic Voltammetry of Conjugated Macrocycles with Terthienyl Units

The wide range of ring sizes, which was obtained for the **C[3T(Bu$_4$)–DA]$_m$** family, allowed for a study of the redox behaviour of fully conjugated macrocycles with an incremental increase in size. It was already mentioned in the previous section that the smallest family member, the cyclic dimer **C[3T(Bu$_4$)–DA]$_2$**, can take up two positive charges in a fully reversible way.[177] However, oxidation becomes increasingly irreversible with growing size. This can be shown by comparison of the cyclic voltammograms for the cycles with m = 2–5 (figure 106 and table 29). Already the cyclic trimer and tetramer are restricted to one partially reversible oxidation wave; further oxidations lead to irreversible side reactions. Consequently, the first oxidation wave of the cyclic pentamer is only slightly reversible.

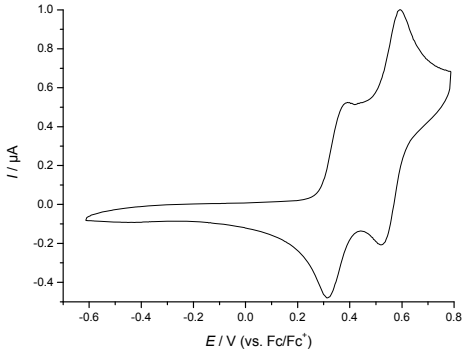

a) C[3T(Bu$_4$)–DA]$_2$[177]
$c = 1.0\times10^{-3}$ M;
$E^{ox}_1 = +0.39$ V ($E^0_1 = +0.35$ V; fully reversible), $E^{ox}_2 = +0.59$ V ($E^0_2 = +0.56$ V; fully reversible)

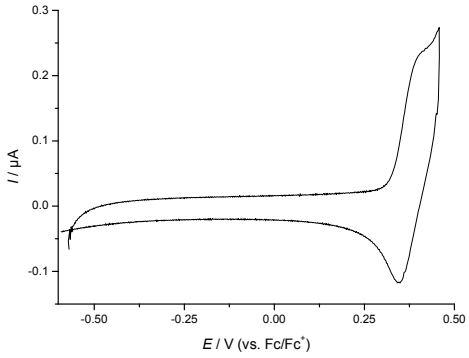

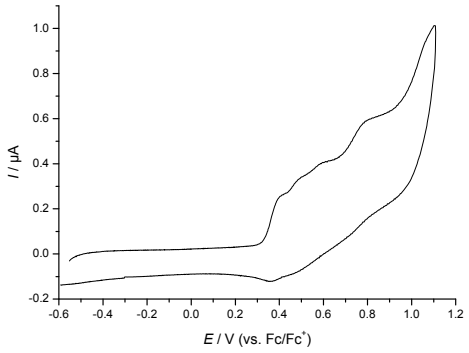

b) C[3T(Bu$_4$)–DA]$_3$
$c = 1.6\times10^{-4}$ M;
left graph: first oxidation peak; $E^{ox}_1 = +0.41$ V ($E^0_1 = +0.38$ V; partially reversible)
right graph: complete oxidative scan; $E^{ox}_2 \approx +0.50$ V, $E^{ox}_3 \approx +0.59$ V, $E^{ox}_4 \approx +0.79$ V

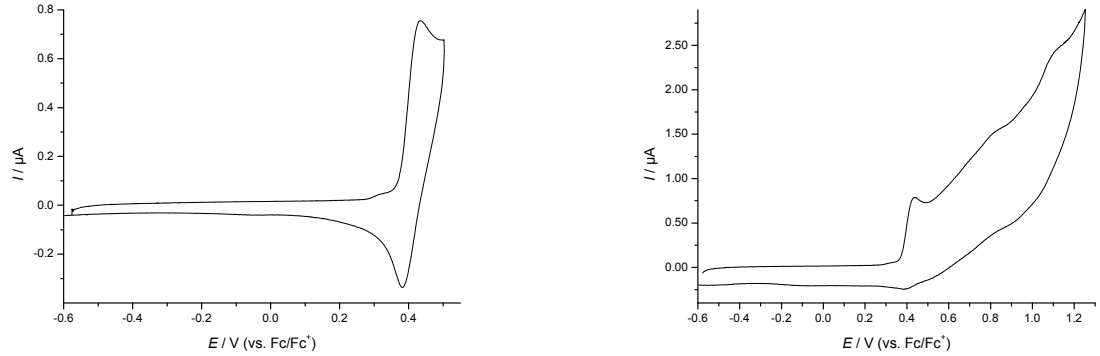

c) C[3T(Bu$_4$)–DA]$_4$
$c = 2.4\times10^{-4}$ M;
left graph: first oxidation peak; $E^{ox}_1 = +0.44$ V ($E^0_1 = +0.41$ V; partially reversible)
right graph: complete oxidative scan; $E^{ox}_2 \approx +0.85$ V, $E^{ox}_3 \approx +1.14$ V

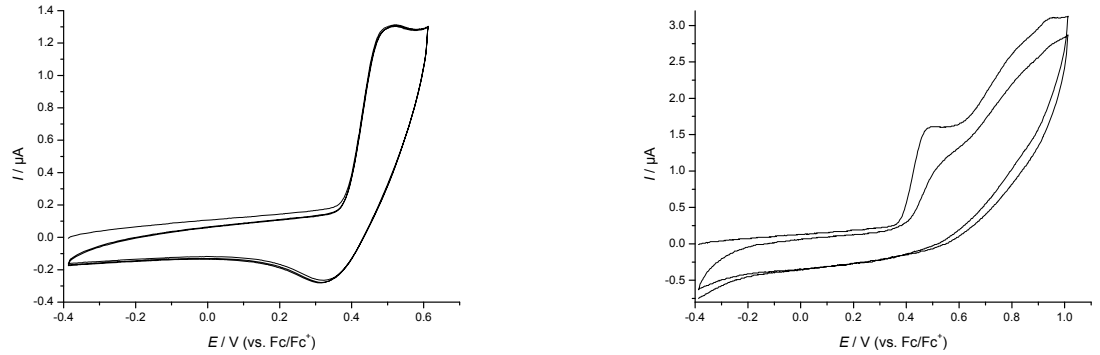

d) C[3T(Bu$_4$)–DA]$_5$
$c = 1.0\times10^{-4}$ M;
left graph: first oxidation peak; $E^{ox}_1 = +0.49$ V ($E^0_1 = +0.42$ V; partially reversible)
right graph: complete oxidative scan (with follow-up cycle); $E^{ox}_2 \approx +0.82$ V, $E^{ox}_3 \approx +0.94$ V

Figure 106: Cyclic voltammograms of the C[3T(Bu$_4$)–DA]$_m$ series (m = 2–5)
all spectra were recorded in CH_2Cl_2 at 295 K at a scan rate of $v = 100$ mV s^{-1}, using 0.1 M Bu_4NPF_6 as supporting electrolyte; the values of the potentials are reported vs. Fc/Fc$^+$

compound	E^{ox}_1 (E^0_1) / V	further E^{ox} / V
C[3T(Bu$_4$)–DA]$_2$[177]	+0.39 (+0.35); fully reversible	+0.59 (+0.56); fully reversible
C[3T(Bu$_4$)–DA]$_3$	+0.41 (+0.38)	≈ +0.50, ≈ +0.59, ≈ +0.79
C[3T(Bu$_4$)–DA]$_4$	+0.44 (+0.41)	≈ +0.85, ≈ +1.14
C[3T(Bu$_4$)–DA]$_5$	+0.49 (+0.42)	≈ +0.82, ≈ +0.94

Table 29: Summary of electrochemical data of the conjugated oligothienyl–diethynyl macrocycles
all potentials are reported vs. Fc/Fc$^+$

The shape of the cyclic voltammograms of the macrocycles with $m > 2$ made it impossible to determine exact values for all oxidations and back reductions except for the first oxidations, which are quasi-reversible with increasing half-wave potentials of E^0_1 = +0.38 V (cyclic trimer), +0.41 V (cyclic tetramer) and +0.42 V (cyclic pentamer). This notable augmentation will be discussed more in detail in section 5.5. A peak separation of approximately 0.06 V at a scan rate of 100 mV s^{-1} indicates one-electron transfer processes for all these waves. As can be seen in figure 106, the reversibility vanishes when the oxidative scan is prolonged, thus additional oxidations and side reactions take place which render the first oxidation completely irreversible. Like for the photophysical data, the differences between the half-wave potentials are decreasing with growing size of the macrocycles.

Furthermore, The shape of the cyclic voltammograms does not change much between the tetramer and the pentamer, indicating "saturation" for the electrochemical values. After the first oxidation, which still has a rather sharp signal, the electric current increases in an almost constant fashion. As an exception, the small macrocycle **C[3T(Bu$_4$)–DA]$_3$** shows more pronounced signals in the oxidative scan. Although exact values could not be determined, the separation of the corresponding cathodic and anodic peak potentials seems to be around 100 mV at a scan rate of 100 mV s^{-1}, i.e. only one electron is transferred during oxidation/reduction. This assumption is supported by the nearly constant height of the first three steps which indicates a successive transfer of one electron each.

5.3 Analytical Cyclic Voltammetry of Oligothienyl Diplatina-Macrocycles

While for the smallest fully conjugated macrocycles a perfectly reversible behaviour towards oxidation could be demonstrated (cf. section 5.2), the cyclic Pt(II) precursors undergo fast reactions already after the first electron transfer, which can be shown by comparison of the electrochemical data of the three differently substituted terthiophene-containing diplatina-macrocycles **C[Pt–A–3T(Bu$_4$)–A]$_2$**, **C[Pt–A–3T(Ph$_4$)–A]$_2$**, and **C[Pt–A–3T(Dodec$_2$)–A]$_2$** (figure 107). The oxidation of the phenyl-substituted **C[Pt–A–3T(Ph$_4$)–A]$_2$** is irreversible even at high scan rates of 1000 mV s^{-1}. This result corresponds to the findings for the other two compounds, summarised in figure 108 and table 30.

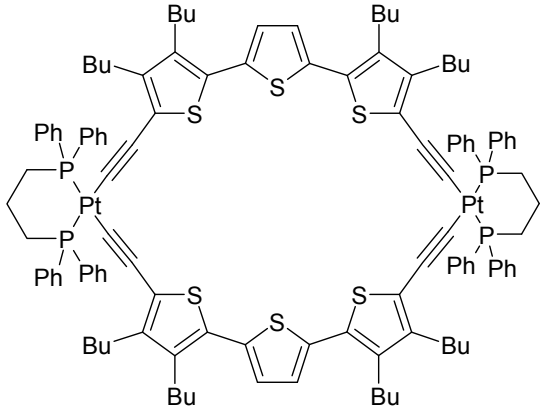

a) C[Pt–A–3T(Bu$_4$)–A]$_2$[177]

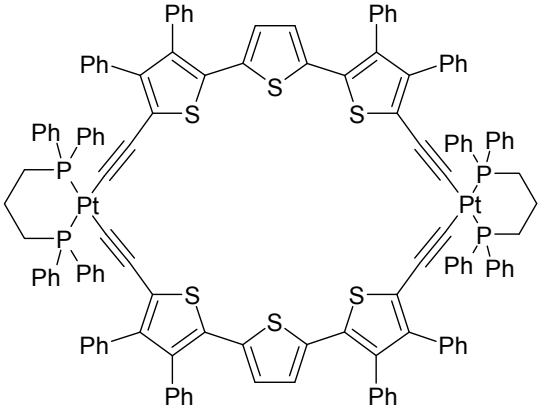

b) C[Pt–A–3T(Ph$_4$)–A]$_2$

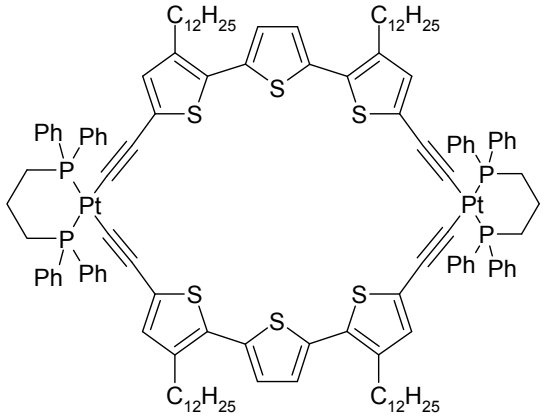

c) C[Pt–A–3T(Dodec$_2$)–A]$_2$[182]

Figure 107: Structures of diplatina macrocycles with terthiophene moieties

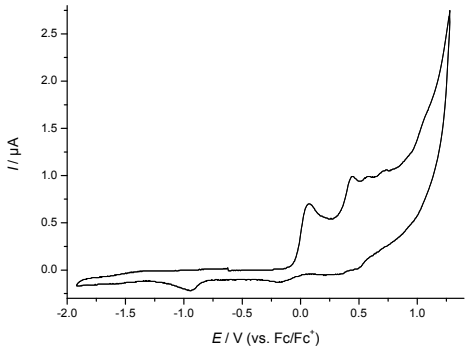

a) C[Pt–A–3T(Bu$_4$)–A]$_2$[177]
$c = 1.0\times10^{-4}$ M;
$E^{ox}_1 = +0.06$ V, $E^{ox}_2 = +0.44$ V, $E^{ox}_3 = +0.57$ V, $E^{ox}_4 = +0.72$ V

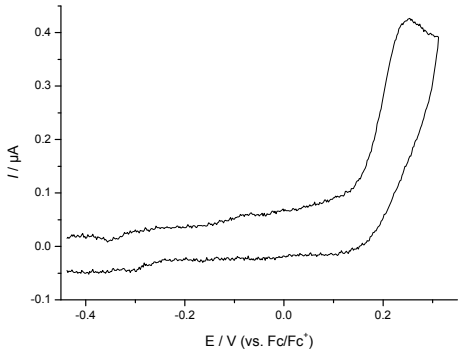

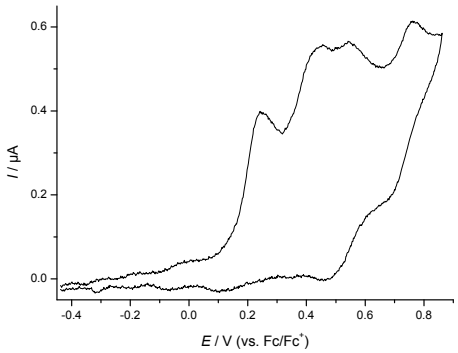

b) C[Pt–A–3T(Ph$_4$)–A]$_2$
$c = 4.0\times10^{-4}$ M;
left graph: first oxidation peak; $E^{ox}_1 = +0.25$ V
right graph: complete oxidative scan; $E^{ox}_2 = +0.45$ V, $E^{ox}_3 = +0.55$ V, $E^{ox}_4 = +0.77$ V

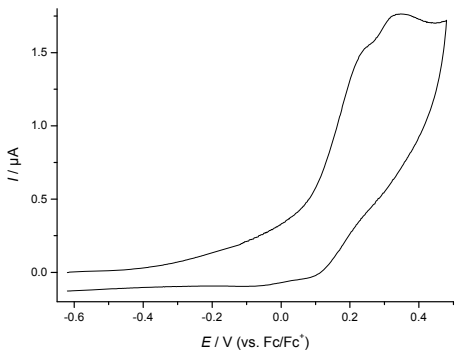

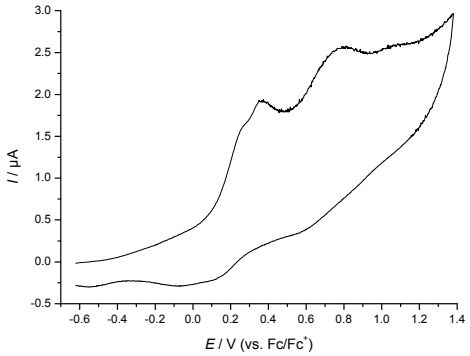

c) C[Pt–A–3T(Dodec$_2$)–A]$_2$[182]
$c = 5.0\times10^{-4}$ M;
left graph: first oxidation peak; $E^{ox}_1 \approx +0.24$ V, $E^{ox}_2 = +0.35$ V
right graph: complete oxidative scan; $E^{ox}_3 = +0.79$ V, $E^{ox}_4 = +1.08$ V

Figure 108: Cyclic voltammograms of diplatina terthiophene macrocycles
all spectra were recorded in CH_2Cl_2 at 295 K at a scan rate of $v = 100$ mV s^{-1}, using 0.1 M Bu_4NPF_6 as supporting electrolyte; the values of the potentials are reported vs. Fc/Fc$^+$

compound	E^{ox}_1 [V]	further E^{ox} [V]
C[Pt–A–3T(Bu$_4$)–A]$_2$[177]	+0.06	+0.44, +0.57, +0.72
C[Pt–A–3T(Ph$_4$)–A]$_2$	+0.25	+0.45, +0.55, +0.77
C[Pt–A–3T(Dodec$_2$)–A]$_2$[182]	≈ +0.24	+0.35, +0.79, +1.08

Table 30: Summary of electrochemical data of diplatina terthiophene macrocycles
all potentials are reported vs. Fc/Fc^+

All tree compounds show cyclic voltammograms of similar shape with a first, rather sharp and irreversible oxidation wave, and 2–3 additional peaks which sometimes overlap. Interestingly, the first oxidation wave of **C[Pt–A–3T(Bu$_4$)–A]$_2$** appears at a significantly lower potential (of +0.06 V vs. Fc/Fc^+; cf. section 5.1.3) compared to that of the other two macrocycles, which is found around +0.25 V. In the case of **C[Pt–A–3T(Dodec$_2$)–A]$_2$,** this first peak almost coincides with a second peak at +0.35 V. While the butyl- and phenyl-substituted molecules, comprising the same substitution pattern, have almost identical follow-up oxidation values of ca. +0.45, +0.55 and +0.75 V, the dodecyl-substituted macrocycle can only be further oxidised at higher potentials of +0.79 and +1.08 V. In subsequent scans, the peak at +0.79 V even disappears, whereas no changes are found in the spectra of **C[Pt–A–3T(Bu$_4$)–A]$_2$** and **C[Pt–A–3T(Ph$_4$)–A]$_2$**. Hence, the different substitution pattern with longer alkyl chains in **C[Pt–A–3T(Dodec$_2$)–A]$_2$** seems to prevent an oxidative follow-up reaction which is possible for the other two macrocycles, either for sterical/structural or for electronic reasons.

5.4 Electrochemically Triggered Reductive Elimination of Pt(II) Centres

Although shifted to a higher oxidation potential of +0.25 V vs. Fc/Fc^+ compared with +0.06 V for **C[Pt–A–3T(Bu$_4$)–A]$_2$** (cf. section 5.3), the similar structure of the cyclic voltammogram of the phenyl analogue **C[Pt–A–3T(Ph$_4$)–A]$_2$** proposed that reductive elimination by electrochemical means should also be possible in this case. For the practical realisation, the solvent turned out to be a major difficulty, as the phenyl-substituted diplatina-macrocycle did not show enough solubility in dichloromethane to provide reasonable concentrations for electrosynthesis. In the search of a better suited solvent, it was found that benzonitrile allowed higher concentrations around 10^{-3} mol L^{-1}. To test its applicability for reductive elimination, the linear *cis*-Pt(II) compound **Pt[A–T]$_2$** was submitted to electrochemical oxidation (scheme 49).

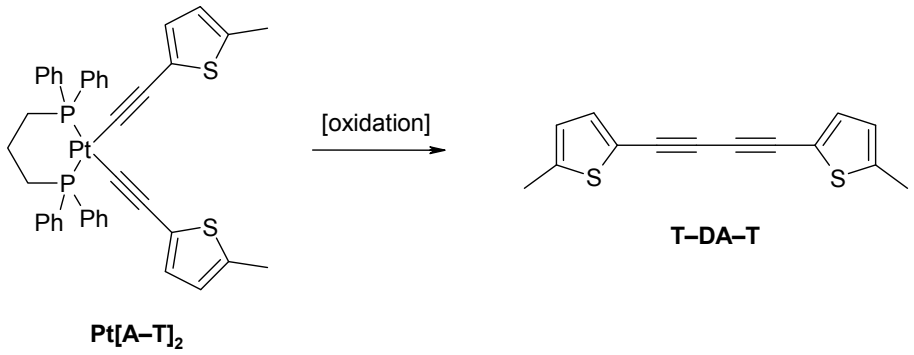

Scheme 49: Reductive elimination of the Pt(II) centre in Pt[A–T]$_2$

At a concentration of 10^{-3} mol L^{-1} in a volume of 5 mL of benzonitrile, the first and second oxidation waves of **Pt[A–T]$_2$** peaked at +0.03 V and +0.22 V vs. Fc/Fc^+ (figure 109a). Hence, the intermediate value of +0.13 V was chosen for the electrochemical oxidation and was applied over a period of 8 h. During this time, the current flow steadily decreased (figure 109b), as **Pt[A–T]$_2$** was converted and less substance was left to be oxidised for charge transport. After 8 h, the initial oxidation peak at +0.13 V had almost vanished (figure 109c), indicating a complete reaction.

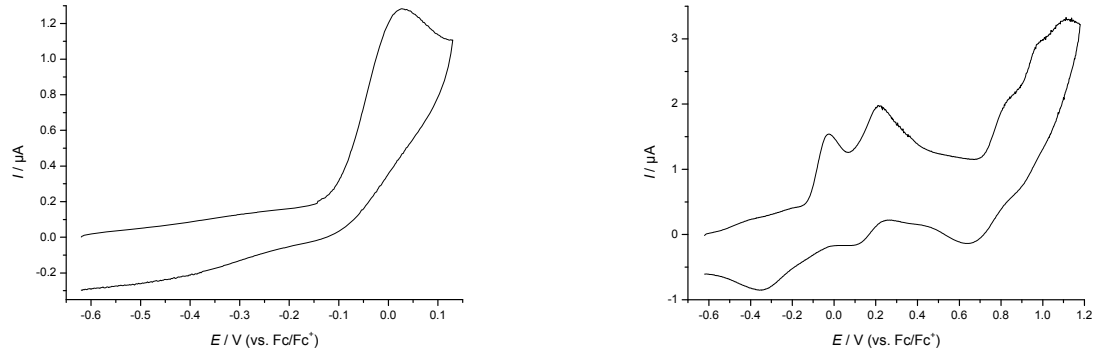

a) cyclic voltammograms before electrochemical elimination
left graph: first oxidation peak; $E^{ox}_1 = +0.03$ V
right graph: complete oxidative scan; $E^{ox}_2 = +0.22$ V, $E^{ox}_3 = +0.83$ V, $E^{ox}_4 \approx +0.98$ V, $E^{ox}_5 \approx +1.11$ V

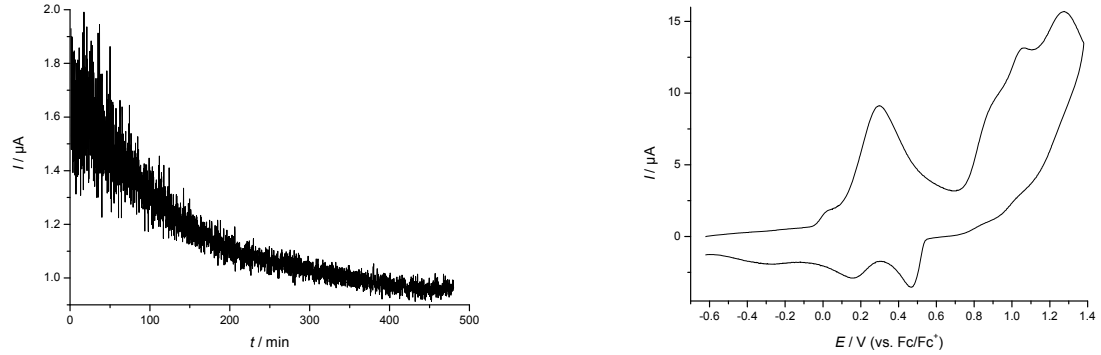

b) decrease of the electric current during oxidation at +0.13 V

c) complete oxidative scan after electrochemical elimination for 8 h;
the first distinct oxidation peak now appears at +0.30 V

Figure 109: Electrochemical curves of a benzonitrile solution of Pt[A–T]$_2$ before, during and after application of an oxidising potential
$c = 1.0\times10^{-3}$ M; all spectra were recorded at 295 K and at a scan rate of $v = 100$ mV s^{-1}, using 0.1 M Bu_4NPF_6 as supporting electrolyte; the values of the potentials are reported vs. Fc/Fc^+

Due to the small amount of **Pt[A–T]$_2$** used in this reaction, work-up to separate the product from the supporting electrolyte was not tried. Instead, as benzonitrile had proven to function as a suitable solvent for an oxidatively induced reductive elimination, it was directly employed in a larger batch of 50 mg (4.1×10^{-4} M) of **C[Pt–A–3T(Ph$_4$)–A]$_2$** in 50 mL of the solvent (scheme 50).

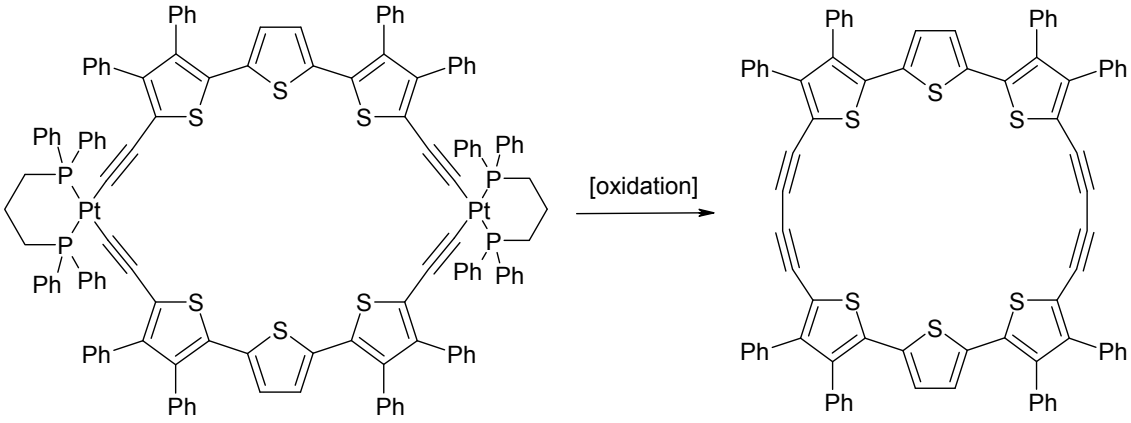

C[Pt–A–3T(Ph$_4$)–A]$_2$ **C[3T(Ph$_4$)–DA]$_2$**

Scheme 50: Reductive elimination of the Pt(II) centres in C[Pt–A–3T(Ph$_4$)–A]$_2$ by electrochemical oxidation

Compared to the cyclovoltammetric curves obtained in dichloromethane, the first oxidation wave in benzonitrile was less distinct (figure 110), but appeared at the same potential of +0.25 V vs. Fc/Fc$^+$. A potential of +0.31 V was then applied over a period of 35 h, during which the Pt-wire counter electrode had to be changed twice due to a black precipitate.

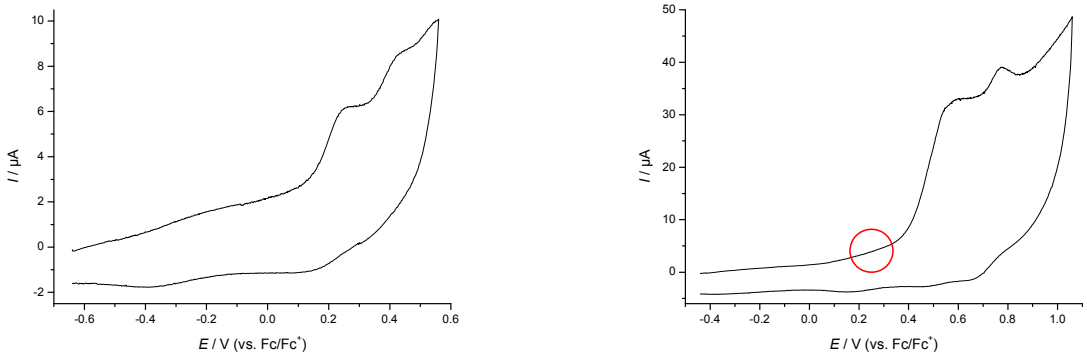

a) before oxidation;
E^{ox}_1 = +0.25 V

b) after oxidation;
the red circle indicates the former position of E^{ox}_1

Figure 110: Cyclic voltammograms of C[Pt–A–3T(Ph$_4$)–A]$_2$ before and after application of an oxidising potential of +0.31 V for 35 h
$c = 4.1\times10^{-4}$ M in benzonitrile; all spectra were recorded at 295 K at a scan rate of $v = 100$ mV s^{-1}, using 0.1 M Bu_4NPF_6 as supporting electrolyte; the values of the potentials are reported vs. Fc/Fc

After the reaction, methanol was added to the mixture to precipitate remaining starting material. Both the filtrate and the filtration residue were worked up using column chromatography. Each separation yielded 10 mg of a fraction that contained the desired conjugated macrocycle, as could be shown by MALDI TOF mass spectrometry (figure 111). However, the main compounds of these fractions seemed to be unreacted Pt(II) macrocycle and an intermediate with one platinum corner left, indicative of a step-wise mechanism of Pt(II) elimination. A further important finding is the

lack of mass signals for conjugated macrocycles larger than the cyclic dimer, which had been found for the iodine-induced elimination reaction (cf. section 3.3).

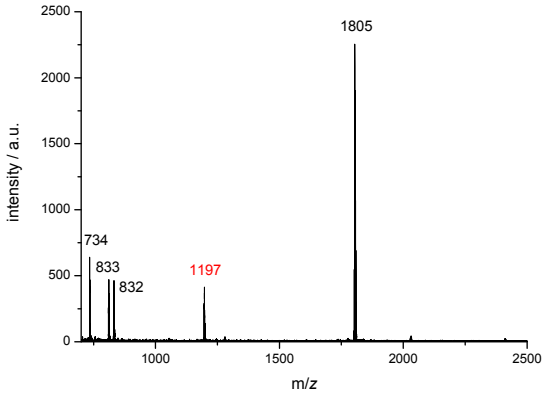

Figure 111: MALDI TOF mass spectrum of the product fractions of electrochemical elimination after column chromatography
m/*z* = 734 [Pt(dppp) + I]$^+$, 811, 832 [Pt(dppp) + matrix]$^+$, 1197 [cyclic dimer]$^+$, 1805 [cyclic dimer with one remaining Pt(dppp) corner]$^+$

The main drawback in this experiment was the incomplete conversion of the starting material. This can be explained by the use of an electrochemical cell designed for cyclic voltammetry: The oxidation process is restricted by small electrode surfaces and a one-compartment setup, leading to the precipitation of electroactive compounds on the counter electrode. Thus, the experiment was repeated in an electrosynthesis cell comprising larger platinum foil electrodes, an $Ag/AgNO_3$ reference electrode (connected by a Luggin capillary), and a compartment for the counter electrode which was separated by a sintered-glass filter. This time, the butyl-substituted diplatina-macrocycle **C[Pt–A–3T(Bu$_4$)–A]$_2$** was employed in order to rule out an incomplete reaction that originates from the nature of the starting material, as electrochemical oxidation of **C[Pt–A–3T(Bu$_4$)–A]$_2$** in a cyclic voltammetry cell had already yielded **C[3T(Bu$_4$)–DA]$_2$** as the only product.[177] In the electrosynthesis cell, cyclic voltammetry of the starting material showed a first oxidation peak at +0.36 V vs. Ag/Ag^+ (figure 112a); therefore the fixed potential for the Pt(II) elimination was set to +0.42 V. After 24 hours, the first oxidation wave was still visible in the cyclic voltammogram, thus the reaction was continued for a total of four days. Unfortunately, a leak caused the reference electrode to run dry during the last 24 hours. As a result, control over the applied potential was lost and no final cyclic voltammogram could be recorded. A MALDI TOF mass spectrum of the crude product showed the desired product peak at m/*z* = 1036.5 and no signals above 1299.5. The mixture was worked up by evaporation of the solvent, extraction with toluene, and column chromatography in order to separate the macrocycle from the supporting electrolyte. In the first few fractions, the

presence of the dimeric macrocycle **C[3T(Bu$_4$)–DA]$_2$** was detected by analytical HPLC, but these fractions — which had yields of only a few milligrams — contained impurities that could not be separated off.

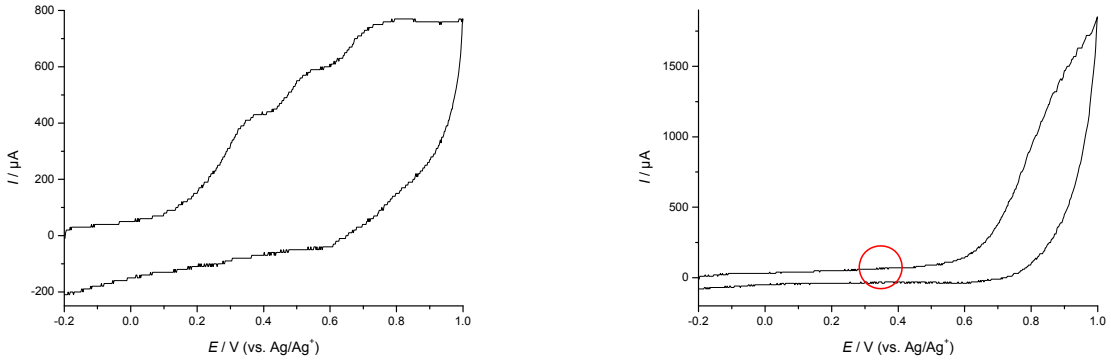

a) before oxidation;
E^{ox}_1 = +0.36 V

b) after 2 days;
the red circle indicates the former position of E^{ox}_1

Figure 112: Cyclic voltammograms of C[Pt–A–3T(Bu$_4$)–A]$_2$ before and after application of an oxidising potential of +0.42 V over two days
$c = 1.0\times10^{-4}$ M in benzonitrile; all spectra were recorded at 295 K at a scan rate of $v = 100$ mV s^{-1}, using 0.1 M Bu_4NPF_6 as supporting electrolyte; the values of the potentials are reported vs. Ag/Ag$^+$

5.5 Discussion of the Electrochemical Results

In the series of the **C[3T(Bu$_4$)–DA]$_m$** cycles, some trends can be withdrawn from the cyclic voltammograms for $m = 2$–5. Most importantly, the fully conjugated oligothienyl macrocycles exhibit an increasingly irreversible behaviour towards oxidation with growing size: Only for **C[3T(Bu$_4$)–DA]$_2$** the first and the second oxidation is fully reversible; for the larger homologues already the first oxidation loses more and more of its reversible character. This finding is in contrast to the results for the acyclic oligothiophenes ***n*T(Bu$_{n+1}$)**:[183] In this linear oligothiophene series, the longer oligomers could be reversibly charged to radical cations and even higher due to the steric shielding of the β substituents at the terminal thiophenes. The shorter linear terthiophene **3T(Bu$_4$)**, however, only showed a quasi-reversible first oxidation wave. (It should be mentioned that, starting from the linear undecithiophene **11T(Bu$_{12}$)**, the peak separation is reduced to less than 59 mV, indicating a transfer of at least two electrons in the first oxidation process.) Such a behaviour of increasing irreversibility is, on the other hand, known for other structures: E.g., the Pt(II) terminated oligoethynylene "wires" **Gladysz9–12** of *Gladysz and coworkers* (figure 113) show a spectrum ranging from full reversibility for a four-carbon chain to zero reversibility for a sixteen-carbon chain.[185] A direct comparison to the macrocycles is not feasible, though, as the wires become less shielded with increasing length, yet (like for the cycles) oxidation becomes thermodynamically less favourable.

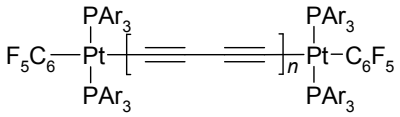

Figure 113: Molecular wires Gladysz9–12 with bulky Pt(II) stoppers
Ar = *p*-toluene;
Gladysz9: $n = 1$
Gladysz10: $n = 2$
Gladysz11: $n = 3$
Gladysz12: $n = 4$

Surprisingly, the direction in which the values of the first oxidation potentials develop is somewhat contradictory: It was expected that — much like for the linear series[183] — the values would shift to lower potentials instead of higher ones due to extended electron delocalisation. Hence, there seems to some kind of stabilisation with growing ring size towards oxidation, or, from another point of view, smaller ring sizes are electronically destabilised. This might be partially caused by the ring strain of the small cycles. On the other hand, already the cyclic tetramer should be strain-free (cf. section 4.7.3). A possible explanation for this seeming contradiction might be a greater twisting

and thus less planarity within the oligothiophene moieties, as flexibility and conformational degrees of freedom increase. This assumption is supported by semiempiric energy optimisations, which show increasing maximum S–C–C–S torsion angles of 40,5° for **C[3T(Bu$_4$)–DA]$_3$** up to 65,7° for **C[3T(Bu$_4$)–DA]$_5$**.[184] Another reason might be a slightly better sterical shielding, as the angles — especially the C–Pt–C angles — in the macrocycles widen and alkyl substituents can get in closer proximity to the Pt(II) corners and to each other.

The follow-up oxidations in the oxidative scan occur in several more or less separate steps. For **C[3T(Bu$_4$)–DA]$_3$**, three such steps could be distinguished, which are assumed to correspond to the formation of cations in the three monomeric units of the cyclic trimer. This would also mean that there is a strong electronic communication between the terthiophene units through the diethynylene bridges, leading to a shift of the potentials for subsequent oxidations. Although the second oxidation wave between +0.50 V and +0.59 V is wavy and seems to contain two processes, a clear interpretation of its electronic nature cannot be made due to the indistinct shape of the curve.

Comparison of the cyclic voltammograms of the phenyl- and dodecyl-substituted platinacycles **C[A–Pt–3T(Ph$_4$)–A]$_2$**, and **C[A–Pt–3T(Dodec$_2$)–A]$_2$** with the results of **C[A–Pt–3T(Bu$_4$)–A]$_2$** underlines the exceptional state of the butyl-substituted variant: Both other macrocycles have a significantly higher first oxidation potential of ca. +0.25 V vs. Fc/Fc$^+$ compared to +0.06 V for **C[A–Pt–3T(Bu$_4$)–A]$_2$**. This also leads to a smaller separation from the following oxidations and might be one drawback for a general preparative electrolysis to obtain Pt-free, fully conjugated macrocycles. However, the bad solubility of the platinacycles is still the biggest problem, as solvents have to be chosen that render the work-up process more difficult. Although electrolysis of **C[A–Pt–3T(Ph$_4$)–A]$_2$** was successful according to mass spectrometry analysis of the products, the separation problems remained. Especially the efficient separation from the conducting electrolyte, which has to be used in excess, is still a challenge even in the electrosynthesis cell setup and diminishes the advantage of a defined elimination process. Besides better soluble Pt(II) precursor cycles, a suitable solvent/electrolyte system for an easier work-up has to be determined.

5.6 Experimental Section

Chemicals:

Solvents and Electrolyte were purified prior to use by the following methods: Dichloromethane (Merck [Suprasolv®]) and benzonitrile (Merck) were dried over P_4O_{10} (Sicapent; Merck), freshly distilled under inert gas (Ar 4.6; MTI) and filtered over basic or neutral aluminium oxide of activation grade 0 (Alumina B Super 1; ICN Biomedicals). Tetra(*n*-butyl)ammonium hexafluorophosphate (Bu_4NPF_6; Avocado) was recrystallised twice from ethanol and stored under inert gas. The internal redox standard ferrocene (Fc/Fc^+; +0.43 V vs. SCE)[186] was recrystallised from cyclohexane.

Preparation of the electrodes:

The Ag/AgCl pseudo-reference electrode was prepared by first polishing a silver wire electrode and subsequently coating it in a 0.55 M $HCl_{(aq)}$ solution at +0.8 V for 20 min. The Pt wire counter electrode was polished prior to use. The Pt working electrode consisted of a Pt wire (∅ = 1.0 mm; $A = 0.785\ mm^2$) which was sealed in a soft glass tube. The electrode surface was polished successively with diamond polishing paste (Buehler) of 6, 3, 1 and finally 0.25 micron to obtain a smooth surface which was controlled with a microscope. Additionally, a neutral surface was built up by electrochemical cleaning in 0.5 M $H_2SO_{4(aq)}$.

Setup and procedure for analytical cyclic voltammetry:

All measurements were performed under inert gas (Ar 4.6; MTI). Solutions were prepared directly in the electrochemical cells, except for the microcompartment setup described below.

Cyclic voltammetry was performed with a computer-controlled EG&G PAR 273 Potentiostat (software: Model 270/250 Research Electrochemistry Software Version 4.40) or a PerkinElmer VMP Multichannel Potentiostat (software: EC-Lab v6.61), usually in a three-electrode single-compartment cell. Prior to the measurements, the electrochemical window of the electrolyte solution (typically 2 or 5 mL of a 0.1 M dichloromethane solution of Bu_4NPF_6) was checked, and the working electrode was cleaned by performing several cyclic sweeps within the determined range. The electroactive species was added to obtain a 10^{-3}–10^{-4} M solution. After the measurements, an equivalent amount of ferrocene was added and the potential for Fc/Fc^+ was determined as the internal standard.

For small amounts of substance, a microcompartment cell setup with a volume of 0.5 mL was used: Here, the working electrode was mounted from below, so that a teflon tube, which was put on top of the electrode, could serve as the compartment. A combined counter/pseudo-reference electrode (Pt ring/[Ag/AgCl]) was vertically lowered into the compartment. To dissolve the electroactive substance, the electrolyte solution was transferred out of and into the cell by a gas-tight syringe.

Setup and procedure for preparative reductive elimination:

Preparative electrochemistry was either performed in a standard three-electrode cell, using the same setup as described above for analytical cyclic voltammetry, or in a special arrangement for electrosynthesis. The latter consisted of a large glass compartment of approx. 600 mL, whose hollow wall provided connections for a thermostat. In its teflon lid, openings allowed the insertion of the working electrode, the reference electrode, the counter electrode compartment, a thermometer and a needle for Argon inlet. All openings were sealed with teflon seals and screws; the lid itself was tightened to the glass cell by metal screws. The working electrode consisted of a Pt foil (25.0 cm^2). The reference electrode consisted of an $Ag/AgNO_3$ electrode (Ag wire, 1.0×10^{-2} M $AgNO_3$ and 1.0×10^{-1} M Bu_4NPF_6 in acetonitrile), which was connected to the compartment by a Luggin capillary (1.0×10^{-1} M Bu_4NPF_6 in acetonitrile) with a Vicor glass membrane. The counter electrode compartment consisted of a glass cylinder with a sintered-glass bottom, into which the Pt-foil counter electrode (25.0 cm^2) and a cooling finger with an Argon inlet were inserted from the top.

Due to the low solubility of the platina-macrocycles in dichloromethane, benzonitrile was used as a solvent. After determination of the first oxidation wave by cyclic voltammetry, a slightly higher potential than that of the corresponding peak value was applied, and the solution was stirred continuously (at least for 24 h) until cyclic voltammetry indicated a completed reaction by disappearance of the initial oxidation peak. Work-up of the reaction was done by toluene extraction of the product from the dried reaction mixture and by subsequent column chromatography.

6 Interactions between Oligothienyl Macrocycles and Receptor Molecules

6.1 The Role of Macrocycles as Host Molecules

Examples of molecular recognition with Pt(II) macrocycles have already been mentioned in section 2.4. These include anion sensing in the cavity (**Lippert4b** on p. 35 ; **Ferrer1** on p. 45, and **Hanan1** on p. 53), rotaxane formation by hydrogen bonds (**Kim1** on p. 38), and metal–π "tweezer" complexations (**Stang3** on p. 42, **TessierYoungs2** on p. 60, and **Tessieryoungs5** on p. 61). However, failure to interact with several potential guest molecules was reported for **Lees3–5** (p. 57). In the following, selected examples of host–guest assemblies with shape-persistent macrocycles will be presented, covering different types of interaction.

Like for the redox properties presented in section 5.1, studies on molecular recognition have primarily been performed on macrocycles comprising functional groups, especially *N* heterocycles. Examples of metals being complexed to nitrogen atoms in the ring structure, sometimes even capable to build up three-dimensional superstructures like lattices, are numerous, especially if one considers metalla-porphyrins with their additional possibility of creating networks by attaching multivalent building blocks to the metal centre. An amazing example is the multiporphyrin array **Aida1** (figure 114) by *Aida and coworkers*, which can include a fifth porphyrin molecule and thereby act as a model for biologic light harvesting systems.[187]

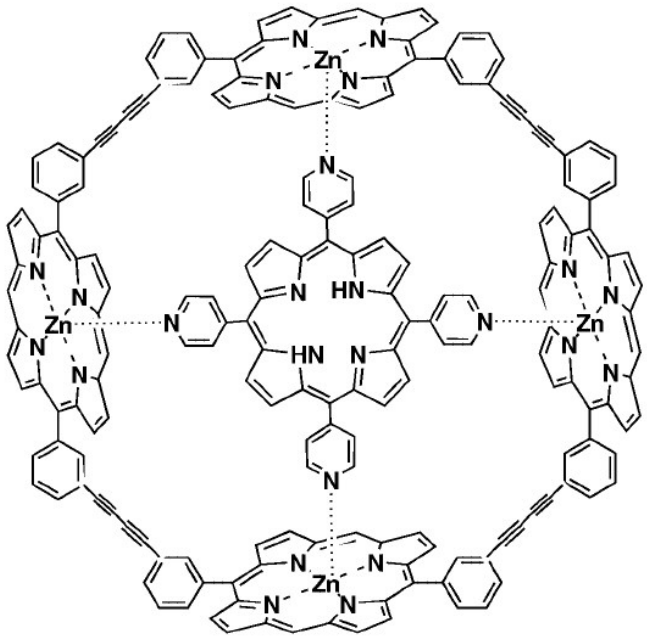

Figure 114: Inclusion complex of tetrakis(4-pyridyl)porphyrin in Aida1[187]

More related to cyclo[*n*]thiophenes are the macrocycles by *Baxter*, who prepared the thiophene-containing **Baxter1** (figure 115) which shows selective interaction with Pd(II), Ni(II), Co(II), Ag(I) and Hg(II).[188] Due to the donor-acceptor nature of the cycle, the changes in the absorption spectra were shifted to significantly lower energies than for the thiophene-free counterparts. Furthermore, the nature of the luminescence sensing differed for the metals: While in most cases a quenching of the fluorescence emission occurred, a bright orange luminescence developed for Ag(I).

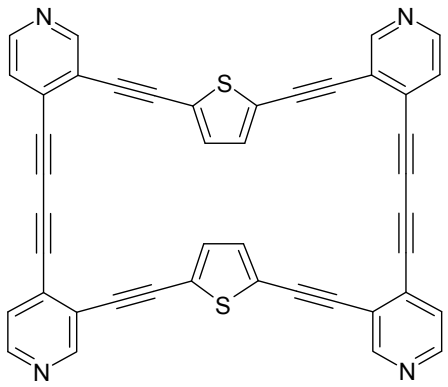

Figure 115: Macrocycle Baxter1

In the context of this thesis, however, a different kind of metal coordination is of more interest: the so-called "tweezer" complexation, in which the metal ion — usually Ag(I) — is complexed by two π-electronic moieties which are connected and held in close vicinity owing to the rigid structure of the molecule. Regarding macrocycles, such a complexation has been found predominantly for smaller specimen, which offer even more sites for metal–π interaction so that the advantage of the chelate effect fully comes into operation. Figure 116 shows a recent demonstration of such Ag(I) complexes with **MartínezBarcina1–2** by *Martínez, Barcina et al.*[189] Further examples can be found in literature.[190]

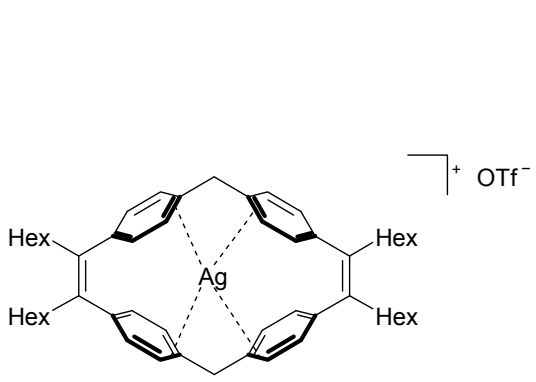

a) MartínezBarcina1

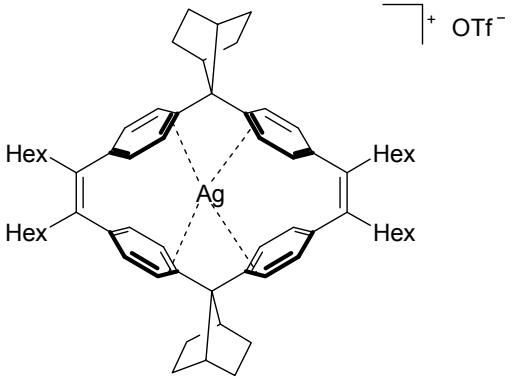

b) MartínezBarcina2

Figure 116: Ag(I) complexes of macrocycles MartínezBarcina1–2

Naturally, the chelate effect is an important factor for molecular recognition with macrocycles. Crown ethers, which are among the oldest applications for this principle, are still extensively used, e.g. in the (multi-)rotaxane motifs by *Stoddart and coworkers*, who use ammonium moieties as docking units.[191] Such hydrogen-bonding interactions are also present in the synthesis of the [2]catenane **Sanders1** (figure 117) by acetylenic coupling, although *Sanders and coworkers* claim the donor–acceptor interaction between the electron-rich naphthalene and the electron-deficient aromatic diimide to be more important.[192]

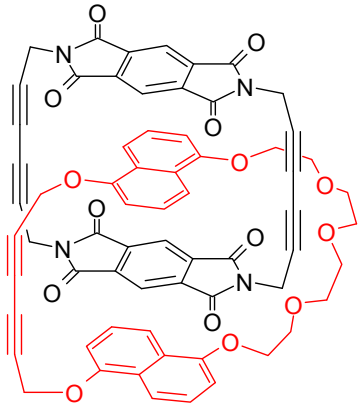

Figure 117: [2]Catenane Sanders1

However, as crown ethers are not shape-persistent, such examples will not be discussed further. Likewise, calixarenes and similar structures, which *are* shape-persistent and can take in a wide range of organic molecules by hydrophobic complexation (e.g. C_{60}[193]), shall only be mentioned, since even a basic overview on their host–guest chemistry would go far beyond the scope of this chapter.

Arene interactions, on the other hand, are of special interest, as they are more relevant for (cyclic) oligothiophenes. An overview on aromatic interactions in recognition processes has recently been presented by *Castellano, Diederich et al.*[194] Maybe the most intriguing example of arene recognition by conjugated macrocycles without functional groups are the "carbon nanorings" by *Kawase, Oda and coworkers*, which comprise ethynylene and either phenylene (**KawaseOda2**, figure 118), 1,4-naphthylene (**KawaseOda1**, cf. figure 3f on page 14) or 2,6-naphthylene units.[195]



a) general structure of cyclic para[*n*+5]-phenyleneacetylenes; *n* = 1–4

c) complex of hexamethylbenzene within the cyclic hexamer (*n* = 1); (calculated structure)

b) complex of C_{60} within the cyclic hexamer (*n* = 1) within the cyclic nonamer (*n* = 4); (calculated structure)

Figure 118: Examples for cyclic paraphenyleneacetylenes KawaseOda2 and their inclusion complexes[195]

These macrocycles possess cavities with a diameter of 1.32–1.98 nm and have been proven to be among the best fluorescence sensors for fullerenes C_{60} and C_{70}, with association constants K_a up to 10^5–10^6 L mol^{-1}. Based on theoretical studies, the authors ascribe the high values to a charge separation for curved aromatic hydrocarbons, as such systems should suffer an anisotropic distribution of π electrons and should therefore be polarised, with the concave side bearing the higher negative potential.[194,195a] Similarly high association constants with C_{60} can be found for the (non–shape persistent) cyclic dimers of metalloporphyrins developed by *Aida, Saigo and coworkers*.[196] There, C_{60} is complexed to two opposite sides by cation–π interactions, while a flexible alkyl spacer between the porphyrin moieties allows an induced fit.

The electron-deficient nature of fullerenes might also be the reason why C_{60} is — to the best of the author's knowledge — the only example of interaction to a (naturally electron-rich) thiophene moiety within a macrocycle.[197] By STM investigation, the deployment of a C_{60} monolayer on a monolayer of **C[12]T** could be monitored (figure 119). Different complexation sites were detected, reflecting the sixfold symmetry of **C[12]T**. Interestingly however, imaging of cavity-bound fullerene molecules was only possible at a low coverage, while a position at the rim of the macrocycle is thermodynamically preferred. The 1:1 donor–acceptor complexes turned out to be stable under the scanning conditions and could be characterised in terms of their semiconductor behaviour. Due to their dipolar nature, they can even induce quadrupoles in adjacent macrocycles, so that with growing coverage a two-dimensional crystalline superstructure with three different types of domains is formed.

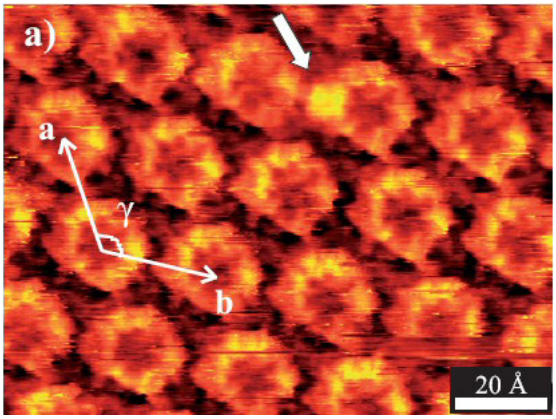

a) STM image of a monolayer of **C[12]T** on HOPG, including a **C[12]T**–C_{60} complex (white arrow); image area: 11.6 nm × 8.7 nm; tunnelling conditions: bias voltage U = −700 mV, tunnelling current I = 44 pA

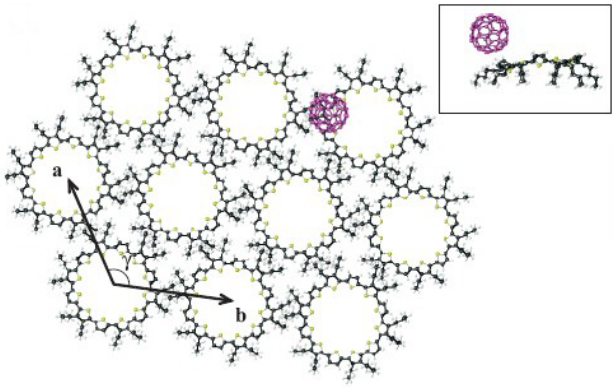

b) calculated model of a closely packed monolayer of **C[12]T** with a hexagonal arrangement including the unit cell parameters; side view of the calculated energy minimum conformation of a **C[12]T**–C_{60} complex (inset)

Figure 119: Complexation of C_{60} on a cyclothiophene monolayer[197]

6.2 Influence of Guest Molecules on the Fluorescence of Oligothienyl Macrocycles

6.2.1 Choice of the Guest Molecules

In general, thiophene is a rather weak partner for intermolecular interaction, as its sulphur atom is a very poor acceptor for hydrogen bonds, owing to a positive residual Mulliken charge of sulphur when attached to sp^2 carbon atoms.[198] Its coordination chemistry typically involves transition metal bonds to either the sulphur atom or the aromatic ring as a sandwich complex.[199]

To explore the character of the oligothiophene macrocycles as host systems, potential guest molecules have been used which provide different modes of interaction, including neutral or ionic aromatic donor–acceptor interactions, hydrogen bonds and metal complexations. The basis for the individual choice is described more in detail in the respective sections.

6.2.2 Addition of Fullerene C_{60} to Oligothienyl Macrocycles

One promising possibility for binding guest molecules to the oligothienyl–diethynyl macrocycles was the coordination of electron-poor compounds like fullerene C_{60} by the electron-rich oligothiophene moieties, which was successfully demonstrated in STM measurements (cf. section 6.1). Furthermore, C_{60} is an interesting partner for recognition, as it is frequently used as an electron acceptor material for photovoltaic devices including oligothiophenes.[168] In this context, even various dyads and triads with oligothiophenes and fullerenes had been prepared and their properties have been determined, especially with respect to energy and charge transfer.[200]

Molecular models of the macrocycles indicated that the cyclic trimer **C[3T(Bu$_4$)–DA]$_3$** exhibits a maximum S–S distance of 13.7 Å within the ring, providing a cavity of roughly 10 Å with respect to the van der Waals radii. Hence, C_{60} with its van der Waals diameter of 10 Å should fit exactly into the rim. Furthermore, the absorption curve of C_{60}, which is different from the absorption of the macrocycles (cf. section 4.2), should allow a good determination of the binding capacity by fluorescence quenching.

Indeed, successive addition of C_{60} to a 6.4×10^{-7} M solution of **C[3T(Bu$_4$)–DA]$_3$** in dichloromethane displayed an effect on the fluorescence intensity. Figure 120 shows the fluorescence decrease of **C[3T(Bu$_4$)–DA]$_3$** upon addition of C_{60}; the corresponding intensities (curve integrals relative to the pristine **C[3T(Bu$_4$)–DA]$_3$** solution) are listed in table 31. As can be deduced from the values, the

fluorescence intensity can be linearly decreased in steps of 10 % by addition of 50 equivalents of C_{60}, indicating a binding constant in the range of $3.4–4.7\times10^3$ L mol^{-1}.

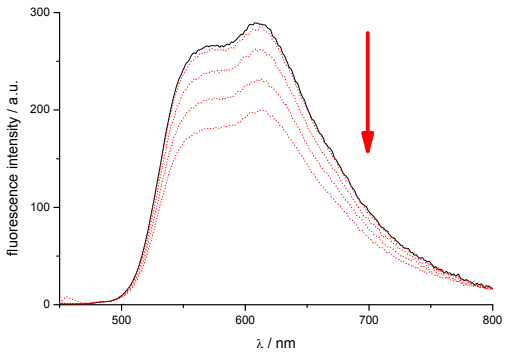

Figure 120: Fluorescence titration of C[3T(Bu$_4$)–DA]$_3$ with C_{60}
the emission intensity of the pristine solution (solid line; 6.4×10^{-7} M in CH_2Cl_2) is reduced upon addition of 10, 45, 95, and 150 equivalents of C_{60} (dotted red lines)

number of C_{60} equivalents	fluorescence intensity relative to pristine solution / %
0	100
10	98
45	91
95	81
150	70

Table 31: Decrease of fluorescence intensity upon addition of C_{60} to C[3T(Bu$_4$)–DA]$_3$

To obtain knowledge whether the size correlation using the van der Waals radii was correct, macrocycles with different sizes were also used as host molecules for C_{60}. As expected, **C[3T(Bu$_4$)–DA]$_4$** — providing a larger cavity — showed a weaker interaction than **C[3T(Bu$_4$)–DA]$_3$**: After addition of almost 100 equivalents of C_{60}, the decrease in fluorescence intensity was only 4 % compared to 20 % for the cyclic trimer (figure 121). This also rules out a decrease of the emission intensity for the **C[3T(Bu$_4$)–DA]$_3$**/C_{60} mixtures in figure 120 due to reabsorption by the fullerene: At energies where the macrocycles possess their emission maxima, C_{60} shows only a broad, flat shoulder in its UV/Vis spectrum. Consequently, all macrocycles should show a similar fluorescence decrease upon addition of C_{60} — which is not the case, as can be seen in the following experiments.

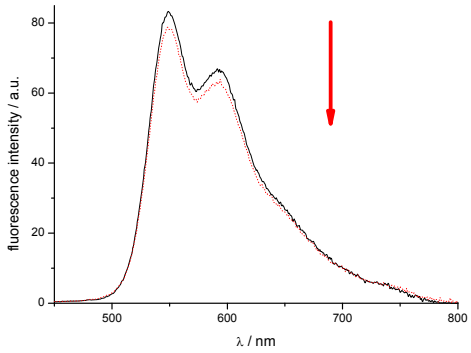

Figure 121: Fluorescence titration of C[3T(Bu$_4$)–DA]$_4$ with C$_{60}$
the emission intensity of the pristine solution (solid line; 1.9×10^{-7} M in CH_2Cl_2) is only slightly reduced upon addition of 95 equivalents of C_{60} (dotted red line)

To enhance quenching, the experimental approach was slightly modified based upon the findings of *Kobayashi et al.*:[201] While seeking evidence for the inclusion of C_{60} into thiaarene-cyclyne macrocycles by absorption titration, they observed higher complexation constants in the range of $7–12\times10^3$ L mol^{-1} only after having heated the chloroform solution to reflux. Consequently, for the recognition in thiophene macrocycles, part of the chloroform host solution with an excess of C_{60} was first put into an ultrasonic bath to facilitate the dissolution of C_{60}, then refluxed for 1 h before addition to the pristine macrocycle solution. The application of chloroform served the purpose of driving the equilibrium towards complexation by the use of a weaker solvent for C_{60}. Experiments were carried out with **C[3T(Bu$_4$)–DA]$_2$**, **C[3T(Bu$_4$)–DA]$_4$**, **C[3T(Bu$_4$)–DA]$_5$** and **C[5T(Bu$_6$)–DA]$_2$** to cover a broader range of host diameters. Due to a lack of larger amounts of **C[3T(Bu$_4$)–DA]$_3$**, this macrocycle could not be used for comparison, as this time a total amount of 50 mL chloroform was used to limit losses during refluxation.

While on a first glance it does not seem reasonable to use a smaller host than the cyclic trimer **C[3T(Bu$_4$)–DA]$_3$**, complexations in cyclic metalla-porphyrin dimers had shown that the distance of C_{60} to the closest host atom can even be less than the sum of the van der Waals radii.[196a] Compared to these stable complexes, the C_{60}–macrocycle distance of more than 3.5 Å for **C[3T(Bu$_4$)–DA]$_3$** can be considered rather large. Unfortunately, for the cyclic dimer **C[3T(Bu$_4$)–DA]$_2$** the already weak fluorescence emission was not altered by the potential guest molecule; therefore no statement can be made about interactions between C_{60} and **C[3T(Bu$_4$)–DA]$_2$**.

Regarding larger macrocycles, the pretreatment by refluxing the fullerene solution showed no effect for **C[3T(Bu$_4$)–DA]$_4$**: Like for the solution prepared at room temperature, there was only a 4 % decay of fluorescence emission after addition of 100 equivalents of C_{60}. A size increase of the host

molecule by application of **C[3T(Bu$_4$)–DA]$_5$** instead of the cyclic tetramer reduced the already weak interaction to zero, i.e. the emission of the macrocycle was not quenched at all.

Finally, a comparison with **C[5T(Bu$_6$)–DA]$_2$** shows that size is not the only parameter with a significant influence on molecular recognition: Having almost the same ring size as **C[3T(Bu$_4$)–DA]$_3$**, titration with a total of 100 equivalents of C_{60} in chloroform lead to a decrease in fluorescence intensity of "only" 13 % (figure 122).

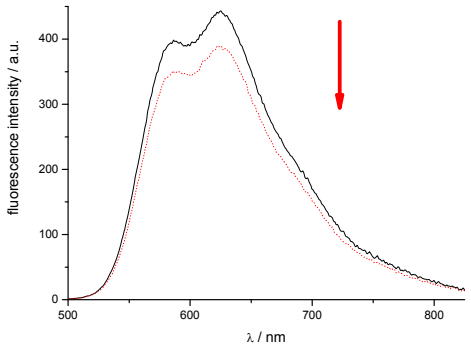

Figure 122: Fluorescence titration of C[5T(Bu$_6$)–DA]$_2$ with C_{60}
the emission intensity of the pristine solution (solid line; 3.1×10^{-7} M in $CHCl_3$) is reduced upon addition of 100 equivalents of C_{60} and heating to reflux for 1.5 h (dotted red line)

6.2.3 Addition of Porphyrins to Oligothienyl Macrocycles

As C_{60} had shown moderate quenching, tests on π–π interactions were continued with porphyrins, which not only provide an extended π system and a good fit to the macrocyclic cavity, but are also capable of forming charge-transfer assemblies and are therefore interesting candidates for recognition experiments.

Due to the more square shape of the porphyrins, the square cyclic tetramer **C[3T(Bu$_4$)–DA]$_4$** was chosen as a host macrocycle. Molecular models showed that, e.g., 5,10,15,20-tetrakis-pyridin-4-yl-21,23*H*-porphyrin **P(Py)$_4$** should fit exactly into the cavity of **C[3T(Bu$_4$)–DA]$_4$**, so that the van der Waals surfaces just get into contact. The porphyrin fills approximately 55 % of the cavity area in a two-dimensional projection.[202] Although this is less than the anticipated value of at least 70 %, which was calculated for a two-dimensional cross section of the "ideal" 55–70 % space filling,[203] the sum of the van der Waals radii can be regarded as a minimum interatomic distance between guest and host atoms, and simple molecular models indicated that this close distance should be reached for a **C[3T(Bu$_4$)–DA]$_4$/P(Py)$_4$** host–guest pair.[204]

Unfortunately, the strong absorption of the porphyrin turned out to be a severe problem for the fluorescence titration of **C[3T(Bu$_4$)–DA]$_4$**. Figure 123a shows that although at 430 nm the main absorption band of **P(Py)$_4$** (with a maximum at 416 nm) is almost passed, the optical density is noticeably higher than for pristine **C[3T(Bu$_4$)–DA]$_4$** already at 30 equivalents of the porphyrin. Furthermore, additional absorption bands at 511, 545 and 587 nm appear, leading to a reabsorption of the fluorescence emission. The result is an almost complete disappearance of the macrocycle emission at high relative concentrations (100–850 equivalents) of **P(Py)$_4$**, while the intensity of the more bathochromic emission bands of **P(Py)$_4$** first increases and then also decreases (figure 123b).

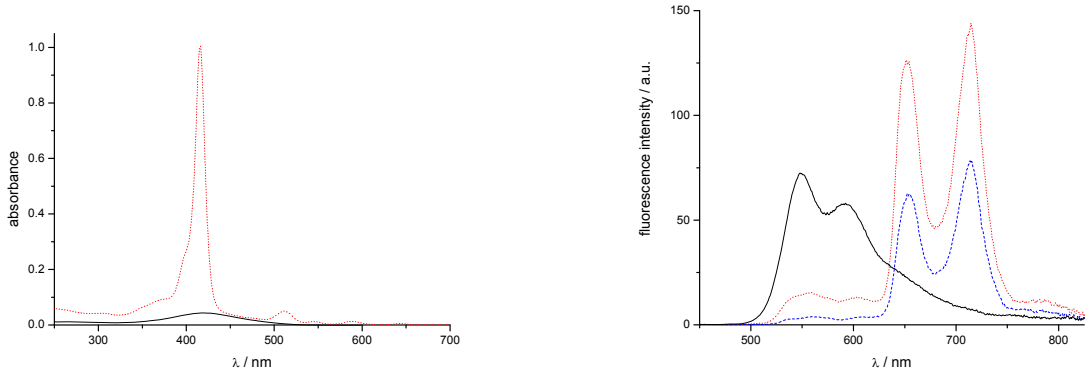

Figure 123: Titration of C[3T(Bu$_4$)–DA]$_4$ with P(Py)$_4$
concentration of the macrocycle: $c = 1.9\times10^{-7}$ M in CH_2Cl_2
left graph: absorption spectra of the pristine macrocycle solution (solid line) and after addition of 30 equivalents of **P(Py)$_4$** (dotted red line)
right graph: emission spectra of the pristine macrocycle solution (solid line) and after addition of 270 (dotted red line) and 850 (dashed blue line) equivalents of **P(Py)$_4$**

6.2.4 Addition of Viologene Derivatives to Oligothienyl Macrocycles

As the recognition of the electron acceptor C_{60} by **C[3T(Bu$_4$)–DA]$_3$** still gives room for improvement, a better acceptor seemed reasonable. Cations not only are acceptors, but they also provide a positive charge and can exhibit cation–π interactions which are typically stronger than π–π interactions.[205] In particular, viologene derivatives are often well recognised by aromatic moieties. An important example for the application of cations in molecular recognition is the work of *Stoddart and coworkers*, who utilise viologene systems to build rotaxanes and catenanes for molecular devices (cf. section 6.1).[206]

Semi-empiric calculations with viologene on an AM1 level[204] indeed predicted an attraction towards oligothienylene–diethynylene macrocycles. Interestingly, in the energy-minimised structure the viologene is not positioned over an oligothienyl moiety, as expected, but ends up with a pyridyl ring parallel to a diethynyl bridge of the macrocycle.

The transfer of this result to a fluorescence-quenching experiment brought up the problem of solubility of the viologene compounds: In general, viologene salts are well soluble in polar solvents like water or acetonitrile, but not in solvents like dichloromethane which are, on the other hand, perfectly suitable for the oligothienyl macrocycles. Thus, a solvent mixture of dichloromethane and acetonitrile (3:2) was employed and two viologene salts were chosen based on criteria regarding solubility and possible interactions: 1,1'-bis(6-thiophene-3-yl-hexyl)-[4,4']bipyridinyl hexafluoro-phosphate **V(Hex–T)$_2$**, comprising long thiophene-modified alkyl side chains which could further interact with the macrocycles, and 1,1'-bis(perdeuteromethyl)-[4,4']bipyridinyl tosylate **VMe$_2$**, which carries only methyl substituents but contains the better soluble tosylate as the counter anion (figure 124). Each of the viologenes was added to **C[3T(Bu$_4$)–DA]$_3$** until a 100-fold excess was reached, but no change in the fluorescence curves was noticeable (figure 125).

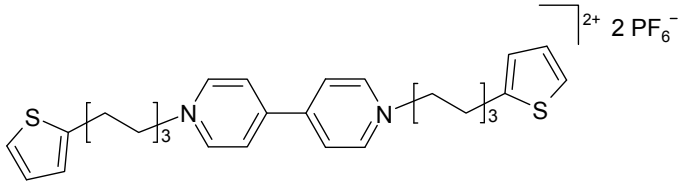

a) V(Hex–T)$_2$

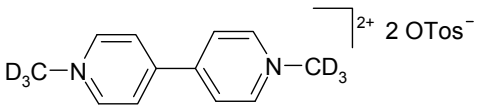

b) VMe$_2$

Figure 124: Viologene derivatives used for fluorescence quenching

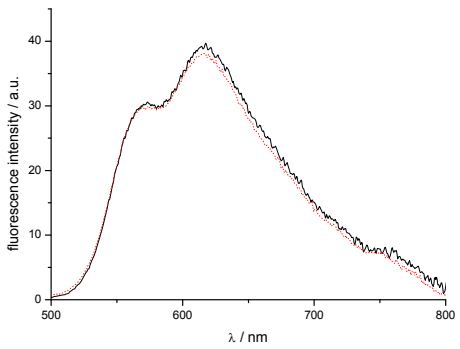

a) titration with **V(Hex–T)$_2$**

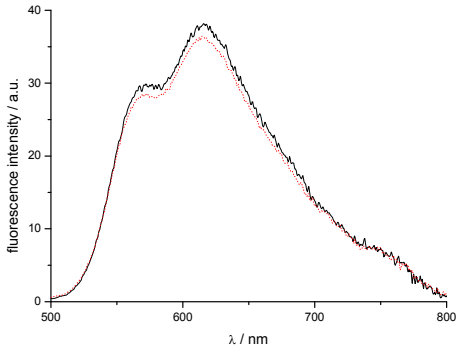

b) titration with **VMe$_2$**

Figure 125: Fluorescence titration of C[3T(Bu$_4$)–DA]$_3$ with viologene derivatives
fluorescence spectra of pristine solutions of the macrocycle (solid lines; $c = 4.1\times10^{-7}$ M in a 3:2 mixture of CH_2Cl_2:MeCN) and upon addition of 100 equivalents of the respective viologene (dotted red lines)

6.2.5 Formation of Gold Clusters

Apart from the π system, the thiophene sulphur atoms of the macrocycles are the only sites where interactions for molecular recognition are rational. However, only few examples for such coordination compounds exist.[199a] In the macrocycles, chances are higher due to multiple coordinating sites and a potentially resulting chelate effect. The affinity of sulphur to silver and gold surfaces and the application of gold in the doping of polythiophenes[207] consequently led to the idea of growing metal clusters inside the macrocycles. In this manner, the 10–20 Å diameters of the cycles would be ideally suited for the inclusion of Au_{55} aggregates. Such gold clusters had been employed before by *Konishi et al.* as templates in the formation of a hexaporphyrin cage.[208]

The most widely used method of a controlled formation of small gold clusters is the reduction of gold salts according to *Brust et al.*[209,210] There, $AuCl_4^-$ ions are first transferred to the organic phase by a phase transfer catalyst and then reduced by $NaBH_4$ in the presence of a surface complexing agent, e.g. a thiol. With this method, stable clusters of 1–3 nm diameters and a narrow size distribution can be prepared.

To determine the applicability of the idea, a reduction of $HAuCl_4 \cdot 3H_2O$ with a freshly prepared $NaBH_4$ solution was performed in a mixture of toluene and water with and without a surface complexing agent. Tetra-*n*-octylammoniumbromid was used as the phase transfer catalyst. Without surfactant, the colour of the organic phase turned from yellow to dark red immediately after addition of $NaBH_4$. Aqueous work-up after 18 h yielded a black solid which was insoluble in common organic solvents. As expected, the uncontrolled growth had led to a large cluster size. Such an aggregation was circumvented by reducing the concentration from 10^{-3} to 10^{-7} mol L^{-1} and addition of dodecanethiol as a surface-complexing agent. In this case, absorption bands were visible in the region of the typical surface plasmon bands for Au clusters of 1–2 nm size (figure 126).[210]

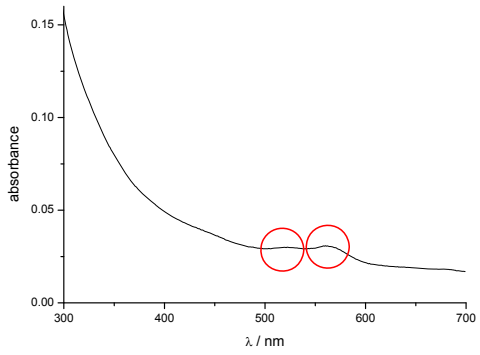

Figure 126: Absorption spectrum of the crude product of the Au^{3+} reduction in CH_2Cl_2
weak absorptions can be seen at 520 and 560 nm (red circles)

A drawback of the above preparation of Au clusters in this very low concentration range is the separation from additives like the phase transfer catalyst, which is virtually impossible. On the other hand, the small amounts of the macrocycles do not allow a preparation in higher concentrations, so that this type of recognition experiment turned out not to be feasible.

6.2.6 Addition of Melamine Compounds

2,4,6-Triamino-1,3,5-triazine (melamine) not only offers the possibility to build up π–π interactions with the oligothiophene moieties of the macrocycles, but also provides polarised N–H bonds that might develop hydrogen bonds to the thiophene sulphur atoms. Moreover, results in literature describing complexations between tetrathiafulvalene and cyclophanes with viologene moieties propose a good chance that recognition of protonated melamine might be successful.[206g]

Unprotonated melamine is insoluble in chlorinated solvents, therefore the fluorescence-quenching experiment with **C[3T(Bu$_4$)–DA]$_3$** was performed in THF. However, the result in this case was disillusioning: Even after addition of 80 equivalents of melamine, no change was noticed in the fluorescence spectra, thus no complexation seems to take place.

Protonation of melamine was tried using different methods described in literature,[211–212] but only the addition of 1.1 equivalents of $HCl_{conc.}$ to an aqueous solution at elevated temperatures, described by *Scoponi et al.*,[211c] yielded the singly protonated melamine in form of the hydrochloride. The titration of **C[3T(Bu$_4$)–DA]$_3$** with the protonated melamine required a slightly different procedure, as the salt was insoluble in THF. Thus, the melamine hydrochloride was dissolved in DMSO and added to a THF solution of the macrocycle. Thereby, the concentration of melamine hydrochloride was chosen high enough that the dilution effects for each titration step could be almost neglected (< 1 %). However, also protonation of melamine did not lead to a change in the complexation behaviour towards the macrocycle (figure 127).

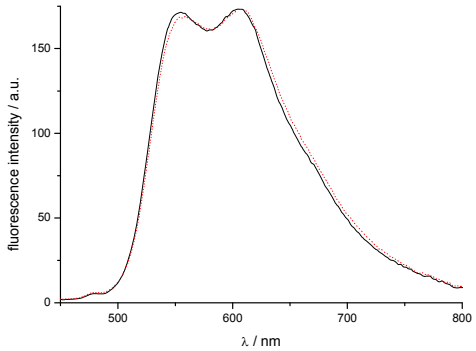

Figure 127: Fluorescence titration of C[3T(Bu$_4$)–DA]$_3$ with melamine hydrochloride
the emission intensity of the pristine solution (solid line; 2.8×10^{-7} M in THF) does not change even after addition of 164 equivalents of melamine hydrochloride (dotted red line);
the fluorescence intensity of the titrated solution was corrected by the concentration change upon addition of the melamine–hydrochloride solution.

6.2.7 Reaction of 3,4,3",4"-tetrabutylterthiophene with ferrocene

A more directed guest recognition would be the complexation of metal ions to the aromatic thiophene moieties of the macrocycles. However, due to its weak electron donor properties, thiophene is a rather bad partner for such reactions. In literature, stable thiophene coordination compounds seem to be restricted to the reaction partners Fe, Ru, Rh and Ir, especially as sandwich-like complexes.[213] E.g., by reaction of ferrocene with tetramethylthiophene and 2,5-dimethylthiophene, respectively, *Guerchais and Astruc* were able to prepare η^5-coordinated Cp–Fe–thiophene complexes.[213f] These compounds could be obtained in 52 and 21 % yield in form of their stable PF_6^- salts by reaction of the thiophene with ferrocene or $CpFe(CO)_2Cl$, respectively, in the presence of $AlCl_3$ at elevated temperatures.

Based on these reaction conditions, preparation of a metal complex was tried first with 3,3",4,4"-tetrabutylterthiophene. As a substitute for the macrocycles, this monomer should give a good indication whether a coordination of metal ions to such a moiety is practicable. Of further interest was the stoichiometry of the reaction, i.e. how many Fe(II) ions would bind to one terthiophene, and the regioselectivity. The applied reaction conditions are presented in scheme 51: Ferrocene and the terthiophene were mixed in heptane under argon atmosphere together with a small amount of water and one equivalent of $AlCl_3$ and Al each. This mixture was heated to reflux for 14 h. After washing with diethyl ether, basic conditions were established by addition of a small amount of half-concentrated ammonia. Then, one equivalent of a 40 % aqueous HBF_4 solution was added. The precipitate was separated by filtration, but neither MALDI TOF mass spectrometry nor

^{1}H NMR spectrometry showed any hints for a thiophene–Fe(II) complex. The diethyl ether washing phase contained large amounts of the starting materials ferrocene and 3,3",4,4"-tetrabutylterthiophene, of which the latter could be recovered in 27 % yield by column chromatography.

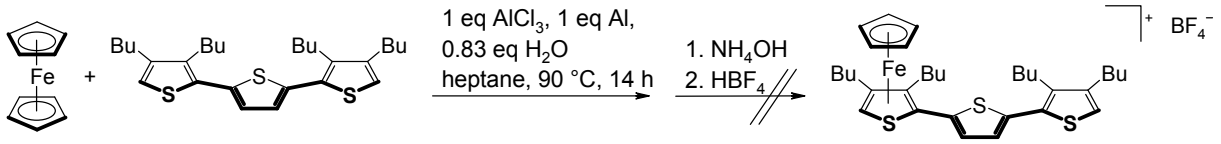

Scheme 51: Reaction scheme of the anticipated complexation of 3,4,3'',4''-tetrabutylterthiophene with ferrocene

6.3 Discussion

From a number of possible guest molecules, taken from various classes of compounds with different sizes, shapes, polarities and charges, only C_{60} showed a significant influence on the optical properties of cyclo(oligothienylene–diethynylene)s. The group of non-interacting molecules includes porphyrin, viologenes, melamine (protonated and unprotonated) and ferrocene, while for gold clusters fluorescence quenching is not a feasible method to detect interactions with the macrocycles in the available concentration range.

In the case of the porphyrin derivative, the strong absorption of the potential guest spoiled the measurements, leading to a disappearance of the emission of **C[3T(Bu$_4$)–DA]$_4$**. Thereby, Förster resonance energy transfer may have happened, but could not be distinguished from reabsorption in the solution. Thus, molecular recognition could not be determined.

With the viologenes, despite their positive charge which should allow cation–π interactions and should therefore alter the fluorescence emission, the attractive forces are too small to show an influence on the optical properties. Other viologene derivatives would probably exhibit the same behaviour, as for the experiments compounds were used that possess factors from which interactions should benefit, i.e. thiophene-containing alkyl side chains or weakly bound counter anions. The lack of spectroscopic response for melamine hydrochloride as another small and positively charged molecule supports this assumption.

In the reaction of ferrocene with a linear terthiophene, no reaction between the starting materials had taken place. Obviously, the butyl-substituted terthiophene system (and consequently, the macrocycles) seem to be sterically too demanding to allow coordination of a $CpFe^+$ fragment. Thus, coordination reactions — even with more reactive species like $CpFe(CO)_2Cl$ — seem not to be suited for the use in molecular sensing applications with cyclothiophenes.

C_{60} was considered to possess the ideal size and optimal electronic properties for interaction with the thiophene macrocycles. However, even with C_{60} these interactions are rather weak compared to other complexations reported in literature: principally, a complete fluorescence quenching is possible already with an equimolar amount of guest molecules. (In such cases, binding constants well above the maximum of $3.4–4.7\times10^3$ L mol^{-1} measured here are effective.) Nevertheless, some distinct relations can be derived from the results: With increasing ring size of the macrocycles, the ability for binding a guest drops off; from a 20 % reduction of fluorescence intensity in the case of **C[3T(Bu$_4$)–DA]$_3$** to zero in the case of **C[3T(Bu$_4$)–DA]$_5$** (upon addition of 100 equivalents of C_{60}). This finding suggests that the binding of C_{60} in solution is not solely based on a π–π interaction

with the π system of the oligothienylene moieties, as otherwise a significant interaction would also be expected for larger macrocycles. Instead, the cavity (ring size) seems to play the major role. Regarding the overlap of the van der Waals radii in molecular models,[204] the size is slightly too small for **C[5T(Bu$_6$)–DA]$_2$** (showing a 13 % fluorescence reduction), while for the "winner" **C[3T(Bu$_4$)–DA]$_3$** (20 % reduction) it is already a little too large for a perfect fit of C_{60}. Although due to the extremely weak emission of **C[3T(Bu$_4$)–DA]$_2$** a statement cannot be sustained by experimental results, it can be deducted that this macrocycle is too small for an interaction with the fullerene.

6.4 Experimental Section

The influence of potential guest molecules on the physicochemical properties of oligothienyl macrocycles was determined by fluorescence quenching:

In 25 mL optically pure dichloromethane (Aldrich) or in a 3:2 mixture of dichloromethane and acetonitrile, approx. 10–20 μg of the macrocycle were dissolved to obtain a concentration in the range 10^{-7}–10^{-6} mol L^{-1} and an optical density of approximately 0.04 cm^{-1} (solution A). To a part of this solution in a quartz cuvette, the guest substance was added in a 100- or 1000-fold excess (solution B). This allowed the addition of a total of 0.5 mL of Solution B to 2.5 mL of solution A in steps of 10–100 μL, while a constant concentration of the macrocycle is maintained. After each addition step, a fluorescence spectrum — for which the longest-wavelength absorption maximum of the macrocycle was used as excitation wavelength — was recorded with a PerkinElmer LS 50B luminescence spectrometer in a 90° setup. All spectra were corrected automatically. Changes in the fluorescence intensity were determined using the ratios of the curve integrals.

7 Summary

7.1 Summary of the Results

Fully conjugated macrocycles based on oligothienyl monomers (figure 128) constitute a new class of materials with exciting prospects: Since they do not possess end groups that interfere with the π system of the conjugated chain, like it is possible for oligo- and polymers, they might be considered "idealised polymers". Their cyclic nature furthermore defines intriguing new electronic properties different to linear oligomers, and their tendency to self-assemble on ordered surfaces is a good basis for an application in molecular electronics.

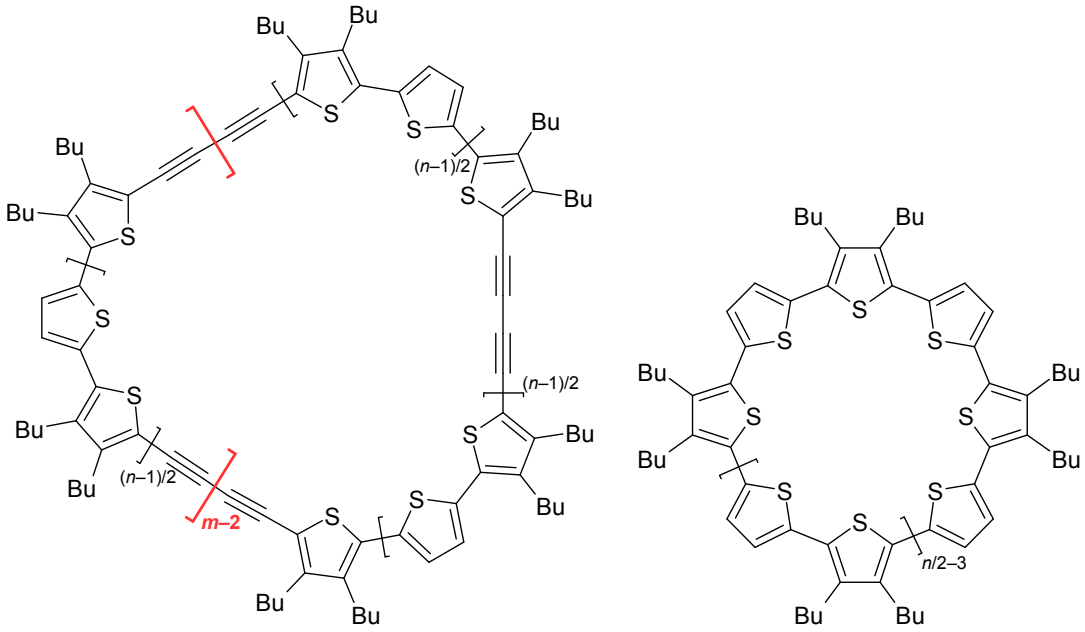

a) C[*n*T(Bu$_{n+1}$)–DA]$_m$ **b) C[*n*]T**

Figure 128: Fully conjugated macrocycles comprising oligothiophene units

The work presented in this thesis can be divided into three main parts: First, the synthesis of a new, aryl-substituted oligothiophene macrocycle by using the so-called "metal template" strategy. Second, the physicochemical characterisation of oligothiophene macrocycles with different monomer units, especially by UV/Vis and fluorescence spectroscopy as well as by electrochemistry. And finally, evaluation of the molecular recognition capabilities for these macrocycles in solution.

For the synthesis of a new macrocycle, a substitution pattern with phenyl moieties in the 3,4,3",4"-positions of a terthiophene was chosen in accordance to existing butyl-substituted cycles. Hence, synthesis principally was followed in analogy to the latter. In one of the first steps,

3,4-diphenylthiophene **T(Ph$_2$)** was prepared in the form of crystals suitable for an X-ray structure analysis, from which interesting aspects regarding intermolecular interactions of the aryl moieties could be determined. One deviation to the route for the butyl analogues was the application of the Negishi instead of the Kumada coupling for building the terthiophene **3T(Ph$_4$)**, thus avoiding an extensive separation of mono- and dibrominated **T(Ph$_2$)** for the coupling. Another deviation resulted from the lower reactivity of **3T(Ph$_4$)** concerning iodination via mercuration, which could only be performed quantitatively by using the more reactive Hg(II) salt of pivalylic acid instead of Hg(OAc)$_2$. While the following reactions up to the protected precursor **TMSA–3T(Ph$_4$)–TMSA** worked well, more serious problems finally occurred at the stage of the Pt(II) macrocycle **C[Pt–A–3T(Ph$_4$)–A]$_2$** (scheme 52), which had been available in good yields of almost 90 %: Similar to the butyl-substituted analogue, the compound is extremely insoluble and was impossible to characterise other than by mass spectrometry. The lack of solubility is probably the reason why reductive elimination to one distinct Pt(II)-free product failed. Instead, a mixture of fully conjugated macrocycles **C[3T(Ph$_4$)–DA]$_m$** of different sizes was obtained, which could not be separated from each other and from remaining Pt fragments. A project of improving the solubility of the macrocycles by attaching long alkyl chains to the aryl substituents was stopped at the terthiophene stage, since the reactivity and the yields had dropped significantly due to the sterical demand of the *p*-dodecylphenyl moieties.

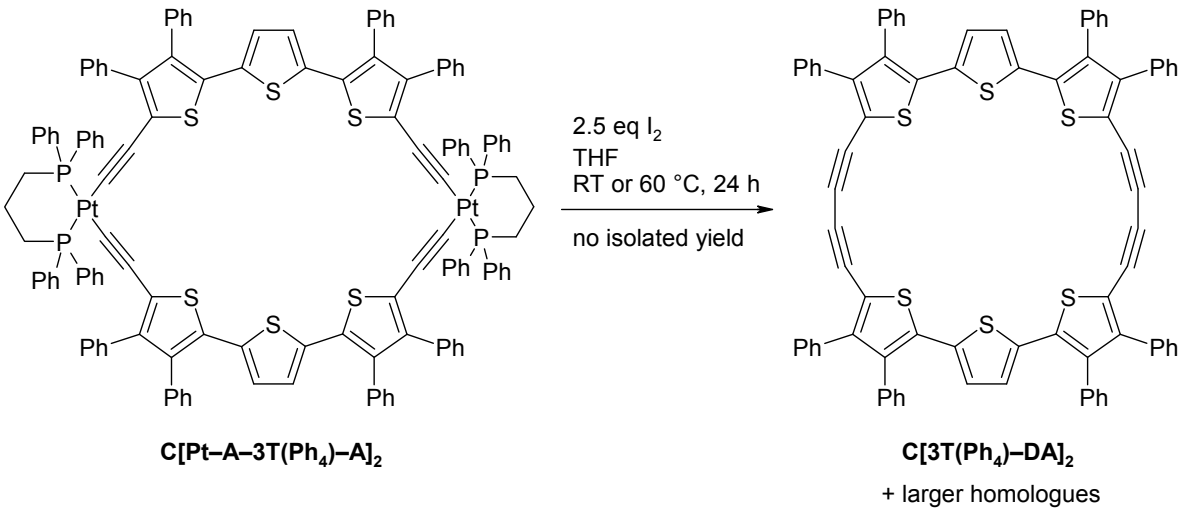

Scheme 52: Preparation of fully conjugated, phenyl-substituted oligothiophene macrocycles by oxidatively induced reductive elimination

Semi-empiric calculations showed that the cyclic dimer, as the major product of the metal template route, has a ring strain similar to cyclopropane of about 100 kJ mol^{-1}, what explains why it could not be synthesised at all with the formerly used statistical cyclisation method.

The electronic nature of the **C[*n*T(Bu$_{n+1}$)–DA]$_m$** and **C[*n*]T** macrocycles is well reflected in their physicochemical properties. Absorption spectra generally show one broad peak between 400 and 445 nm (figure 129), while emission and excitation spectra are more structured, indicative of the expected chinoidal structure of the excited state.

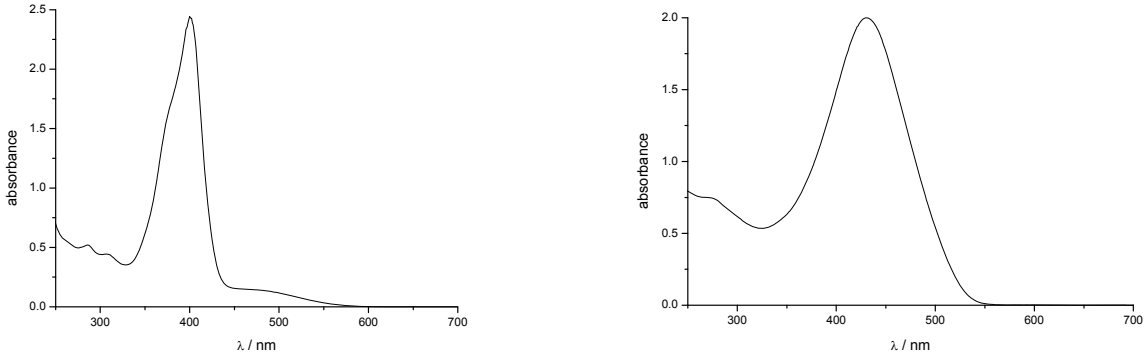

Figure 129: Absorption spectra of two members of the C[3T(Bu$_4$)–DA]$_m$ series
left graph: absorption spectrum of **C[3T(Bu$_4$)–DA]$_2$**
right graph: absorption spectrum of **C[3T(Bu$_4$)–DA]$_5$** (representative for the series)

Differences could be shown by comparing macrocycles of the same size, but with a varying ratio of thienyl to diethynyl units: As the (usually twisted) oligothienyl units require a somewhat stronger rearrangement to reach a chinoidal state, the Stokes shift becomes larger for cycles with a higher thiophene quota. Absorption and emission maxima follow a trend which is known from the linear oligothienyl pendants, where both properties asymptotically approach a limit value which remains constant even for a further extension of the π system (figure 130).

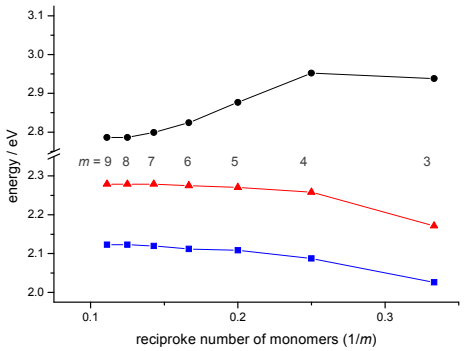

Figure 130: Plot of absorption/emission maxima vs. reciprocal number of 3T(Bu$_4$)–DA units in the C[3T(Bu$_4$)–DA]$_m$ series (m = 3–9)
black line (●): absorption maxima ($S_0 \rightarrow S_2$ transition)
red (▲) and blue (■) line: first and second emission maxima (vibronic splitting)

However, the linear compounds show an absorption maximum at higher wavelengths, approximately at the value of a macrocycle with twice as much monomer units, what corresponds well to theoretical calculations on the basis of a Frenkel exciton model. This model also predicted that the LUMO energy for the cycles remains constant and that the first electronic transition is forbidden, which was indeed found in the absorption spectra of the smallest macrocycles (cf. left graph of figure 129). There, the absorption band was much smaller and a second very weak band at ca. 490 nm was seen, corresponding to the first transition. Since the transition is already located only on half the cycle, the metal centres in the platinacycles rather expand this conjugation than interrupt it, hence the absorption maximum is red-shifted for **C[Pt–A–3T(Bu$_4$)–A]$_2$**. Further insight into the conjugated macrocycles was gained by special spectroscopic techniques. Although fluorescence correlation spectrocopy (FCS) failed due to rapid photobleaching of the compounds, low temperature measurements resulted in more structured spectra which support the picture of a chinoidal excited state.

Electrochemical characterisation by cyclic voltammetry showed that the **C[3T(Ph$_4$)–DA]$_m$** macrocycles are rather instable upon oxidation, as the first oxidation waves shift to higher potentials and become more and more irreversible with growing ring size (figure 131). Follow-up oxidations occurred in several steps so that a strong electronic communication between the terthiophene moieties seems to exist.

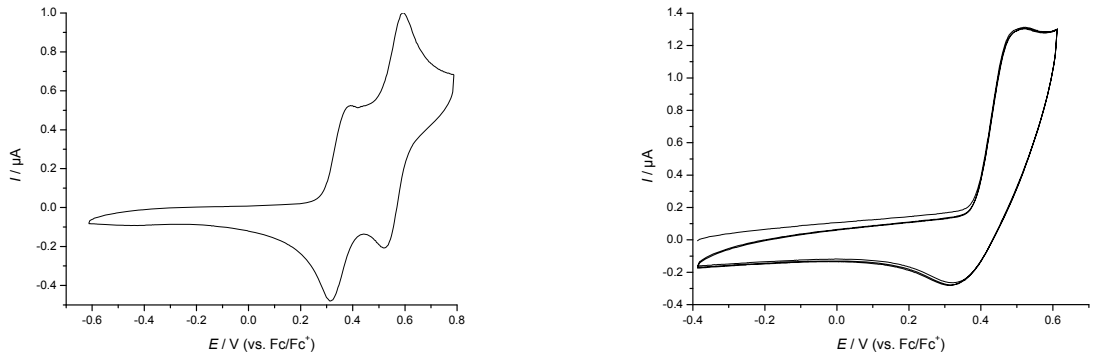

Figure 131: Cyclic voltammograms of two members of the C[3T(Bu$_4$)–DA]$_m$ series
left graph: first and second (reversible) oxidation waves of **C[3T(Bu$_4$)–DA]$_2$**
right graph: first (only partially reversible) oxidation wave of **C[3T(Bu$_4$)–DA]$_5$**

The irreversibility of the first oxidation also for **C[Pt–A–3T(Ph$_4$)–A]$_2$** was utilised for an electrochemical elimination of the Pt(II) corners to obtain the fully conjugated **C[3T(Ph$_4$)–DA]$_2$**. Mass spectrometry indicated that the elimination proceeds in a step-wise mechanism and that, in contrast to the iodine-induced elimination, no larger homologues were formed. However, work-up

was again not successful due to solubility problems. A comparison of differently substituted Pt(II)–oligothienyl macrocycles furthermore revealed that oxidation of the butyl-substituted species **C[Pt–A–3T(Bu$_4$)–A]$_2$** takes place at a potential which is ca. 0.2 V lower than that for the other compounds. Although the reason for this exceptional behaviour is not quite clear, this finding may explain why oxidatively induced metal elimination proceeded smoothly only for this platina-macrocycle.

In terms of molecular recognition, oligothiophene macrocycles only provide weak possibilities for binding guests. From a number of potential guests with different modes of interaction, only C_{60} with its electron-deficient surface managed to significantly quench the fluorescence of the macrocycles (figure 132). Even here, the interaction was strongly dependent on the cavity size: The highest binding constant of ca. 5×10^3 L mol^{-1} was observed with **C[3T(Bu$_4$)–DA]$_3$**, while already **C[3T(Bu$_4$)–DA]$_5$** showed no interaction at all.

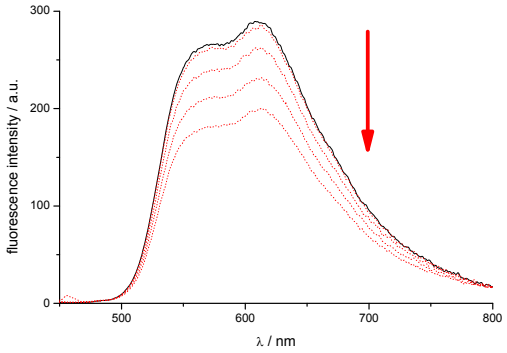

Figure 132: Fluorescence titration of C[3T(Bu$_4$)–DA]$_3$ with up to 150 equivalents of C_{60}

Based on these results, a template synthesis of the macrocycles in presence of a suitable guest, like anticipated in the introduction to this thesis, seems unrealistic, so that the metal template route still is the most efficient method of synthesis. As a further conclusion, any introduction of functionality can best be done at the substituents. Future efforts on the topic of oligothiophene macrocycles should therefore concentrate on substitution patterns which on one hand provide a good solubility, possibly a symmetrical *N*,*N*-dimethyleneamine bridge with an alkyl chain of medium size (like hexyl) attached to the nitrogen atom, and on the other hand possess an (occasionally protected) functional group that allows covalent linkage to other molecules, e.g. to a C_{60} derivative or to a functionalised surface.

7.2 Zusammenfassung der Ergebnisse

Vollständig konjugierte Makrocyclen aus Oligothiophen-Monomeren (Abbildung 133) bilden eine neue Substanzklasse mit fesselnden Perspektiven: Da sie keine Endgruppen besitzen, die störend mit dem π-System der konjugierten Kette wechselwirken – wie es für Oligo- und Polymere oft der Fall ist –, können sie als „idealisierte Polymere“ betrachtet werden. Ihr cyclischer Aufbau hebt sie mit neuen und einzigartigen Eigenschaften von den linearen Oligomeren ab, und ihre Tendenz zur Selbstorganisation auf strukturierten Oberflächen bietet eine solide Basis für Anwendungen in der molekularen Elektronik.

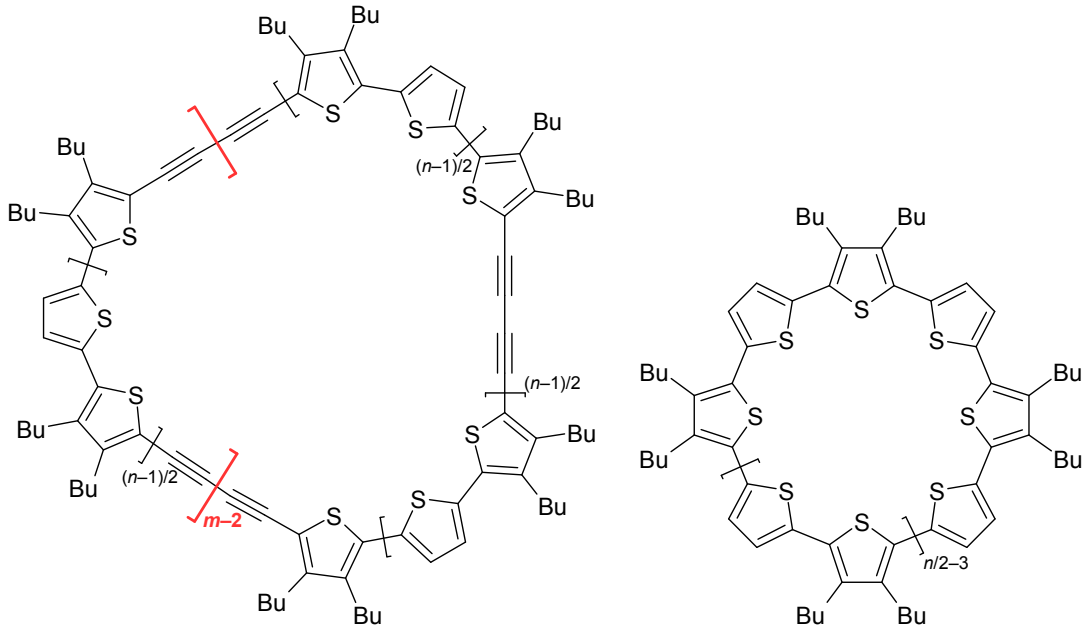

a) **C[*n*T(Bu$_{n+1}$)–DA]$_m$** **b)** **C[*n*]T**

Abbildung 133: Vollständig konjugierte Oligothiophen-Makrocyclen

Die vorliegende Arbeit gliedert sich in drei Hauptteile: Erstens die Synthese eines neuen, phenyl-substituierten Makrocyclus mittels der so genannten „Metall-Templat“-Methode; zweitens die physikalisch-chemische Charakterisierung von Oligothiophen-Makrocyclen mit unterschiedlichen Monomereinheiten, insbesondere durch UV/Vis- und Fluoreszenzspektroskopie sowie durch Cyclovoltammetrie; und schließlich Untersuchungen über die molekulare Erkennung dieser Cyclen in Lösung.

Für die Synthese eines neuen Makrocyclus wurde, entsprechend bereits bestehenden butyl-substituierten Cyclen, ein Substitutionsmuster am Terthiophen mit Phenylgruppen in den 3,4,3",4"-Positionen gewählt. Die Synthese erfolgte daher auch prinzipiell in Analogie zur Herstellung der Cyclen mit Butylresten. Einer der ersten Schritte umfasste die Darstellung von

3,4-Diphenylthiophen **T(Ph$_2$)**, welches in Form von Kristallen anfiel, die für eine Röngtenstruktur-analyse geeignet waren. Diese erlaubte interessante Rückschlüsse auf zwischenmolekulare Wechselwirkungen der Arylgruppen. Im weiteren Verlauf wurde, abweichend vom Syntheseweg für die Butyl-Analoga, die Negishi- anstelle der Kumada-Kupplung zur Darstellung des Terthiophens **3T(Ph$_4$)** eingesetzt. So konnte eine aufwändige Trennung von mono- und dibromiertem **T(Ph$_2$)** als Edukt für die Kupplung vermieden werden. Eine weitere Abweichung ergab sich durch die geringere Reaktivität von **3T(Ph$_4$)** hinsichtlich der Mercurierung/Iodierung, die erst nach Austausch von $Hg(OAc)_2$ durch das reaktivere Hg(II)-Pivalylsäuresalz quantitativ erfolgte. Während die weiteren Reaktionsschritte bis hin zum geschützten Precursor **TMSA–3T(Ph$_4$)–TMSA** problemlos verliefen, stellten sich schließlich auf der Stufe des Platinacyclus **C[Pt–A–3T(Ph$_4$)–A]$_2$** (Schema 53), welcher in fast 90%-iger Ausbeute erhalten wurde, schwerwiegende Probleme ein: Wie das butylsubstituierte Pendant ist auch diese Verbindung äußerst schwerlöslich und konnte lediglich durch Massenspektrometrie charakterisiert werden. Diese mangelnde Löslichkeit war vermutlich auch ausschlaggebend dafür, dass die reduktive Eliminierung zu einem einzigen, definierten Pt(II)-freien Produkt fehlschlug. Stattdessen entstand eine Mischung aus vollständig konjugierten Makrocyclen mit verschiedenen Größen der Serie **C[3T(Ph$_4$)–DA]$_m$**, die weder voneinander noch von verbleibenden Platinfragmenten abgetrennt werden konnten. Ein Ansatz, die Löslichkeit der Makrocyclen durch Verwendung von Aryl-Substituenten mit längeren Alkylresten zu verbessern, wurde auf der Stufe des entsprechenden Terthiophens eingestellt, da sowohl die Reaktivität als auch die Ausbeuten aufgrund des sterischen Anspruchs der *p*-Dodecylphenylgruppen drastisch gesunken waren.

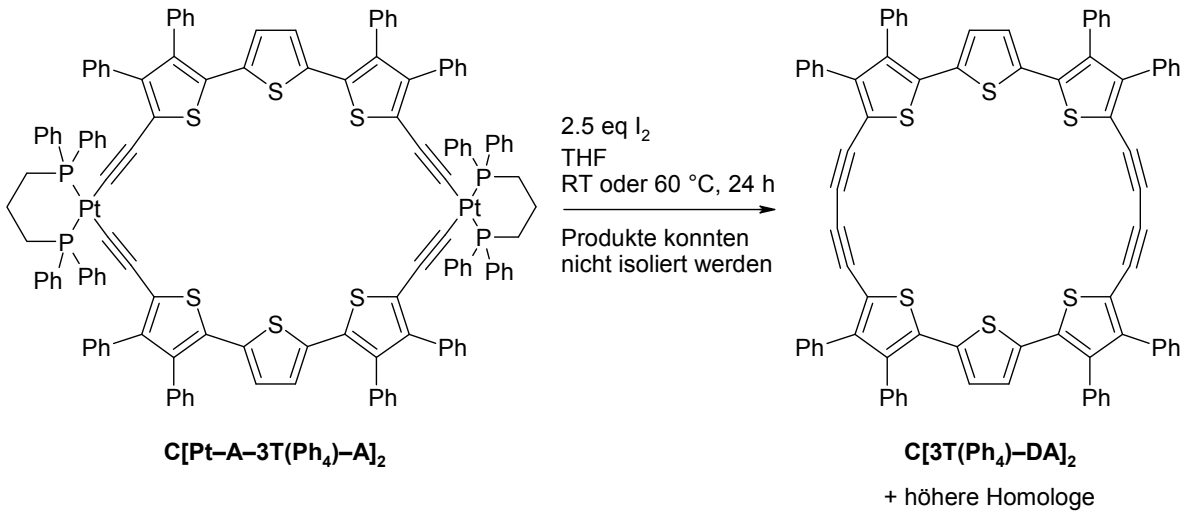

Schema 53: Darstellung vollständig konjugierter, phenylsubstituierter Makrocyclen durch oxidativ induzierte reduktive Eliminierung

Semi-empirische Rechnungen zeigten, dass das cyclische Dimer (als Hauptprodukt der Metall-Templat-Synthese) eine dem Cyclopropan vergleichbare Ringspannung von etwa 100 kJ mol^{-1} besitzt, was erklärt, warum es mit der früher verwendeten statistischen Cyclisierungsmethode überhaupt nicht dargestellt werden konnte.

Die elektronische Beschaffenheit der Makrocyclen aus den Familien **C[*n*T(Bu$_{n+1}$)–DA]$_m$** und **C[*n*]T** wird durch die physikalisch-chemischen Eigenschaften recht gut widergespiegelt. Die Absorptionsspektren zeigen üblicherweise eine breite Bande mit einem Maximum zwischen 400 und 450 nm (Abbildung 134), während die Emissions- und Anregungsspektren stärker strukturiert sind, was wie erwartet auf einen chinoiden Anregungszustand hindeutet.

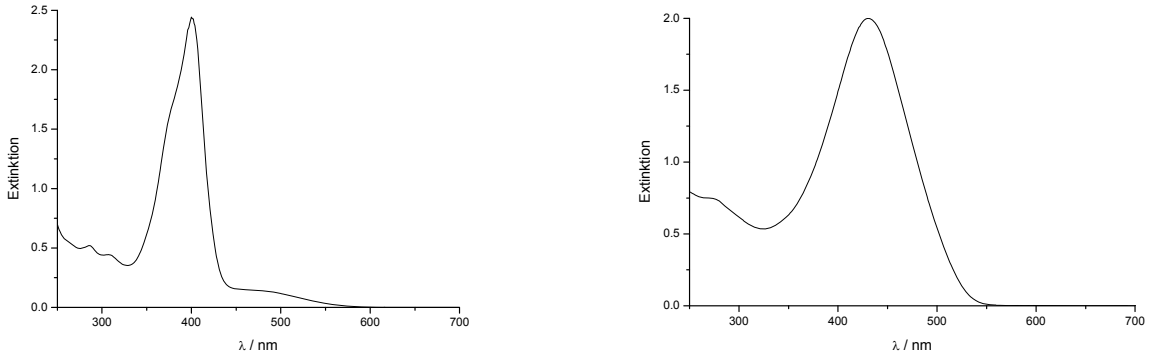

Abbildung 134: Absorptionsspektren zweier Makrocyclen der C[3T(Bu$_4$)–DA]$_m$-Serie
linkes Diagramm: Absorptionsspektrum von **C[3T(Bu$_4$)–DA]$_2$**
rechtes Diagramm: Absorptionsspektrum von **C[3T(Bu$_4$)–DA]$_5$** (repräsentativ für die gesamte Serie)

Verschiedenheiten zeigten sich im Vergleich von Makrocyclen mit gleicher Größe aber unterschiedlichem Verhältnis von Thienyl- zu Diethinyleinheiten: Da die normalerweise gegeneinander verdrehten Thienyleinheiten eine größere Konformationsänderung zum Erreichen eines chinoiden Zustands benötigen, ist der Stokes-Shift für Cyclen mit höherem Thiophenanteil größer. Sowohl Absorption als auch Emission folgen dabei einem Trend, der bereits von den linearen Oligothiophenen her bekannt ist, wonach sich beide Eigenschaften asymptotisch einem Grenzwert nähern, der auch bei weiterer Ausdehnung des π-Systems konstant bleibt (Abbildung 135).

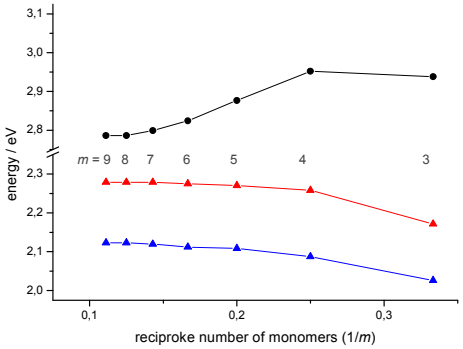

Abbildung 135: Auftragung der Absorptions- und Emissionsmaxima gegen die reziproke Zahl an 3T(Bu_4)–DA-Einheiten in der C[3T(Bu_4)–DA]$_m$-Serie (m = 3–9)
schwarze Linie (●): Absorptionsmaxima (Übergang $S_0 \rightarrow S_2$)
rote (▲) and blaue (■) Linie: erste und zweite Emissionsmaxima (vibronisch aufgespalten)

Im Vergleich zu den Cyclen liegen die Absorptionsmaxima der linearen Oligothiophene allerdings bei deutlich höheren Wellenlängen, in etwa bei den Werten für Makrocyclen mit der doppelten Anzahl an Monomereinheiten, was hervorragend mit Berechnungen auf Basis eines Frenkel-Exciton-Modells übereinstimmt. Dieses Modell sagt weiterhin ein konstantes Niveau für die LUMO-Energie der Cyclen sowie ein Verbot des ersten elektronischen Übergangs voraus, was auch tatsächlich aus den Absorptionsspektren der kleinsten Makrocyclen ersichtlich ist (vgl. linkes Diagramm in Abbildung 134). In diesen ist die Absorptionsbande deutlich schmaler, wodurch eine sehr schwache weitere Bande bei ca. 490 nm sichtbar ist, die dem ersten elektronischen Übergang entspricht. Da dieser Übergang nur auf einer Hälfte des Makrocyclus lokalisiert ist, können in den Platinacyclen die Metallzentren die Konjugation erweitern statt sie zu unterbrechen, weshalb das Absorptionsmaximum von **C[Pt–A–3T(Bu_4)–A]$_2$** zu längeren Wellenlängen verschoben ist. Weitere Einblicke in die Struktur der konjugierten Makrocyclen wurden durch spezielle Spektroskopietechniken erhalten. Obwohl mit Fluoreszenz-Korrelations-Spektroskopie (FCS) wegen des raschen Ausbleichens der Verbindungen keine verwertbaren Ergebnisse erzielt werden konnten, unterstützten die durch Tieftemperaturspektroskopie erhaltenen, stärker strukturierten Spektren die Annahme eines chinoiden Anregungszustands.

Die elektrochemische Charakterisierung mittels Cyclovoltammetrie zeigte eine deutliche Instabilität gegenüber Oxidation für die **C[3T(Bu_4)–DA]$_m$**-Serie, da sich die erste Oxidationswelle mit zunehmender Ringgröße zu höheren Potenzialen verschob und zunehmend irreversibel wurde (Abbildung 136). Weitere Oxidationen erfolgten in mehreren Schritten, was auf eine starke elektronische Verbindung zwischen den Terthiopheneinheiten hinweist.

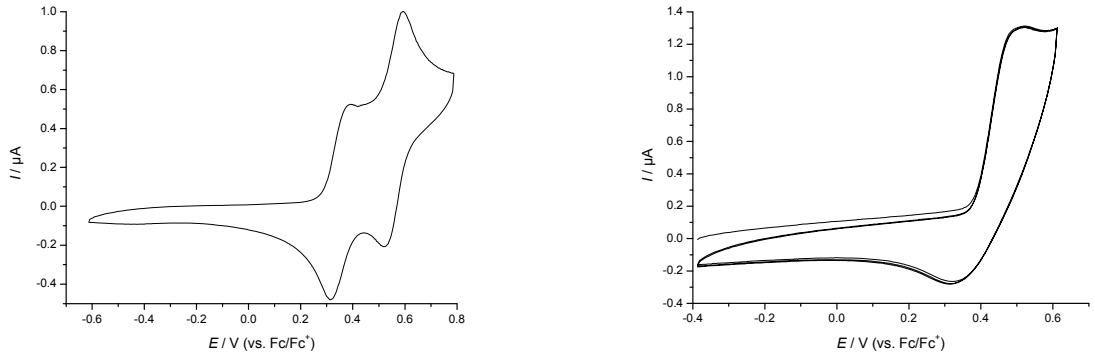

Abbildung 136: Cyclovoltammogramme zweier Cyclen der C[3T(Bu$_4$)–DA]$_m$-Serie
linkes Diagramm: erste und zweite (reversible) Oxidationswelle von **C[3T(Bu$_4$)–DA]$_2$**
rechtes Diagramm: erste (nur partiell reversible) Oxidationswelle von **C[3T(Bu$_4$)–DA]$_5$**

Der irreversible Charakter der Erstoxidation, welcher ebenfalls für den Platinacyclus **C[Pt–A–3T(Ph$_4$)–A]$_2$** zu beobachten war, wurde ausgenutzt, um durch elektrochemische Elimination der Pt(II)-Ecken den vollständig konjugierten Cyclus **C[3T(Ph$_4$)–DA]$_2$** darzustellen. Massenspektrometrische Messungen lassen einen schrittweisen Prozess annehmen; zudem konnten im Gegensatz zu den durch Iod induzierten Eliminierungsreaktionen keine Verunreinigungen durch höhere Homologe festgestellt werden. Dennoch scheiterte die Aufarbeitung erneut an Löslichkeitsproblemen. Ein Vergleich verschieden substituierter Pt(II)-Oligothienyl-Makrocyclen zeigte, dass die Erstoxidation der butyl-substituierten Spezies **C[Pt–A–3T(Bu$_4$)–A]$_2$** bei einem um 0.2 V niedrigeren Potenzial als bei den restlichen Verbindungen erfolgte. Obwohl die Ursache des außergewöhnlichen Verhaltens nicht ganz klar ist, erklärt dieser Befund möglicherweise, warum die oxidativ induzierte Metall-Eliminierung bislang nur für diesen einen Platinacyclus glatt ablief.

In Bezug auf die molekulare Erkennung boten die Oligothiophen-Makrocyclen eine nur schwache Leistung bei der Komplexierung von Gastmolekülen. Aus einer Reihe von potenziellen Gästen, mit verschiedenen Möglichkeiten zur Wechselwirkung, konnte lediglich C_{60} mit seiner elektronenarmen Oberfläche die Fluoreszenzintensität der Makrocyclen bemerkenswert reduzieren (Abbildung 137). Selbst dabei war der Effekt noch stark vom Durchmesser der Cyclen abhängig: Die höchste Bindungskonstante von ca. 5×10^3 L mol^{-1} erzielte **C[3T(Bu$_4$)–DA]$_3$**, während bereits das Pentamer **C[3T(Bu$_4$)–DA]$_5$** keinerlei Wechselwirkung mehr zeigte.

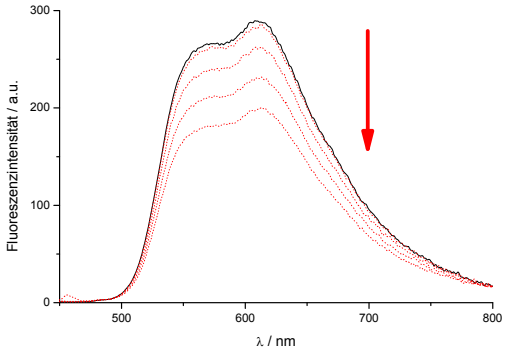

Abbildung 137: Fluoreszenztitration von C[3T(Bu_4)–DA]$_3$ mit bis zu 150 Äquivalenten C_{60}

Basierend auf diesen Ergebnissen erscheint eine Templatsynthese der Makrocyclen in Gegenwart von geeigneten Gästen, wie sie in der Einleitung zu dieser Arbeit angestrebt wurde, unrealistisch, so dass die Metall-Templat-Strategie weiterhin den effizientesten Syntheseweg darstellt. Zudem folgt daraus, dass eine Einführung von Funktionalität am besten an den Substituenten geschieht. Zukünftige Arbeiten auf dem Gebiet der Oligothiophen-Makrocyclen sollten daher den Fokus auf Substitutionsmustern haben, welche zu einen eine gute Löslichkeit gewährleisten können – möglicherweise eine symmetrische *N*,*N*-Dimethylenamin-Brücke mit einem Alkylrest mittlerer Länge (z. B. Hexyl) am Stickstoffatom –, und zum anderen eine (zunächst geschützte) funktionelle Gruppe beinhalten, die eine kovalente Anknüpfung an andere Moleküle wie beispielsweise C_{60}-Derivate oder funktionalisierte Oberflächen ermöglicht.

8 Literature References

To provide a good readability, references are numbered throughout the whole document and divided by the main sections (with sections 2 and 2.4, due to their large number of references, being further divided). Therefore, identical references may be mentioned several times if they appear in different sections. If possible, line breaks are arranged in a way that the details about the journal remain within one line.

Section 0 (Conventions and Abbreviations)

[1] A good summary can be found under the entry "dash" at the free encyclopedia Wikipedia, http://en.wikipedia.org/wiki/Dash.

Section 1 (Preface)

[2] a) A. Gesquière, P. Jonkheijm, A. P. H. J. Schenning, E. Mena-Osteritz, P. Bäuerle, S. De Feyter, F. C. De Schryver, E. W Meijer, *J. Mater. Chem.* **2003**, *13*, 2164–2167;
b) E. Mena-Osteritz, *Adv. Mater.* **2002**, *14*, 609–616;
c) E. Mena-Osteritz, A. Meyer, B. M. W. Langeveld-Voss, R. A. J. Janssen, E. W. Meijer, P. Bäuerle, *Angew. Chem.* **2000**, *112*, 2792–2796; *Angew. Chem. Int. Ed.* **2000**, *39*, 2680–2684;
d) R. Azumi, G. Götz, T. Debaerdemaeker, P. Bäuerle, *Chem. Eur. J.* **2000**, *6*, 735–744.

[3] further recent examples are:
a) L. Jiang, R. C. Hughes, D. Y. Sasaki, *Chem. Commun.* **2004**, 1028–1029;
b) P. Samori, V. Francke, V. Enkelmann, K. Müllen, J. P. Rabe, *Chem. Mater.* **2003**, *15*, 1032–1039;
c) F.-R. F. Fan, J. Yang, L. Cai, D. W. Price Jr., S. M. Dirk, D. V. Kosynkin, Y. Yao, A. M. Rawlett, J. M. Tour, A. J. Bard, *J. Am. Chem. Soc.* **2002**, *124*, 5550–5560.

[4] a) U. Mitschke, P. Bäuerle, *J. Chem. Soc. Perkin Trans. 1* **2001**, 740–753;
b) J. Krömer, P. Bäuerle, *Tetrahedron* **2001**, *57*, 3785–3794;
c) P. Bäuerle, *Oligothiophenes* in *Electronic Materials: The Oligomer Approach* (Eds.: K. Müllen, G. Wegner), Wiley–VCH, Weinheim, **1999**, pp. 105–197.

[5] further recent examples are:
a) M.-H. Yoon, S. A. DiBenedetto, A. Facchetti, T. J. Marks, *J. Am. Chem. Soc.* **2005**, *127*, 1348–1349;
b) A. R. Murphy, J. M. J. Fréchet, P. Chang, J. Lee, V. Subramanian, *J. Am. Chem. Soc.* **2004**, *126*, 1596–1597;
c) M. Melucci, G. Barbarella, M. Zambianchi, P. Di Pietro, A. Bongini, *J. Org. Chem.* **2004**, *69*, 4821–4828;
d) A. Facchetti, M. Mushrush, M.-H. Yoon, G. R. Hutchinson, M. A. Ratner, T. J. Marks, *J. Am. Chem. Soc.* **2004**, *126*, 13859–13874;
e) A. Facchetti, M.-H. Yoon, C. L. Stern, G. R. Hutchinson, M. A. Ratner, T. J. Marks, *J. Am. Chem. Soc.* **2004**, *126*, 13480–13501;

f) J. Casado, T. M. Pappenfus, L. L. Miller, K. R. Mann, E. Ortí, P. M. Viruela, R. Pou-Amérigo, V. Hernández, J. T. López Navarrete, *J. Am. Chem. Soc.* **2003**, *125*, 2524–2534;
g) T. M. Pappenfus, M. W. Burand, D. E. Janzen, K. R. Mann, *Org. Lett.* **2003**, *5*, 1535–1538;
h) A. Wakamiya, D. Yamazaki, T. Nishinaga, T. Kitagawa, K. Komatsu, *J. Org. Chem.* **2003**, *68*, 8305–8314;
i) T. Izumi, S. Kobashi, K. Takimiya, Y. Aso, T. Otsubo, *J. Am. Chem. Soc.* **2003**, *125*, 5286–5287.

[6] a) G. Fuhrmann, PhD thesis, University of Ulm, **2006**;
b) G. Fuhrmann, T. Debaerdemaeker, P. Bäuerle, *Chem. Commun.* **2003**, 948–949;
c) M. Ammann, M. Enßle, G. Fuhrmann, A. Kaiser, P. Kilickiran, E. Mena-Osteritz, P. Bäuerle, *Polymer Preprints* **2003**, *44*, 379–380;
d) P. Bäuerle, E. Mena-Osteritz, G. Fuhrmann, A. Kaiser, M. Ammann, *Polym. Mater. Sci. Eng.* **2002**, *86*, 34;
e) E. Mena-Osteritz, P. Bäuerle, *Adv. Mater.* **2001**, *13*, 243–246;
f) G. Fuhrmann, J. Krömer, P. Bäuerle, *Synth. Met.* **2001**, *119*, 125–126;
g) J. Krömer, I. Rios-Carreras, G. Fuhrmann, C. Musch, M. Wunderlin, T. Debaerdemaeker, E. Mena-Osteritz, P. Bäuerle, *Angew. Chem.* **2000**, *112*, 3623–3628; *Angew. Chem. Int. Ed.* **2000**, *39*, 3481–3486.

Section 2 (Introduction: The "Metal-Template" Approach to Oligothiophene Macrocycles)

Section 2.1 (Introduction to Shape-Persistent Macrocycles)

[7] For recent reviews see:
a) Y. Yamaguchi, Z.-i. Yoshida, *Chem. Eur. J.* **2003**, *9*, 5431–5440;
b) D. Zhao, J. S. Moore, *Chem. Commun.* **2003**, 807–818;
c) J. A. Marsden, G. J. Palmer, M. M. Haley, *Eur. J. Org. Chem.* **2003**, 2355–2369;
d) G. J. Bodwell, T. Satou, *Angew. Chem.* **2002**, *114*, 4175–4178; *Angew. Chem. Int. Ed.* **2002**, *41*, 4003–4006;
e) C. Grave, A. D. Schlüter, *Eur J. Org. Chem.* **2002**, 3075–3098;
f) M. M. Haley, J. J. Pak, S. C. Brand, *Top. Curr. Chem.* **1999**, *201*, 81–130;
g) A. de Meijere, S. I. Koszushkov, *Top. Curr. Chem.* **1999**, *201*, 1–42;
h) W. J. Youngs, C. A. Tessier, J. D. Bradshaw, *Chem. Rev.* **1999**, *99*, 3153–3180.

[8] X. Shen, D. M. Ho, R. A. Pascal Jr., *Org. Lett.* **2003**, *5*, 369–371.

[9] a) S. Höger, *Chem. Eur. J.* **2004**, *10*, 1320–1329;
b) M. Fischer, G. Lieser, A. Rapp, I. Schnell, W. Mamdouh, S. De Feyter, F. C. De Schryver, S. Höger, *J. Am. Chem. Soc.* **2004**, *126*, 214–222;
c) M. Fischer, S. Höger, *Eur. J. Org. Chem.* **2003**, 441–446;
d) S. Höger, K. Bonrad, A. Mourran, U. Beginn, M. Möller, *J. Am. Chem. Soc.* **2001**, *123*, 5651–5659;
e) S. Rosselli, A.-D. Ramminger, T. Wagner, B. Silier, S. Wiegand, W. Häußler, G. Lieser, V. Scheumann, S. Höger, *Angew. Chem.* **2001**, *113*, 3234–3237; *Angew. Chem. Int. Ed.* **2001**, *40*, 3137–3141;
f) S. Höger, V. Enkelmann, K. Bonrad, C. Tschierske, *Angew. Chem.* **2000**, *112*, 2356–2358; *Angew. Chem. Int. Ed.* **2000**, *39*, 2267–2270.

[10] a) U. H. F. Bunz, *Acc. Chem. Res.* **2001**, *34*, 998–1010;
b) P.-H. Ge, W. Fu, W. A. Herrmann, E. Herdtweck, C. Campana, R. D. Adams, U. H. F. Bunz, *Angew. Chem.* **2000**, *112*, 3753–3756; *Angew. Chem. Int. Ed.* **2000**, *39*, 3607–3610;

[11] a) Y. Tobe, I. Ohki, M. Sonoda, H. Niino, T. Sato, T. Wakabayashi, *J. Am. Chem. Soc.* **2003**, *125*, 5614–5615;
b) Y. Tobe, R. Umeda, N. Iwasa, M. Sonoda, *Chem. Eur. J.* **2003**, *9*, 5549–5559;
c) Y. Tobe, N. Utsumi, K. Kawabata, A. Nagano, K. Adachi, S. Araki, M. Sonoda, K. Hirose, K. Naemura, *J. Am. Chem. Soc.* **2002**, *124*, 5350–5364;
d) Y. Tobe, R. Furukawa, M. Sonoda, T. Wakabayashi, *Angew. Chem.* **2001**, *113*, 4196–4198; *Angew. Chem. Int. Ed.* **2001**, *40*, 4072–4074;
e) Y. Tobe, N. Utsumi, A. Nagano, M. Sonoda, K. Naemura, *Tetrahedron* **2001**, *57*, 8075–8083;
f) Y. Tobe, T. Fujii, H. Matsumoto, K. Tsumuraya, D. Nogushi, N. Nakagawa, M. Sonoda, K. Naemura, Y. Achiba, T. Wakabayashi, *J. Am. Chem. Soc.* **2000**, *122*, 1762–1775.

[12] a) Y. Saiki, K. Nakamura, Y. Nigorikawa, M. Yamaguchi, *Angew. Chem.* **2003**, *115*, 5348–5350; *Angew. Chem. Int. Ed.* **2003**, *42*, 5190–5192;
b) K. Nakamura, H. Okubo, M. Yamaguchi, *Org. Lett.* **2001**, *3*, 1097–1099.

[13] a) T. Kawase, L. Tanaka, N. Shiono, Y. Seirai, M. Oda, *Angew. Chem.* **2004**, *116*, 1754–1756; *Angew. Chem. Int. Ed.* **2004**, *43*, 1722–1724;
b) T. Kawase, N. Fujiwara, M. Tsutumi, M. Oda, Y. Maeda, T. Wakahara, T. Akasaka, *Angew. Chem.* **2004**, *116*, 5170–5172; *Angew. Chem. Int. Ed.* **2004**, *43*, 5060–5062;
c) T. Kawase, K. Tanaka, Y. Seirai, N. Shiono, M. Oda, *Angew. Chem.* **2003**, *115*, 5755–5758; *Angew. Chem. Int. Ed.* **2003**, *42*, 5597–5600;
d) T. Kawase, Y. Seirai, H. R. Darabi, M. Oda, Y. Sarakai, K. Tashiro, *Angew. Chem.* **2003**, *115*, 1659–1662; *Angew. Chem. Int. Ed.* **2003**, *42*, 1621–1624;
e) T. Kawase, K. Tanaka, N. Fujiwara, H. R. Darabi, M. Oda, *Angew. Chem.* **2003**, *115*, 1662–1666; *Angew. Chem. Int. Ed.* **2003**, *42*, 1624–1628;
f) T. Kawase, N. Ueda, K. Tanaka, Y. Seirai, M. Oda, *Tetrahedron Lett.* **2001**, *42*, 5509–5511.

[14] a) W. B. Wan, R. C. Chiechi, T. J. R. Weakley, M. M. Haley, *Eur. J. Org. Chem.* **2001**, 3485–3490;
b) S. Lahiri, J. L. Thompson, J. S. Moore, *J. Am. Chem. Soc.* **2000**, *122*, 11315–11319;

[15] a) M. Srinivasan, S. Sankararaman, H. Hopf, B. Varghese, *Eur. J. Org. Chem.* **2003**, 660–665;
b) M. Ohkita, K. Ando, T. Tsuji, *Chem. Commun.* **2001**, 2570–2571;
c) M. B. Nielsen, M. Schreiber, Y. G. Baek, P. Seiler, S. Lecomte, C. Boudon, R. R. Tykwinsky, J.-P. Gisselbrecht, V. Gramlich, P. J. Skinner, C. Bosshard, P. Günter, M. Gross, F. Diederich, *Chem. Eur. J.* **2001**, *7*, 3263–3280.

[16] a) K. Campbell, R. McDonald, M. J. Ferguson, R. R. Tykwinski, *Organometallics* **2003**, *22*, 1353–1355;
b) K. Campbell, C. J. Kuehl, M. J. Ferguson, P. J. Stang, R. R. Tykwinski, *J. Am. Chem. Soc.* **2002**, *124*, 7266–7267;
c) K. Campbell, R. McDonald, R. R. Tykwinsky, *J. Org. Chem.* **2002**, *67*, 1133–1140;
d) K. Campbell, R. McDonald, N. R. Branda, R. R. Tykwinsky, *Org. Lett.* **2001**, *3*, 1045–1048.

[17] a) Y. Yamaguchi, S. Kobayashi, S. Miyamura, Y. Okamoto, T. Wakamiya, Y. Matsubara, Z.-i. Yoshida, *Angew. Chem.* **2004**, *116*, 370–373; *Angew. Chem. Int. Ed.* **2004**, *43*, 366–369;
b) S.-S. Sun, A. J. Lees, *Organometallics* **2001**, *20*, 2353–2358.

[18] a) P. N. W. Baxter, *J. Org, Chem.* **2004**, *69*, 1813–1821;
b) P. N. W. Baxter*, Chem. Eur. J.* **2003**, *9*, 5011–5022;
c) P. N. W. Baxter, *Chem. Eur. J.* **2003**, *9*, 2531–2541;
d) P. N. W. Baxter*, Chem. Eur. J.* **2002**, *8*, 5250–5264.

[19] a) C. Grave, D. Lentz, A. Schäfer, P. Samori, J. P. Rabe, P. Franke, A. D. Schlüter, *J. Am. Chem. Soc.* **2003**, *125*, 6907–6918;
b) O. Henze, D. Lentz, A. D. Schlüter, *Chem. Eur. J.* **2000**, *6*, 2362–2367;
c) V. Hensel, A. D. Schlüter, *Chem. Eur. J.* **1999**, *5*, 421–429;
d) V. Hensel, K. Lützow, J. Jakob, K. Gessler, W. Saenger, A.-D. Schlüter, *Angew. Chem.* **1997**, *109*, 2768–2770; *Angew. Chem. Int. Ed. Engl.* **1997**, *36*, 2654–2656.

[20] c) M. Schmittel, H. Ammon, *Synlett* **1999**, *6*, 750–752.

[21] S. Maruyama, H. Hokari, T. Wada, H. Sasabe, *Synthesis* **2001**, 1794–1799.

[22] a) A. Srinivasan, T. Ishizuka, A. Osuka, H. Furuta, *J. Am. Chem. Soc.* **2003**, *125*, 878–879;
b) S. Shimizu, J.-Y. Shin, H. Furuta, R. Ismael, A. Osuka, *Angew. Chem.* **2003**, *115*, 82–86; *Angew. Chem. Int. Ed.* **2003**, *42*, 78–82.

[23] a) V. G. Anand, S. Venkatraman, H. Rath, T. K. Chandrashekar, W. Teng, K. Ruhlandt-Senge, *Chem. Eur. J.* **2003**, *9*, 2282–2290;
b) C.-H. Hung, J.-P. Jong, M.-Y. Ho, G.-H. Lee, S.-M. Peng, *Chem. Eur. J.* **2002**, *8*, 4542–4548;
c) N. Sprutta, L. Latos-Grażyński, *Chem. Eur. J.* **2001**, *7*, 5099–5112.

[24] a) J. C. Hawley, N. Bampos, J. K. M. Sanders, *Chem. Eur J.* **2003**, *9*, 5211–5222;
b) L. Yu, J. S. Lindsey, *J. Org. Chem.* **2001**, *66*, 7402–7419.

[25] M. J. Cook, M. J. Heeney, *Chem. Eur. J.* **2000**, *6*, 3958–3967.

[26] a) T. Köhler, Z. Ou, J. T. Lee, D. Seidel, V. Lynch, K. M. Kadish, L. J. Sessler, *Angew. Chem.* **2005**, *117*, 85–89; *Angew. Chem. Int. Ed.* **2005**, *44*, 83–87.
b) D. Seidel, V. Lynch, J. L. Sessler, *Angew. Chem.* **2002**, *114*, 1480–1483; *Angew. Chem. Int. Ed.* **2002**, *41*, 1422–1425.

[27] a) G. Fuhrmann, T. Debaerdemaeker, P. Bäuerle, *Chem. Commun.* **2003**, 948–949;
b) M. Ammann, M. Enßle, G. Fuhrmann, A. Kaiser, P. Kilickiran, E. Mena-Osteritz, P. Bäuerle, *Polymer Preprints* **2003**, *44*, 379–380;
c) P. Bäuerle, E. Mena-Osteritz, G. Fuhrmann, A. Kaiser, M. Ammann, *Polym. Mater. Sci. Eng.* **2002**, *86*, 34;
d) E. Mena-Osteritz, P. Bäuerle, *Adv. Mater.* **2001**, *13*, 243–246;
e) G. Fuhrmann, J. Krömer, P. Bäuerle, *Synth. Met.* **2001**, *119*, 125–126;
f) J. Krömer, I. Rios-Carreras, G. Fuhrmann, C. Musch, M. Wunderlin, T. Debaerdemaeker, E. Mena-Osteritz, P. Bäuerle, *Angew. Chem.* **2000**, *112*, 3623–3628; *Angew. Chem. Int. Ed.* **2000**, *39*, 3481–3486.

[28] J. Krömer, PhD thesis, University of Ulm, **2000**.

[29] G. Fuhrmann, PhD thesis, University of Ulm, **2006**.

[30] M. Mayor, C. Didschies,
Angew. Chem. **2003**, *115*, 3284–3287; *Angew. Chem. Int. Ed.* **2003**, *42*, 3176–3179.

[31] a) J. R. Nitschke, T. D. Tilley, *J. Am. Chem. Soc.* **2001**, *123*, 10183–10190;
b) J. R. Nitschke, S. Zürcher, T. D. Tilley, *J. Am. Chem. Soc.* **2000**, *122*, 10345–10352.

[32] a) P. Siemsen, R. C. Livingston, F. Diederich,
Angew. Chem. **2000**, *112*, 2740–2767; *Angew. Chem. Int. Ed.* **2000**, *39*, 2632–2657;
b) P. J. Stang, F. Diederich, *Modern Acetylene Chemistry*, VCH, Weinheim, **1995**;
c) L. Brandsma, *Preparative Acetylenic Chemistry*, Elsevier, Amsterdam, **1988**.

[33] K. Sonogashira, *Cross-coupling Reactions to sp Carbon Atoms* in *Metal-catalyzed Cross-coupling Reactions* (Eds.: F. Diederich, P. J. Stang), Wiley–VCH, Weinheim, **1998**, pp. 203–229.

Section 2.2 (Preparation of Oligothiophene Macrocycles by Glaser-Type Coupling)

[34] a) U. Fritzsche, S. Hünig, *Tetrahedron Lett.* **1972**, 4831–4834;
b) A. Vaitiekunas, F. F. Nord, *J. Am. Chem. Soc.* **1954**, *76*, 2733–2736;
c) C. Glaser, *Chem. Ber.* **1869**, *2*, 422–424.

[35] G. Eglinton, A. R. Galbraith, *J. Chem. Soc.* **1959**, 889–896.

[36] a) K. Okuhara, *Bull. Chem. Soc. Jpn.* **1981**, *54*, 2045–2052;
b) A. S. Hay, *J. Org. Chem.* **1962**, *27*, 3320–3321.

[37] J. P. P. Stewart, MOPAC Program Package, QCPE 455, Indiana University, Bloomington IN.

Section 2.3 (The Metal-Template Route as a Combination of Synthetic Strategies)

[38] a) R. Rossi, A. Carpita, C. Bigelli, *Tetrahedron Lett.* **1985**, *26*, 523–526;
b) K. Sonogashira, Y. Tohda, N. Hagihara, *Tetrahedron Lett.* **1975**, *16*, 4467–4470.

[39] Q. Liu, D. J. Burton, *Tetrahedron Lett.* **1997**, *38*, 4371–4374.

Section 2.4 (Survey of Macrocycles Comprising Pt(II) Building Blocks)

Section 2.4.1 (Usage of Pt(II) Units as Supramolecular Building Blocks)

[40] a) F. Diederich, P. J. Stang (Eds.), *Templated Organic Synthesis*, Wiley–VCH, Weinheim, **2000**;
b) J.-P. Sauvage, M. W. Hosseini (Eds.), *Templating, Self-assembly and Self-organization*. As vol. 9 of: J.-M. Lehn (Chair Ed.), *Comprehensive Supramolecular Chemistry*, Pergamon Press, Oxford, **1996**;
c) J.-M. Lehn, *Supramolecular Chemistry — Concepts and Perspectives*, Wiley–VCH, Weinheim, **1995**;
d) F. Vögtle, *Supramolecular Chemistry*, Wiley, Chichester, **1991**.

[41] B. J. Holliday, C. A. Mirkin,
Angew. Chem. **2001**, *113*, 2076–2098; *Angew. Chem. Int. Ed.* **2001**, *40*, 2022–2043.

[42] a) G. F. Swiegers, T. J. Malefetse, *Coord. Chem. Rev.* **2002**, *225*, 91–121;
b) G. F. Swiegers, T. J. Malefetse, *Chem. Rev.* **2000**, *100*, 3483–3537.

[43] C. J. Jones, *Chem. Soc. Rev.* **1998**, *27*, 289–299.

[44] a) M. Fujita, *Chem. Soc. Rev.* **1998**, *27*, 417–425;
b) M. Fujita, K. Ogura, *Bull. Chem. Soc. Jpn.* **1996**, *69*, 1471–1482.

[45] a) S. R. Seidel, P. J. Stang, *Acc. Chem. Res.* **2002**, *35*, 972–983;
b) S. Leininger, B. Olenyuk, P. J. Stang, *Chem. Rev.* **2000**, *100*, 853–908;
c) B. Olenyuk, A. Fechtenkötter, P. J. Stang,
J. Chem. Soc. Dalton Trans. **1998**, 1707–1728;
d) P. J. Stang, B. Olyenuk, *Acc. Chem. Res.* **1997**, *30*, 502–518.

[46] P. H. Dinolfo, J. T. Hupp, *Chem. Mater.* **2001**, *13*, 3113–3125.

[47] C. A. Schalley, A. Lützen, M. Albrecht, *Chem. Eur. J.* **2004**, *10*, 1072–1080.

[48] D. W. Johnson, K. N. Raymond, *Supramolec. Chem.* **2001**, *13*, 639–659.

[49] R. Vilar,
Angew. Chem. **2003**, *115*, 1498–1516; *Angew. Chem. Int. Ed.* **2003**, *42*, 1460–1477.

[50] A. Kaiser, P. Bäuerle, *Top. Curr. Chem.* **2005**, *249*, 127–201.

Section 2.4.2 (Strategic Choice of Building Blocks for Pt(II) Macrocycles)

[51] E. Bosch, C. L. Barnes, *Organometallics* **2000**, *19*, 5522–5524.

[52] a) K. Campbell, C. A. Johnson II, R. McDonald, M. J. Ferguson, M. M. Haley,
R. R. Tykwinski,
Angew. Chem. **2004**, *116*, 6093–6097; *Angew. Chem. Int. Ed.* **2004**, *43*, 5967–5971**;**
b) K. Campbell, R. McDonald, M. J. Ferguson, R. R. Tykwinski,
J. Organomet. Chem. **2003**, *683*, 379–387.

Section 2.4.3 (Choice of Reaction Conditions)

[53] K. Sonogashira, T. Yatake, Y. Tohda, S. Takahahi, N. Hagihara,
J. Chem. Soc. Chem. Commun. **1977**, 291–292.

Section 2.4.4 (Characterisation of Pt(II) Macrocycles)

[54] J. A. Whiteford, E. M. Rachlin, P. J. Stang,
Angew. Chem. **1996**, *108*, 2643–2648; *Angew. Chem. Int. Ed. Engl.* **1996**, *35*, 2524–2529.

[55] a) S. Sakomoto, M. Yoshizawa, T. Kusukawa, M. Fujita, K. Yamaguchi,
Org. Lett. **2001**, *3*, 1601–1604;
b) S. Sakamoto, M. Fujita, K. Kim, K. Yamaguchi, *Tetrahedron* **2000**, *56*, 955–964.

[56] C. A. Schalley, T. Müller, P. Linnartz, M. Witt, M. Schäfer, A. Lützen,
Chem. Eur. J. **2002**, *8*, 3538–3551.

Section 2.4.6 (Macrocycles with Pt–N Coordination Containing Nucleobases)

[57] C. J. L. Lock, H. J. Peresie, B. Rosenberg, G. Turner,
J. Am. Chem. Soc. **1978**, *100*, 3371–3374.

[58] D. Neugebauer, B. Lippert, *Inorg. Chim. Acta.* **1982**, *67*, 151–158.

[59] Y.-T. Fanchiang, *J. Chem. Soc. Dalton. Trans.* **1986**, 135–140.

[60] a) S. E. Sherman, D. Gibson, A. H.-J. Wang, S. J. Lippard,
J. Am. Chem. Soc. **1988**, *110*, 7368–7381;
b) S. E. Sherman, D. Gibson, A. H.-J. Wang, S. J. Lippard, *Science* **1985**, *230*, 412–417.

[61] a) B. Longato, G. Bandoli, G. Trovó, E. Marasciulo, G. Valle,
Inorg. Chem. **1995**, *34*, 1745–1750;
b) L. Schenetti, G. Bandoli, A. Dolmella, G. Trovó, B. Longato,
Inorg. Chem. **1994**, *33*, 3169–3176.

[62] a) J. A. R. Navarro, B. Lippert, *Coord. Chem. Rev.* **2001**, *221*, 219–250;
b) E. Zangrando, F. Pichierri, L. Randaccio, B. Lippert, *Coord. Chem. Rev.* **1996**, *156*, 275–332;
c) B. Lippert, *Prog. Inorg. Chem.* **1989**, *37*, 1–97.

[63] a) I. B. Rother, M. Willermann, B. Lippert, *Supramolec. Chem.* **2002**, *14*, 189–197;
b) R.-D. Schnebeck, E. Freisinger, F. Glahé, B. Lippert, *J. Am. Chem. Soc.* **2000**, *122*, 1381–1390;
c) J. A. R. Navarro, E. Freisinger, B. Lippert, *Inorg. Chem.* **2000**, *39*, 2301–2305;
d) J. A. R. Navarro, E. Freisinger, B. Lippert, *Eur. J. Inorg. Chem.* **2000**, 147–151;
e) J. A. R. Navarro, M. B. L. Janik, E. Freisinger, B. Lippert, *Inorg. Chem.* **1999**, *38*, 426–432;
f) R.-D. Schnebeck, E. Freisinger, B. Lippert, *Angew. Chem.* **1999**, *111*, 235–238; *Angew. Chem. Int. Ed.* **1999**, *38*, 168–171;
g) R.-D. Schnebeck, E. Freisinger, B. Lippert, *Chem. Commun.* **1999**, 675–676;
h) R.-D. Schnebeck, L. Randaccio, E. Zangrando, B. Lippert, *Angew. Chem.* **1998,** *110*, 128–130; *Angew. Chem. Int. Ed.* **1998**, *37*, 119–121;
i) M. S. Lüth, E. Freisinger, F. Glahé, B. Lippert, *Inorg. Chem.* **1998**, *37*, 5044–5045;
j) M. S. Lüth, E. Freisinger, F. Glahé, J. Müller, B. Lippert, *Inorg. Chem.* **1998**, *37*, 3195–3203;
k) H. Rauter, I. Mutikainen, M. Blomberg, C. J. L. Lock, P. Amo-Ochoa, E. Freisinger, L. Randaccio, E. Zangrando, E. Chiarparin, B. Lippert, *Angew. Chem.* **1997**, *109*, 1353–1357; *Angew. Chem. Int. Ed. Engl.* **1997**, *36*, 1296–1301;
l) H. Rauter, E. C. Hillgeris, A. Erxleben, B. Lippert, *J. Am. Chem. Soc.* **1994**, *116*, 616–624;
m) A. Schreiber, E. C. Hillgeris, B. Lippert, *Z. Naturforsch.* **1993**, *48b*, 1603–1612;
n) H. Rauter, E. C. Hillgeris, B. Lippert, *J. Chem. Soc. Chem. Commun.* **1992**, 1385–1386;
o) B. Lippert, *Inorg. Chem.* **1981**, *20*, 4326–4343;

Section 2.4.7 (Macrocycles with Pt–N Coordination Containing Exocyclic Diamine Ligands)

[64] a) S.-Y. Yu, H. Huang, H.-B. Liu, Z.-N. Chen, R. Zhang, M. Fujita, *Angew. Chem.* **2003**, *115*, 710–714; *Angew. Chem. Int. Ed*. **2003**, *42*, 686–690;
b) M. Aoyagi, K. Biradha, M. Fujita, *Bull. Chem. Soc. Jpn.* **1999**, *72*, 2603–2606;
c) M. Fujita, J. Yazaki, K. Ogura, *Tetrahedron Lett.* **1991**, *32*, 5589–5592;
d) M. Fujita, J. Yazaki, K. Ogura, *Chem. Lett.* **1991**, 1031–1032.

[65] a) J. K. Bera, J. Basca, B. W. Smucker, K. R. Dunbar, *Eur. J. Inorg. Chem.* **2004**, 368–375;
b) J. K. Bera, B. W. Smucker, R. A. Walton, K. R. Dunbar, *Chem. Commun.* **2001**, 2562–2563;

[66] a) K.-M. Park, S.-Y. Kim, J. Heo, D. Whang, S. Sakamoto, K. Yamaguchi, K. Kim, *J. Am. Chem. Soc.* **2002**, *124*, 2140–2147;
b) D. Whang, K.-M. Park, J. Heo, P. Ashton, K. Kim, *J. Am. Chem. Soc.* **1998**, *120*, 4899 –4900.

[67] a) Z. Qin, M. C. Jennings, R. J. Puddephatt, *Inorg. Chem.* **2003**, *42*, 1956–1965;
b) Z. Qin, M. C. Jennings, R. J. Puddephatt, *Chem. Commun.* **2001**, 2676–2677.

Section 2.4.8 (Square Pt–N Coordinated Macrocycles with Exocyclic Ligands Other than ...)

[68] a) J. Fan, J. A. Whiteford, B. Olenyuk, M. D. Levin, P. J. Stang, E. B. Fleischer, *J. Am. Chem. Soc.* **1999**, *121*, 2741–2752;
b) C. Müller, J. A. Whiteford, P. J. Stang, *J. Am. Chem. Soc.* **1998**, *120*, 9827–9837;
c) J. A. Whiteford, C. V. Lu, P. J. Stang, *J. Am. Chem. Soc.* **1997**, *119*, 2524–2533;
d) J. Manna, C. J. Kuehl, J. A. Whiteford, P. J. Stang, D. C. Muddiman, S. A. Hofstadler, R. D. Smith, *J. Am. Chem. Soc.* **1997**, *119*, 11611–11619;
e) P. J. Stang, J. Fan, B. Olenyuk, *Chem. Commun.* **1997**, 1453–1454;
f) P. J. Stang, D. H. Cao, S. Saito, A. M. Arif, *J. Am. Chem. Soc.* **1995**, *117*, 6273–6283;
g) P. J. Stang, D. H. Cao, *J. Am. Chem. Soc.* **1994**, *116*, 4981–4982.

[69] C. M. Drain, J.-M. Lehn, *J. Chem. Soc. Chem. Commun.* **1994**, 2313–2315; *J. Chem. Soc. Chem. Commun.* **1995**, 503.

[70] a) F. Würthner, A. Sautter, D. Schmid, P. J. A. Weber, *Chem. Eur. J.* **2001**, *7*, 894–902;
b) F. Würthner, A. Sautter, *Chem. Commun.* **2000**, 445–446.

[71] a) S.-S. Sun, J. A. Anspach, A. J. Lees, *Inorg. Chem.* **2002**, *41*, 1862–1869;
b) S.-S. Sun, J. A. Anspach, A. J. Lees, P. Y. Zavalij, *Organometallics* **2002**, *21*, 685–693.

[72] T. W. Kim, M. S. Lah, J.-I. Hong, *Chem. Commun.* **2001**, 743–744.

Section 2.4.9 (Molecular Polygons Other than Squares (...) and Equilibira Thereof)

[73] a) T. Yamamoto, A. M. Arif, P. J. Stang, *J. Am. Chem. Soc.* **2003**, *125*, 12309–12317;
b) K.-W. Chi, C. Addicott, A. M. Arif, N. Das, P. J. Stang, *J. Org. Chem.* **2003**, *68*, 9798–9801;
c) Y. K. Kryschenko, S. R. Seidel, A. M. Arif, P. J. Stang, *J. Am. Chem. Soc.* **2003**, *125*, 5193–5198;
d) M. Schweiger, S. R. Seidel, A. M. Arif, P. J. Stang, *Inorg. Chem.* **2002**, *41*, 2556–2559;
e) C. J. Kuehl, S. D. Huang, P. J. Stang, *J. Am. Chem. Soc.* **2001**, *123*, 9634–9641;
f) M. Schweiger, S. R. Seidel, A. M. Arif, P. J. Stang, *Angew. Chem.* **2001**, *113*, 3575–3577; *Angew. Chem. Int. Ed.* **2001**, *40*, 3467–3469;
g) M. Schmitz, S. Leininger, J. Fan, A. M. Arif, P. J. Stang, *Organometallics* **1999**, *18*, 4817–4824.

[74] M. Ferrer, L. Rodríguez, O. Rossell, *J. Organomet. Chem.* **2003**, *681*, 158–166.

[75] A. Sautter, D. G. Schmid, G. Jung, F. Würthner, *J. Am. Chem. Soc.* **2001**, *123*, 5424–5430.

[76] S.-W. Lai, M. C.-W. Chan, S.-M. Peng, C.-M. Che, *Angew. Chem.* **1999**, *111*, 708–710; *Angew. Chem. Int. Ed.* **1999**, *38*, 669–671.

[77] N. C. Gianneschi, E. R. T. Tiekink, L. M. Rendina, *J. Am. Chem. Soc.* **2000**, *122*, 8474–8479.

[78] T. Habicher, J.-F. Nierengarten, V. Gramlich, F. Diederich, *Angew. Chem.* **1998**, *110*, 2019–2022; *Angew. Chem. Int. Ed.* **1998**, *37*, 1916–1919.

[79] A. J. Baer, B. D. Koivisto, A. P. Côté, N. J. Taylor, G. S. Hanan, H. Nierengarten, A. V. Dorsselaer, *Inorg. Chem.* **2002**, *41*, 4987–4989.

[80] S.-Y. Chang, H.-Y. Jang, K.-S. Jeong, *Chem. Eur. J.* **2003**, *9*, 1535–1541.

Section 2.4.10 (Macrocycles with Bridging Cyanide and Isocyanide Ligands)

[81] S.-W. Lai, K.-K. Cheung, M. C.-W. Chan, C.-M. Che, *Angew. Chem.* **1998**, *110*, 193–195; *Angew. Chem. Int. Ed.* **1998**, *37*, 182–184.

[82] L. R. Falvello, M. Tomás, *Chem. Commun.* **1999**, 273–274.

[83] J. Forniés, J. Gómez, E. Lalinde, M. T. Moreno, *Chem. Eur. J.* **2004**, *10*, 888–898.

[84] P. Espinet, K. Soulantica, J. P. H. Charmant, A. G. Orpen, *Chem. Commun.* **2000**, 915–916.

Section 2.4.11 (Macrocycles with Bridging Acetylide Ligands)

[85] M. I. Bruce, K. Costuas, J.-F. Halet, B. C. Hall, P. J. Low, B. K. Nicholson, B. W. Skelton, A. H. White, *J. Chem. Soc. Dalton. Trans.* **2002**, 383–398.

[86] R. Faust, F. Diederich, V. Gramlich, P. Seiler, *Chem. Eur. J.* **1995**, *1*, 111–117.

[87] a) S. M. ALQaisi, K. J. Galat, M. Chai, D. G. Ray III, P. L. Rinaldi, C. A. Tessier, W. J. Youngs, *J. Am. Chem. Soc.* **1998**, *120*, 12149–12150;
b) D. Zhang, D. B. McConville, C. A. Tessier, W. J. Youngs, *Organometallics* **1997**, *16*, 824–825;
c) J. D. Bradshaw, L. Guo, C. A. Tessier, W. J. Youngs, *Organometallics* **1996**, *15*, 2582–2584.

[88] a) J. J. Pak, T. J. R. Weakley, M. M. Haley, *Organometallics* **1997**, *16*, 4505–4507.
b) C. A. Johnson II, M. M. Haley, personal communication.

[89] B. Olenyuk, J. A. Whiteford, P. J. Stang, *J. Am. Chem. Soc.* **1996**, *118*, 8221–8230.

[90] a) J. Hua, W. Lin, *Org. Lett.* **2004**, *6*, 861–864;
b) H. Jiang, W. Lin, *J. Am. Chem. Soc.* **2003**, *125*, 8084–8085;
c) H. Jiang, A. Hu, W. Lin, *Chem. Commun.* **2003**, 96–97;
d) S. J. Lee, A. Hu, W. Lin, *J. Am. Chem. Soc.* **2002**, *124*, 12948–12949.

[91] S. Takahashi, K. Onitsuka, F. Takei, *Macromol. Symp.* **2000**, *156*, 69–77.

[92] Y. Mori, T. Kasai, T. Takesada, H. Komatsu, H. Yamazaki, M.-a. Haga, *Chem. Lett.* **2001**, 996–997.

[93] G. Fuhrmann, P. Kilickiran, P. Bäuerle, unpublished results.

[94] M. Ammann, A. Rang, C. A. Schalley, P. Bäuerle, *Eur. J. Org. Chem.* **2006**, 1940-1948.

[95] C. Fave, P. Bäuerle, unpublished results.

Section 2.4.12 (Macrocycles by Pt–P Coordination)

[96] C. A. Bessel, P. Aggarwal, A. C. Marschilok, K. J. Takeuchi, *Chem. Rev.* **2001**, *101*, 1031–1066.

[97] a) T. Shima, E. B. Bauer, F. Hampel, J. A. Gladysz, *J. Chem. Soc. Dalton Trans.* **2004**, 1012–1028;
b) E. B. Bauer, F. Hampel, J. A. Gladysz, *Organometallics* **2003**, *22*, 5567–5580;
c) E. B. Bauer, S. Szafert, F. Hampel, J. A. Gladysz, *Organometallics* **2003**, *22*, 2184–2186;
d) J. Ruwwe, J. M. Martín-Alvarez, C. R. Horn, E. B. Bauer, S. Szafert, T. Lis, F. Hampel, P. C. Cagle, J. A. Gladysz, *Chem. Eur. J.* **2001**, *7*, 3931–3950;
e) E. B. Bauer, J. Ruwwe, J. M. Martín-Alvarez, T. B. Peters, J. C. Bohling, F. A. Hampel, S. Szafert, T. Lis, J. A. Gladysz, *Chem. Commun.* **2000**, 2261–2262.

[98] C. G. Arena, D. Drommi, F. Faraone, C. Graiff, A. Tiripicchio, *Eur. J. Inorg. Chem.* **2001**, 247–255.

[99] E. Lindner, R. Veigel, K. Ortner, C. Nachtigal, M. Steimann, *Eur. J. Inorg. Chem.* **2000**, 959–969.

[100] T. Baumgartner, K. Huynh, S. Schleidt, A. J. Lough, I. Manners, *Chem. Eur. J.* **2002**, *8*, 4622–4632.

[101] L. R. Falvello, J. Forniés, J. Gómez, E. Lalinde, A. Martín, F. Martínez, M. T. Moreno, *J. Chem. Soc. Dalton Trans.* **2001**, 2132–2140.

[102] see, e.g.,
a) D. Xu, H. J. Murfee, W. E. van der Veer, B. Hong, *J. Organomet. Chem.* **2000**, *596*, 53–63;
b) W. Oberhauser, C. Bachmann, T. Stampfl, P. Brüggeller, *Inorg. Chim. Acta.* **1997**, *256*, 223–234.

[103] R. J. Puddephatt, *Chem. Soc. Rev.* **1983**, *12*, 99–127.

Section 2.4.13 (Macrocycles by Unusual Pt(II) Coordination)

[104] a) P. S. Mukherjee, N. Das, Y. K. Kryschenko, A. M. Arif, P. J. Stang, *J. Am. Chem. Soc.* **2004**, *126*, 2464–2473;
b) N. Das, P. S. Mukherjee, A. M. Arif, P. J. Stang, *J. Am. Chem. Soc.* **2003**, *125*, 13950–13951.

[105] N. N. Greenwood, A. Earnshaw, *Chemistry of the Elements*, Pergamon, Oxford, **1984**.

[106] P. Teo, L. L. Koh, T. S. A. Hor, *Inorg. Chem.* **2003**, *42*, 7290–7296.

Section 2.4.14 (Concluding Remarks on Pt(II) Macrocycles)

[107] M. Fujita, O. Sasaki, T. Mitsuhashi, T. Fujita, J. Yazaki, K. Yamaguchi, K. Ogura, *Chem. Commun.* **1996**, 1535–1536.

[108] B. L. Edelbach, R. J. Lachicotte, W. D. Jones, *J. Am. Chem. Soc.* **1998**, *120*, 2843–2853.

[109] a) F. Diederich, P. J. Stang (Eds), *Templated Organic Synthesis*, Wiley–VCH,Weinheim, **2000**;
b) N. V. Gerbeleu, V. B. Arion, J. Burgess, *Template Synthesis of Macrocyclic Compounds*,Wiley–VCH,Weinheim, **1999**;
c) J. P. Sauvage, C. Dietrich-Buchecker (Eds.), *Molecular Catenanes, Rotaxanes, and Knots*,Wiley–VCH,Weinheim, **1999**.

[110] M. Ammann, PhD thesis, University of Ulm, **2004**.

Section 3 (Synthesis of Aryl-Substituted Oligothienyl Macrocycles)

[111] a) M. Janda, J. Šrogl, I. Stibor, M. Němec, P. Vopatrná, *Synthesis* **1972**, 545–547;
b) S. Gronowitz S., *Acta Chem. Scand.* **1959**, *13*, 1045–1046.

[112] a) D. Kotkar, V. Joshi, P. K. Ghosh, *Chem. Commun.* **1988**, 917–918;
b) K. Tamao, S. Kodama, I. Nakajima, M. Kumada, A. Minato, K. Suzuki, *Tetrahedron* **1982**, *38*, 3347–3354;
c) W. Steinkopf, *Liebigs Ann. Chem.* **1921**, *424*, 23–61;
d) O. Hinsberg, *Chem. Ber.* **1915**, *48*, 1611–1614;.

[113] G. Fuhrmann, PhD thesis, University of Ulm, **2006**.

[114] M. Ammann, personal communication.

[115] E.-i. Negishi, F. Liu, *Palladium- or Nickel-catalyzed Cross-coupling with Organometals Containing Zinc, Magnesium, Aluminium, and Zirconium* in *Metal-catalyzed Cross-couling Reactions* (Eds.: F. Diederich, P. J. Stang), Wiley–VCH, Weinheim, **1998**.

[116] J. Krömer, P. Bäuerle, *Tetrahedron* **2001**, *57*, 3785–3794.

[117] a) G. W. Gray, M. Hird, D. Lacey, K. J. Toyne, *J. Chem. Soc. Perkin Trans. 2* **1989**, 2041–2053;
b) M. Wehmeier, M. Wagner, K. Müllen, *Chem. Eur. J.* **2001**, *10*, 2197–2205.

[118] X-ray-structural analysis and quantum-chemical calculations were performed in the labs of PD Dr. C. Strohmann, University of Würzburg.

[119] Illustrations of crystal structures were made with the program ORTEP-3: L. L. Farrugia, *J. Appl. Cryst.* **1997**, *30*, 565.

[120] a) A. D. Becke, *J. Chem. Phys.* **1993**, *98*, 5648–5652;
b) C. Lee, W. Yang, R. G. Parr, *Phys. Rev. B: Condens. Matter.* **1988**, *37*, 785–789.

[121] Gaussian 98, Revision A.7, M. J. Frisch, G. W. Trucks, H. B. Schlegel, G. E. Scuseria, M. A. Robb, J. R. Cheeseman, V. G. Zakrzewski, J. A. Montgomery, Jr., R. E. Stratmann, J. C. Burant, S. Dapprich, J. M. Millam, A. D. Daniels, K. N. Kudin, M. C. Strain, O. Farkas, J. Tomasi, V. Barone, M. Cossi, R. Cammi, B. Mennucci, C. Pomelli, C. Adamo, S. Clifford, J. Ochterski, G. A. Petersson, P. Y. Ayala, Q. Cui, K. Morokuma, D. K. Malick, A. D. Rabuck, K. Raghavachari, J. B. Foresman, J. Cioslowski, J. V. Ortiz, A. G. Baboul, B. B. Stefanov, G. Liu, A. Liashenko, P. Piskorz, I. Komaromi, R. Gomperts, R. L. Martin, D. J. Fox, T. Keith, M. A. Al-Laham, C. Y. Peng, A. Nanayakkara, C. Gonzalez, M. Challacombe, P. M. W. Gill, B. Johnson, W. Chen, M. W. Wong, J. L. Andres, C. Gonzalez, M. Head-Gordon, E. S. Replogle, J. A. Pople, Gaussian, Inc., Pittsburgh (PA), **1998**.

[122] HyperChem^{TM} 6.03, Hypercube, Inc., 1115 NW 4th Street, Gainesville, FL 32601, USA.

[123] E. A. Meyer, R. K. Castellano, F. Diederich, *Angew. Chem.* **2003**, *115*, 1244–1287; *Angew. Chem. Int. Ed.* **2003**, *42*, 1210–1250.

[124] P. Kilickiran, personal communication.

[125] P. Kilickiran, C. Fave, personal communication.

[126] W. Steinkopf, H. Jacob, H. Penz, *Liebigs Ann. Chem.* **1934**, *512*, 136–164.

[127] V. Meyer, H. Kreis, *Chem. Ber.* **1884**, *17*, 1558–1563.

[128] S. Fukuzumi, J. K. Kochi, *J. Phys. Chem.* **1981**, *85*, 648–654.

[129] T. G. Appleton, M. A. Bennett, I. B. Tomkins, *J. Chem. Soc., Dalton Trans.* **1976**, 439–446.

[130] D. R. Coulson, *Inorg. Synth.* **1972**, 121–124.

[131] a) G. M. Sheldrick, SHELXS-90, Structure Solving Program for Crystal Structure Determination; University of Goettingen (Germany): Goettingen, **1990**;
b) G. M. Sheldrick, SHELXL-97, A Computer Program for Refinement of Crystal Structures; University of Goettingen (Germany): Goettingen, **1997**.

Section 4 (Photophysical Properties of Oligothienyl Macrocycles)

[132] H. Shirakawa, E. J. Louis, A. G. MacDiarmid, C. K. Chiang, A. J. Heeger, *J. Chem. Soc. Chem. Commun*. **1977**, 578–580.

[133] see, e.g.:
a) D. Fichou (Ed.), *Handbook of Oligo- and Polythiophenes*, Wiley–VCH, Weinheim, **1999**;
b) P. Bäuerle, *Oligothiophenes* in *Oligothiophenes in Electronic Materials: The Oligomer Approach* (Eds.: K. Müllen, G. Wegner), Wiley–VCH, Weinheim, **1998**, pp. 105–197.

[134] recent examples include:
a) G. Sonmez, F. Wudl, *J. Mater. Chem.* **2005**, *15*, 20–22;
b) G. Sonmez, C. K. F. Shen, Y. Rubin, F. Wudl, *Angew. Chem.* **2004**, *116*, 1523–1528; *Angew. Chem. Int. Ed.* **2004**, *43*, 1498–1502.
c) P. Furuta, J. Brooks, M. E. Thompson, J. M. J. Fréchet, *J. Am. Chem. Soc.* **2003**, *125*, 13165–13172;
d) M. Mazzeo, V. Vitale, F. Della Sala, D. Pisignano, M. Anni, G. Barbarella, L. Favaretto, A. Zanelli, R. Cingolani, G. Gigli, *Adv. Mater.* **2003**, *15*, 2060–2063;
e) T. Otsubo, Y. Aso, K. Takimiya, *J. Mater. Chem.* **2002**, *12*, 2565–2575;
f) L. Zhu, H. Tang, Y. Harima, K. Yamashita, D. Hirayama, Y. Aso, T. Otsubo, *Chem. Commun.* **2001**, 1830–1831;
g) U. Mitschke, P. Bäuerle, *J. Chem. Soc. Perkin Trans. 1* **2001**, 740–753.

[135] recent examples include:
a) M.-H. Yoon, S. A. DiBenedetto, A. Facchetti, T. J. Marks, *J. Am. Chem. Soc.* **2005**, *127*, 1348–1349;
b) A. R. Murphy, J. M. J. Fréchet, P. Chang, J. Lee, V. Subramanian, *J. Am. Chem. Soc.* **2004**, *126*, 1596–1597;
c) Y. Kunugi, K. Takimiya, N. Negishi, T. Otsubo, *J. Mater. Chem.* **2004**, *14*, 2840–2841;
d) B.-H. Huisman, J. J. P. Valeton, W. Nijssen, J. Lub, W. ten Hoeve, *Adv. Mater.* **2003**, *15*, 2002–2005;
e) A. Yassar, F. Demanze, A. Jaafari, M. El Idrissi, C. Coupry, *Adv. Func. Mater.* **2002**, *12*, 699–707;
f) T. M. Pappenfus, R. J. Chesterfield, C. D. Frisbie, K. R. Mann, J. Casado, J. D. Raff, L. L. Miller, *J. Am. Chem. Soc.* **2002**, *124*, 4184–4185;
g) H. E. Katz, Z. Bao, S. L. Gilat, *Acc. Chem. Res.* **2001**, *34*, 359–369;
h) J. M. Tour, *Acc. Chem. Res.* **2000**, *33*, 791–804.

[136] e.g.,
a) R. de Bettignies, Y. Nicholas, P. Blanchard, E. Levillain, J.-M. Nunzi, J. Roncali, *Adv. Mater.* **2003**, *15*, 1939–1943;
b) N. Noma, T. Tsuzuki, Y. Shirota, *Adv. Mater.* **1995**, *7*, 647–648.

[137] a) T. Izumi, S. Kobashi, K. Takimiya, Y. Aso, T. Otsubo, *J. Am. Chem. Soc.* **2003**, *125*, 5286–5287 (96-mer);
b) T. Otsubo, Y. Aso, K. Takimiya, *Bull. Chem. Soc. Jpn.* **2001**, *74*, 1789–1801 (72-mer and 48-mer);
c) J. Krömer, P. Bäuerle, *Tetrahedron* **2001**, *57*, 3785–3794 (11-mer);
d) T. Kirschbaum, C.A. Briehn, P. Bäuerle, *J. Chem. Soc. Perkin Trans. 1* **2000,** 1211–1216 (12-mer);

e) J. Krömer, PhD thesis, University Ulm, **2000** (19-mer);
f) H. Nakanishi, N. Sumi, Y. Aso, T. Otsubo, *J. Org. Chem.* **1998**, *63*, 8632–8633 (27-mer);
g) A. H. Mustafa, M. K. Shepherd, *Chem. Commun*. **1998**, 2743–2744 (24-mer);
h) P. R. L. Malenfrant, L. Groenendaal, J. M. Frechet, *J. Am. Chem. Soc.* **1998**, *120*, 10990–10991 (17-mer),
i) M. Sato, M. Hiroi, *Polymer* **1996**, *37*, 1685–1689 (15-mer);
j) P. Bäuerle, T. Fischer, B. Bildlingmeier, A. Stabel, J. P. Rabe, *Angew. Chem.* **1995**, *107*, 335–339; *Angew. Chem. Int. Ed. Engl.* **1995**, *34*, 303–307 (16-mer).

[138] a) R. E. Martin, F. Diederich, *Angew. Chem.* **1999**, *111*, 1440–1469; *Angew. Chem. Int. Ed.*, *38*, 1350–1377;
b) I. Jestin, P. Frère, P. Blanchard, J. Roncali, *Angew. Chem.* **1998**, *110*, 990–993; *Angew. Chem. Int. Ed.* **1998**, *37*, 942–945;
c) J. Roncali, *Chem. Rev.* **1997**, *97*, 173–205;
d) H. Meier, U. Stalmach, H. Kolshorn, *Acta Polym.* **1997**, *48*, 379–384.

[139] a) W. ten Hoeve, H. Wynberg, E. E. Havinga, E. W. Meijer, *J. Am. Chem. Soc.* **1991**, *113*, 5887–5889;
b) E. E. Havinga, I. Rotte, E. W. Meijer, W. ten Hoeve, H. Wynberg, *Synth. Met.* **1991**, *41*, 473–478.

[140] M. Bednarz, P. Reineker, E. Mena-Osteritz, P. Bäuerle, *J. Lumin.* **2004**, *110*, 225–231.

[141] G. Fuhrmann, PhD thesis, University of Ulm, **2006**.

[142] a) G. Fuhrmann, T. Debaerdemaeker, P. Bäuerle, *Chem. Commun.* **2003**, 948–949;
b) M. Ammann, M. Enßle, G. Fuhrmann, A. Kaiser, P. Kilickiran, E. Mena-Osteritz, P. Bäuerle, *Polymer Preprints* **2003**, *44*, 379–380.

[143] S. M. ALQaisi, K. J. Galat, M. Chai, D. G. Ray III., P. L. Rinaldi, C. A. Tessier, W. J. Youngs, *J. Am. Chem. Soc.* **1998**, *120*, 12149–12150.

[144] Experimental work of Dr. P. Kilickiran, University of Ulm, unpublished.

[145] J. Widengren, R. Rigler, Ü. Mets, *J. Fluoresc.* **1994**, *4*, 255–258.

[146] all low temperature spectroscopic experiments were performed in the labs of Prof. U. Nienhaus, University of Ulm.

[147] S. Brawer, *Relaxation in Viscous Liquids and Glasses*, Am. Ceram. Soc., Columbus (OH), **1985**, pp. 6–11.

[148] HyperChem™ 6.03, Hypercube, Inc., 1115 NW 4th Street, Gainesville, FL 32601, USA.

[149] PC Spartan 1.0.5, Wavefunction, Inc., Irvine (CA).

[150] e.g.,
a) S. Goeb, A. De Nicola, R. Ziessel, *J. Org. Chem.* **2005**, *70*, 1518–1529;
b) A. Facchetti, M. Mushrush, M.-H. Yoon, G. R. Hutchinson, M. A. Ratner, T. J. Marks, *J. Am. Chem. Soc.* **2004**, *126*, 13859–13874;
c) L. Zhao, I. F. Perepichka, F. Türksoy, A. S. Batsanov, A. Beeby, K. S. Findlay, M. R. Bryce, *New J. Chem.* **2004**, *28*, 912–918;
d) L. Guyard, C. Dumas, F. Miomandre, R. Pansu, R. Renault-Méallet, P. Audebert, *New J. Chem.* **2003**, *27*, 1000–1006;
e) C. Ringenbach, A. De Nicola, R. Ziessel, *J. Org. Chem.* **2003**, *68*, 4708–4719.

[151] a) M. Mayor, C. von Hänisch, H. B. Weber, J. Reichert, D. Beckmann, *Angew. Chem.* **2002**, *114*, 1228–1231; *Angew Chem. Int. Ed.* **2002**, *41*, 1183–1186;
b) P. Siemsen, U. Gubler, C. Bosshard, P. Günter, F. Diederich, *Chem. Eur. J.* **2001**, *7*, 1333–1341.

[152] a) H. Jiang, W. Lin, *J. Am. Chem. Soc.* **2003**, *125*, 8084–8085;
b) M. Hissler, R. Ziessel, *J. Chem. Soc. Dalton Trans.* **1995**, 893–896.

[153] L. A. Sacksteder, E. Baralt, B. A. DeGraff, C. M. Lukehart, J. N. Demas, *Inorg Chem.* **1991**, *30*, 2468–2476.

[154] J. N. Demas, G. A. Crosby, *J. Phys. Chem.* **1971**, *75*, 991–1024.

[155] a) H. G. O. Becker (Ed.), *Einführung in die Photochemie*, Verlag der Wissenschaften, Berlin, **1991**, p. 455.
b) *EPA Newsletter* **1986**, *28*, p. 27.

[156] R. Sjöback, J. Nygren, M. Kubista, *Spectrochim. Acta Part A* **1995**, *51*, L7–L21.

Section 5 (Electrochemical Properties of Oligothienyl Macrocycles)

[157] see, e.g.,
a) D. W. Steuerman, H.-R. Tseng, A. J. Peters, A. H. Flood, J. O. Jeppesen, K. A. Nielsen, J. F. Stoddart, J. R. Heath, *Angew. Chem.* **2004**, *116*, 6648–6653; *Angew. Chem. Int. Ed.* **2004**, 47, 6486–6491;
b) M. Venturi, S. Dumas, V. Balzani, J. Cao, J. F. Stodart, *New. J. Chem.* **2004**, *28*, 1032–1037;
c) H. Yu, Y. Luo, K. Beverly, J. F. Stoddart, H.-R. Tseng, J. R. Heath, *Angew. Chem.* **2003**, *115*, 5884–5889; *Angew. Chem. Int. Ed.* **2003**, *42*, 5706–5711;
d) S. Chia, J. Cao, J. F. Stoddart, J. I. Zink; *Angew. Chem.* **2001**, *113*, 2513–2517; *Angew. Chem. Int. Ed.* **2001**, *40*, 2447–2451;
e) P. R. Ashton, V. Baldoni, V. Balzani, A. Credi, H. D. A. Hoffmann, M.-V. Martínez-Díaz, F. M. Raymo, J. F. Stoddart, M. Venturi, *Chem. Eur. J.* **2001**, *7*, 3482–3493;
f) V. Balzani, P. Ceroni, A. Credi, M. Gómez-López, C. Hamers, J. F. Stoddart, R. Wolf, *New J. Chem.* **2001**, *25*, 25–31;
g) V. Balzani, A. Credi, G. Mattersteig, O. A. Matthews, F. M. Raymo, J. F. Stoddart, M. Venturi, A. J. P. White, D. J. Williams, *J. Org. Chem.* **2000**, *65*, 1924–1936.

[158] a) A. N. Shipway, I. Willner, *Chem. Commun.* **2001**, 2035–2045;
b) A. N. Shipway, E. Katz, I. Willner, *ChemPhysChem* **2000**, *1*, 18–52.

[159] Y. Inokuma, T. Matsunari, N. Ono, H. Uno, A. Osuka, *Angew. Chem.* **2005**, *117*, 1890–1894; *Angew. Chem. Int. Ed.* **2005**, *44*, 1856–1860.

[160] a) L. N. Lucas, J. J. D. de Jong, J. H. van Esch, R. M. Kellogg, B. L. Feringa, *Eur. J. Org. Chem.* **2003**, 155–166;
b) A. Peters, N. R. Branda, *J. Am. Chem. Soc.* **2003**, *125*, 3404–3405.

[161] T. Köhler, Z. Ou, J. T. Lee, D. Seidel, V. Lynch, K. M. Kadish, L. J. Sessler, *Angew. Chem.* **2005**, *117*, 85–89; *Angew. Chem. Int. Ed.* **2005**, *44*, 83–87.

[162] N. Sprutta, L. Latos-Grażyński, *Chem. Eur. J.* **2001**, *7*, 5099–5112.

[163] M. B. Nielsen, M. Schreiber, Y. G. Baek, P. Seiler, S. Lecomte, C. Boudon, R. R. Tykwinsky, J.-P. Gisselbrecht, V. Gramlich, P. J. Skinner, C. Bosshard, P. Günter, M. Gross, F. Diederich, *Chem. Eur. J.* **2001**, *7*, 3263–3280.

[164] K. Hara, M. Hasegawa, Y. Kuwatani, H. Enozawa, M. Iyoda, *Chem. Commun.* **2004**, 2042–2043.

[165] a) U. Mitschke, P. Bäuerle, *J. Chem. Soc. Perkin Trans. 1* **2001**, 740–753;
b) J. Krömer, P. Bäuerle, *Tetrahedron* **2001**, *57*, 3785–3794;
c) P. Bäuerle, *Oligothiophenes* in *Electronic Materials: The Oligomer Approach* (Eds.: K. Müllen, G. Wegner), Wiley–VCH, Weinheim, **1999**, pp. 105-197.

[166] further recent examples are:
a) M.-H. Yoon, S. A. DiBenedetto, A. Facchetti, T. J. Marks, *J. Am. Chem. Soc.* **2005**, *127*, 1348–1349;
b) A. R. Murphy, J. M. J. Fréchet, P. Chang, J. Lee, V. Subramanian, *J. Am. Chem. Soc.* **2004**, *126*, 1596–1597;
c) M. Melucci, G. Barbarella, M. Zambianchi, P. Di Pietro, A. Bongini, *J. Org. Chem.* **2004**, *69*, 4821–4828;
d) A. Facchetti, M. Mushrush, M.-H. Yoon, G. R. Hutchinson, M. A. Ratner, T. J. Marks, *J. Am. Chem. Soc.* **2004**, *126*, 13859–13874;
e) A. Facchetti, M.-H. Yoon, C. L. Stern, G. R. Hutchinson, M. A. Ratner, T. J. Marks, *J. Am. Chem. Soc.* **2004**, *126*, 13480–13501;
f) J. Casado, T. M. Pappenfus, L. L. Miller, K. R. Mann, E. Ortí, P. M. Viruela, R. Pou-Amérigo, V. Hernández, J. T. López Navarrete, *J. Am. Chem. Soc.* **2003**, *125*, 2524–2534;
g) T. M. Pappenfus, M. W. Burand, D. E. Janzen, K. R. Mann, *Org. Lett.* **2003**, *5*, 1535–1538;
h) A. Wakamiya, D. Yamazaki, T. Nishinaga, T. Kitagawa, K. Komatsu, *J. Org. Chem.* **2003**, *68*, 8305–8314;
i) T. Izumi, S. Kobashi, K. Takimiya, Y. Aso, T. Otsubo, *J. Am. Chem. Soc.* **2003**, *125*, 5286–5287.

[167] a) E. Mena-Osteritz, P. Bäuerle, *Adv. Mater.* **2006**, *18*, 447–451;
b) E. Mena-Osteritz, P. Bäuerle, *Adv. Mater.* **2001**, *13*, 243–246;
c) J. Krömer, I. Rios-Carreras, G. Fuhrmann, C. Musch, M. Wunderlin, T. Debaerdemaeker, E. Mena-Osteritz, P. Bäuerle, *Angew. Chem.* **2000**, *112*, 3623–3628; *Angew. Chem. Int. Ed.* **2000**, *39*, 3481–3486.

[168] see, e.g.,
a) Y. Kunugi, K. Takimiya, N. Negishi, T. Otsubo, Y. Aso, *J. Mater. Chem.* **2004**, *14*, 2840–2841;
b) T. Otsubo, Y. Aso, K. Takimiya, *J. Mater. Chem.* **2002**, *12*, 2565–2575;
c) A. Cravino, N. S. Sariciftci, *J. Mater. Chem.* **2002**, *12*, 1931–1943;
d) C. J. Brabec, C. Winder, N. S. Sariciftci, J. C. Hummelen, A. Dhanabalan, P. A. van Hal, R. A. Janssen, *Adv. Funct. Mater.* **2002**, *12*, 709–712.

[169] a) F. Paul, C. Lapinte, *Coord. Chem. Rev.* **1998**, 178–180;
b) J. J. Pak, T. J. R. Weakley, M. M. Haley, *Organometallics* **1997**, *16*, 4505–4507.

[170] a) M. O. Wolf, PhD thesis, Massachusetts Institute of Technology, **1994**;
b) G. Frapper, M. Kertesz, *Inorg. Chem.* **1993**, *32*, 732–740.

[171] a) M. Mayor, C. von Hänisch, H. B. Weber, J. Reichert, D. Beckmann, *Angew. Chem.* **2002**, *114*, 1228–1231; *Angew Chem. Int. Ed.* **2002**, *41*, 1183–1186;

b) P. Siemsen, U. Gubler, C. Bosshard, P. Günter, F. Diederich, *Chem. Eur. J.* **2001**, *7*, 1333–1341;
c) Y. Mori, T. Kasai, T. Takesada, H. Komatsu, H. Yamazaki, M.-a. Haga, *Chem. Lett.* **2001**, 996–997.

[172] a) F. Würthner, A. Sautter, D. Schmid, P. J. A. Weber, *Chem. Eur. J.* **2001**, *7*, 894–902;
b) F. Würthner, A. Sautter, *Chem. Commun.* **2000**, 445–446.

[173] W.-Y. Wong, K.-H. Choi, G.-L. Lu, J.-X Shi, *Macromol. Rapid Commun.* **2001**, *22*, 461–465.

[174] J. Lewis, N. J. Long, P. R. Raithby, G. P. Shields, W.-Y. Wong, M. Younus, *J. Chem. Soc. Dalton Trans.* **1997**, 4283–4288.

[175] a) R. J. Puddephatt, *Angew. Chem.* **2002**, *114*, 271–273; *Angew. Chem. Int. Ed.* **2002**, *41*, 261–263;
b) G. S. Hill, G. P. A. Yap, R. J. Puddephatt, *Organometallics* **1999**, *18*, 1408–1418;
c) L. M. Rendina, R. J. Puddephatt, *Chem. Rev.* **1997**, *97*, 1735–1754;
d) G. S. Hill, R. J. Puddephatt, *Organometallics* **1997**, *16*, 4522–4524;
e) S. Roy, R. J. Puddephatt, J. D. Scott, *J. Chem. Soc. Dalton Trans.* **1989**, 2121–2125;
f) M. P. Brown, R. J. Puddephatt, C. E. E. Upton, *J. Chem. Soc. Dalton Trans.* **1974**, 2457–2460.

[176] a) D. M. Crumton-Bregel, K. I. Goldberg, *J. Am. Chem. Soc.* **2003**, *125*, 9442–9456;
b) K. L. Bartlett, K. I. Goldberg, W. T. Borden, *J. Am. Chem. Soc.* **2000**, *122*, 1462–1465;
c) D. M. Crumpton, K. I. Goldberg, *J. Am. Chem. Soc.* **2000**, *122*, 962–963.

[177] G. Fuhrmann, PhD thesis, University of Ulm, **2006**.

[178] a) G. Fuhrmann, T. Debaerdemaeker, P. Bäuerle, *Chem. Commun.* **2003**, 948–949;
b) M. Ammann, M. Enßle, G. Fuhrmann, A. Kaiser, P. Kilickiran, E. Mena-Osteritz, P. Bäuerle, *Polymer Preprints* **2003**, *44*, 379–380.

[179] M. Sato, E. Mogi, *Organometallics* **1995**, *14*, 3157–3159.

[180] M. Ammann, PhD thesis, University of Ulm, **2004**.

[181] R. N. Adams, *Electrochemistry at Solid Electrodes*, Marcel Dekker, New York, **1969**, p. 146.

[182] Experimental work of Dr. P. Kilickiran, University of Ulm, unpublished.

[183] J. Krömer, PhD thesis, University of Ulm, **2000**.

[184] a) HyperChem™ 6.03, Hypercube, Inc., 1115 NW 4th Street, Gainesville, FL 32601, USA.
b) PC Spartan 1.0.5, Wavefunction, Inc., Irvine (CA).

[185] W. Mohr, J. Stahl, F. Hampel, J. A. Gladysz, *Chem. Eur. J.* **2003**, *9*, 3324–3340.

[186] a) J. van Haare, PhD thesis, TU Eindhoven, **1997**, p. 47;
b) J. Pommerehne, H. Vestweber, W. Guss, R.F. Mahrt, H. Bässler, M. Porsch, J. Daub, *Adv. Mater.* **1995**, *7*, 551–554.

Section 6 (Interactions between Oligothienyl Macrocycles and Receptor Molecules)

[187] M.-S. Choi, T. Yamazaki, I. Yamazaki, T. Aida,
Angew. Chem. **2004**, *116*, 152–160; *Angew. Chem. Int. Ed.* **2004**, *43*, 150–158.

[188] P. N. W. Baxter, *J. Org, Chem.* **2004**, *69*, 1813–1821.

[189] A. G. Martínez, J. O. Barcina, M. del Rosario Colorado Heras, A. de Fresno Cerezo, M. del Rosario Torres Salvador, *Chem. Eur. J.* **2003**, *9*, 1157–1165.

[190] a) S. Cerezo, J. Cortès, E. Lago, E. Molins, M. Moreno-Mañas, T. Parella, R. Pleixats, J. Torrejón, A. Vallribera, *Eur. J. Org. Chem.* **2001**, 1999–2006;
b) Y. Kuwatani, T. Yoshida, A. Kusaka, M. Oda, K. Hara, M. Yoshida, H. Matsuyama, M. Iyoda, *Tetrahedron* **2001**, *57*, 3567–3576;
c) W. J. Youngs, C. A. Tessier, J. D. Bradshaw, *Chem. Rev.* **1999**, *99*, 3153–3180;
d) L. Guo, J. D. Bradshaw, C. A. Tessier, W. J. Youngs,
Organometallics **1995**, *14*, 586–588;
e) J. E. McMurry, G. J. Haley, J. R. Matz, J. C. Clardy, J. Mitchell,
J. Am. Chem. Soc. **1986**, *108*, 515–516.

[191] a) J. D. Badjić, V. Balzani, A. Credi, J. N. Lowe, S. Silvi, J. F. Stoddart,
Chem. Eur. J. **2004**, *10*, 1926–1935;
b) V. Balzani, M. Clemente-León, A. Credi, J. N. Lowe, J. D. Badjić, J. F. Stoddart, D. J. Williams, *Chem. Eur. J.* **2003**, *9*, 5348–5360;
c) M. V. Martínez-Díaz, N. S. Fender, M. S. Rogríguez-Morgade, M. Gómez-López, F. Diederich, L. Echegoyen, J. F. Stoddart, T. Torres,
J. Mater. Chem. **2002**, *12*, 2095–2099;
d) S.-H. Chiu, S. J. Rowan, S. J. Cantrill, J. F. Stoddart, A. J. P. White, D. J. Williams,
Chem. Eur. J. **2002**, *8*, 5170–5183.

[192] D. G. Hamilton, L. Prodi, N. Feeder, J. K. M. Sanders,
J. Chem. Soc. Perkin Trans. 1 **1999**, 1057–1065.

[193] see, e.g.,
a) J. L. Atwood, L. J. Barbour, M. W. Heaven, C. L. Raston,
Chem. Commun. **2003**, 2270–2271;
b) G.-B. Pan, J.-M. Liu, H.-M. Zhang, L.-J. Wan, Q.-Y. Zheng, C.-L. Bai,
Angew. Chem. **2003**, *115*, 2853–2857; *Angew. Chem. Int. Ed.* **2003**, *42*, 2747–2751.

[194] E. A. Meyer, R. K. Castellano, F. Diederich,
Angew. Chem. **2003**, *115*, 1244–1287; *Angew. Chem. Int. Ed.* **2003**, *42*, 1210–1250.

[195] a) T. Kawase, L. Tanaka, N. Shiono, Y. Seirai, M. Oda,
Angew. Chem. **2004**, *116*, 1754–1756; *Angew. Chem. Int. Ed.* **2004**, *43*, 1722–1724;
b) T. Kawase, N. Fujiwara, M. Tsutumi, M. Oda, Y. Maeda, T. Wakahara, T. Akasaka,
Angew. Chem. **2004**, *116*, 5170–5172; *Angew. Chem. Int. Ed.* **2004**, *43*, 5060–5062;
c) T. Kawase, K. Tanaka, Y. Seirai, N. Shiono, M. Oda,
Angew. Chem. **2003**, *115*, 5755–5758; *Angew. Chem. Int. Ed.* **2003**, *42*, 5597–5600;
d) T. Kawase, Y. Seirai, H. R. Darabi, M. Oda, Y. Sarakai, K. Tashiro,
Angew. Chem. **2003**, *115*, 1659–1662; *Angew. Chem. Int. Ed.* **2003**, *42*, 1621–1624;
e) T. Kawase, K. Tanaka, N. Fujiwara, H. R. Darabi, M. Oda,
Angew. Chem. **2003**, *115*, 1662–1666; *Angew. Chem. Int. Ed.* **2003**, *42*, 1624–1628.

[196] a) J.-Y. Zheng, K. Tashiro, Y. Hirabayashi, K. Kinbara, K. Saigo, T. Aida, S. Sakamoto, K. Yamaguchi,
Angew. Chem. **2001**, *113*, 1909–1913; *Angew. Chem. Int. Ed.* **2001**, *40*, 1858–1861;
b) T. Nishioka, K. Tashiro, T. Aida, J.-Y. Zheng, K. Kinbara, K. Saigo, S. Sakamoto, K. Yamaguchi, *Macromolecules* **2000**, *39*, 9182–9184;
c) K. Tashiro, T. Aida, J.-Y. Zheng, K. Kinbara, K. Saigo, S. Sakamoto, K. Yamaguchi, *J. Am. Chem. Soc.* **1999**, *121*, 9477–9478.

[197] E. Mena-Osteritz, P. Bäuerle, *Adv. Mater.* **2006**, *18*, 447–451.

[198] F. H. Allen, C. M. Bird, R. S. Rowland, P. R. Raithby, *Acta Cryst.* **1997**, *B53*, 696–701.

[199] a) T. B. Rauchfuss, *Prog. Inorg. Chem.* **1991**, *39*, 259–329;
b) R. J. Angelici, *Coord. Chem. Rev.* **1990**, *105*, 61–76.

[200] see, e.g.,
a) J. L. Segura, N. Martín, D. M. Guldi, *Chem. Soc. Rev.* **2005**, *34*, 31–47;
b) H. Kanato, K. Takimiya, T. Otsubo, Y. Aso, T. Nakamura, Y. Araki, O. Ito, *J. Org. Chem.* **2004**, *69*, 7183–7189;
c) P. A. van Hal, E. H. A. Beckers, S. C. J. Meskers, R. A. J. Janssen, B. Jousselme, P. Blanchard, J. Roncali, *Chem. Eur. J.* **2002**, *8*, 5415–5429;
d) C. Martineau, P. Blanchard, D. Rondeau, J. Delaunay, J. Roncali, *Adv. Mater.* **2002**, *14*, 283–287;
e) D. Hirayama, K. Takimiya, Y. Aso, T. Otsubo, T. Hasobe, H. Yamada, H. Imahori, S. Fukuzumi, Y. Sakata, *J. Am. Chem. Soc.* **2002**, *124*, 532–533;
f) S.-G. Liu, C. Martineau, J.-M. Raimundo, J. Roncali, L. Echegoyen, *Chem. Commun.* **2001**, 913–914;
g) A. Cravino, G. Zerza, M. Maggini, S. Bucella, M. Svensson, M. R. Andersson, H. Neugebauer, N. S. Sariciftci, *Chem. Commun.* **2000**, 2487–2488.

[201] S. Kobayashi, Y. Yamaguchi, T. Wakamiya, Y. Matsubara, Z.-i. Yoshida, *5th intern. conf. on func. π-electron systems Fπ5* (Ithaca, NY) **2004**, poster 5541_0017; oral communication.

[202] The value was determined by printing a two-dimensional projection of a CPK model and subsequent weighing of the cut-out pieces.

[203] a) K. Nakano, K. Sada, Y. Kurozumi, M. Miyata, *Chem. Eur. J.* **2001**, *7*, 209–220;
b) S. Mecozzi, J. Rebek Jr., *Chem. Eur. J.* **1998**, *4*, 1016–1022.

[204] HyperChem™ 6.03, Hypercube, Inc., 1115 NW 4th Street, Gainesville, Florida 32601, USA.

[205] E. A. Meyer, R. K. Castellano, F. Diederich, *Angew. Chem.* **2003**, *115*, 1244–1287; *Angew. Chem. Int. Ed.* **2003**, *42*, 1210–1250.

[206] see, e.g.,
a) D. W. Steuerman, H.-R. Tseng, A. J. Peters, A. H. Flood, J. O. Jeppesen, K. A. Nielsen, J. F. Stoddart, J. R. Heath, *Angew. Chem.* **2004**, *116*, 6648–6653; *Angew. Chem. Int. Ed.* **2004**, 47, 6486–6491;
b) M. Venturi, S. Dumas, V. Balzani, J. Cao, J. F. Stoddart, *New. J. Chem.* **2004**, *28*, 1032–1037;
c) H. Yu, Y. Luo, K. Beverly, J. F. Stoddart, H.-R. Tseng, J. R. Heath, *Angew. Chem.* **2003**, *115*, 5884–5889; *Angew. Chem. Int. Ed.* **2003**, *42*, 5706–5711;
d) S. Chia, J. Cao, J. F. Stoddart, J. I. Zink; *Angew. Chem.* **2001**, *113*, 2513–2517; *Angew. Chem. Int. Ed.* **2001**, *40*, 2447–2451;

e) P. R. Ashton, V. Baldoni, V. Balzani, A. Credi, H. D. A. Hoffmann, M.-V. Martínez-Díaz, F. M. Raymo, J. F. Stoddart, M. Venturi, *Chem. Eur. J.* **2001**, *7*, 3482–3493;
f) V. Balzani, P. Ceroni, A. Credi, M. Gómez-López, C. Hamers, J. F. Stoddart, R. Wolf, *New J. Chem.* **2001**, *25*, 25–31;
g) V. Balzani, A. Credi, G. Mattersteig, O. A. Matthews, F. M. Raymo, J. F. Stoddart, M. Venturi, A. J. P. White, D. J. Williams, *J. Org. Chem.* **2000**, *65*, 1924–1936.

[207] see, e.g.,
a) L. Zhai, R. D. McCullough, *J. Mater. Chem.* **2004**, *14*, 141–143;
b) M. S. A. Abdou, S. Holdcroft, *Chem. Mater.* **1996**, *8*, 26–31;
c) M. S. A. Abdou, S. Holdcroft, *Synth. Metals* **1993**, *60*, 93–96.

[208] T. Inomata, K. Konishi, *Chem. Commun.* **2003**, 1282–1283.

[209] M. Brust, M. Walker, D. Bethell, D. J. Schiffrin, R. Whyman, *J. Chem. Soc. Chem. Commun.* **1994**, 801–802.

[210] R. Wang, J. Yang, Z. Zheng, M. D. Carducci, J. Jiao, S. Seraphin, *Angew. Chem.* **2001**, *113*, 567–570; *Angew. Chem. Int. Ed.* **2001**, *40*, 549–552.

[211] a) J. Janzcak, G. J. Perpétu, *Acta Cryst.* **2001**, *C57*, 1120–1122;
b) J. Janzcak, G. J. Perpétu, *Acta Cryst.* **2001**, *C57*, 873–875;
c) M. Scoponi, E. Polo, F. Pradella, V. Bertolasi, V. Parassiti, P. Goderti, *J. Chem. Soc. Perkin Trans. 2* **1992**, 1127;
d) C. E. Barnett, *J. Chem. Phys.* **1930**, *34*, 1497–1504.

[212] Protonation of melamine was also performed in analogy to lit. [211c] using trifluoroacetic acid instead of hydrochloric acid, but the yields in this case were significantly lower.

[213] see, e.g.,
a) D. A. Weinberger, T. B. Higgins, C. A. Mirkin, L. M. Liable-Sands, A. L. Rheingold, *Angew. Chem.* **1999**, *117*, 2748–2750; *Angew. Chem. Int. Ed.* **1999**, *38*, 2565–2568;
b) S. Luo, T. B. Rauchfuss, A. L. Rheingold, *J. Organomet. Chem.* **1994**, *472*, 295–302;
c) J. W. Benson, R. J. Angelici, *Organometallics* **1992**, *11*, 922–927;
d) J. Chen, R. J. Angelici, *Organometallics* **1990**, *9*, 849–852;
e) A. E. Skaugset, T. B. Rauchfuss, C. L. Stern, *J. Am. Chem. Soc.* **1990**, *112*, 2432–2433;
f) V. Guerchais, D. Astruc, *J. Organomet. Chem.* **1986**, *316*, 335–341;
g) D. Catheline, D. Astruc, *J. Organomet. Chem.* **1984**, *272*, 417–426.

List of Publications

Publications

a) *Macrocycles and Complex Three-Dimensional Structures Comprising Pt(II) Building Blocks*: A. Kaiser, P. Bäuerle, *Top. Curr. Chem.* **2005**, *249*, 127;

b) *Functional π-Electron Materials for Nanoelectronics*: M. Ammann, M. Enßle, G. Fuhrmann, A. Kaiser, P. Kilickiran, E. Mena-Osteritz, P. Bäuerle, *Polymer Preprints* **2003**, *44*, 379.

Poster Contributions

a) A. Kaiser, G. Fuhrmann, E. Mena-Osteritz, P. Bäuerle, *Electronic Properties of Macrocyclic Oligothiophenes*:
6th International Symposium on Functional π-Electron Systems (Fπ6), Ithaca, NY, **2004**;

b) A. Kaiser, C. Fave, G. Fuhrmann, P. Kilickiran, P. Bäuerle, *Electrochemical Properties of Macrocyclic Oligothiophenes*:
Workshop of the Graduate College 328 and the Collaborative research centre SFB 569, Ulm, **2004**;

c) A. Kaiser, P. Bäuerle, *The Metal Template Route to Fully Conjugated Macrocycles*:
4th Workshop of Conjugated Oligomers and Polymers (KOPO ´03), Blaubeuren, **2003**;
Workshop of the Graduate College 328 and the Collaborative research centre SFB 569, Ulm, **2003**;

d) A. Kaiser, P. Bäuerle, *Spectroscopic and Electronic Properties of Macrocyclic Oligothiophene-diacetylenes*:
5th International Symposium on Functional π Electron Systems (Fπ5), Ulm, **2002**;

e) A. Kaiser, G. Fuhrmann, E. Mena-Osteritz, P. Bäuerle, *Spectroscopic Properties of Cyclic Oligo(terthiophene-diyne)s*:
Workshop of the Graduate College 328 and the Collaborative research centre SFB 569, Ulm, **2001**;

f) A. Kaiser, G. Fuhrmann, E. Mena-Osteritz, P. Bäuerle, *Molecular Spiders and Honeycombs: The Perspectives of Cyclothiophenes*:
Frühjahrssymposium of the GDCh Young Chemists´ Forum, Leipzig, **2001**;
5th Int. Symposium of the VW-Stiftung on Intra- and Intermolecular Electron Transfer, Chemnitz, **2001**;
GDCh Annual Conference 2001, Würzburg, **2001**.

Erklärung

Ich erkläre hiermit, dass ich die vorliegende Arbeit selbstständig und nur mit den angegebenen Hilfsmitteln angefertigt habe.

(Achim Kaiser)